Ultrasonic Reflection for Measurement of Oil Film Thickness and Contact between Dissimilar Materials

by

Dedison Gasni

March 2012

Thesis submitted for the degree of Doctor of Philosophy

Department of Mechanical Engineering

University of Sheffield

Summary

The contact between dissimilar materials occurs in many machine elements where one of the contacting parts is manufactured from low modulus materials such as lip seals, o-rings, and metal on polymer prosthetic hip joints. Contacts of this sort of are often operated in the iso-viscous elastohydrodynamic lubrication (I-EHL) regime. Typically, they have been studied using a numerical approach due to lack of sensor of instrumentation for measuring oil film thickness. By developing the technology of sensors such as electromagnetic radiation and magnetic resistance techniques, the phenomenon of lubrication in I-EHL regime has shown results which are better understood. However, the experimental study that has been conducted to date is only appropriate for laboratory-based measurements.

This thesis deals with the ultrasonic reflection methods to measure an oil film thickness and contact between dissimilar materials where these methods could be applied in-situ. This warrants special attention because there are two drawbacks of measuring of oil film thickness and contact by using bulk longitudinal wave between dissimilar materials (such as rubber and steel) which have mismatched acoustic impedance. One is the attenuation. The ultrasonic signal will be reduced when passed through the rubber. The other is accessibility. The wave must pass normally through the interface and so the transducer must be mounted on the rubber itself.

There are two methods that can be used to measure oil film thickness using ultrasonic reflection: amplitude and phase shift. The amplitude method has been proved successfully for measuring oil film thickness between two similar materials and between two materials with little difference in acoustic impedance, but it fails for contact between two acoustically dissimilar materials. In this case, the phase shift method has the potential to measure oil film thickness. The results show that this method is valid for measuring thin films ($h < 40$ μm) for contact between Perspex and steel.

The application of ultrasonic reflection techniques to measure the lubricant film thickness in iso-viscous elastohydrodynamic lubrication regime has been investigated. The reflection of ultrasonic pulses from the interface between the nitrile sphere and Perspex disk was recorded for a range of lubricated, dry, static, and dynamic contact conditions. In this way, profiles of oil film thickness were created for various loads and sliding speeds. The phenomenon of a wedge-shaped constriction in lubricant film was observed, especially at low speeds. It was also possible to observe cavitation effects on the signal in the exit region. The measured central film thickness results are compared with published models of the lubrication mechanism and experimental data obtained from optical methods. The result shows that the oil film thickness was measured in the region of 1 to 6 μm. The data was shown to be consistent with previous published experimental work using optical methods but somewhat lower than theoretical solutions.

Ultrasonic surface waves that are commercially used for non-destructive evaluation (NDE) and damage detection have been also developed to measure contact between soft and hard materials. The measurements were made by using variable and fixed wedge transducers. The reflection coefficient of Rayleigh waves at point and line contacts was measured to study the characteristic of compliant contacts in dry and lubricated conditions. The results show that the increased load causes a decreased reflection coefficient. Therefore, the reflection coefficient of Rayleigh wave at interface between soft and hard materials can be developed as a sensor for o-ring and lip seals and this sensor could be positioned remotely from the contact.

Acknowledgments

I would like to offer my sincere gratitude to my supervisor, Professor Rob Dwyer-Joyce, for his help and guidance, and for his support and patience. He provides great knowledge and experience in the field of Tribology, which has been of great value for the results presented here.

I am very grateful to Dr. Connor Myant for the sharing of his experimental data in Chapter 5, measurement of film thickness I-EHL regime.

During the past three years, I have enjoyed the pleasant working environment in the Leonardo Centre for Tribology Group and I want to thank to research assistants: Robin Mills and Stephen Lewis, research technician Dave Butcher, and Phd students: Kamel Wan Ibrahim, Juan Zhu, Hendry Brunskill, Steve Pugh, Emin Yusuf Avan, and Daniel Ooi for their help and support.

I am grateful to the directorate general higher education (DGHE) scholarship, Republic Indonesia, which has funded my PhD. Many thanks to vice rector for academic Andalas University, Indonesia and education and culture attaché of Republic Indonesia in London for supporting and helping as long as I studied in UK.

Finally, I would like to thank my family for their encouragement and infinite patience and in particular my wife, Sabrina, for her strength and reassurance.

Table of contents

Nomenclature

All symbols are also defined in the text.

Symbol	Description	Units
a	contact radius	m
A	amplitude of reduced signal	volt
A_I	amplitude of incident wave	m
A_T	amplitude of transmitted wave	m
A_R	amplitude of reflected wave	m
A_0	amplitude of signal	volt
$A(f)$	amplitude of the signal reflected from the lubricant-film layer	volt
$A_0(f)$	amplitude of the reference signal	volt
c	speed of sound	m/s
c_1	speed of sound of material 1	m/s
c_2	speed of sound of material 2	m/s
c_w	speed of sound water	m/s
c_{tm}	speed of sound test material	m/s
c_m	material sound velocity	m/s
c_{1L}	longitudinal speed of sound of material 1	m/s
c_{2L}	longitudinal speed of sound of material 2	m/s
c_{2T}	transversal speed of sound of material 2	m/s
D_c	transducer element diameter	m
$d_f(-6dB)$	spot diameter	m
e	natural	dimensionless
E	Young's modulus	Pa

E_1	Young's modulus of material 1	Pa
E_2	Young's modulus of material 2	Pa
E^*	reduced Young's modulus	Pa
f	frequency	Hz
F	transducer focal length	m
F	force	N
G	dimensionless material parameter	dimensionless
h	film thickness	m
h_c	central film thickness	m
$\hat{H}_{cen}$	dimensionless central film thickness	dimensionless
K	stiffness of the layer	Pa/m^2
k	ellipticity parameter	dimensionless
k_T	wave number for transversal wave	m^{-1}
k_L	wave number for longitudinal wave	m^{-1}
k_1	wave number for media 1	m^{-1}
k_2	wave number for media 2	m^{-1}
l_w	focal length	m
L	Moes dimensionless speed	dimensionless
M	Moes dimensionless load	dimensionless
m	Mode number of resonant frequency	dimensionless
P	force	N
r	constant, $exp\{1-6/(L+8)\}$	dimensionless
r	refracted angle	rad
R	reflection coefficient	dimensionless
R	radius	m
R_0	the reflection coefficient of the reference interface	dimensionless
R_x	effective radius in x direction	
s	constant, $12-10exp(M^{-2})$	dimensionless
t	constant, $1-exp\left\{-0.9\frac{M^{1/6}}{L^{1/6}}\right\}$	dimensionless
t	time	s
T	material thickness	m
u_i	displacement wave of incident wave	m
u_r	displacement wave of reflected wave	m
u_t	displacement wave of transmitted wave	m
U_1	displacement wave in media 1	m
U_2	displacement wave in media 2	m
U	dimensionless speed parameter	dimensionless
W	dimensionless load parameter	dimensionless
z	distance	m
Z_1	acoustic impedance material 1	kg/m^{2}s
Z_2	acoustic impedance material 2	kg/m^{2}s
α	attenuation coefficient	dimensionless
α_L	angle of incidence of longitudinal wave	degree
α_T	angle of incidence of shear wave	degree
α_{LT}	reflected angle of longitudinal wave	degree
α_{TT}	reflected signal of shear wave	degree
β_{TT}	refracted angle of shear wave	degree
β_{TL}	refracted angle of longitudinal wave	degree

v	Poisson's ratio	dimensionless
σ_1	stress field in media 1	N/m^2
σ_2	stress field in media 2	N/m^2
ρ	material density	kgm^{-3}
ω	frequency	rad/s
μ_1	Lame constant for material 1	dimensionless
μ_2	Lame constant for material 2	dimensionless
θ_1	angle of incidence	degree
θ_2	refracted angle	degree
θ_{1L}	incidence angle of longitudinal wave	degree
θ_{2L}	refracted angle of longitudinal wave	degree
θ_{2T}	refracted angle of shear wave	degree
θ_{cr1}	first critical angle	degree
θ_{cr2}	second critical angle	degree
λ_1	Lame constant for material 1	dimensionless
λ_2	Lame constant for material 2	dimensionless
ϕ	phase difference	rad

Abbreviations

BS	bottom face reflection of steel plate
BW	bottom face reflection of wedge
DPT	digital piezoelectric translator
EHL	elastohydrodynamic lubrication
FFT	fast Fourier transform
HD	hydrodynamic
I-EHL	isoviscous viscous elastohydrodynamic lubrication
Lab VIEW	graphical array-handling programming language
LIF	laser induce fluorescence
LHS	left-hand side
L	longitudinal wave
MLMI	multigrid and multi-level multi-integration
MP	Material thickness
NDT	non destructive testing
NDE	non destructive evaluation
PC	personal computer
PDMS	polydimethyl silixone
RLL	reflection factor for longitudinal reflected wave
RLS	reflection factor for longitudinal transmitted wave
RSL	reflection of solid-liquid interface
RSS	reflection of solid-solid interface
S	shear wave
UPR	ultrasonic pulse receiver
ToF	time of flight
TS	reflected surface wave
TW	top face reflection of wedge
TLL	refraction factor for longitudinal reflected wave
TLS	refraction factor for longitudinal transmitted wave

List of tables

List of figures

using variable wedge transducer.

Chapter 1

Introduction

1.1 Statement of problem

Contact stress and oil film formation are two fields of Tribology that are crucial in design of bearing components. The measurements of oil film thickness and contact between hard and hard materials have been carried out extensively. These methods have been applied in engineering components, such as ball bearings, gears, journal bearings, metal on metal hip joints, and piston rings. By contrast, the study of Tribology between soft and hard materials is not well understood and few investigators get involved despite its importance in many applications of engineering and biological Tribology, such as rubber seals, metal on polymer prosthetic hip joints, and natural synovial joints.

The foundation of numerical approach to measure film thickness between soft and hard materials has been proposed by Hamrock and Dowsons [1978] who obtained a formula to measure centre film thickness for fully flooded, isothermal, and elastohydrodynamic elliptical contact. Several experimental studies have been made to deduce the oil film thickness between soft and hard materials using the electromagnetic radiation and magnetic resistance techniques. Myant [2010] has obtained the film thickness map for compliant contact by using the electromagnetic radiation techniques, so the principles of iso-viscous

elastohydrodynamic lubrication (I-EHL) become clearer. However, both techniques require modifications in implementation to bearing technology and frequently preclude their application outside of the laboratory.

During the past 50 years, ultrasound has been used in non-destructive testing (NDT), such as inspection of cracks, internal flaws, and defects. In the last decade, ultrasonic reflection technique has showed potentially to measure the oil film thickness and contact between hard and hard materials, because this technique has some advantages: non-invasive, safe and portable. However, this technique has not been widely accepted due to lack of calibration, testing and validation (Reddyhoff [2006]). Contact between two materials occurs between not only hard and hard materials but also between soft and hard materials and soft and soft materials. In this thesis, ultrasonic reflection methods have been explored to measure such contacts.

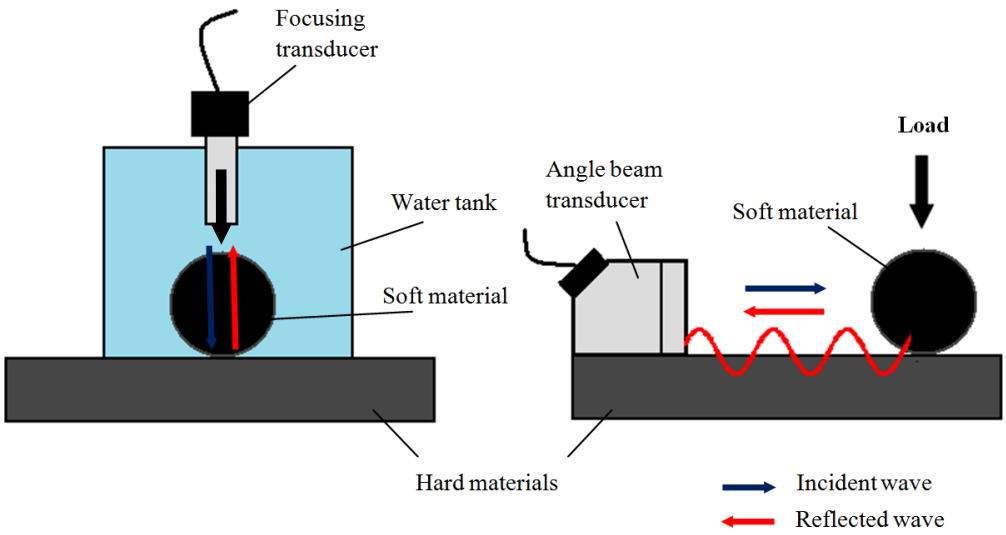

Figure 1.1 Comparison between (a) bulk waves and (b) surface waves in detecting an interface contact between soft and hard materials.

There are two drawbacks using bulk longitudinal wave of ultrasonic reflection technique to measure a contact between soft and hard materials, which have mismatched acoustic impedance. One is the attenuation. The ultrasonic signal will be reduced when passed through the rubber material. The other is accessibility.

The wave must pass normally through the interface and so the transducer must be mounted on the soft material itself. In addition, amplitude methods have failed used to measure oil film thickness and contact between two acoustically dissimilar materials. Phase shift method can be explored to measure such a contact and Rayleigh surface wave, as alternative, can be applied to measure contact between soft and hard materials. The sensor can remotely sense an interface and it can be put somewhere on the surface of hard material as shown in Figure 1.1b.

1.2 Research objectives

The aim of this thesis is to develop experimentally ultrasonic reflection techniques to measure the oil film thickness and contact between two dissimilar materials by expanding the theory behind it and finding new experimental methods. The objectives of this work are:

1. To develop the phase shift method to calculate the oil film thickness between two acoustically dissimilar materials in contact.

2. To develop the ultrasonic reflection techniques to measure the oil film thickness in iso-viscous elastohydrodynamic lubrication (I-EHL) regime.

3. To develop the reflection of Rayleigh waves as a sensor to measure contact between soft and hard materials.

The development of ultrasonic reflection techniques as a tool to measure an oil film thickness and contact could be explored for many applications of bearing technology with various types of material in contact. In addition, the phase shift method based on stiffness interface model to measure oil film thickness has been developed for contact between two acoustically dissimilar materials. The measurement of oil film thickness in I-EHL regime using ultrasonic reflection technique could be used to understand lubricating properties between soft and hard materials. The measurement of contact between soft and hard materials using

reflection coefficient of Rayleigh wave has been developed as a sensor for o-ring and lip seals in the future.

1.3 Thesis layout

This thesis is divided into the following chapters:

1. Chapter 1 explains the statement of the problem and objectives of the research. It also explains the thesis layout.

2. Chapter 2 outlines a literature review on measuring the oil film thickness in iso-viscous elastic lubrication (I- EHL) regime that purposes to identify the gaps in the current state of knowledge and covers some fundamental principles of ultrasound useful to measure the oil film thickness. Formula to measure the oil film thickness for soft EHL is explained. In the last section of this chapter, the measurement of contact using ultrasound is discussed.

3. Chapter 3 begins by laying out the ultrasonic background, and looks at how to measure lubricant oil film thickness by using ultrasonic reflection. In calculation of the oil film thickness, both amplitude and phase shift methods are discussed.

4. Chapter 4 describes ultrasonic equipment and how to choose an ultrasonic transducer, which will be used to measure the oil film thickness and contact in Chapters 5, 6 and 7. The steps of capturing and processing signal in measuring of reflection coefficient and phase difference are described in detail.

5. Chapter 5 gives the first experimental work to measure the oil film thickness between two acoustically dissimilar materials. The experimental study is performed to compare the result of oil film thickness between amplitude and phase shift methods. The phase shift method is used when the amplitude method fails for acoustically dissimilar materials.

6. Chapter 6 shows the second experimental work to measure the oil film thickness in the iso-viscous elastohydrodynamic lubrication (I-EHL) regimes. The contact between Perspex disk and a nitrile ball is studied.

7. Chapter 7 presents the third experimental work in measuring contact between soft and hard materials by using Rayleigh waves. A method of ultrasonic reflection is proposed.

8. The last chapter summaries the work done in this study and the future work is also explained. Recommendations are given for future research.

Chapter 2

Literature review

This chapter presents a literature review to measure oil film thickness in I-EHL regime by numerical and experimental approaches. In the following sections, the comparison between experimental and numerical results for central film thickness is also described. The measurement of contact mechanics using ultrasound is discussed at the end of this chapter.

2.1 Introduction

The isoviscous elastohydrodynamic lubrication (I-EHL) or soft-EHL regime relates to materials of low elastic modulus when one or both of the containing surfaces are in the contact. Hooke [1997] has distinguished lubrication of soft contact from lubrication of hard contact by two characteristics. The first is the relatively low contact pressure (around 1 to 10 MPa) which is insufficient to cause any substantial increase in viscosity. The second is the large elastic deformations where displacements of some hundreds of microns are common. The film thickness which is typically 1 μm thus depends on the elastic properties of the surfaces but not on the pressure-viscosity coefficient of the lubricant.

The soft EHL regime can be applied in many practical lubricated engineering and biological Tribology. Friction of windscreen wipers (Fuji [2007]), road in tyre contact (Heinrich and Kluppel [2008], performance of rubber seals (Drotowski [1968], Poll and Gabelli [1992], Poll *et al.* [1992], Kaneta [2000], Anderson *et al,* [1999], Anderson *et al.* [2000], Anderson *et al.* [2001]), studies of natural synovial joint lubrication (Jin and Dowson [2005], Dowson and Neville [2006]), oral processing (Bongaerts *et al.* [2007]), taste and taste perception of foodstuffs and beverages (Stokes and Telford [2004]), the feel and function of cosmetics and skin cream (Adams *et al.* [2007]) are examples of their application.

The tribological interface of I-EHL consists of un-lubricated and lubricated cases. Lubricated contact depends on the thickness of lubricating film and its physical properties. The integrity and performance of the oil film are key to the successful protection of the contacting surfaces. If the asperity contacts are small, the lubricant films are thin, so these problems are difficult to achieve in experimental methods.

The experimental studies of I-EHL have been focused on the frictional characteristics (de Vicente *et al.* [2005a], de Vicente *et al.* [2005b], Myant [2010]), oil film thickness (Poll and Gabelli [1992], Poll *et al.* [1992], Kaneta [2000], Myant [2010], Myant *et al.* [2010]), and compliant contact (Drotowski [1968]). The research to date has tended to focus on the frictional characteristics and oil film thickness rather than compliant contact.

2.2 Experimental measurements of film thickness

The researches on I-EHL regimes have been conducted in numerical modelling and experimental study. The numerical works (Herrebrugh [1968], Hooke and O'Donoghue [1972], Biswas and Snidel [1976], and Hamrock and Dowson [1978]) have simultaneously solved the Reynolds and elasticity equations in order to identify the range of conditions over which elastic-isoviscous analysis is valid and to develop regression equations for predicting minimum and central film thickness. Venner [1991] used an alternative numerical technique to solve the

EHL problem by using multigrid and multi-level multi-integration (MLMI) method.

In experimental measurement of oil film thickness in the I-EHL regime, there have been relatively few experimental measurements of film thickness. This is probably because it is quite difficult to measure oil film thickness in soft contacts compared with hard contacts.

The techniques for measuring lubricant film thickness on soft-EHL regime within lubricated contacts can be divided into three main groups: electromagnetic radiation, magnetic resistance and ultrasonic techniques. The electromagnetic radiation techniques are consisted of optical interferometry and laser induced fluorescence.

2.2.1 Electromagnetic radiation techniques

2.2.1.1 Optical Interferometry

The optical method was employed for the first time by Robert and Tabor [1968] to measure oil film thickness and profile of fluid film for rubber lubrication. The main obstacle was quality of the rubber surface which ordinary rubber surfaces were rough and poorly reflecting, so making interferometric observations difficult.

To improve imaging, the surface of the rubber should be smooth and reflected. Myant [2010] made a test specimen of spherical polydimethyl silixone (PDMS) ball created using a candle dipping process. A 19 mm stainless steel ball was coated by 1-2 mm in thickness of uncured PDMS. The thickness of PDMS layer was thick enough compared to the contact size, so that the steel substrate had negligible effect the mechanical properties of the PDMS layer. Opaque filler was added to the PDMS to prevent this absorbing any non-reflected light.

The basic principle of optical interferometry in measuring an oil film thickness in soft EHL regime is based on the optical interference. An Abbe prism is used instead of the flat glass disk due to the low reflectivity of the PDMS ball. The optical window made from BK7 glass will produce the most visible interference fringes for aqueous solutions (Myant [2010]). The film thickness in the contact area between the BK7 glass prism optical window and PDMS ball can be determine by the light intensity value between the minimum and the maximum values, which is called by relative light intensity.

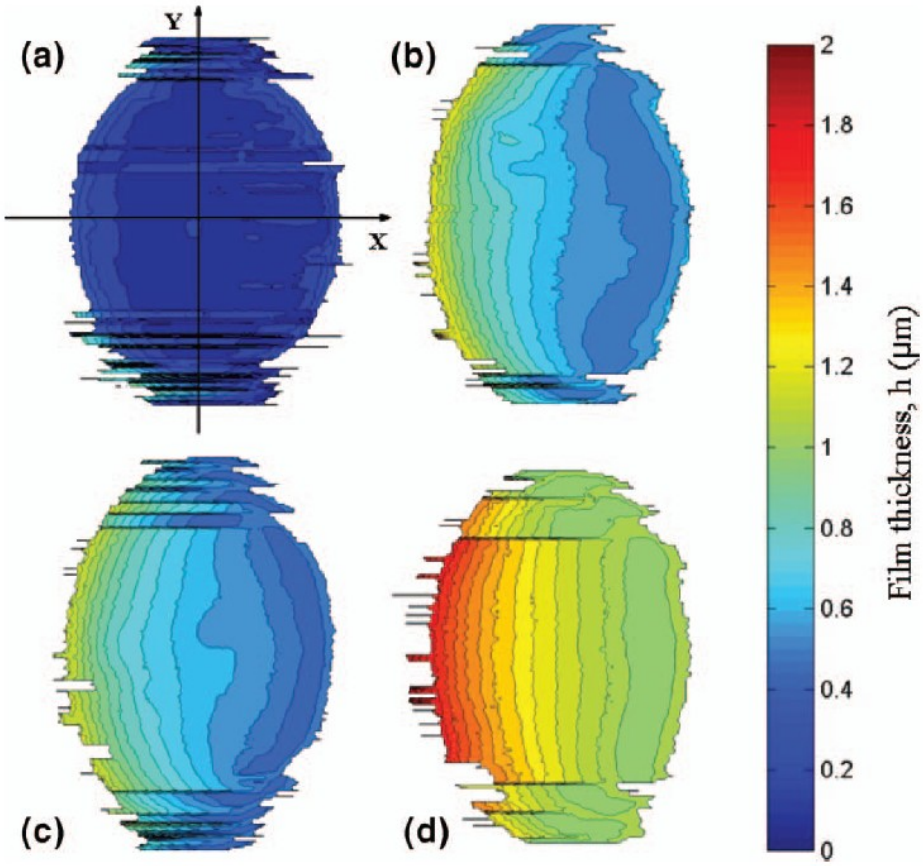

Figure 2.1 Film thickness maps in sliding complaint contact for different entrainment speeds. At U= 0.02, 0.25, 0.33, and 1.31 mm/s for images (a), (b), (c), and (d), respectively (Myant *et al*. [2010]).

An optical interferometric technique is developed for measuring nano-scale thickness in compliant contact. The thickness of EHL film is the same order of magnitude as the wavelength of visible light, thus interferometry is seen to have the potential to study this lubrication regime. The using of white, monochromatic

and duo chromatic lights is limited to minimum film thickness of 45~75 nm. The developing of ultra thin film interferometric techniques is capable to measure *ca* 1 nm.

Recently, Myant [2010] used monochromatic optical interferometry for measuring lubricant film thickness in compliant contacts. The film thickness maps were produced from this method as shown in Figure 2.1. This technique is suitable to measure thin films of h < 2μm. From his experiment, the following best-fit was obtained to measure central film thickness and given by;

$$\frac{h_c}{R_x} = 3.3U^{0.63}W^{-0.13} \tag{2.1}$$

The result of regression equations to predict film thickness has given the exponents of the dimensionless parameters. The meaning of the symbols used will be explained in section 2.3.

2.2.1.2 Laser induced fluorescence (LIF)

The drawback of optical interferometry is the coherence of the illuminating light, which is reduced as the separating gap is increased. The reduced coherence of the illuminating light causes reduced interference image quality and measurements of film thickness are eventually no longer obtainable.

Laser induced fluorescence (LIF) technique based on photo-excitation of a flurophore or fluroscent dye is known as laser induced fluorescence (LIF). Fluorescent dyes can absorb light at one frequency and subsequently re-emit (fluoresce) light at a different frequency. The fluorescent light emitted from the contact will be observed and captured by the camera. A computer-processing technique is used to analyse captured image and create film thickness maps based on grey scale intensity. These intensity profiles are then plotted against the Hertzian equation for the gap outside the central contact region (Wedeven [1970]). The film thickness can be determined based on the intensity images of the contact between elastomer hemisphere (PDMS ball) and transparent optical window.

Poll *et al.* [1992] and Gabelli and Poll [2002] used fluorescence to investigate lubricant film thickness in rubber rotary lip seals where sub-micron film thickness measurements were achieved. Elsewhere, Myant [2010] has used LIF to investigate lubricant film thickness in contact between elastomer ball and glass disk in pure sliding condition, where film thickness measurements were made for both fully flooded and starved conditions. This technique could enable measurement of lubricant thickness of relatively thick films in compliant contacts. He found that the thickness of oil film could be measured by LIF technique for thick film thickness from 30 μm to 300 nm. The advantage of fluorescence techniques is no reflective coating on the contacting surface. The reflective coatings are expensive and prone to wear.

2.2.2 Magnetic resistance

Poll *et al,* [1992] and Poll and Gabelli [2002] used an approach involving magnetic flux measurement to measure film thickness in a rotary lip seal. The magnetic particles, which were using surfactant molecules to protect against oxidation and coagulation, were dispersed within the lubricant. This particles were claimed to be sufficiently small (10 nm diameter) to avoid effecting film formation or wear. The magnetic flux was directed through the seal contact by using a magnetic circuit. The amount of fluid present can be calibrated by providing the magnetic potential, due to the high permeability of magnetite, the inductivity and impedance of the coil.

The magnetic resistance has showed that this method can be used to measure a lubricant film thickness under seal lips. The experimental result has showed a good agreement with theoretical prediction. The disadvantage of this method is necessary to disperse magnetic particles into lubricant.

2.2.3 Ultrasonic techniques

In the beginning of 1970's ultrasonic has been employed in studying contact interfaces by using the properties of reflection and transmission of waves at the

surfaces of separation between media by Matsuko and Ito [1969] and Kendal and Tabor [1971]. However, the relationship between reflection and transmission of waves at the interface was not been formulated. Tattersall [1973] proposed a model of interface by spring model where the reflection of wave at the interface is function of both stiffness of the layer and acoustic impedance between two materials.

In 2003, Dwyer-Joyce *et al.* [2003] adopted a spring model of Tattersall [1973] for modelling a liquid layer between two solid bodies. They developed a method for the measurement of oil film thickness using the reflection of ultrasound. Reflected signal from a liquid layer between two solid bodies depends on ultrasonic frequency, the acoustic properties of solid and liquid, and the layer thickness. If the layer thickness is small compared to the wavelength of incident ultrasound, the spring model of the interface is applied.

Some authors (Dwyer-Joyce *et al*. [2003], Zhang *et al.* [2005], Reddyhoff [2006], Harper [2008]) have validated this technique using the fluid wedges apparatus, annular oil-film apparatus, glass plate test, and digital piezoelectric translator (DPT). The results obtained from these tests show the good agreement between the measured film thickness and theoretical ones.

There are two methods to approach measuring film thickness by using reflection techniques: amplitude and phase shift, because the reflection coefficient contains complex quantity phase and amplitude information (Reddyhoff *et al.* [2005], Reddyhoff [2006]). Both methods have been proven to measure experimental film thickness in journal bearings and contact between glass and glass in static condition (Reddyhoff *et al.* [2005], Reddyhoff [2006]).

The application of ultrasonic reflection for measuring oil film thickness has been developed widely in elastohydrodynamic and hydrodynamic of hard contacts, such as ball bearings (Zhang *et al.* [2006]), journal bearings (Reddyhoff [2006], Harper [2008], Kasolong *et al.* [2008], piston rings (Harper [2008], Avan *et al.* [2010]), hip joints (Harper [2008]), and silicon carbide face seal (Reddyhoff *et al.*

[2006]). This method can be used principally for a wide range of liquid layers trapped between hard and hard contacts of solid surfaces.

2.3 Numerical investigation for film thickness

Several numerical methods for determination of film thickness on I-EHL have been reported. The first author who studied I-EHL was Herrebrough [1968]. He has solved a numerical solution of an integral equation for constant viscosity for a large range of loading conditions. At high load, the pressure curve merges very well with the Hertzian semi elliptic contact pressure distribution, and the pressure spikes is found in the pressure distribution. Hooke and O'Donoghue [1972], Biswas and Snidel [1976], and Hamrock and Dowson [1978] have solved numerically for elastohydrodynamic lubrication for low elastic modulus material.

The foundation of the quantitative film thickness lubrication theory for low-elastic materials was proposed by Hamrock and Dowson [1978]. The numerical solution for I-EHL was generated in smooth point contacts and Newtonian fluids. They studied the film thickness as a function of speed, load, geometry, material, and lubricant properties under fully flooded condition. This enabled a composite central film thickness formula for a fully flooded, isothermal, and elastohydrodynamic elliptical contact for low-elastic modulus materials to be written as;

$$\frac{h_c}{R_x} = 7.32(1-0.72e^{-0.28k})U^{0.64}W^{-0.22} \qquad (2.2)$$

where h_c is the central film thickness and R_x is reduced contact radius in the entrainment speed. k is the ellipticity parameter, which is equal to 1 for the circular contact. The dimensionless operating parameters are;

dimensionless speed parameter, $U = \dfrac{\eta_0 u}{E^* R_x}$

dimensionless load parameter, $W = \dfrac{F}{E^* R_x^2}$

where u is the entrainment speed, F the applied load, η_o the lubricant dynamic viscosity, R_x and E^* the reduced elastic modulus. The latter two terms are defined

$1/R_x = 1/R_{x1} + 1/R_{x2}$ and $2/E^* = (1-\nu_1)/E_1 + (1-\nu_2)/E_2$, respectively, where R_{x1}, R_{x2}, E_1, E_2, υ_1 and υ_2 denote the radii in the entrainment direction, the Young's modulus, and the Poisson's ratio of two contacting bodies.

Venner [1991] and Venner and Nappel [1992] used the multigrid and multi-level-multi-integration (MLMI) method, derived by Mose, and proposed a formula for central film thickness which covers all regimes of lubrication. They give a general asymptotic formula for point contact for the central film thickness, h_c. It covers all regimes of lubrication up to very high loads.

$$\frac{h_c}{R_x} = \left[\left\{ \left(1.70M^{-1/9}L^{3/4}t\right)^r + \left(1.96M^{-1/9}\right)^r \right\}^{s/r} + \left(47.3M^{-2}\right)^s \right]^{1/s} \qquad (2.3)$$

where r, s and t are dimensionless variables where the value are $r = e^{(1-6/(L+8))}$, $s = 12 - 10e^{M^{-2}}$, $t = 1 - e^{-0.9M^{1/6}/L^{1/6}}$. The formula is presented in terms of the Moes dimensionless point contact parameters M and L, dimensionless operating parameter are;

Moes dimensionless speed, $L = (G)(U)^{1/4}$

Moes dimensionless load, $M = \dfrac{W}{(U)^{3/4}}$

where G is the dimensionless material parameter, $G = E^*\alpha$, where α is the lubricant pressure viscosity coefficient.

As well, de Vincent *et al.* [2005] produced a set of numerical prediction for I-EHL film thickness in dimensionless speed and load parameters as given Eq. 2.4;

$$\frac{h_c}{R_x} = 3.3U^{0.60}W^{-0.14} \qquad (2.4)$$

2.4 Comparison between numerical and experimental results for film thickness

Each investigator as mentioned above has calculated film thickness by approaching set of numerical prediction with difference range of the values of dimensionless speed (U) and load (W). The experimental approaches that were conducted by Myant [2010] using interferometric techniques were in condition pure sliding compliant contact, where the ranges of dimensionless speed (U) and load (W) parameters were over a range of values of U = $9\text{x}10^{-12}$ to $5\text{x}10^{-9}$ and load

W = $3x10^{-6}$ to $5x10^{-5}$. He proposed a best fit for measuring central film thickness as stated in Eq. 2.1.

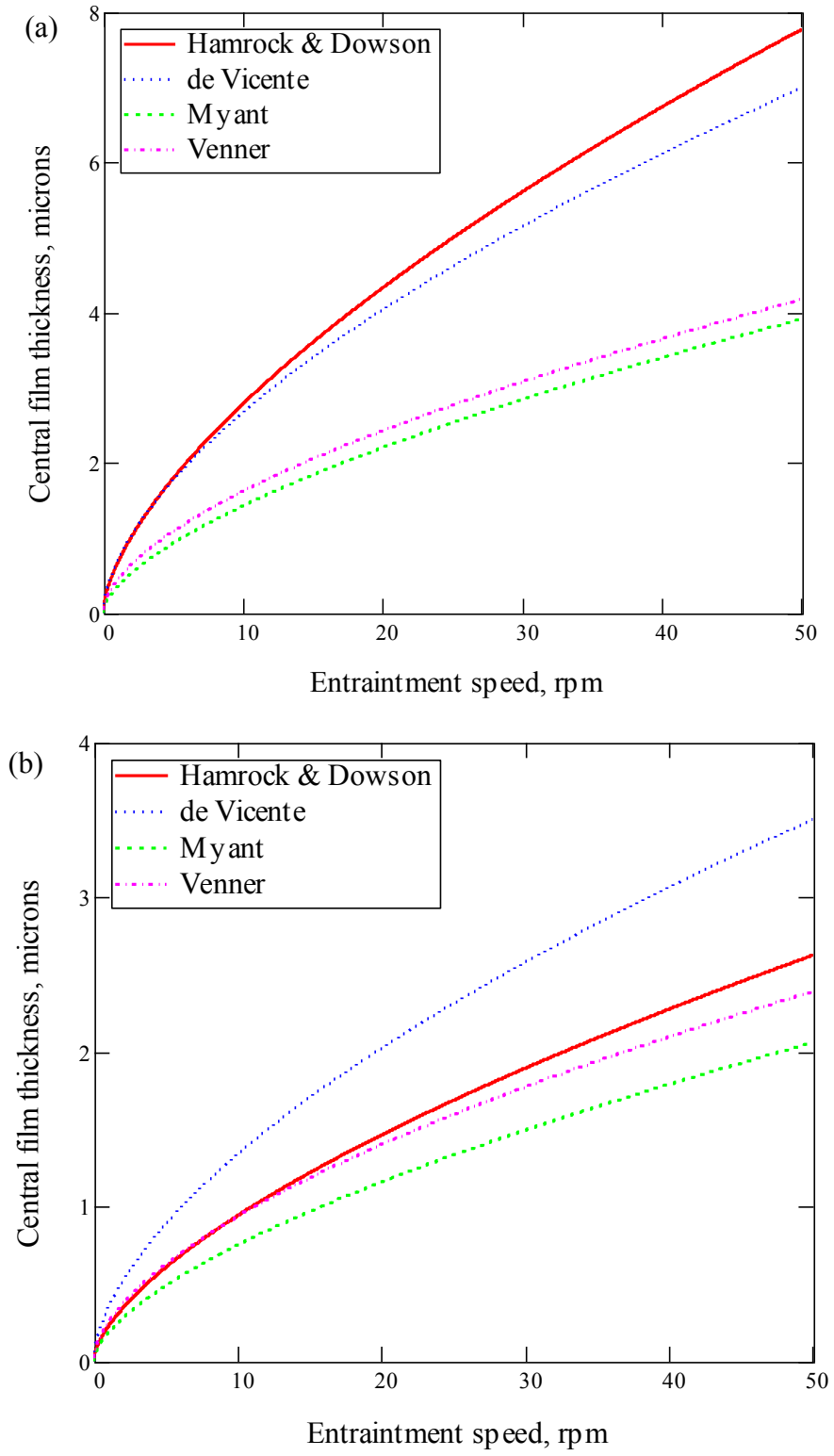

Figure 2.2 Comparison between central film thickness and entrainment speed among formulae for contact between Perspex and 19 mm nitrile ball with (a) W = 8.149 x 10^{-5} and (b) W = 1.1 x 10^{-2}, where U = 1.789 x 10^{-11} to 8.89 x 10^{-8} (Hamrock and Dowson [1978], Venner [1991], de Vicente [2005], Myant [2010]).

The predictions of central film thickness from the formulae above are recorded in Figure 2.2, which the contact is between Perspex and 19 mm nitrile ball. The central film thickness is plotted against entrainment speed that keeps constant in range of nondimensionless speed (U) parameters of Hamrock and Dowson [1978] and Myant [2010]. The nondimensionless load (W) parameter is variable based on Myant [2010] ($W = 8.149 \times 10^{-5}$) and Hamrock and Dowson [1978] ($W = 1.1 \times 10^{-2}$). It is seen that there is remarkably little difference among formulae.

The regression equations of Venner and Myant are close together for low and high loads. In high loads, regression of Hamrock and Dowson is close with regression of Venner and Myant, otherwise de Vicente is not.

2.5 Bulk and surface ultrasonic waves for measurement of dry contacts.

The study of contact mechanics using ultrasound to date has tended to focus on hard and hard contacts rather than soft and hard contacts. The investigation of contact between hard and hard materials using ultrasonic method has focused on using bulk ultrasonic waves. The bulk ultrasonic wave has been used by Tattersall [1973] to model the strength of the coupling between two media is denoted by stiffness, K. The elastic stiffness of interface is to rely on the transmitted pulse. The interface could be modelled as a distributed spring, if the wavelength of the ultrasound was large compared to the scatters at the interface. This idea has been proven experimentally by Baik and Thompson [1984], Krolikowsky and Szczepek [1991], Nagy [1992], Drinkwater *et al.* [1996], Drinkwater and Cawley [1997], and Dwyer-Joyce *et al.* [2001].

The use of bulk ultrasonic waves for measuring contact between soft and hard materials is difficult to apply due to attenuation. Surface wave as an alternative method to measure contact between soft and hard materials will be developed where this wave has been employed for non-destructive evaluation (NDE) and damage detection. There is a difference between bulk ultrasonic waves and

surface wave. Bulk ultrasonic waves refer to wave propagation in infinite media, where they do not require a boundary for support. Surface waves, on the other hand, require a boundary for propagation and they propagate in the surface of solid material.

The propagation of surface wave along solid-solid interface has been considered by a number of authors. Rokhlin *et al.* [1991] used Rayleigh wave propagating along a thin layer adhesive between two elastic half-spaces. The Rayleigh wave propagates on the surface of the elastic half-space. The strength of the adhesive bonds is related with the phase velocity of the interface wave and the effective shear modulus of the interface film. Drinkwater *et al.* [2003] used the propagation of both A_0 and S_0 Lamb modes to determine the normal and shear stiffness of a compressively loaded solid-solid interface. The spring layer model in a continuum model of the system was used to describe the interface. The measured A_0 and S_0 Lamb wave attenuation are related to both normal and shear stiffness of the interface. The normal stiffness of the interface is in good agreement with the normal incidence of longitudinal wave ultrasound as shown in Figure 2.3.

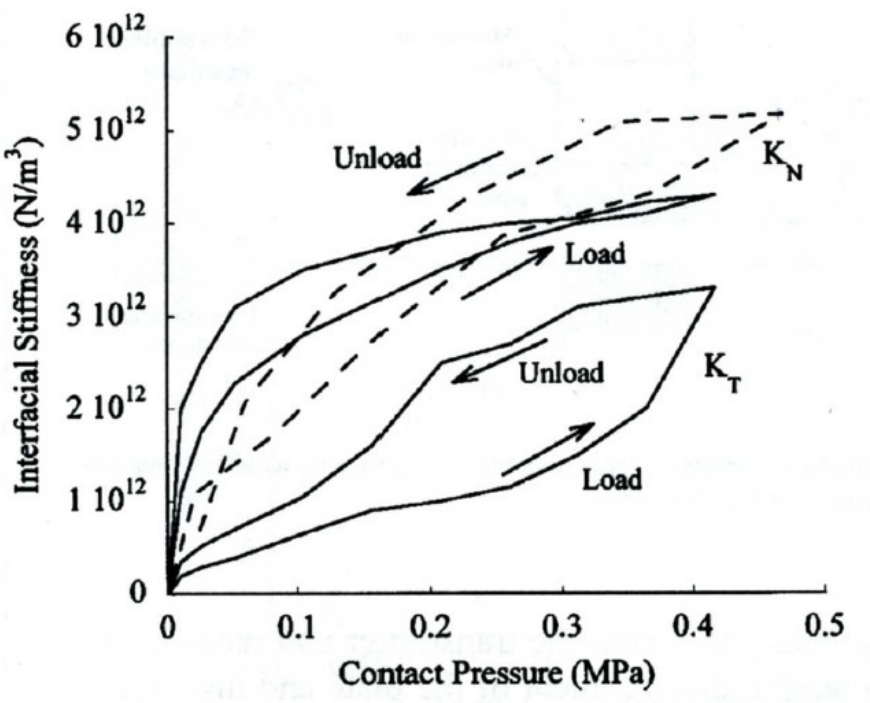

Figure 2.3 Comparison of normal stiffness interface between A_0 lamb wave (solid line) and longitudinal wave (dash line) (Drinkwater *et al*. [2003]).

Murty and Kumar [1991] studied analytically and experimentally the problem of wave propagation along the interface between two elastic, isotropic and homogeneous half-spaces. The measurement of speed and attenuation of an interfacial wave can be used to assess bonding condition at an interface between elastic materials.

2.6 Conclusions

The several techniques to measure film thickness in I-EHL regime have been discussed. The film thickness within lubricated compliant contact is a particular interest, which is a wider application in engineering and biological contacts. The electromagnetic radiation and magnetic resistance techniques have been showed that these techniques have been successfully measuring film thickness within lubricated contact between soft and hard contacts. Unfortunately, these techniques only can be used in laboratory and they are difficult to apply in real components.

The ultrasonic technique appears to answer the problems above, because the measurement of film thickness in hard contact, such as; ball bearings, cylinder engines and journal bearings has shown promising results. By developing phase shift methods in the case of soft materials, the challenges in measurement of film thickness in compliant contacts could be answered.

Bulk ultrasonic waves have been employed successfully to investigate contact between hard and hard materials. However, it is difficult to apply to contact between soft and hard materials due to attenuation. The surface wave, as alternative way, could be used to study contact between soft and hard materials where surface wave can propagate in the contact area.

Chapter 3

Ultrasonic background

This chapter describes background to understand theory behind the ultrasonic techniques used to investigate oil film thickness and contact mechanics between dissimilar materials. The ultrasonic reflection and spring interface model are approached to calculate oil film thickness by using amplitude and phase shift methods. A technique to generate surface wave in solid-solid media using wedge transducer is demonstrated with the potential to be used as a sensor for soft contact. In the last section, the calibrations that have been done by previous investigators for ultrasonic reflection method are discussed

3.1 Introduction

Ultrasound has been employed extensively in many applications, because there are two unique features of ultrasonic waves; these travel slowly, about 100,000 times slower than electromagnetic wave, and they can easily penetrate opaque materials (Cheeke [2002]). Therefore, the applications of ultrasound occur in very broad range of disciplines, covering engineering, physics, medicine, etc. In addition, the use of ultrasound is a non-invasive, safe and portable technique (Reddyhoff [2006]).

Tattersall [1973] used the principle of ultrasonic reflection in detecting flaws using ultrasonic pulse-echo techniques. Both perfect and imperfect interfaces between dissimilar materials always reflect the ultrasonic signal. He proposed a model of interface in order to represent any slackness in interface by a density of springs between two media. Pialucha and Cawley [1994] employed ultrasonic as the most promising method for the detection and characterization of thin embedded layers within a structure. Within an engineering context, non destructive technique (NDT) ultrasound is most commonly used to detect flaws, such as void, crack, porosity, and de-lamination or inclusion in components. More recently, applications of ultrasound are becoming increasingly widespread using commercial ultrasonic transducers to determine rough surface contact (Królikowski *et al.* [1989], Królikowski and Szczepek [1991], Polijaniuk and Kaczmarek [1993], Drinkwater *et al*. [1994], Dwyer-Joyce *et al.* [2001], Baltazar *et al.* [2002], Marshall *et al.* [2006]), interfacial stiffness of contacts (Drinkwater and Cawley [1997], Gonzales-Valades *et al.* [2010]), mapping contact pressure distribution (Dwyer-Joyce *et al.* [2001], Marshall *et al.* [2004], Marshall [2005]), area of contact (Pau [2003], Tohmyoh and Saka [2003], Aymerich and Pau [2004]), measurement of viscosity (Kasolong *et al.* [2008]), wear surface (Birring and Kwun [1989], Ahn and Kim [2001]), and oil film thickness (Dwyer-Joyce *et al.* [2003], Dwyer-Joyce *et al.* [2004], Dwyer-Joyce [2005], Kasolong *et al.* [2008], Zhang and Drinkwater [2008]).

3.2 Basic principles of ultrasound

3.2.1 Ultrasonic waves

An ultrasonic wave is defined as a wave frequency above 20 kHz, where the frequencies cannot be detected by the human ear. It continues up to MHz and GHz ranges, and into the hypersonic regime. Figure 3.1 shows the spectrum where typical ranges for the phenomena of interest are indicated. The application of measurement film thickness and contact by using ultrasound method is in range of 1 to 50 MHz.

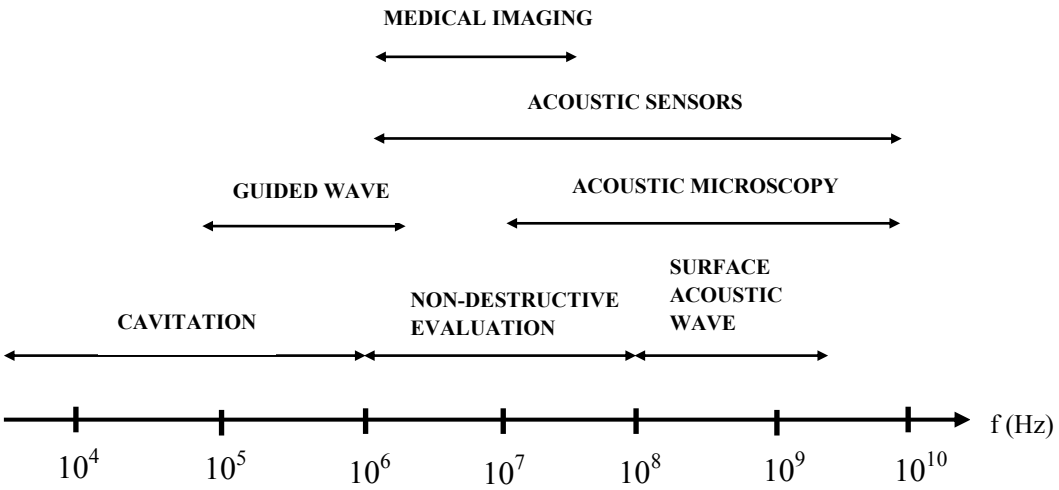

Figure 3.1 Frequency spectrum ranges for various ultrasonic processes, modified from Cheeke [2002].

3.2.1.1 Longitudinal waves

A longitudinal wave is where the particle displacement is parallel to direction of wave propagation. Figure 3.2a shows a longitudinal sound wave progressing through a host medium. The particles are excited from left to right, resulting in the zones of expansion and compression. Longitudinal waves are also known as pressure or compression waves.

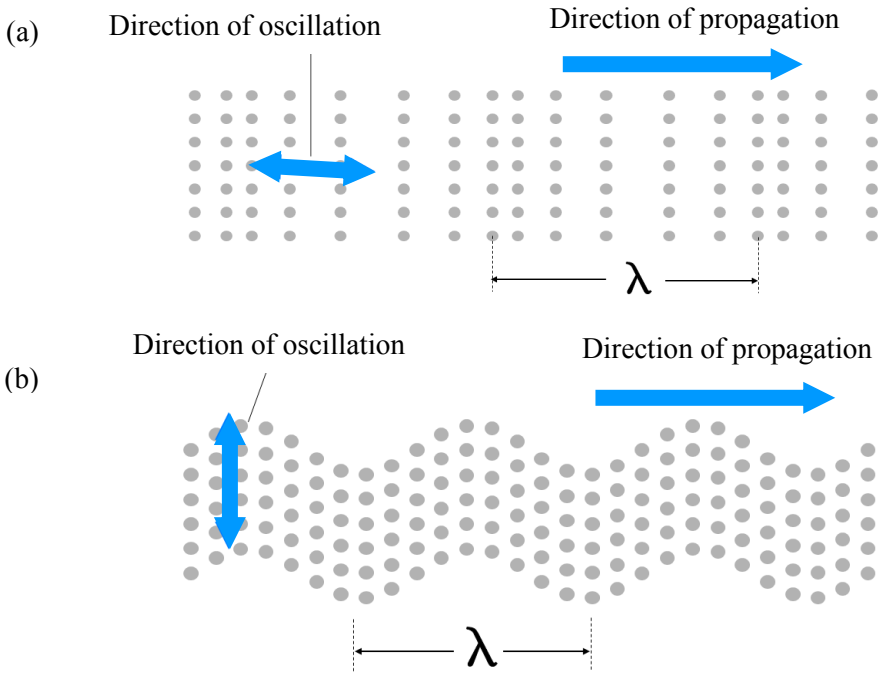

Figure 3.2 (a) Longitudinal and (b) transversal sound waves.

3.2.1.2 Shear waves

A shear waves is where the particle displacement is perpendicular to direction of wave propagation. The direction of propagation could be in an up or down direction, Figure 3.2b, or in any direction within that plane. This wave type is only produced in medium capable of supporting shear, i.e. solids.

3.2.1.3 Surface waves

Surface waves are actually made up of a superposition of longitudinal and shear wave particle velocity component. The longitudinal and shear motions are intimately coupled together in Rayleigh waves and they travel at a common velocity, penetrating to a depth of approximately one wavelength, where the amplitude of the wave decays rapidly with depth. The conditions for the propagation of waves at the interface between two homogeneous and isotropic elastic half-spaces are known as Stoneley waves, between solid and liquid are known as Shcolte waves, and between solid and gas are known as Rayleigh waves as shown in Figures 3.3 and 3.4.

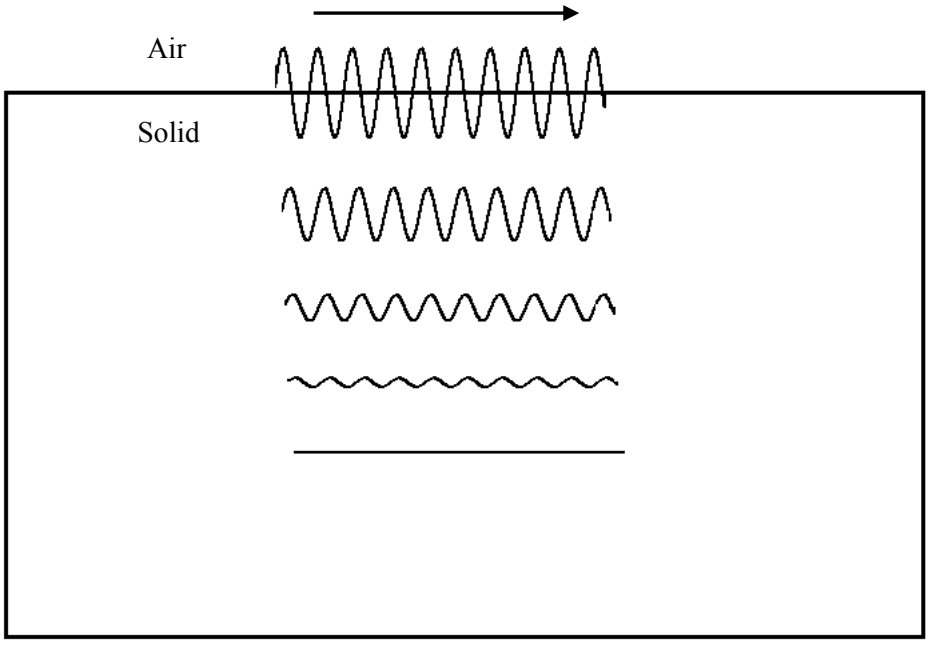

Figure 3.3 Rayleigh waves schematic.

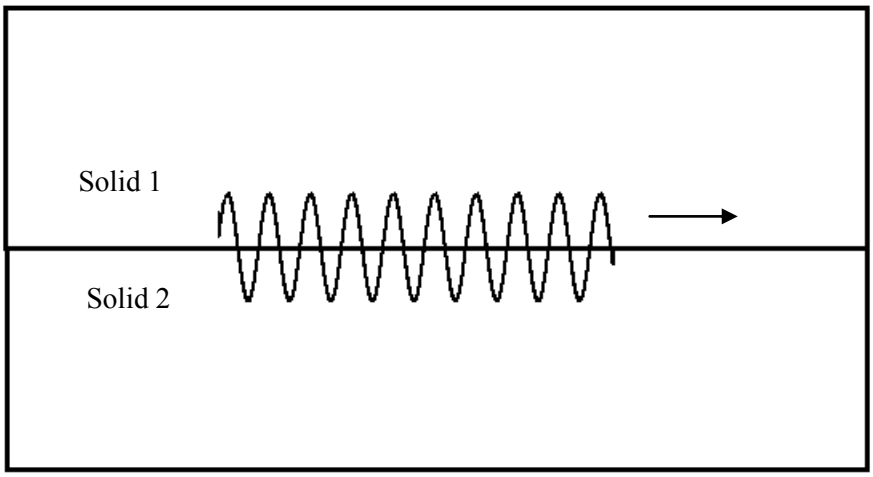

Figure 3.4 Stoneley waves schematic.

3.2.2 Material properties

3.2.2.1 Speed of sound

The speed of sound is a property of the medium, because sound travels through different media at different speeds. Propagation of sound wave occurs due to the elastic forces between constituent particles. Elastic forces depend on the host material; it takes less or more time to transmit the wave. The speed of sound, c, is defined as product of frequency, f, and wave length, λ, by the following relationship;

$$c = f\lambda \tag{3.1}$$

3.2.2.2 Acoustic impedance of material

A measurement of the material's ability to transmit ultrasound is known as the acoustic impedance, which is a useful concept in ultrasound. The acoustic impedance, z, is the product of the density, ρ, of a material and the speed that sound will travel through it, c, as follows:

$$z = \rho c \tag{3.2}$$

The units for acoustic impedance are $kgm^{-2}s^{-1}x10^{6}$, otherwise known as MRayls.

3.2.2.3 Attenuation of a sound wave

The physical properties of natural materials produce an effect, which further weakens the sound. This further weakening results from attenuation. Attenuation is a function of material properties, distance, and frequency. The attenuation is a combined effect of scattering and absorption. Scattering is the reflection of the sound in directions other than its original direction of propagation due to inhomogeneous nature of materials. Such boundaries can be caused by voids, inclusions and grain boundaries. Absorption is the conversion of the sound energy to other forms of energy. In this way, the strength of an ultrasonic signal reduces as it propagates through a given material.

The decay rate of the wave as it propagates through the material is called ultrasonic attenuation. The amplitude change of a decaying plane wave can be expressed by:

$$A = A_0 e^{-\alpha x} \tag{3.3}$$

where A_o is the attenuation the propagating wave at some location. The amplitude A is the reduced amplitude after the wave has travelled a distance x from that initial location. In this expression, α is an attenuation coefficient.

To measure the attenuation coefficient a common technique in that, the signal amplitude transmitted through two samples of different length is compared. The attenuation α, in units of nepers per unit length is determined from the magnitudes of the signals: A_1 through a specimen of length L_1, A_2 through a specimen of length L_2:

$$\alpha = \frac{\ln\left({}^{A_1}/_{A_2}\right)}{(L_1 - L_2)} \tag{3.4}$$

One neper is a decrease in amplitude of a factor of 1/e. Sometimes attenuation is expressed in terms of decibels (dB), a logarithmic scale.

3.2.3 Reflection and transmission of ultrasonic waves

3.2.3.1 Snell's law and mode conversion

When plane ultrasonic wave encounters an interface between two materials at some inclined angle, two things are happen. The first, refraction of the ultrasonic wave occurs in the same way for optical light wave using Snell's law. The second, the energy of the ultrasonic wave is distributed into longitudinal and shear waves in the second material, known as mode conversion. Some energy is also reflected, where the angle of reflection is equal to the angle of incidence. From Snells's law, the refracted angle can be computed as:

$$c_1 \sin\theta_2 = c_2 \sin\theta_1 \tag{3.5}$$

The concept of mode conversion is associated with a superposition of two specific motions: one associated with a normal force and normal wave propagation, the second associated with a shear force and shear wave propagation. The both normal and shear wave would be produced in both materials, and the superposition process would generate wave that could travel along the inteface of the two materials. Figure 3.5 shows the mode conversion of ultrasonic wave based on Snell's law.

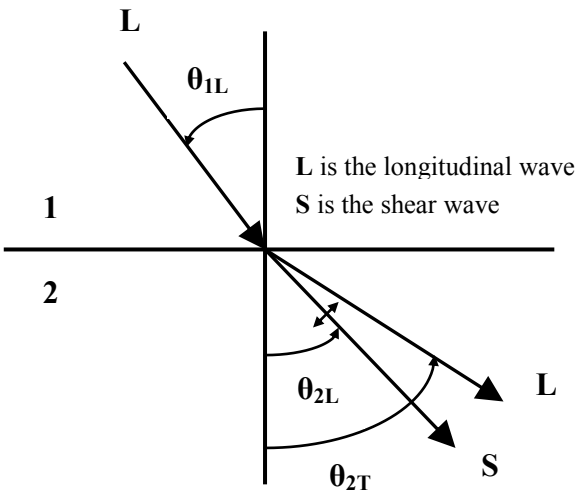

$$c_{1L} \sin\theta_{2L} = c_{2L} \sin\theta_{1L}$$

$$c_{1L} \sin\theta_{2T} = c_{2T} \sin\theta_{1L}$$

Figure 3.5 Snell's law and mode conversion for incident longitudinal wave .

Two critical angles exist with respect to the refraction process based on Snell's law. The first critical angle occurs when the longitudinal refracted angle is 90^0 and is defined as $\theta_{cr1} = \sin^{-1}\frac{c_1}{c_{1L}}$ when $\theta_2 = 90^0$ (Figure 3.6a). The longitudinal energy is either reflected or converted to an interface wave, whereas the shear wave remains in the second material. The second critical angle occurs when the shear refracted angle is 90^0 and defines as $\theta_{cr2} = \sin^{-1}\frac{c_1}{c_{1T}}$ when $\theta_2 = 90^0$ (Figure 3.6b). All of the energy is either reflected or transformed into interface wave propagation.

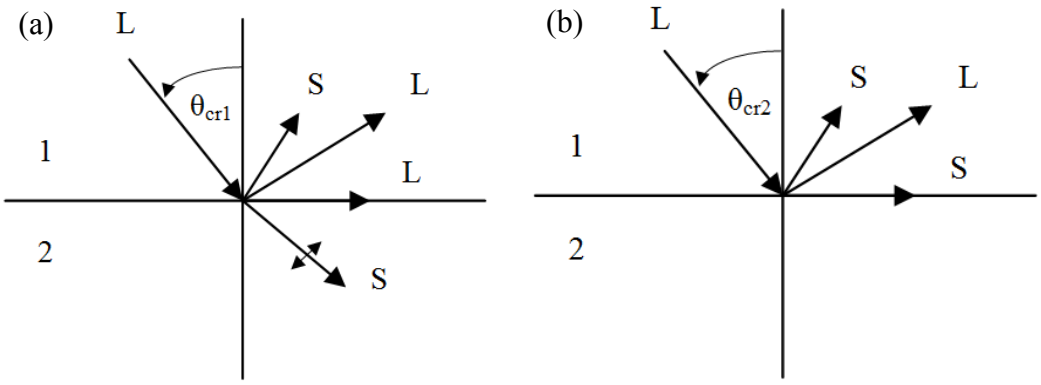

Figure 3.6 (a) The first critical angle and (b) second critical angle.

When the incident longitudinal wave is the first critical angle, only shear waves are propagated into the second material, the longitudinal wave produces an interface wave. In this case, both longitudinal and shear waves are reflected. An incident longitudinal wave beyond the second critical angle, there will produce no ultrasonic energy in the second material, because both longitudinal and shear wave are reflected as shown in Figure 3.6b.

3.2.3.2 Reflection and transmission at normal incidence

Plane ultrasonic waves that strike an interface between two perfectly bonded materials (Figure 3.7) are partially reflected at front face of layer and partially go through it to the back face. Ultrasound will be transmitted into to the second material and energy will be extracted from the incident ultrasonic wave, to produce amplitude and phase change in the reflected wave.

Consider the incident acoustic displacement wave as

$$u_i = A_I \exp\ i(\omega t - k_1 x) \tag{3.6}$$

and the reflected and transmitted wave displacements be

$$u_r = A_R \exp\ i(\omega t + k_1 x) \tag{3.7}$$

$$u_t = A_T \exp\ i(\omega t - k_2 x) \tag{3.8}$$

where A_I, A_R and A_T are amplitude of incident, reflected and transmitted waves and k_1 and k_2 are wave number of media 1 and 2, respectively.

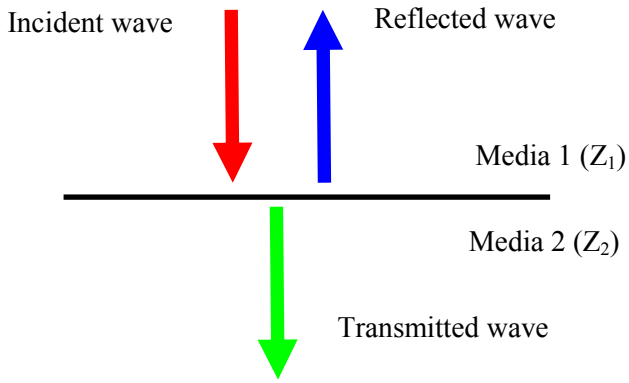

Figure 3.7 Configuration of reflection and transmision at normal incidence between two media.

Thus the displacements in media *1* and *2* are given respectively by

$$U_1 = A_I \exp i(\omega t - k_1 x) + A_R\ \exp i(\omega t + k_1 x) \tag{3.9}$$

$$U_2 = A_T \exp i(\omega t - k_2 x) \tag{3.10}$$

The stress fields in media *1* and *2* are respectively

$$\sigma_1 = E_1 \frac{\partial U_1}{\partial x} = -i\omega Z_1 \exp \mathrm{i}(\omega t - k_1 x) + i\omega Z_1 A_R \exp i(\omega t + k_1 x) \tag{3.11}$$

$$\sigma_2 = E_2 \frac{\partial U_2}{\partial x} = -i\omega Z_2\ A_T \exp \mathrm{i}(\omega t - k_2 x) \tag{3.12}$$

where E_1 and E_2 are modulus elasticity of material *1* and *2*, respectively.

Boundary conditions are as follows:

$$U^1|_{x=0} = U^2|_{x=0} \tag{3.13}$$

$$\sigma^1|_{x=0} = \sigma^2|_{x=0} \tag{3.14}$$

Substituting Eqs. (3.9) and (3.10) into (3.13) yields

$$1 + A_R = A_T \tag{3.15}$$

From Eqs. (3.11), (3.12) and (3.14), it follows that

$$Z_1(1 - A_R) = Z_2 A_T \tag{3.16}$$

Solution of Eqs. (3.15) and (3.16) gives A_R and A_T

$$A_R = \frac{Z_1 - Z_2}{Z_1 + Z_2} A_I \text{ and } A_T = \frac{2 Z_1}{Z_1 + Z_2} A_I \quad (3.17)$$

The stress reflection and transmission coefficient are obtained

$$R = \left. \frac{\sigma_x^{(R)}}{\sigma_x^{(I)}} \right|_{x=0} = \frac{A_R}{A_I} \quad (3.18)$$

$$T = \left. \frac{\sigma_x^{(T)}}{\sigma_x^{(I)}} \right|_{x=0} = \frac{A_T}{A_I} \quad ..(3.19)$$

The reflection coefficient, *R*, and the transmission coefficient, *T*, can be written by substituting Eq. 3.17 to Eqs. 3.18 and 3.19 where *R* and *T* depend on the acoustic impedance mismatch between the two materials:

$$R = \frac{z_1 - z_2}{z_1 + z_2} \quad (3.20)$$

$$T = \frac{2z_2}{z_1 + z_2} \quad (3.21)$$

(where suffices *1* and *2* refer to the materials on either side of the interface). The acoustic impedance, *z* of a material is a product of its density and the speed of sound through it.

3.2.3.3 Solid-solid media interface

The wave reflection and refraction are topics associated with the subject of stress wave propagation in solid materials. The reflected (transmitted) factor is defined as ratio of the amplitude of reflected (transmitted) wave to the amplitude of the incident wave. The factor depends on the angle of incident, wave velocites, and possibly frequency, depending on the interface condition (Rose [1991]). Figure 3.8 shows the reflection and refraction at a solid-solid interface for longitudinal and shear wave incidence.

The reflection factor can be calculated by considering the particle velocity-displacement relationship, the strain-displacement relationship, and the stress-strain relationship for two-dimensional plane strain in isotropic media. The stress-particle velocity relationship can be obtained by subsituting the boundary condition equations; the reflection factor equations can be given by (Rose [1991]):

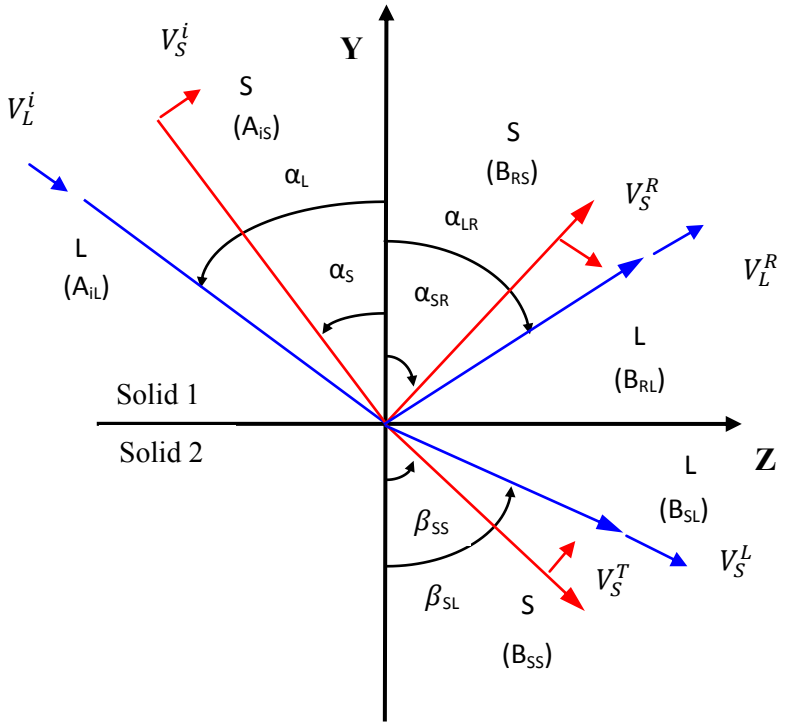

Figure 3.8 Reflection and transmission at a solid-solid media interface (β_{SS} and β_{SL} for shear input, but change to β_{LS} and β_{LL} longitudinal inputs).

$$M \begin{bmatrix} RLL \\ RLS \\ TLL \\ TLS \end{bmatrix} = a \tag{3.22}$$

Where a is a 4 x 1 matrix and M is a 4 x 4 matrix:

$$M = \begin{bmatrix} -\cos\alpha_{LR} & \sin\alpha_{SR} & -\cos\beta_{SL} & \sin\beta_{ST} \\ -\sin\alpha_{LR} & -\cos\alpha_{SR} & \sin\beta_{SL} & \cos\beta_{ST} \\ -k_{L1}(\lambda_1+2\mu_1)\cos 2\alpha_{SR} & k_{T1}\mu_1 \sin 2\alpha_{SR} & k_{L2}(\lambda_2+2\mu_2)\cos 2\beta_{ST} & -k_{T2}\mu_2 \sin 2\beta_{ST} \\ -k_{L1}\mu_1 \sin 2\alpha_{LR} & -k_{T1}\mu_1 \cos 2\alpha_{SR} & -k_{L2}\mu_2 \sin 2\beta_{SL} & -k_{T2}\mu_2 \cos 2\beta_{ST} \end{bmatrix} \tag{3.23}$$

Where k_T and k_L are wave number for longitudinal and transversal waves as given by

$$K_T = \frac{\omega}{C_S} \text{ and } K_L = \frac{\omega}{C_L} \tag{3.24}$$

C_S and C_L are speed of transversal and longitudinal materials, λ and μ are Lamé constant.

For longitudinal wave incidence,

$$a = \begin{bmatrix} -\cos\alpha_L \\ \sin\alpha_L \\ k_{L1}(\lambda_1 + 2\mu_1)\cos 2\alpha_L \\ -k_{L1}\mu_1 \sin 2\alpha_L \end{bmatrix} \tag{3.25}$$

reflection and refraction factors are defined as

$$RLL = \frac{B_{rl}}{A_{il}}, \qquad RLS = \frac{B_{rs}}{A_{il}}, \qquad TLL = \frac{B_{tl}}{A_{il}}, \qquad TLS = \frac{B_{ts}}{A_{il}} \tag{3.26}$$

Where the first element in the left-hand side (LHS) is either *R* or *T* (reflected or transmited wave), the second element is for the incident wave, S or *L* (shear or longitudinal), and the third is for longitudinal or shear *L* or *S* waves. A_{in} is the amplitude of the incident shear or longitudinal wave (A_{is} or A_{il}) and Bmn is the amplitude of the reflected or transmitted (*m* = *r* or *t*, respectively) wave *n* (longitudinal or shear, resppectively *l* or *s*).

The reflected and refracted factors of longitudinal incidence for oblique incident angles from 0^0 to 90^0 onto Perspex – steel interface are shown in Figure 3.9. At normal incidence, the reflected and refracted factors become that given in Eqs. 3.20 and 3.21. Its value depends on the acoustic impedance between Perspex and steel. Only the longitudinal wave is transmited and no shear wave is transmitted at normal incidence. As incident angle increses, longitudinal and shear wave are excited in the steel. Refracted longitudinal factor stays more or less constant until the first critical angle, at which point it rises sharply to spike at refracted longitudinal factor equal 0.35. At this angle, the longitudinal wave propagates along the surface so no energy is propagated into the steel. The refracted shear wave amplitude goes to zero at this angle. As incident angle increases further, the second critical angle is reached at incident angle 64.8^0 for refracted shear waves, which now propogate along the surface. At the second critial angle, reflected shear factor rises sharply to 1.2 and the surface waves are generated at this point. From the second critical angle to 90^0 , there is sudden change in phase from 0 to about 2π in the region of the second critical angle. This is due to the excitation of Rayleigh surface wave at an incidence angle larger than the second critical angle. This effect is called the Rayleigh dip (Cheeke [2002]).

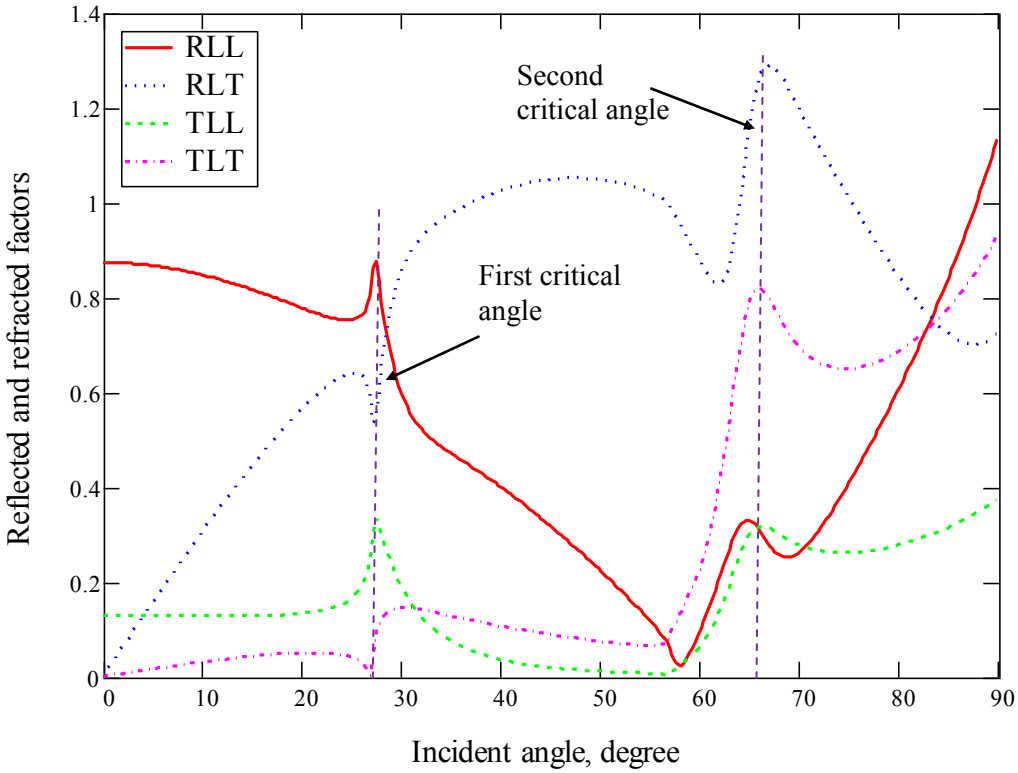

Figure 3.9 Reflection and refraction factors for oblique incidence onto Perspex – steel interface.

3.3 Measurement of film thickness by using ultrasound

There are three main approaches for calculating lubricant-film thickness using reflected ultrasonic signal:

a. Time of flight (ToF)
b. The resonant-layer model
c. The spring-layer model

a. Time of flight (ToF)

In the case of thick films, these reflections from the top and bottom bearing surfaces can be received and the time between each reflection can be measured to give the time of flight. This means that if the speed of sound of the layer is known

then the thickness can easily be determined by measuring time of flight between the two reflections using the equation 3.27.

$$h = \frac{c.t}{2} \tag{3.27}$$

where c is the speed of sound in the layer, h is thickness of the layer and t is the time taken for a sound wave to travel through the layer.

This technique is known as the time of flight (ToF) technique. The ToF method can measure film thickness greater than 40 μm (thick-film) (Dwyer-Joyce et al. [2003]). As the lubricant film becomes thinner, the ToF approach becomes difficult to apply because the distance between two signals becomes closer depended on frequency of transducer.

b. The resonant-layer model

Films of intermediate thickness can be determined by measuring the frequency at which the film resonates. Pialucha and Cawley [1994] used a resonant-layer model approach to show that the thickness of the layer, h, is related to the resonant frequencies of an embedded layer and acoustic properties by

$$h = \frac{cm}{2f_m} \tag{3.28}$$

where c is the speed of sound lubricant layer, m is the mode number of the resonant frequency and f_m is the resonant frequency of m-th mode.

The resonant-layer model is valid for all layer thicknesses and allows the prediction of the through-thickness resonant frequencies of the lubricant layers. In practice, this method is suitable for measuring film in typical bearing application down as thin as 30 μm. Below this the high frequencies of transducer are limited due to attenuation (Dwyer-Joyce *et al*. [2002]).

c. The spring-layer model

The spring model is suitable for thin lubricant films in which the wavelength of the ultrasound is much larger than the layer thickness. The region of spring model

is below the first resonance of spring-mass system where the deflection of the mass is dependent purely on the applied load and the spring stiffness. Hosten [1991] showed that the interaction of ultrasound with a very thin layer in determined by the stiffness of that layer. The film thickness is stated by function of stiffness per unit area, *K*, given by

$$h = \frac{\rho c^2}{K} \tag{3.29}$$

where ρ is density of the layer and c is speed of sound of the layer.

3.3.1 Ultrasonic reflection and spring interface model

The reflection coefficient of ultrasonic wave that strikes between two media is influenced of the type of interface or layer, which is separated between them. Figure 3.10 shows two types of interface: perfectly bonded material (Figure 3.10a) and not perfectly bonded material, there is a thin layer lubricant (Figure 3.10b). For perfectly bonded material, the reflection coefficient can be calculated using Eq. 3.20 as explained in section 3.2.3.2.

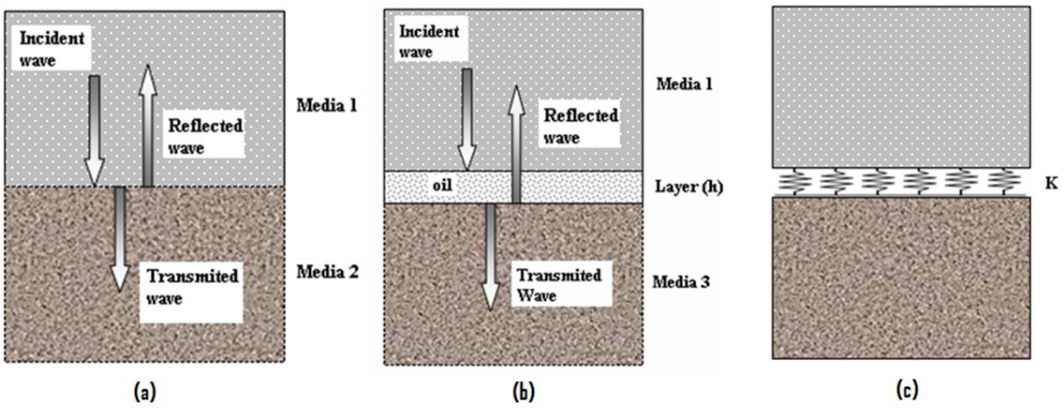

Figure 3.10 Model of interface: (a) perfectly bonded material, (b) thin layer, and (c) spring interface model.

If the layer is not perfectly bonded or there is a thin layer lubricant, the interface acts as a single reflector. The ultrasonic wave that strike the front and back faces of a thin layer lubricant on three-layered system will overlap and it becomes impossible to distinguish from the discrete reflections. To extract the thickness information from the reflections that are overlapping in the time domain and frequencies domain, an approach is used. A so-called spring model of the

interface is constructed (Figure 3.10c). This applies when the layer thickness is small compared to the wavelength of incident ultrasound. It is then the stiffness of the layer, *K*. Tattersall [1973] proposed the relation between reflection coefficient and layer stiffness, as follow:

$$R = \frac{z_1 - z_2 + i\omega(z_1 z_2 / K)}{z_1 + z_2 + i\omega(z_1 z_2 / K)} \tag{3.30}$$

where ω is the angular frequency of the ultrasonic wave. The stiffness of an interface, expressed per unit area, is given by the rate of change of pressure, p with approach of the surfaces, h

$$K = -\frac{dp}{dh} \tag{3.31}$$

The stiffness of the interface can then be related to asperity deformation mechanics and contact pressure. The approach has also been used to determine the thickness and integrity of adhesive in glued joints. If the interfacial layer is a liquid then the stiffness is obtained from its bulk modulus, B, which is the pressure, required to cause unit change in volume, V

$$B = -\frac{dp}{dV / V} \tag{3.32}$$

If the sound wave is large compared to the layer thickness, then a liquid layer is constrained to deform across its thickness only (*i.e.*, the fluid area remains constant). Then dV/V=dh/h and:

$$B = -h\frac{dp}{dh} \tag{3.33}$$

Combining (3.31)–(3.33) gives

$$K = \frac{B}{h} \tag{3.34}$$

The speed of sound through a liquid, c is related to the density, ρ and bulk modulus by

$$c = \sqrt{\frac{B}{\rho}} \tag{3.35}$$

Combining (3.34) and (3.35) gives the stiffness of the layer in terms of its acoustic properties

$$K = \frac{\rho c^2}{h} \tag{3.36}$$

where h is film thickness of the layer.

The reflection coefficient (from Eq. 3.30) contains complex quantity phase and amplitude information. Eq. 3.30 can be separated real and imaginary parts by multiplying the complex conjugate of the denominator and, after some simplification becomes:

$$R = \frac{(z_1^2 - z_2^2) + z_1^2 z_2^2 (\omega/K)^2}{(z_1 + z_2)^2 + z_1^2 z_2^2 (\omega/K)^2} + i\left[\frac{2z_1 z_2^2 (\omega/K)}{(z_1 + z_2)^2 + z_1^2 z_2^2 (\omega/K)^2}\right] \tag{3.37}$$

Figure 3.11 shows an Argand diagram where both the amplitude and the phase can be used to determine the oil film thickness (Reddyhoff [2006]).

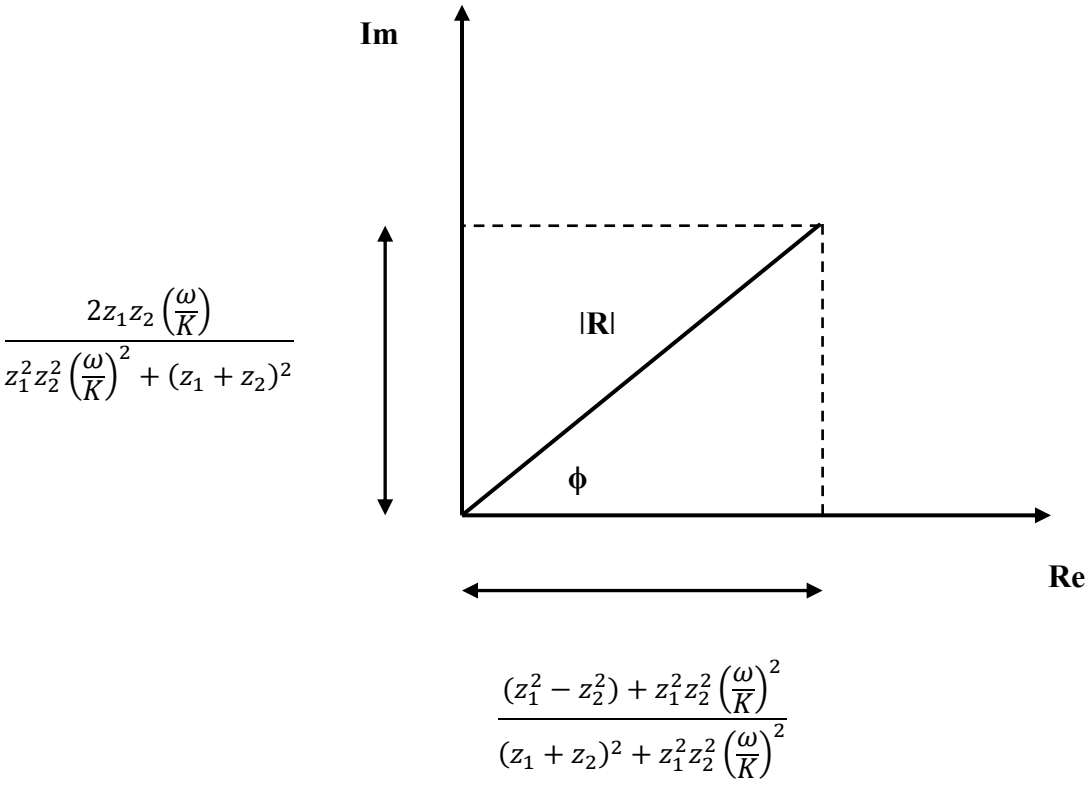

Figure 3.11 An Argand diagram that represents the complex quantity phase difference and reflection coefficient information.

3.3.2 Amplitude methods

From Figure 3.11, the modulus of the reflection coefficient is obtained from trigonometry:

$$|R| = \sqrt{\frac{(\omega z_1 z_2)^2 + K^2 (z_1 - z_2)^2}{(\omega z_1 z_2)^2 + K^2 (z_1 + z_2)^2}} \tag{3.38}$$

By combining Eqs. (3.38) and (3.36) and rearranging, it gives the film thickness in terms of the amplitude of the reflection coefficient, then the basic amplitude spring model, Eq. 3.39, is obtained:

$$h = \frac{\rho c^2}{\omega z_1 z_2} \sqrt{\frac{R^2 (z_1 + z_2)^2 - (z_1 - z_2)^2}{1 - R^2}} \tag{3.39}$$

This relationship (Eq. (3.39)) has been plotted out in Figure 3.12, for a Perspex – oil – rubber layer system for three values of layer thickness, *h*. The minimum of reflection coefficient that occurs when the layer falls to 0.2 (and the two opposing surfaces are assumed to be fully in contact) is given by Eq. (3.20).

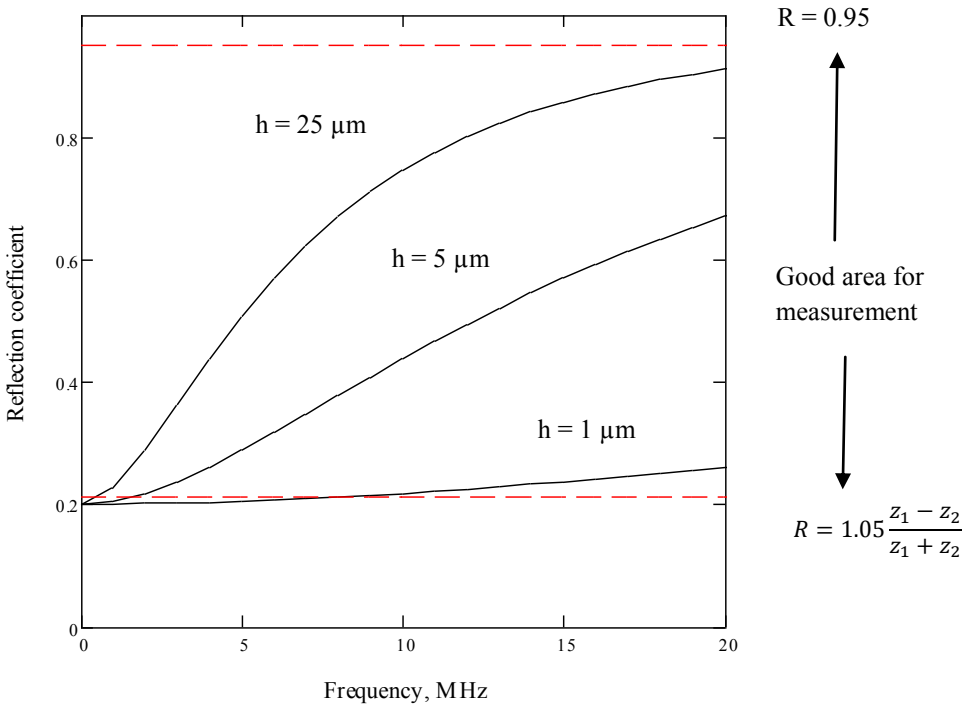

Figure 3.12 Reflection coefficient spectra between Perspex and rubber for arrange of fluid film thickness.

Inspection of Eq. (3.39) shows that when $R \rightarrow 1$ and $R \rightarrow \frac{z_2 - z_1}{z_2 + z_1}$ small errors in *R* lead to large errors in the determined value of *h*. Investigation that has been done by Dwyer-Joyce *et al*. [2003] in measuring oil film thickness using ultrasound showed that the upper limit measurement of *R* less than 0.9 yields

satisfactory results and for the minimum limit of measurement is for R = 0.1. In the same way, Reddyhoff *et al.* [2006] have only shown that the best measurements for measuring oil film thickness in a silicon carbide face seal are achieved typically for the region $(z_1 - z_2)/(z_1 + z_2) < R < 0.90$. The upper limit of measurement of film thickness using spring interface model is depended on value of R where it approaches 1, the film thickness tends to infinity in Eq. 3.39. The lower limit of measurement film thickness is influenced by its acoustic impedance between two materials in contact (Eq.3.20). In this thesis, the measurement range of R adopted is indicated on Figure 3.13 where the upper and lower limits of R are $1.05\,(z_1 - z_2)/(z_1 + z_2) < R < 0.95$. These measurement limits are more moderate than the investigators above. The consideration of these limits will depend on signal to noise ratio. The effect of noise in the recorded signal becomes significant outside this range. The exact width of this measurement region (and how close to R=1 can be achieved) will depend on the electrical noise, voltage stability, and any internal equipment filtering. These parameters are highly equipment and environment dependent and will vary from application to application. The quality of surface material and material its self have also contribution. These measurement limits should therefore be viewed as an experimental guide and not as fixed physical limits.

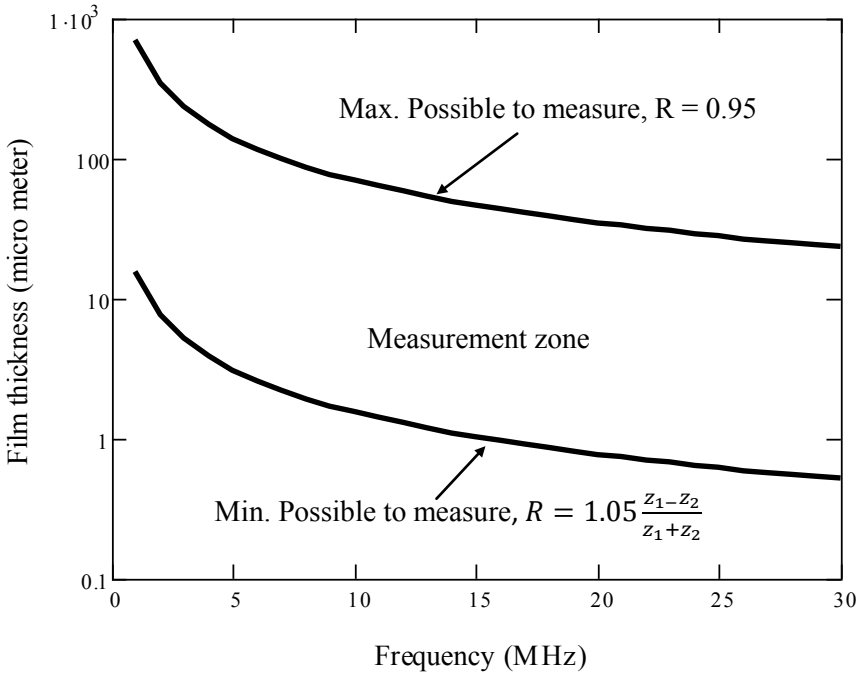

Figure 3.13 Measurable film ranges for contact between rubber and Perspex with an oil film by using the amplitude method.

The predicted oil film thickness at the two measurement limits using Eq. 3.39 for $R = 1.05\frac{z_1 - z_2}{z_1 + z_2}$ and R = 0.95 is shown in Figure 3.13. Thus for a 10 MHz transducer, as used in this study, film thickness in the range 1 to 100 µm are measureable. Clearly higher frequencies are sensitive to thinner oil films.

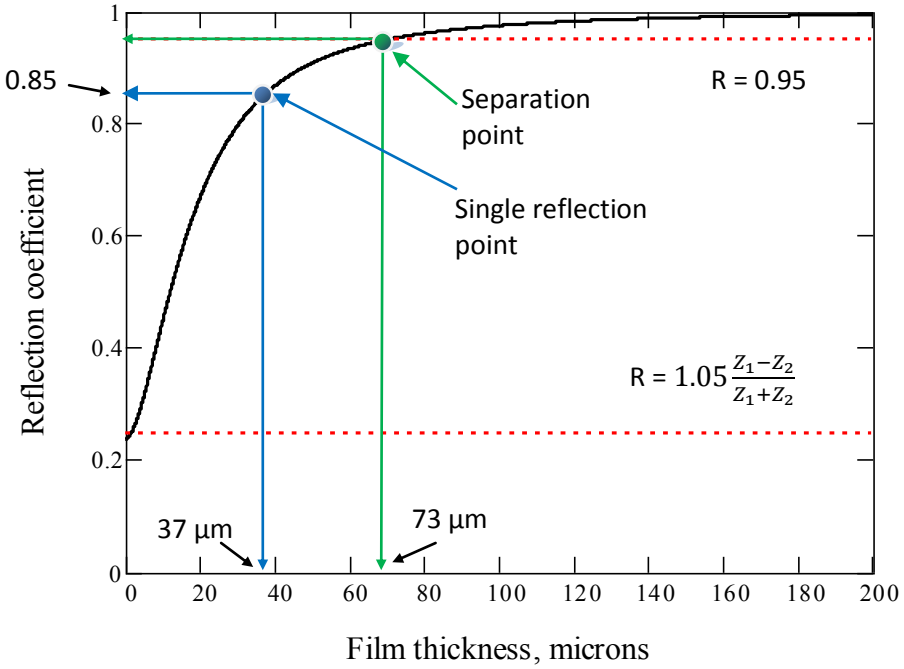

Figure 3.14 Reflection coefficient spectra between Perspex and rubber for 10 MHz frequency transducer.

The upper limit of R in measuring oil film thickness using spring interface model could be shifted from the upper limit of measurement as mentioned above depended on interface of two materials in contact as shown in Figure 3.14. This figure shows the reflection coefficient spectra between Perspex and rubber for 10 MHz frequency transducer. When the thickness of oil film is 73 µm (assuming that the thickness of oil is the same as the wavelength (t≈0.1 µs) of signal in the oil based on the limitation of ToF model), the reflected signals from the interface will be separated each other. As the film becomes thinner, the reflected signals from the interface will be approach each other until both signals united. If the single reflection is formed at half of wavelength (or equivalent to 37 µm), the maximum upper limit for R will be 0.85.

3.3.3 Phase shift methods

From Fig. 3.11, phase difference (ϕ) can be obtained by trigonometry from Eq. (3.30) as follow,

$$\phi = \arctan\left(\frac{2z_1z_2^2\left(\frac{\omega}{K}\right)}{\left(z_1^2 - z_2^2\right) + z_1^2z_2^2\left(\frac{\omega}{K}\right)^2}\right) \tag{3.40}$$

Where phase difference is the difference of the phase shift between the incident and reflected waves. It is associated with film thickness (Reddyhoff *et al.* [2005], Reddyhoff [2006]).

The film thickness can be expressed in terms of the phase difference by combining Eqs. (3.40) and (3.36).

$$h = \frac{\rho c^2\left(z_1z_2^2 \pm \sqrt{\left(z_1z_2^2\right)^2 - \tan^2\phi z_1^2z_2^2\left(z_1^2 - z_2^2\right)}\right)}{\omega\tan\phi z_1^2z_2^2} \tag{3.41}$$

From Eq. 3.41, it can be seen that there are two values in the bracket, negative and positive. These values are related to the Figure 3.15 where if we plot the relationship between phase difference in radians and frequency of transducer to vary film thickness for a Perspex – oil – rubber system based on Eq. 3.40, the graph shows a polynomial curve. The positive tangent and negative tangent lines of this curve are associated with the negative and positive values of Eq. 3.41, respectively.

The phase difference for contact between Perspex and rubber, between an incident wave and a reflected wave, varies from 0 for thick film ($K\rightarrow 0$) to 0.67 (0.22π) for a thin film ($K\rightarrow \infty$) for positive and from 0.67 (0.22π) for a thick film ($K\rightarrow 0$) to 0 for thin film ($K\rightarrow \infty$) for negative.

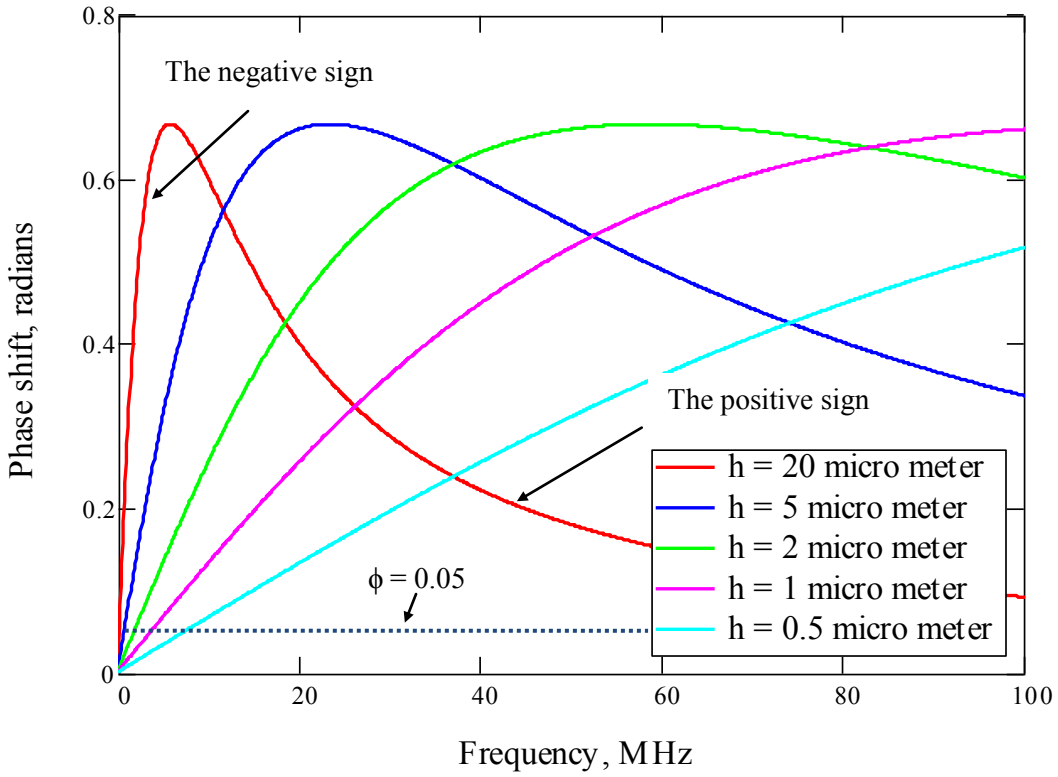

Figure 3.15 Phase shift difference spectra between Perspex and rubber for arrange of fluid film thickness.

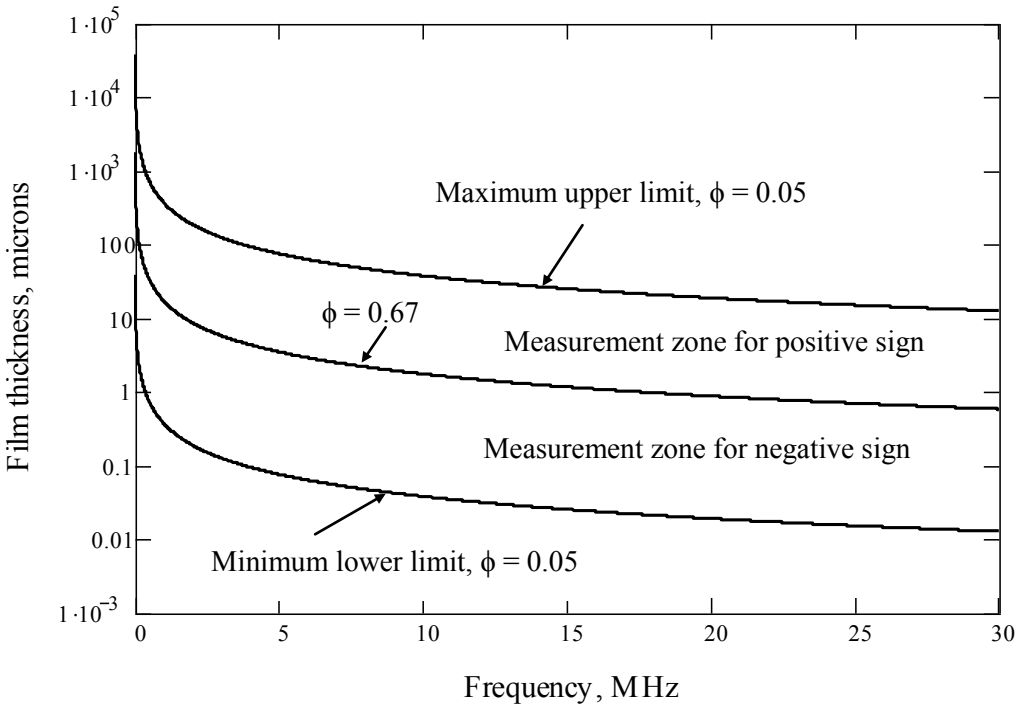

Figure 3.16 Measurement zone for contact between Perspex and rubber by using phase shift method.

The predicted oil film thickness at the measurement limit using Eq. 3.41 for ϕ = 0.05 is shown in Figure 3.16. Thus for a 10 MHz transducer, as used in this study, film thickness in the range 0.1 to 5 μm are measureable for negative sign and 5 to 100 μm are measurable for positive sign. Clearly higher frequencies are sensitive to thinner oil films.

3.3.4 Relationship between reflection coefficient and phase difference

Equating equations 3.39 and 3.41 give reflection coefficient in terms of phase difference. For the case of $z_1 = z_2$, reflection coefficient is stated as:

$$R = \sqrt{\frac{1}{\tan^2 \phi + 1}} \tag{3.42}$$

For the case of $z_1 \neq z_2$

$$R = \sqrt{\frac{(z_1 - z_2)^2 + A^2}{(z_1 + z_2)^2 + A^2}} \tag{3.43}$$

where

$$A = \frac{\left(z_1 z_2^2 \pm \sqrt{\left(z_1 z_2^2\right)^2 - \tan^2 \phi z_1^2 z_2^2 \left(z_1^2 - z_2^2\right)} \right)}{\tan \phi z_1 z_2}$$

The Figure 3.17 shows the relationship between reflection coefficient and phase difference (Eqs. 3.42 and 3.43) for contact cases between steel-steel and Perspex – rubber. For the contact between Perspex and rubber, the negative sign of Eq. 3.43 shows that the phase shift value is to indicate thin oil films.

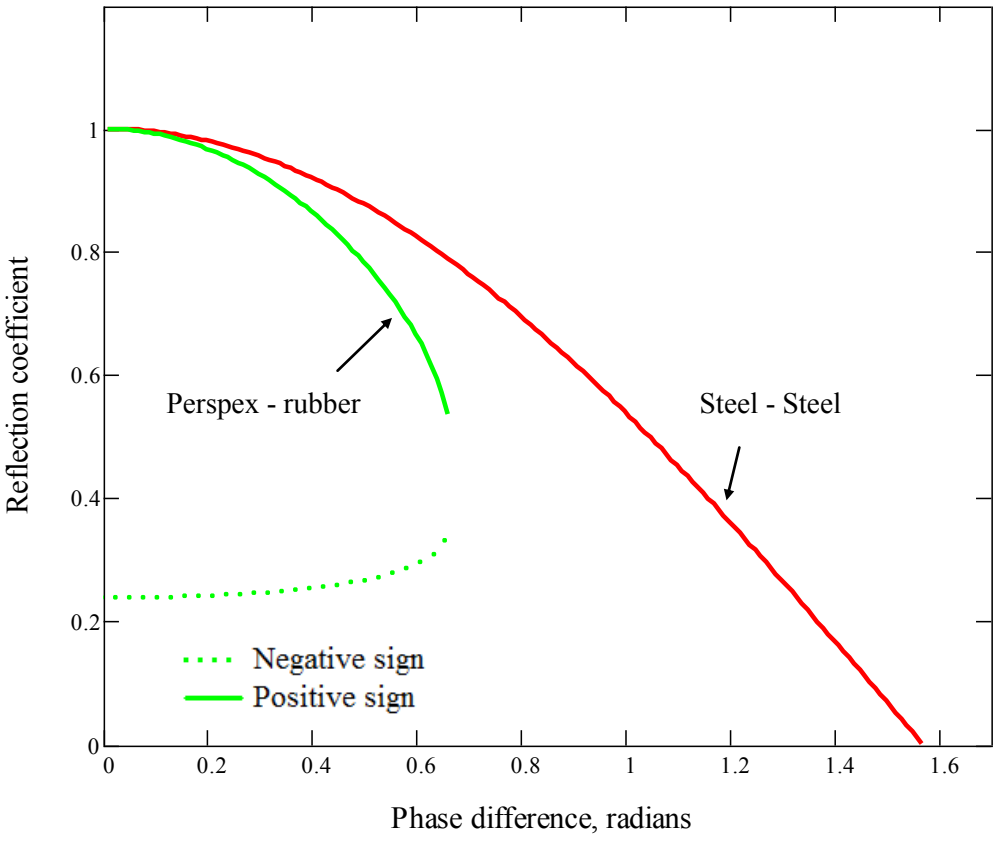

Figure 3.17 Relationship between reflection coefficient and phase difference for contact between steel-steel and Perspex-rubber based on Eqs. 3.42 and 3.43.

3.4 Calibration of lubricant film thickness

The ultrasonic reflection technique is still in its infancy and has not been widely used due to lack of calibration, testing and validation (Reddyhoff [2006]). The application of ultrasonic techniques has been limited by the lack of a robust calibration procedure (Zhang *et al.* [2005]), so the standard procedure to measure film thickness by using ultrasound has not been standardized or a robust method has not been found. Nevertheless, some authors have proposed the methods of calibration by using liquid-wedge (Reddyhoff [2006], Harper [2008]), journal geometry (Dwyer-Joyce *et al.* [2003], Dwyer-Joyce *et al.* [2004], Harper [2008]), glass plate test (Harper [2008]) and digital piezoelectric translator (DPT) technique (Zhang *et al.* [2005]).

3.4.1 Liquid-wedge experiment

This technique used a method for comporting physical geometry provided a wedge of fluid trapped between two solids. Two glass sheets of 6 mm thick were separated by a shim of known thickness at one end. The geometry of the fluid-wedge formed by the shim could estimate the film thickness of the liquid layer at any measuring location as shown in Figure 3.18.

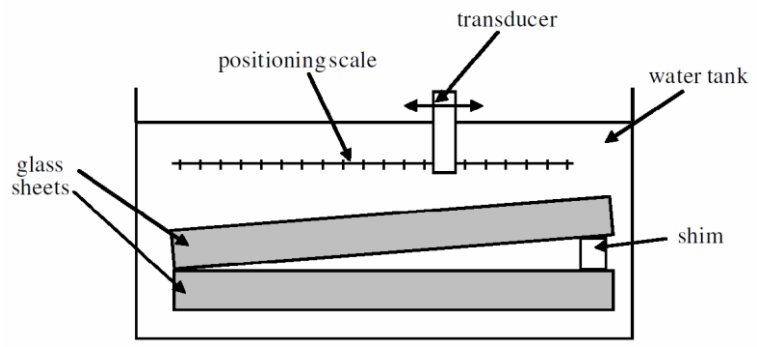

Figure 3.18 Schematic representation of liquid-wedge experiment (Dwyer-Joyce *et al.* [2003]).

The calculation of film thickness using ultrasonic method was approached by spring interface model for thickness lower than 25 μm and resonant layer models for thickness larger than 25 μm. The Figure 3.19 shows that the good agreement between the measured film thickness and theoretical ones for thin films.

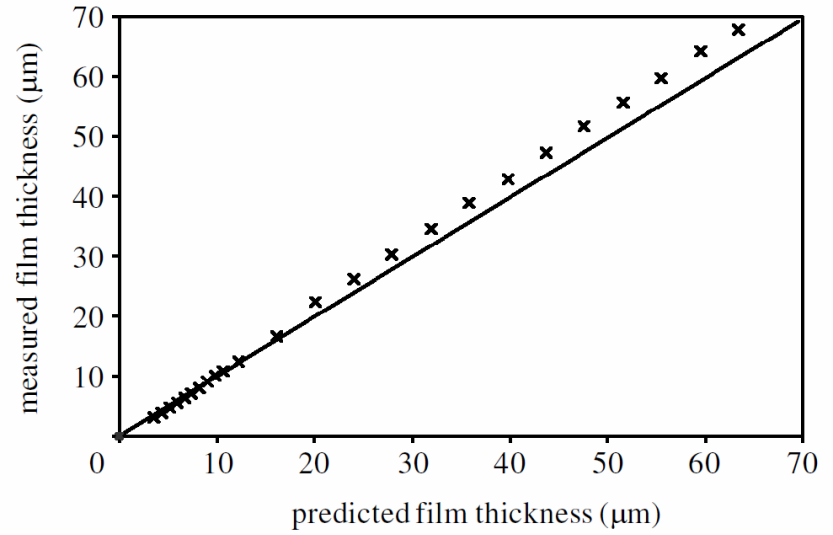

Figure 3.19 Ultrasonic measurement of the thickness of liquid compared with the geometrical prediction of the layer thickness (Dwyer-Joyce *et al.* [2004]).

3.4.2 Journal geometry experiment

Figure 3.20 shows a schematic of apparatus to create an oil wedge between a ring and shaft. The shaft and ring were connected by spring by changing the position of loading point, so the gap thickness in the region above transducer could be varied.

A 25 MHZ focus transducer was mounted on bearing holder of journal bearing. The measurement film thickness was conducted in static condition. The results of measurement film thickness, which are approached by resonant layer model are plotted in Fig. 3.21. The relation of measurement and theoretical film thickness is reasonable.

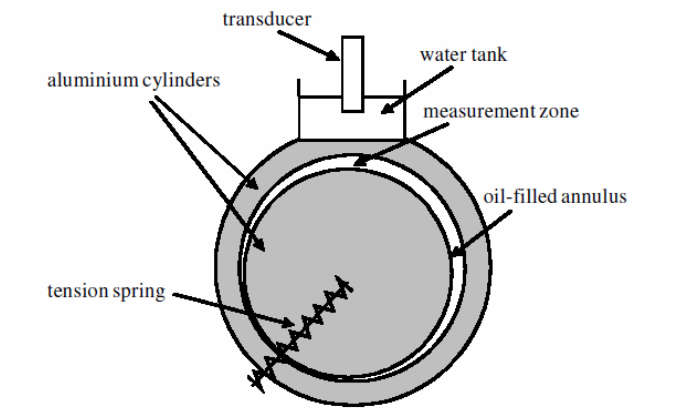

Figure 3.20 Schematic representation of apparatus used to create journal geometry experiment (Dwyer-Joyce *et al.* [2003]).

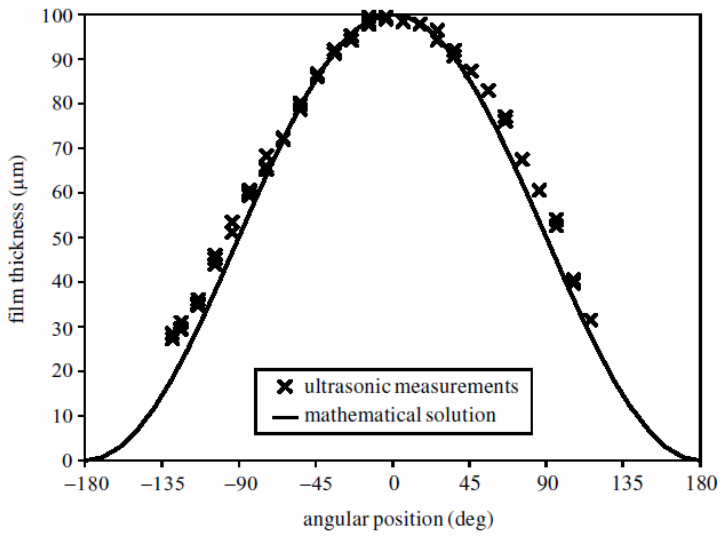

Figure 3.21 Measured oil film thickness round the circumference of a journal bearing for a fixed load and speed (Dwyer-Joyce *et al.* [2003]).

3.4.3 Glass plate test

This experiment was carried out on a static oil film by approaching amplitude and phase shift methods. Figure 3.22 shows the schematic representation of apparatus to measure film thickness. A 2 MHz piezoelectric transducer was bonded directly to the upper glass sheet. The two sheets of float glass 5 mm in thickness were used in this experiment and a static oil film was created by sandwiching a drop of oil between two glasses. The oil film thickness in the range 3 µm to 30 µm could be obtained in this way. The oil drop is pressed into a circle and given the mass, density and diameter of the oil circle formed can calculate the thickness of the circle by using the volume of the oil circle. The thickness of oil film was varied by changing the quantity of oil used or by pressing the glass sheets together.

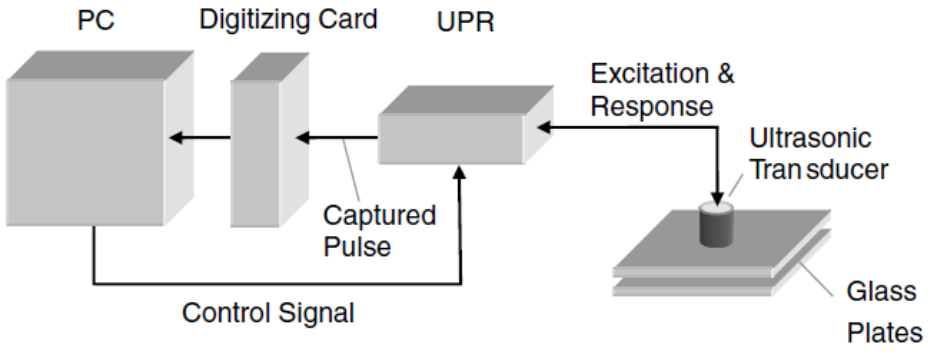

Figure 3.22 Schematic of apparatus to measure film thickness by sandwiching a drop of oil film between two glasses (Reddyhoff [2006]).

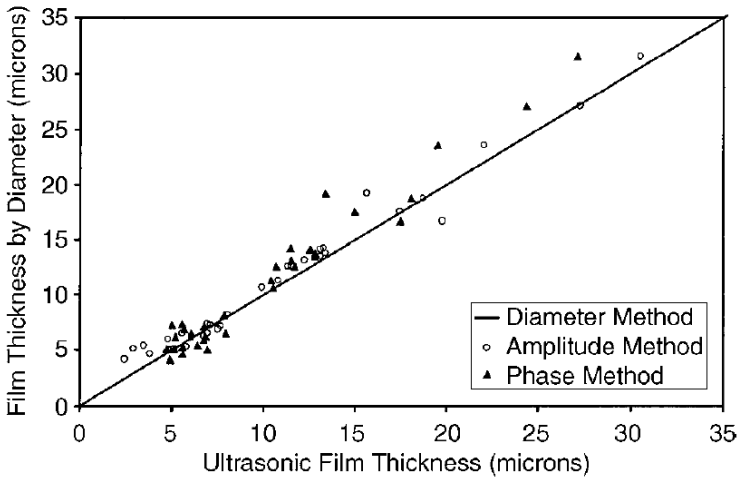

Figure 3.23 Comparison of amplitude and phase methods of film thickness measurement with thickness of the diameter of circle oil spot (Reddyhoff [2006]).

This measured film thickness, which was measured by amplitude and phase methods, was then compared with the thickness of the diameter of circle oil spot. The film thickness could be approximated with accuracy 5% as shown in Figure 3.23. There is good agreement between the three methods.

3.4.4 Digital piezoelectric translator (DPT) techniques

Zhang *et al*. [2005] proposed a method of calibration based around a digital piezoelectric translator (DPT) which is used to adjust lubricant-film thickness by displacing one the steel surface, whilst the others remains fixed as shown in Figure 3.24. The three layer systems consisted of steel-oil-steel were used and the lubricant films are static. The transducer had a centre frequency of 50 MHz, an active diameter of 6 mm and a focal length in a water of 22.86 mm.

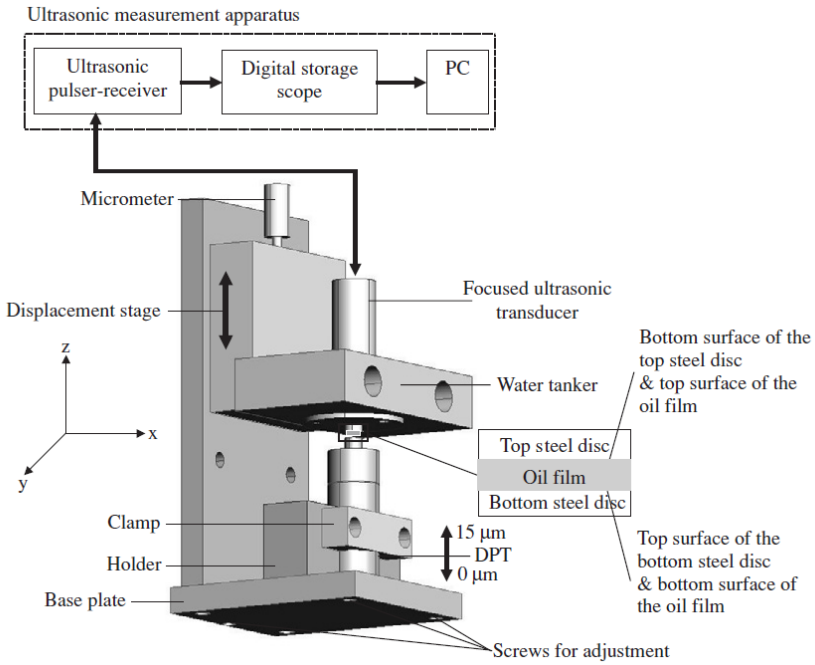

Figure 3.24 The schematic diagram of the experimental apparatus used to calibrate thin film thickness using DPT technique (Zhang *et al.* [2005]).

The resonant-layer model was used to calculate the lubricant-film thickness for the thick films (h > 10 µm). The spring layer model was used to calculate the

thickness of thin lubricant films in the range 0.5 to 1.3 µm. Figure 3.25 shows that the spring layer model gives good quantitative prediction of the lubricant film thickness.

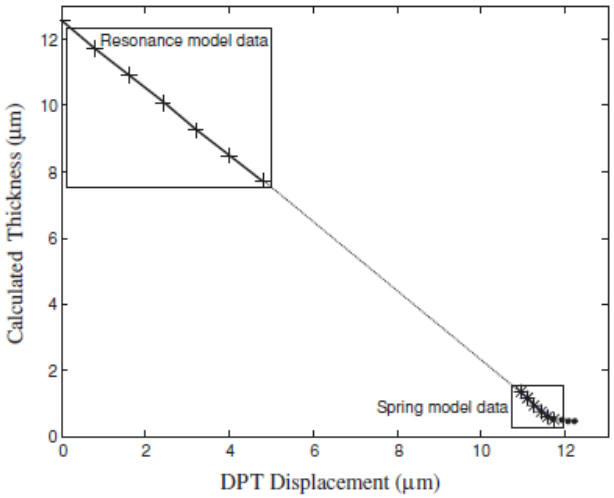

Figure 3.25 Comparison of resonance model data and spring model data with the DPT displacement (Zhang *et al.* [2005]).

3.5 Conclusion

The basic principles of ultrasound have been discussed in this chapter. These principles have been applied to determinate reflection and transmission of ultrasonic waves when the propagates in media. In the section 3.2.2 the mode conversion of ultrasonic wave when propagates in solid-solid media interface has been developed to generate surface wave by measuring reflected factor.

Measurement of film thickness using ultrasonic reflection has been developed for measuring different thickness films by using three methods: time of flight (ToF), the resonant-layer model, and spring layer model, respectively. To calculate thin film thickness between two lubricated contacts using ultrasonic reflection, the Eq. 3.25 is used by approaching spring interface model. The reflection equation (3.23) contains complex quantity phase difference and reflection coefficient information. The reflection coefficient and phase difference have been developed in order to predict lubricant film thickness by amplitude and phase shift methods.

In section 3.4, several methods have been discussed calibration using ultrasonic method, which has been performed by several authors. Until now, there has not been a robust method to calibrate ultrasound before using it.

Chapter 4

Ultrasonic equipments and measurement systems

In this chapter, the ultrasonic equipment and methods employed to measure an oil film thickness and contact between dissimilar materials are described. The hardware that is employed in measuring oil film thickness and contact is addressed. The characteristics of focusing transducers are discussed before choosing an ultrasonic transducer. The steps of measurement systems are explained from capturing reflection signal to calculating oil film thickness.

4.1 Introduction

A schematic diagram of the equipment used for generation and measurement of ultrasonic waves is shown in Figure 4.1. The ultrasonic apparatus consists of an ultrasonic transducer, an ultrasonic pulse-receiver (UPR), an oscilloscope, and a personal computer. A piezoelectric transducer can send and receive pulses to the interface or layer of lubricant being investigated. The transducer is driven by UPR, which is used to generate a series of short duration voltage pulses. The piezoelectric element will resonate due to the pulses. The transducer operates in pulse-echo mode and receives reflection back from the oil film. An oscilloscope

or PC digitizer card is used to capture and record the reflected signal. This is then passed to a PC for processing and displayed results with LabView programs.

In this chapter, the various steps of the measurement systems used in the measurement of experiments in Chapters 5 to 7 are described in principle. The measurement systems of signal processing, reflection coefficient, and phase difference are outlined.

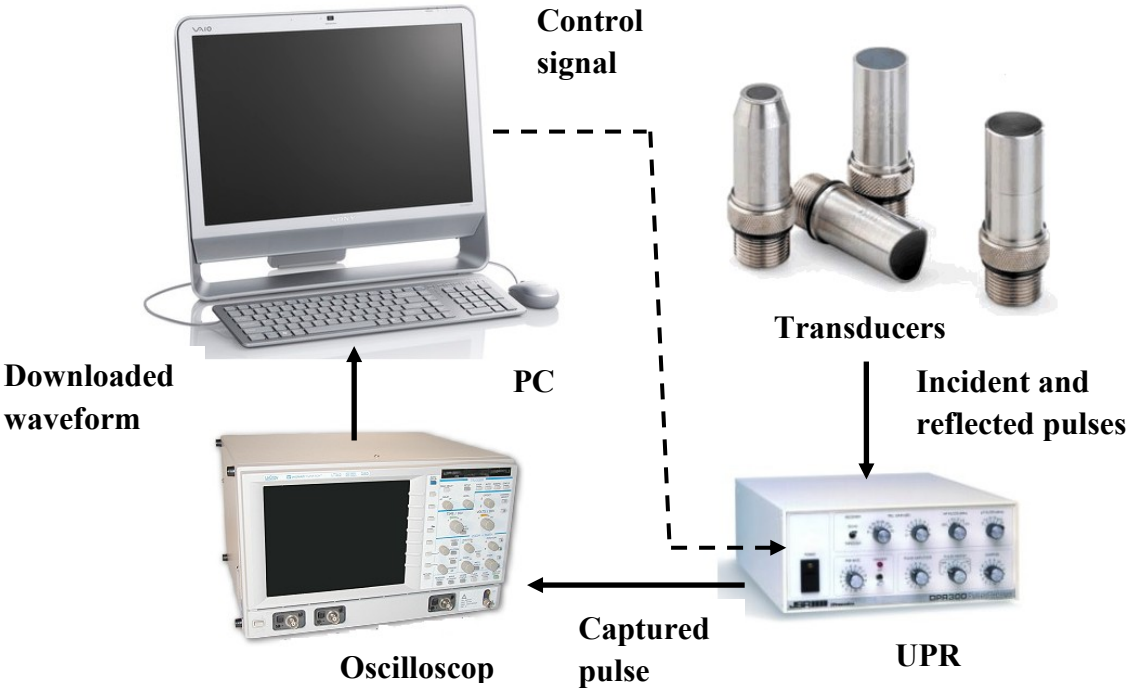

Figure 4.1 Schematic diagrams of the ultrasonic apparatus.

4.2 Hardware

4.2.1 Ultrasonic transducer

Various types of ultrasonic transducers are available, depending on assembly, whether the transducer element produces longitudinal or shear wave, and whether or not the pulse is focused. A tree diagram showing the classification of ultrasonic transducers is shown in Figure 4.2.

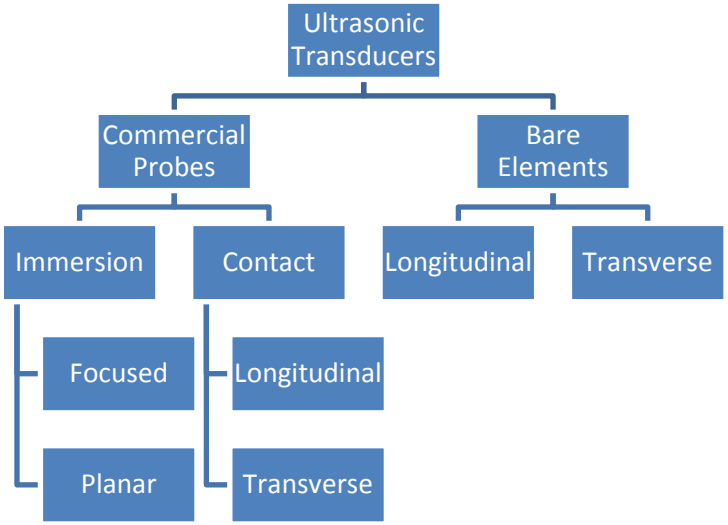

Figure 4.2 Tree diagram shows types of ultrasonic transducers used for oil film measurement and contact mechanics.

Three generic types of transducers are commonly used and are shown schematically in Figure 4.3. Longitudinal transducers generate waves where the direction of oscillation is parallel to the direction of propagation. These can be directly coupled to the specimen using an adhesive or gel (Figure 4.3a and 4.3b), or bonded to a focusing lens and used immersed in a liquid bath (Figure 4.3c). Shear transducers generate waves where the vibration is transverse to the direction of propagation (Figure 4.3b). Shear waves cannot propagate through liquids and so are not useful for measuring oil films (other than the presence or absence of film). Ultrasonic transducers that can generate shear waves require the use of a special couplant of high viscosity in order to transmit the wave.

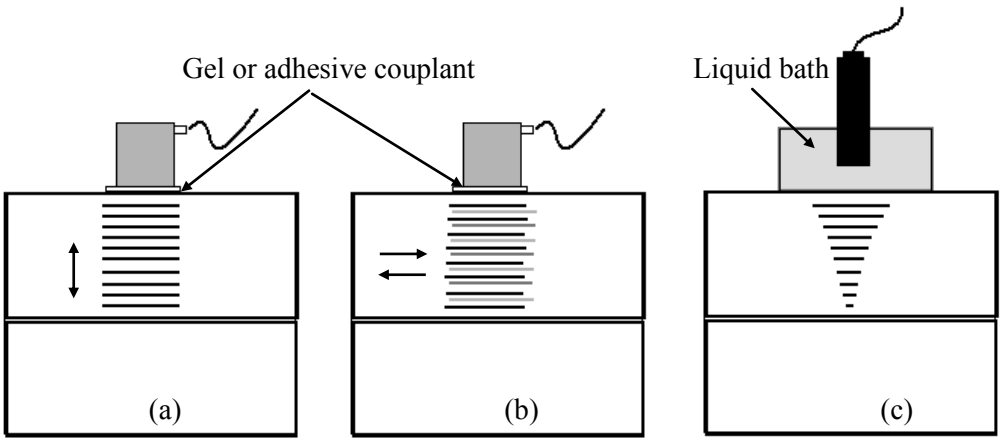

Figure 4.3 Schematic of three types of transducers used for studying tribological interfaces (a) longitudinal contact, (b) shear, and (c) longitudinal focusing.

4.2.2 Wedge transducers

Wedges are inserted between an ultrasonic transducer and a specimen to provide the transducer, which is set on the sloping surface of the wedge. The wedge is acoustically coupled through one of its faces to the surface of the test solid. Wedges are generally made of acrylic. Wedge transducers can be used to generate a surface wave when angle of the critical angle is as described in section 3.2.2.1. In commercial wedge transducers, there are two kinds of wedge transducers: fixed and variable transducers as shown in Figure 4.4.

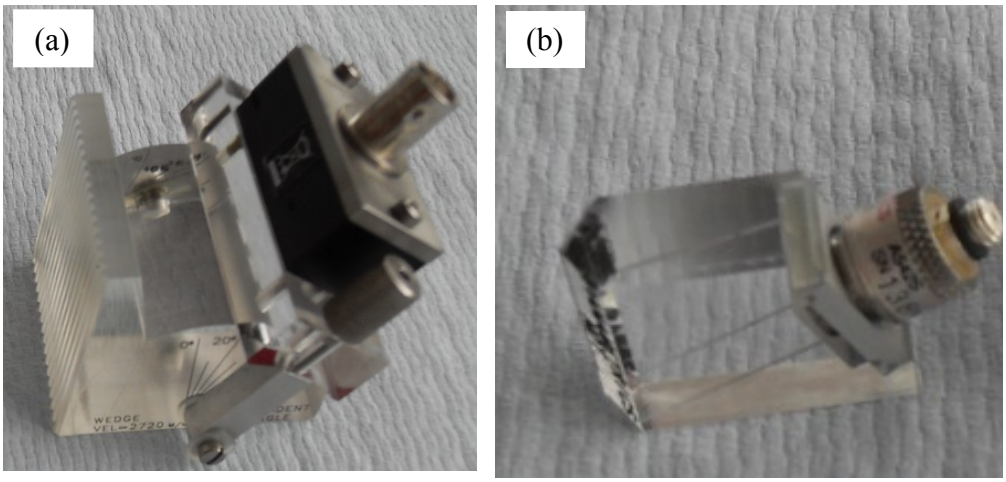

Figure 4.4 Wedge transducers: (a) variable wedge transducer and (b) fixed wedge transducer.

4.2.3 Ultrasonic pulser receiver (UPR)

An ultrasonic pulser receiver (UPR) (NDT solution Ltd) is functioned as tool to produce a voltage signal, which excites the piezoelectric transducer. It causes resonance and sends an ultrasonic pulse into the medium, where it is couple to. The excitation signal is controlled in order that the transducer produces the desired centre frequency.

The produced voltage signal when a transducer receives an ultrasonic signal will be amplified by UPR. The gain of amplification could be adjusted. This UPR has an excellent signal to noise ratio, high speed pulse repetition rate (up to 10 kHz),

high frequency pulsing (set-able up to 30 MHz), and two software selectable channels.

4.2.4 Digital oscilloscope

A commercial digital oscilloscope (LeCroy WaveRunner LT342) that receives and registers the signal from the UPR was used. This allowed a variety of display and processing option to be performed even before the PC-based processing stage. The oscilloscope can sample at 500 MHz bandwidth and 500 M sample/second. For each waveform, 5000 data points were used as well and average of 100 sweeps.

4.2.5 Signal acquisition and data processing

The generating and receiving waves to and from the transducer, it is carried out by the UPR. This apparatus in turns is controlled by means of the driver, in where the frequency, pulse rate, voltage, and gain can be varied on demand. The width frequency band and voltage pulses are generated in order to actuate the piezo-electric transducers. The transducer used to send the signal also receives the reflected pulse. The reflected voltage is then captured by the UPR and stored as a waveform on a digital oscilloscope. From this step onwards signal processing takes place. The waveform of interest is then passed to a PC for signal processing. Next, the sub VI of LabView programme is applied to get a fast Fourier transform (FFT) for each level of load. The FFT results in magnitude and phase. Thus, from the magnitude and phase, the reflection coefficient and phase difference are directly obtained. Finally, film thickness in terms of the frequency can be calculated by using the spring model of Eqs. 3.39 and 3.41.

4.3 Characteristic of focusing transducers

The focusing transducer is one the type of immersion transducers, which the pulse can be focused in a similar way to light. It achieves higher sensitivity and

resolution, by concentrating waves into a small region. The commonly focused down of ultrasound is to point, known as spherical focusing (Figure 4.5).

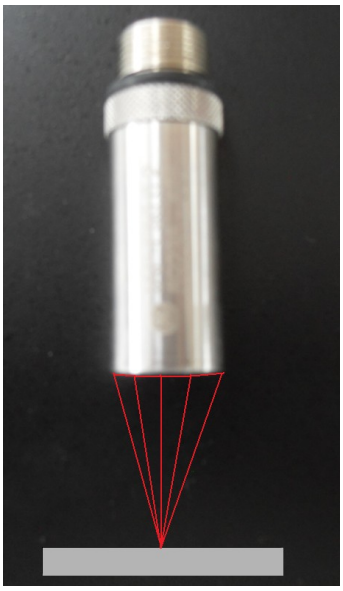

Figure 4.5 A spherically focused transducer with sketch of ultrasonic wave by ignoring beam divergence.

An immersion transducer is a single element longitudinal wave transducer with a 1/4 wavelength layer acoustically matched to water. More ultrasonic energy will concentrate upon the focal spot, if the sound field is focused.

4.3.1 Water path

The focal length of a transducer is dependent on the material, because different materials have different sound velocity. If the velocity of sound of a material is higher than water, focal length in water is shortened due to refraction. The sound path will have to pass from water into the testing material. Because the two materials have different sonic velocities and the sound beam is converging, refraction will occur at the interface between the water and testing material as shown in Figure 4.6. To determine the appropriate water path (WP) to compensate for the focus effect in the test material, Eq. 4.1 can used, and Figure 4.6 shows the ultrasonic beam passes from water to the testing material.

$$WP = F - MP(^{c_{tm}}/_{c_w}) \quad (4.1)$$

where here F is focal length, MP is material thickness and c_{tm} and c_w respectively are speed of sound testing material and water.

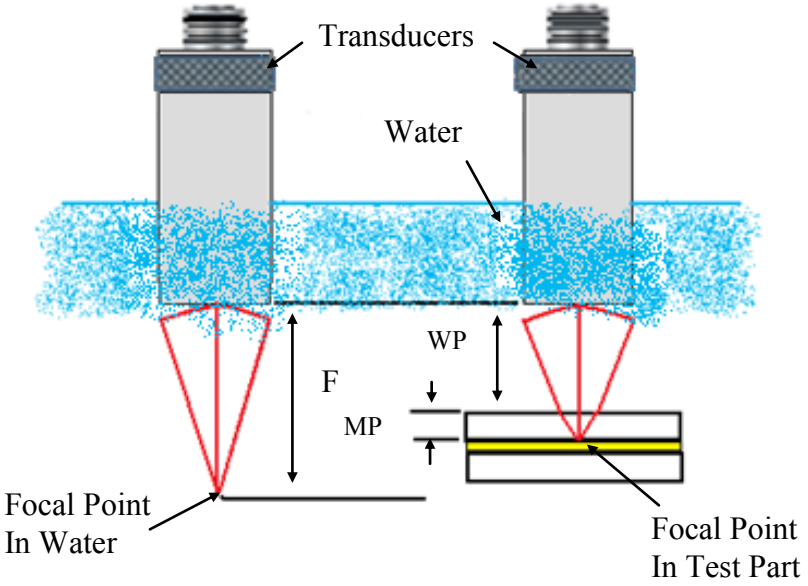

Figure 4.6 The effective shortening of the focal length when the ultrasonic beam passes from water to the testing material.

4.3.2 Focal spot diameter and contact diameter

The spring model (Eq. 3.24) is only valid when the ultrasonic pulse is incident fully over a region where a liquid layer is confined between flat parallel surfaces. It thus assumes both smooth surfaces and a parallel layer. An assumption is made here that this holds provided the pulse falls entirely within the central region of the EHL contact. Any roughness or thickness variation will therefore be averaged across the beam width.

It is important, therefore that the diameter of the focused ultrasonic wave should be less than the diameter of the contact region. The radius of the area of contact between the sphere and plate is given by (Stachwiak and Batchelor [2001]);

$$a = \left(\frac{3PR}{E^*} \right)^{1/3} \tag{4.2}$$

where P is the normal load, R is radius of rubber sphere and E^* is effective elastic modulus. The diameter of the focal spot depends on the frequency of the ultrasonic pulse used. For a 6 dB reduction in signal, the spot diameter can be estimated from the following empirical relationship (Silk [1984]):

$$d_f(-6dB) = 1.025\frac{l_w c_w}{f d_c} \tag{4.3}$$

where, c_w and l_w are the speed of sound and the focal length of the transducer in water respectively and d_c is the diameter of the piezoelectric element of frequency f.

Figure 4.7 shows the relation between spot diameter (Eq. 4.3) and contact diameter for the rubber loaded against Perspex disk (Eq. 4.2). The spot diameter reduces with transducer frequency, and the contact diameter increases with applied load. When the diameter of focal spot is smaller than the contact area, then the spring model is valid and a satisfactory measurement can be made.

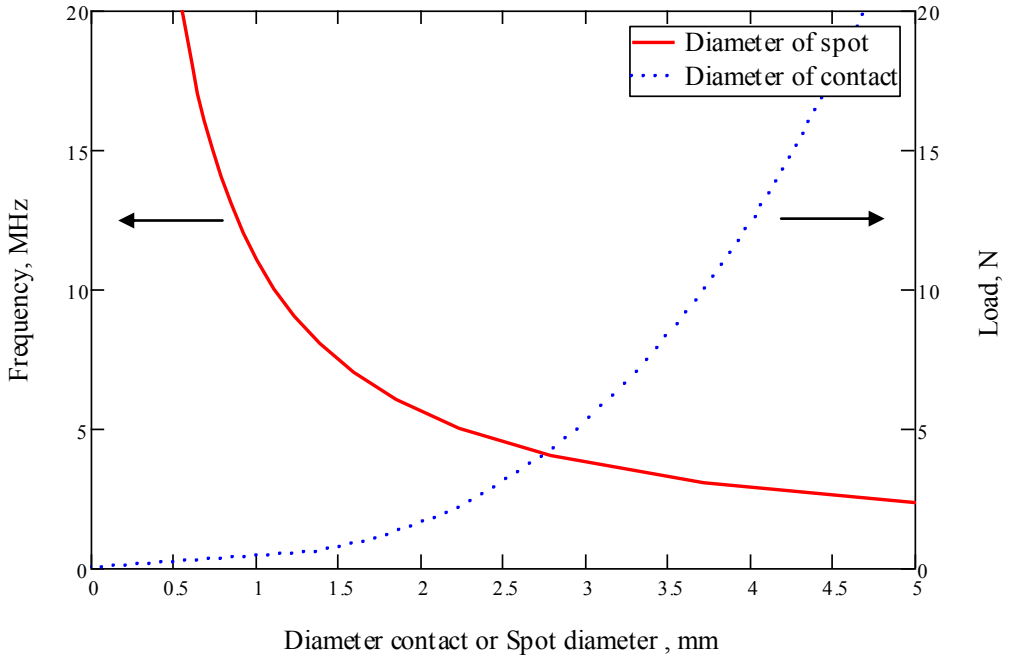

Figure 4.7 Variation of the focused spot diameter, d_f with frequency (for a 50 mm focal length and 12.7 mm element diameter transducer) and the variation of the contact diameter, $2a$ for a nitrile sphere pressed against Perspex with a load, P.

Figure 4.8 shows the locus of frequency and load values for which this is the case. For all combinations above the line, the spot size falls within the contact and

meaningful results are achieved. Clearly, a transducer should be selected such that this is the case. For these relatively large contact areas (compared to metal on metal contacts) this can be achieved with low frequencies.

Inspection of Eq. 4.3 shows that spot diameter is influenced not only by frequency of transducer, but also by the speed of sound of materials. Figure 4.8 indicates the variation of different contact cases to load and frequency. The contact case between steel and steel gives the smallest area above the curve in choosing frequency and load.

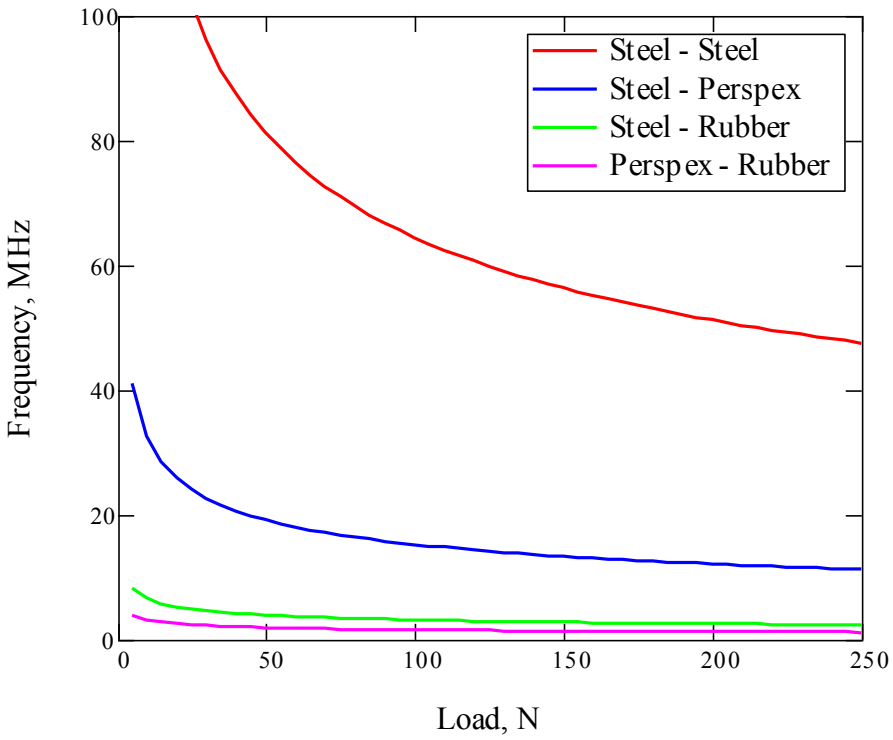

Figure 4.8 Curve where focal spot equal the size of the contact area. Above the line locus spot is smaller than contact area.

4.3.3 Measurement of water path

The focal length can be measured experimentally by adjusting step by step the position of immersion transducer (10 MHz) to surface of Perspex (known as water path, WP, as shown in Figure 4.6). The signal was captured and changed to maximum amplitude of Fourier transform. This was repeated for different water

path and a relation between water paths and amplitude's FFT was obtained as shown in Fig. 4.9. It shows that if the amplitude's FFT is high, more ultrasonic energy is concentrated upon the focal point. The area, which is bordered dot line, is area for region measurement. From Eq. 4.1, the value of the water path (WP) is 32.65 mm and it compared with the actual value specified by the transducer focal length.

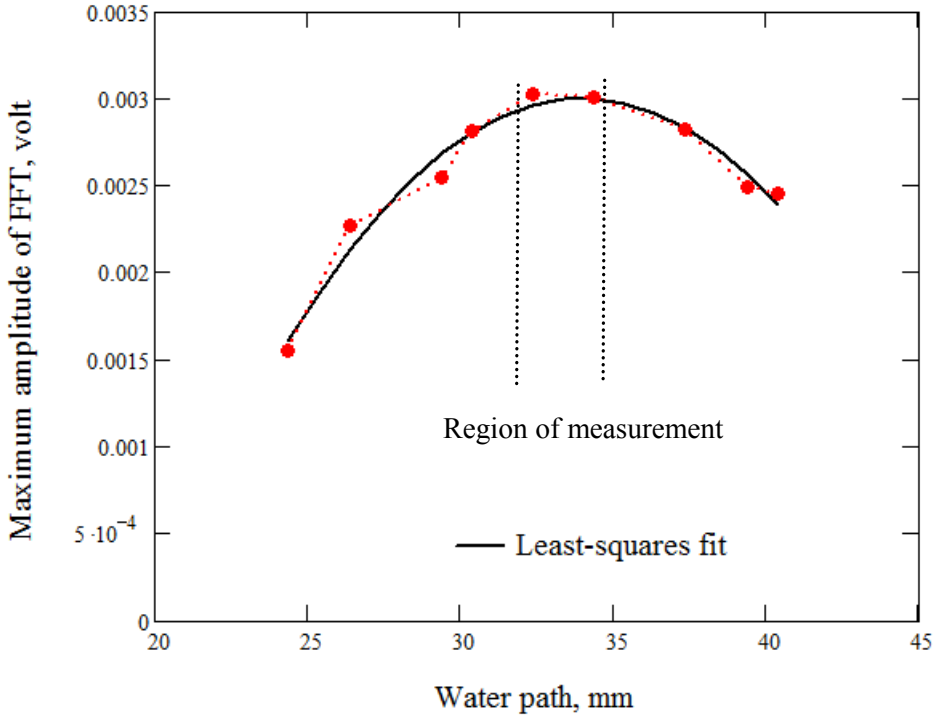

Figure 4.9 Variation of water path with maximum amplitude of FFT for 10 MHz transducer between water and Perspex.

4.3.4 Influence of water path

The ultrasonic waves are focused to enhance the resolution of the ultrasonic technique. The ultrasonic energy is concentrated at a set axial distance from transducer surface, where the sound waves are focused. The experiment was conducted to see the effect of water path against measured film thickness. A schematic of EHL test rig employed is shown in Figure 4.10 where a 10 MHz transducer was mounted on a holder that can be moved vertically. A load, 3.38 N, was applied with a small hydraulic loading cylinder on the nitrile ball that was

rotated 235 rpm by an electric motor. The contact was fully flooded with a mineral oil (Turbo Shell T68). The holder was moved step by step, so the distance of water path to ultrasonic transducer was from unfocused condition to focused condition and then back to unfocused condition. Each position, the reference signal and reflected signal from the lubricant were captured to get reflection coefficient. The film thickness for each position was calculated by using equation (3.25).

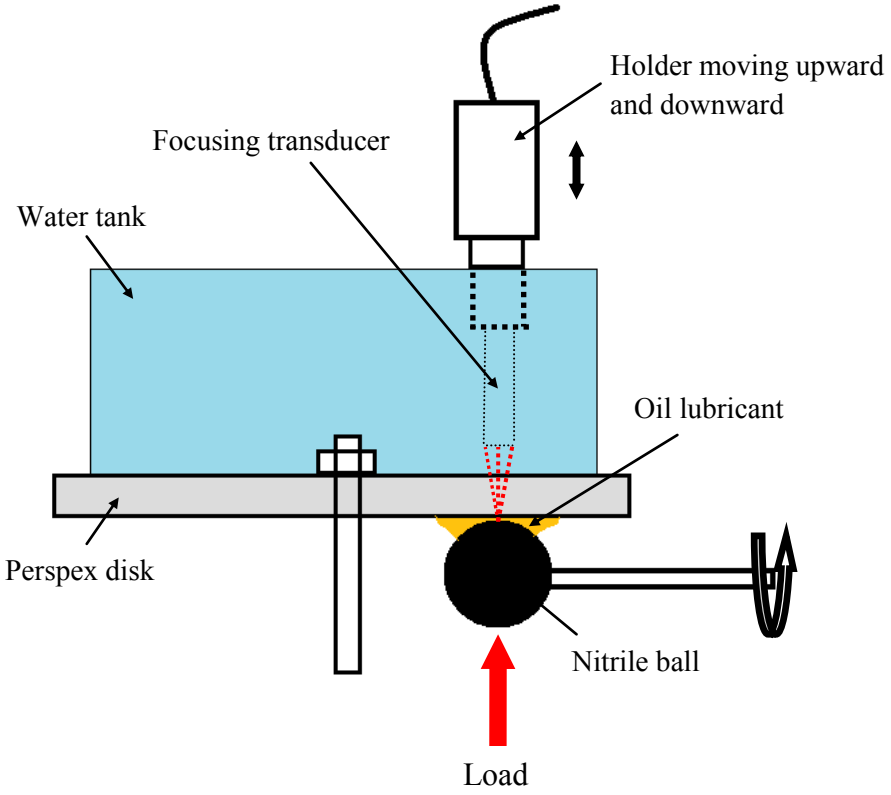

Figure 4.10 Schematic of EHL test rig to see effect of water path against measurement of oil film thickness.

The distance of water path to transducer and calculated film thickness are plotted, as shown in Figure 4.11. There is an influence of the value of measured film thickness against the distance of water path to transducer. It shows that if the transducer is not in focus, the value of measured film thickness will be higher or lower than in the correct measurement region. Outside of the region of measurement, the ultrasonic wave will be attenuated so that amplitude of ultrasound will decrease. The film thickness that is obtained outside of the focus region where the transducer is focused is shown as in Figure 4.12. The error of the calculated film thickness in outside of focus

length is between 39.1% and 0.9% when the water path is 27.2 mm and 31.2 mm, respectively. It is clear from Figures 4.11 and 4.12 that obtaining the correct focal length is important for the correct film thickness measurement.

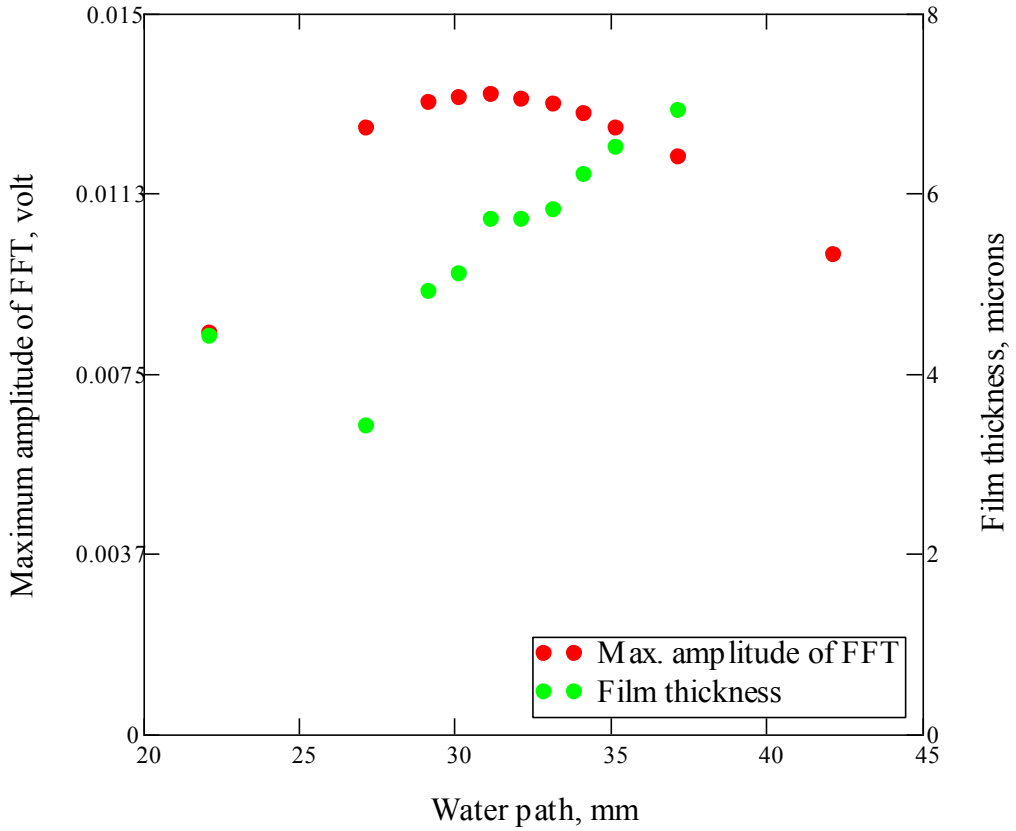

Figure 4.11 Relationship between maximum amplitude of FFT of different water paths and calculated film thickness. Contact between Perspex disk and 19 mm Nitrile ball with load 3.38 N and rotated 235 rpm.

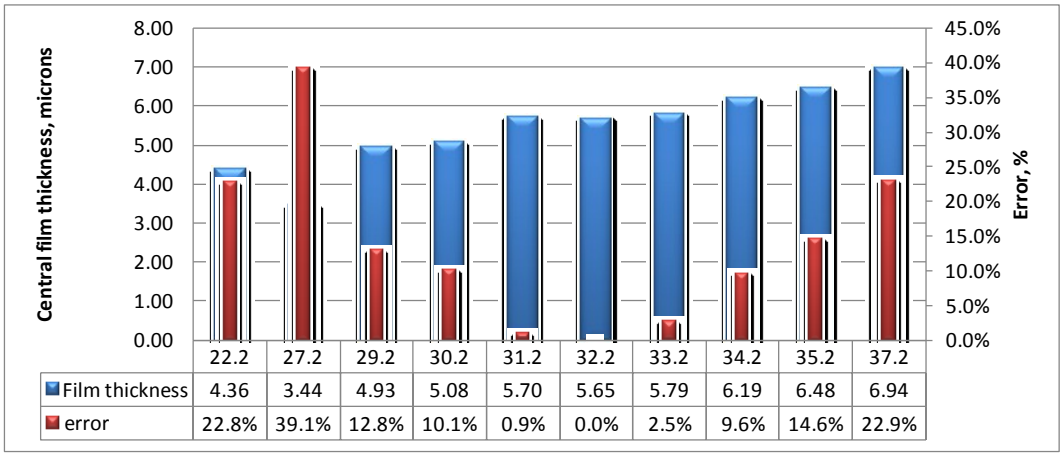

Figure 4.12 Error of measuring central film thickness based on difference between film thicknesses at the correct focus length and the outside of focus length. Contact between Perspex disk and 19 mm Nitrile ball with load 3.38 N and rotated on 235 rpm.

4.3.5 Effect of wave attenuation on centre frequency of transducer

In section 3.2.3.3, the attenuation of a sound wave has been discussed and it shows that the level of attenuation depends on the material, and on the frequency of the sound wave travelling through it. The experiment was conducted by propagating longitudinal wave in 10 mm Perspex and steel disks with 5 and 10 MHz ultrasonic transducers as shown in Figure 4.13. The propagation of ultrasonic sound in Perspex and steel will result discrepancy in centre of frequency. The centre frequency of transducer on Perspex reduced dramatically is compared with steel due to attenuation. The centre frequency of transducer for the case of steel has changed from 3.2 and 3.76 MHz for 5 and 10 MHz ultrasonic focus transducers, respectively.

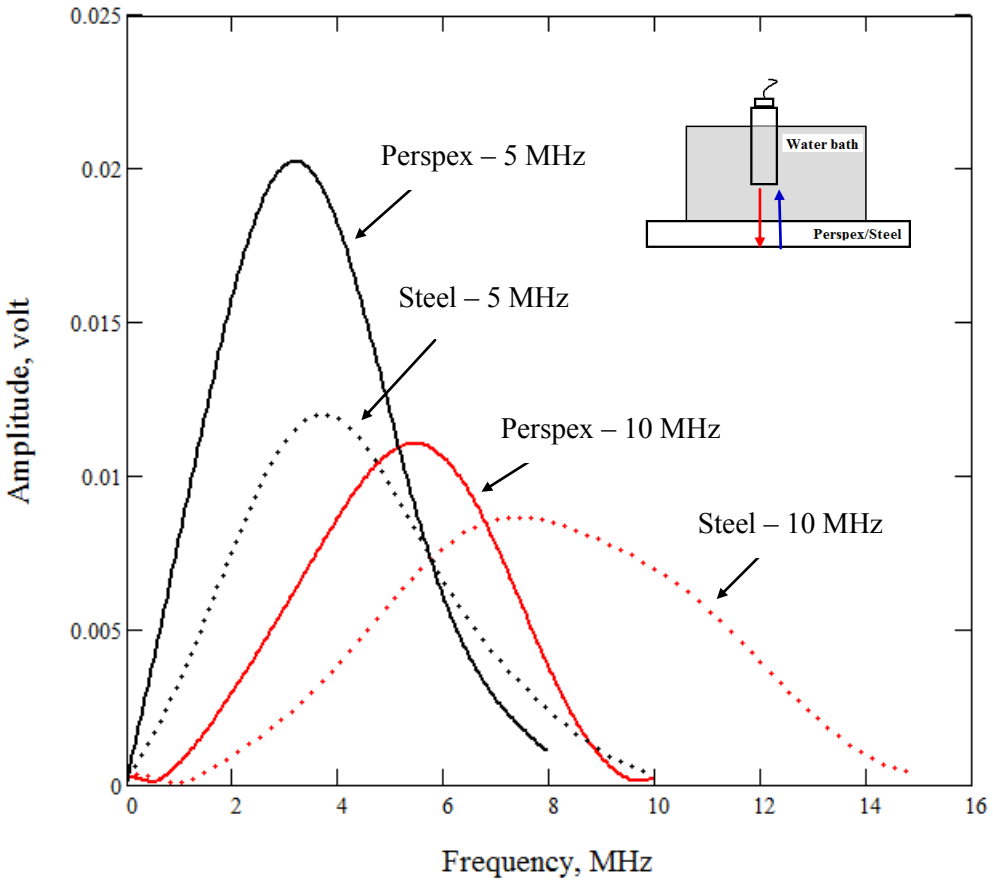

Figure 4.13 Comparison between amplitude and frequency of reflected signal from 10 mm thick of Perspex and steel using both 5 and 10 MHz transducers.

4.4 Measurement of the reflection coefficient and phase difference

4.4.4 Reflection coefficient

In order to measure film thickness of oil between Perspex and elastomer, an ultrasonic transducer is coupled onto the elastomer back face such that a pulse is emitted normal to the oil film. The transducer acts as both a transmitter and a receiver. The reflected wave is captured and digitized. The digitized time domain signals are converted into the frequency domain using an FFT to obtain the amplitude spectra. The reflection coefficient amplitude, required for Eq. (4.4), is obtained by comparing the signal reflected from the interface of interest to that from a known reference signal (Dwyer-Joyce *et al.* [2004]);

$$R(f) = \frac{A(f)}{A_0(f)} R_0 \tag{4.4}$$

where $A(f)$ is the amplitude of the signal reflected from the lubricant-film layer, $A_0(f)$ is the amplitude of the reference signal and R_0 is the reflection coefficient of the reference interface. The reference interface can be achieved by removing the elastomer specimen and the oil film. Then the reflection coefficient amplitude (from a Perspex–air interface) is very close to unity (R_0 = 0.999743273).

4.4.5 Phase difference

The reflection coefficient phase is defined as the difference between the phase shift of the incident wave and the phase shift of the reflected wave as stated in Eq. 4.5. In the same way as with the reflection coefficient amplitude and assuming that the phase shift of the incident signal remains the same as the phase shift of reflected signal, the reflection coefficient phase is obtained by subtracting the phase shift of the reflected signal from a known reference interface to that from the phase shift of the reflected signal of the interface of interest (Reddyhoff [2006]):

$$\Phi_{R(f)} = \phi_0(f) - \phi(f) \tag{4.5}$$

where $\phi_0(f)$ is the phase shift of the reference signal and $\phi(f)$ is the phase shift of the reflected signal from the lubricant film. The amplitude and phase shift of the displacement of a reflected pulse from a typical metal-air are shown schematically in Figure 4.14*a*, while those from a thin oil film reference interface are shown in Figure 4.14b; here, the amplitude and phase shift of the reflected pulse effectively equal those of the incident pulse for metal-air interface.

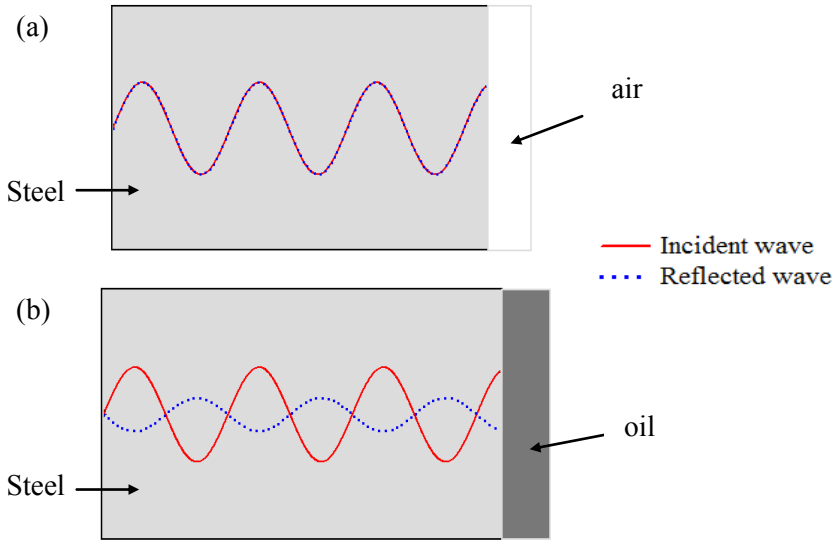

Figure 4.14 Schematic diagrams of pulses from (a) a metal-air interface and (b) a thin oil film.

4.5 Signal processing

There are several steps needed to be taken from capturing a reflected signal to arriving at a film thickness value. The commercial software package LabView is used for signal processing where recorded waveforms were digitized and passed to a PC for storage and analysis. A LabView software interface was also used to control the UPR and digitizer. Figure 4.15a shows a typical reflection signal. Peaks from the front and back face of the Perspex disk and subsequent repeating echoes can be seen. The back face peak (i.e. the signal reflected from the Perspex-rubber interface) was extracted from the signal. Figure 4.15b shows this oil film reflection and its variation as the speed is changed. As the film thickness reduces, more of the ultrasonic pulse is transmitted and the amplitude of the reflected signal reduces. The reflection from this location when there is no ball present is a reference condition and since a Perspex-air interface would fully reflect all the

ultrasound (i.e. R=1) it is equal to the incident signal. Thus dividing all subsequent signals by this reference signal gives the reflection coefficient.

Each of the reflection pulses is passed through a fast Fourier transform (FFT) to give amplitude against frequency plot (Figure 4.15c). Dividing each signal from an oil film by the FFT of the reference signal gives the reflection coefficient spectra (Figure 4.15d).

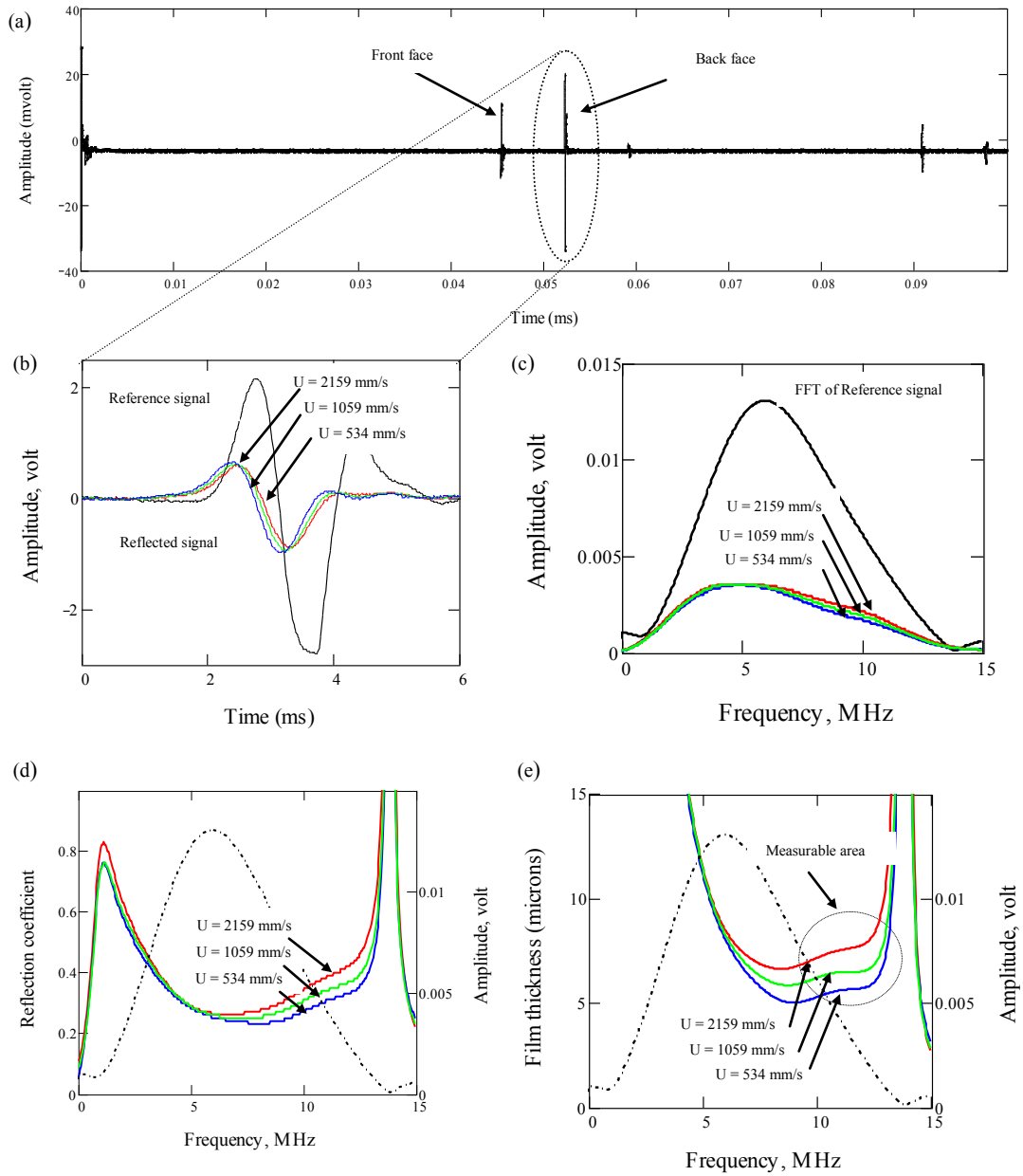

Figure 4.15 Sequence of digital signal processing steps (a) a typical waveform, (b) extracted peaks corresponding to the oil film, (c) FFT of the reflected peaks, (d) reflection coefficient spectra, (e) film thickness variation with frequency. The contact between Perspex and nitrile rubber ball.

The reflection coefficient is then used in Eq. 3.39 to determine the oil film thickness. This is performed for each pair of reflection coefficient and frequency data. The result is therefore a plot of the film thickness determined at each the constituent frequencies in the measurable area (Figure 4.15e). Clearly, the film thickness should not vary with measurement frequency and so a straight line would be expected. Figure 4.15e shows that at the higher frequencies (10 to 12 MHz as shown on the figure), this is the case and these frequencies are used for the measurement. As explained above a higher frequency implies that the focus spot size will be small and therefore more likely to fall fully within the contact region between the nitrile sphere and Perspex disc.

4.6 Measurement of speed of sound

In measurement of film thickness and contact using ultrasonic reflection, the speed of sound of two materials in contact and oil lubricant separated them must be accurately known. There are three methods to determine speed of sound of materials:

a. Time of flight (ToF)
b. Reflection of solid-liquid interface (RSL)
c. Reflection of solid-solid interface (RSS)

4.6.1 Time of flight (ToF)

To measure speed of sound of solid materials, the time-of-flight (ToF) method can be employed by measuring the time-of-flight between two reflections. Based on thickness of the material and round trip time of flight through the material, the speed of sound can be calculated as follows;

$$c = \frac{2T}{t} \tag{4.6}$$

where c is speed of sound, T is material thickness and t is time of flight.

There are two transducers that can be used to measure speed of sound of solid materials, which have high speed of sound velocity: contact and immersion focus transducers. For thick materials, the contact transducer could be attached directly

on the surface of the materials and the immersion focus transducer and a measured material are immersed in water simultaneously. For thin materials, contact transducer could be attached with a delay lines (as shown in Figure 4.16).

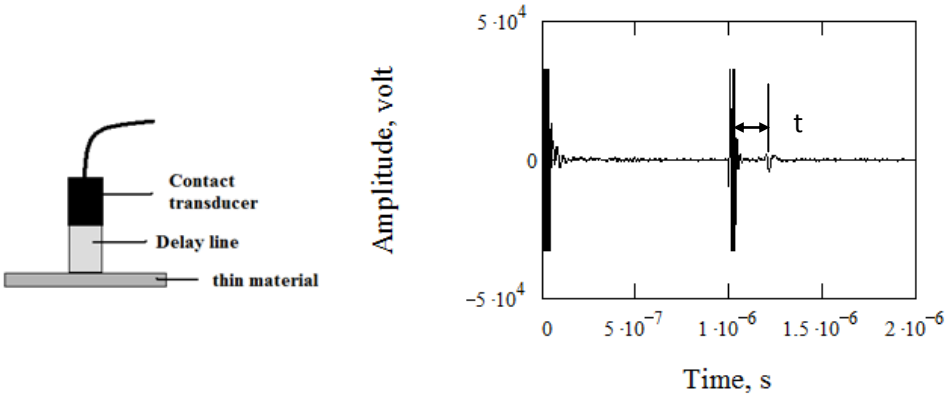

Figure 4.16 Schematic of ultrasonic transducer to measure acoustic impedance of thin material using a contact transducer.

4.6.2 Reflection of solid-liquid interface (RSL)

To measure speed of sound of liquid materials, such as a lubricant, the reflection of solid-liquid interface method can be employed. The principle of measurement can be seen in Figure 4.17. A 5 MHz focusing transducer is mounted perpendicular above Perspex disk, which is immersed in water bath. The capturing reflected signals are conducted in two stages: the first stage, Figure 4.17a, the capturing reflected signal without oil and the second stage, Figure 4.17b, with oil.

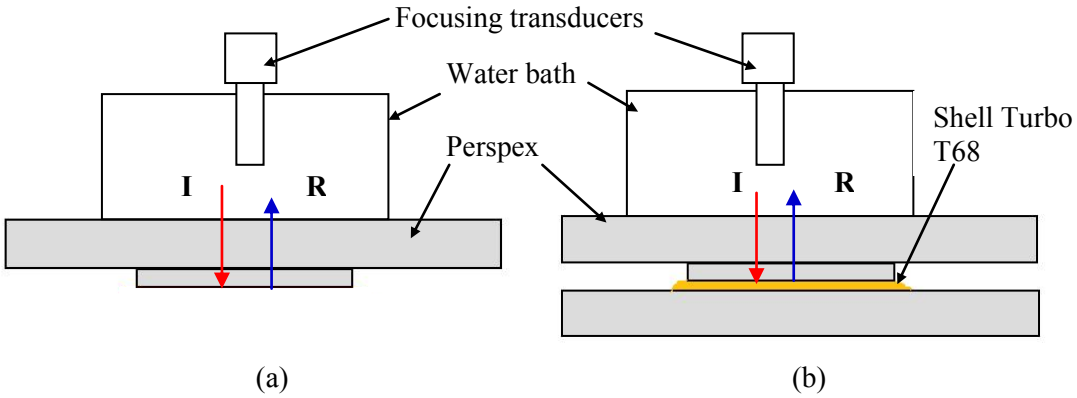

Figure 4.17 Principle of measurement of speed of sound of liquid materials of reflection of ultrasonic wave solid-liquid interface; (a) first stage and (b) second stage.

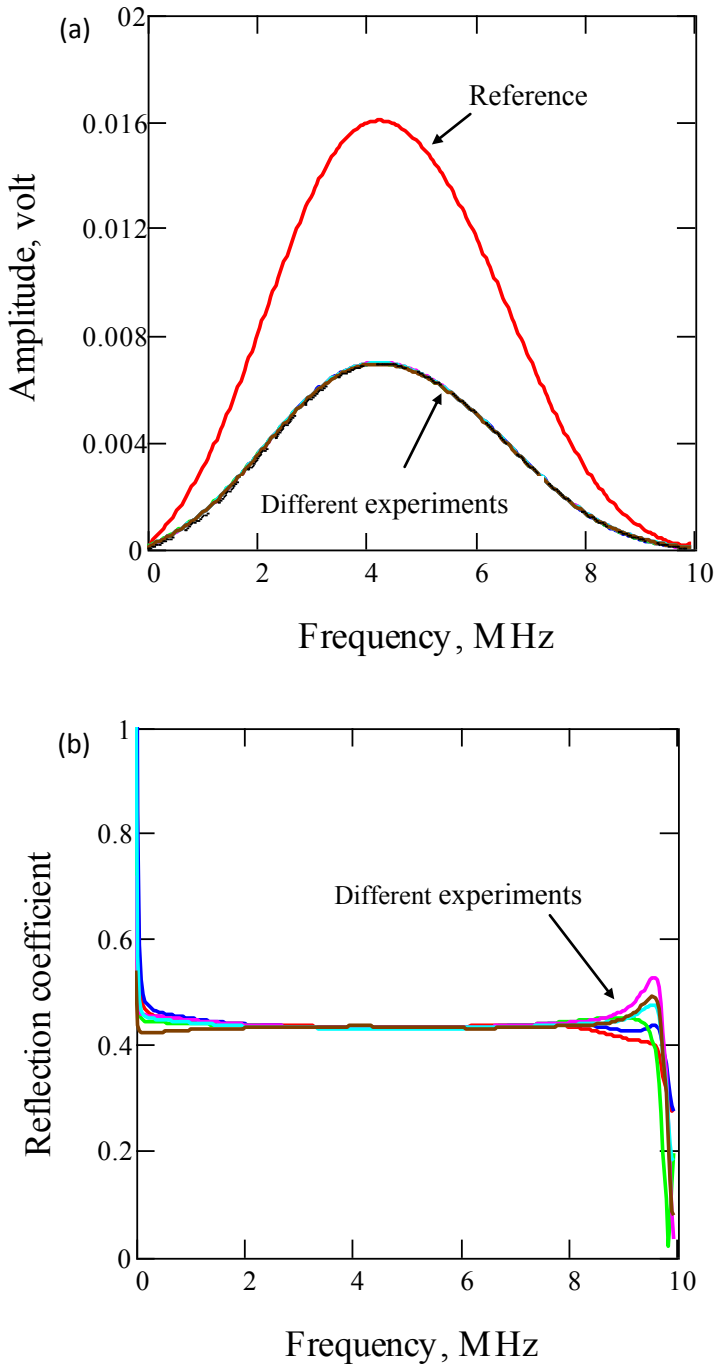

Figure 4.18 An FFT and reflection coefficient of reflected signals (Perspex and Shell Turbo T68).

The reflected signals that have captured were converted to FFT and reflection coefficient of each reflected signal was obtained by dividing by the FFT of reference signal (Figure 4.18). To determine the speed of sound of liquid, the Eq. 3.20 (case of perfectly bonded material) can be used where speed of sound and density of Perspex were known and density of the oil is needed as well.

4.6.3 Reflection of solid-solid interface (RSS)

For the materials that have low speed of sound, such as: rubber, plastic, and polymer, are difficult to measure their speed of sound. The thickness of these materials also would influence the result of measurement. If these materials are too thick, the ultrasonic signal would attenuate due to the viscoelastic effect. To get the speed of sound of these materials, the reflection of a solid-solid interface was used as shown in Figure 4.19. Prior to capture reflected signal from the contact when low modulus material was pressed against Perspex, the reference signal must be taken first by removing low modulus materials as shown in Figure 4.19b.

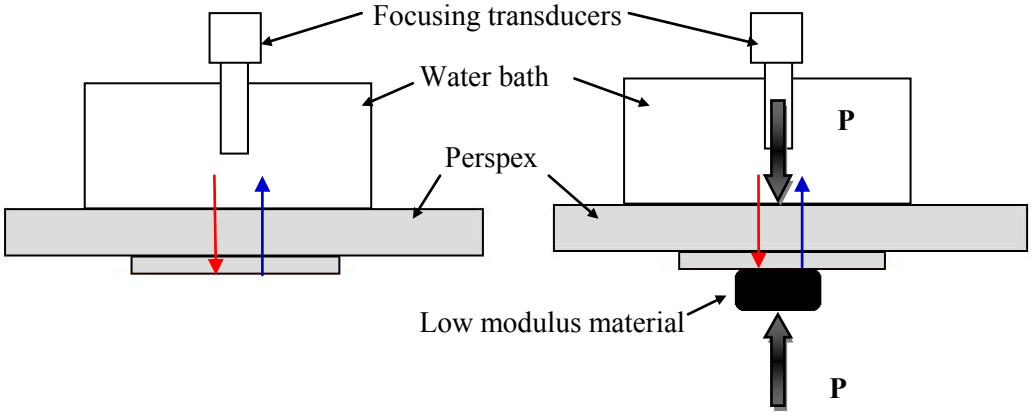

Figure 4.19 Principle of measurement of speed of sound of solid materials of reflection of ultrasonic wave from solid-solid interface: (a) first stage and (b) second stage.

Table 4.1 The results of measurement speed of sound of some materials.

No	Name of materials	Speed of sound (m/s)		
		ToF method	RSL method	RSS method
1	Perspex	2730	-	-
2	Steel	5900	-	-
3	PTFE	1391	-	-
4	Nitrile	1618	-	1648
5	Nylon6	1130	-	-
6	UHMWPE-N	2380	-	-
7	UHMWPE-B	2225	-	-
8	Shell Turbo T68	1460	1465	-
9	Nitrile cord	-	-	1890

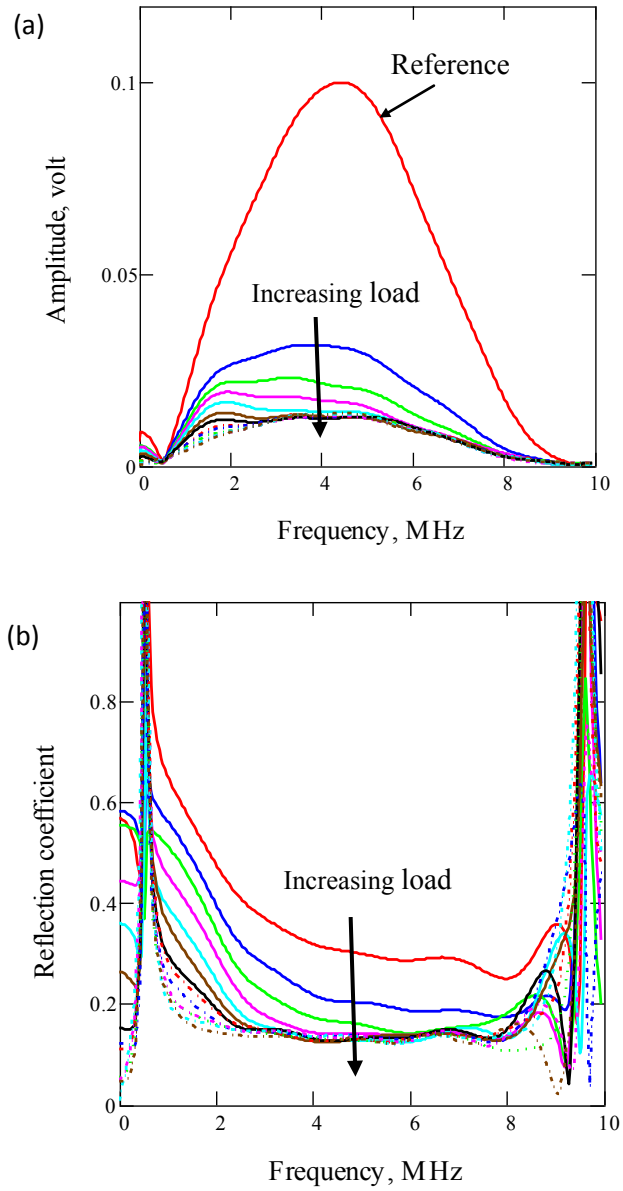

Figure 4.20 An FFT and reflection coefficient of reflected signals of contact between nitrile cord and Perspex.

The reflected signals that have been captured were converted to FFT and reflection coefficient spectrum of each reflected signal was obtained by dividing by the FFT of reference signal (Figure 4.20). To arrive the speed of sound of low modulus materials, the Eq. 3.20 (case of perfectly bonded material) was used where speed of sound and density of Perspex were known and the density of low modulus material was known as well. The results of measurement of speed of sound some materials using the methods above can be shown in Table 4.1. The error of speed of sound between ToF and RSL methods for Shell Turbo T68 was 0.34 per cent and between ToF and RSS methods for Nitrile ball was 1.85 per

cent. This is error due to difficulty to measure perfect contact happened. As shown in Figure 4.20, when the load was increased where there was no change of the amplitude of reflected signal, the perfect contact had obtained.

4.7 Conclusions

In this chapter, the ultrasonic apparatus, consisting of an ultrasonic transducer, an UPR, an oscilloscope, and a personal computer, have been explained their respective functions to get reflected signal from the layer. The steps of signal processing of reflected signal have described from captured signal to calculate oil film thickness using both amplitude and phase shift methods.

To get good and accurate results, the characteristic of ultrasonic focusing transducer must be understood. Their characteristics are focal spot diameter and focus length. The focal spot diameter is associated with the selection of focusing transducer. The ratio between focal spot diameter and contact diameter should be considered. When the diameter of focal spot is smaller than the contact area, then the spring model is valid and a satisfactory measurement can be made. The focal length is related to the accuracy of measurement. The correct focal length is important for the correct film thickness measurement.

Measurement of the speed of sound of the test materials is important in measuring film thickness by using the ultrasonic method. There are three methods that can be employed to measure speed of sound of materials: time of flight (ToF), reflection of solid-liquid interface (RSL), and reflection of solid-solid interface (RSS). For the materials that have low modulus elasticity, such as rubber and plastics, the reflection of solid-solid interface could be used. To measure speed of sound of liquid material, the reflection of solid-solid interface is a new and quick alternative. From the experiment, it shows that the error of speed of sound between ToF and RSL methods for Shell Turbo T68 was 0.34 per cent and between ToF and RSS methods for Nitrile ball was 1.85 per cent.

Chapter 5

Film thickness between two acoustically dissimilar materials

The measurement of oil film thickness between two acoustically dissimilar materials in contact is important for machine components like o-ring, lip seals, and metal on polymer prosthetic hip joints. This chapter explores the phase shift method to measure oil film thickness between two acoustically dissimilar materials when the amplitude method is difficult to apply because of the minimum reflection coefficient approaching 1. The result is discussed and then the proof of concept is presented.

5.1 Introduction

The bearing materials in machine elements fall into two major categories: metallic (babbitts, bronzes, aluminium alloys, porous metals, and metal overlays, such as silver and indium), and non metallic (plastics, rubber, ceramics, and metal oxides). The contact between two bearing materials could be metallic-metallic contact, non metallic-non metallic contact, and metallic-non metallic contact.

The measurement of film thickness by using ultrasonic reflection depends on the acoustic impedance between two materials in contact. When two materials are in contact, the minimum reflection coefficient depends upon acoustic impedance mismatch between two materials. Where each material has unique acoustic impedance, it varies from high to low acoustic impedance. It depends upon application in machine elements.

Heretofore, there are two methods that could be used to measure film thickness using ultrasonic reflection techniques: amplitude and phase shift. Both methods have been proved by Reddyhoff *et al.* [2005] not only for a static model of an oil film but also a rotating journal bearing using a contact transducer. The results are in a good agreement with independent assessments of the oil film thickness. In addition, the application of phase shift method has been employed by Allen and Cooper [1983] in measuring of residual stress in metal using ultrasonic impulse and also by Królikowski and Szczepek [1992] used phase shift of reflection coefficient of ultrasonic wave in the study of the contact interface.

Inspection of the spring model for ultrasonic reflection from a thin film between two dissimilar materials (Eq. 3.39) using amplitude method shows that *R* depends upon the two acoustic impedances, where they are identical and the range of measurements is $0 < R < 1$, when they are dissimilar and the range is $\left|\frac{z_1-z_2}{z_1+z_2}\right| < R < 1$. These if the materials have very different acoustic properties, $Z_1 << Z_2$, then $\left|\frac{z_1-z_2}{z_1+z_2}\right| \rightarrow 1$ and the measurement range is very small. Table 5.1 shows the minimum reflection coefficient between steel and other materials in contact. In practice, it is not possible to measure oil film thickness, for example between steel and rubber, because the range is $0.916 < R < 1$ (as shown in Table 5.1). If the upper and lower limits of measurement (as discussed on section 3.3.2) are applied, the minimum reflection coefficient will be $R = 0.968$.

The phase shift method, however, does not depend on the acoustic impedance mismatch in quite the same way as the amplitude method. It will be shown here for $Z_1 << Z_2$ and $Z_1 < Z_2$ (the first material lesser dense and less dense than the second material), the phase shift method can be used to calculate film thickness,

whereas the amplitude method fails. The shifted phase between the reflected wave and the incident wave when they are reflected will be explored as an oil film changes. In this chapter this phase shift is evaluated as an alternative means to measure oil film thickness for the special case where the first material is lesser dense and less dense than the second material ($Z_1 << Z_2$ and $Z_1 < Z_2$). In the spring model, there is a relationship between the shifted phases of reflected ultrasonic wave, frequency and the film properties.

Table 5.1 The variation of contact between steel and other materials against the minimum reflection coefficient.

Material 1	Material 2	Z_1 (MRayls)	Z_2 (MRayls)	$R = \frac{z_1 - z_2}{z_1 + z_2}$
Steel	Steel	45.63*	45.63*	0.000
Steel	Brass	45.63*	37.30**	0.100
Steel	Aluminium	45.63*	17.06**	0.456
Steel	Perspex	45.63*	3.22*	0.868
Steel	PTFE	45.63*	3.13*	0.872
Steel	Nylon-6	45.63*	2.21*	0.908
Steel	UHMWPE-N	45.63*	2.21*	0.908
Steel	UHMWPE-B	45.63*	2.07*	0.913
Steel	Nitrile	45.63*	2.04*	0.914
Steel	Rubber	45.63*	1.99**	0.916

*Experiment

**Data book

5.2 Limit of the spring model using amplitude methods

The range of measurement of oil film thickness by using amplitude method depends on acoustic impedance between two materials in contact as shown in Figures 5.1 to 5.5. In these figures the upper and lower limits are plotted using Eq. 3.39 based on maximum and minimum reflection coefficient as discussed in section 3.3.2 (R=0.05 and R=0.95, respectively). It will be noted from Figure 5.1 that the sensor with the lower frequency bandwidth will be able to measure film thickness from approximately 0.1 μm. The sensor with the higher frequency bandwidth will be able to measure film thickness from approximately 0.05 μm. This means that a sensor with a lower frequency will be able to measure a range

of thick films; otherwise, the sensor with the higher frequencies will be able to measure a range of thinner films.

Figures 5.1 and 5.3 show that the contacts between two materials having large acoustic impedance (Z_1 and Z_2 >>) can measure very thin film. However, the contact between two materials having low acoustic impedance (Z_1 and Z_2 <<) can measure very thick films as shown in Figures 5.2 and 5.4. The contacts between two materials having a small difference of acoustic impedance would give wide measurement range of film thickness. However, if the acoustic impedance mismatch is too great, it will result in a narrow range of measurable zone for film thickness as shown in Figure 5.5. It means that amplitude method cannot be used to measure film thickness for the contacts between two acoustically dissimilar materials.

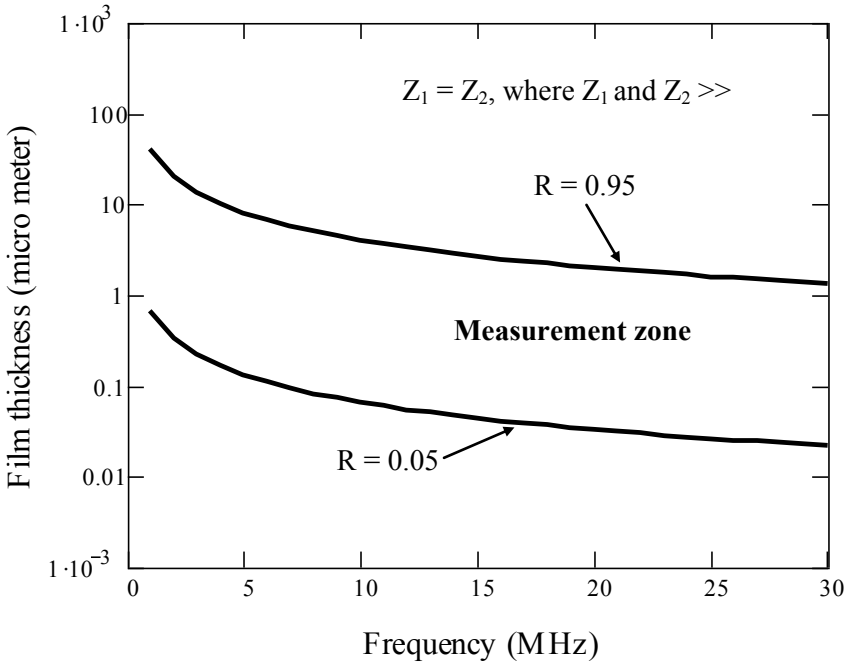

Figure 5.1 Measurement zone for both the first and second medium are acoustically the same and both acoustic impedances are high (Z_1= Z_2, where Z_1 and Z_2 >>) based on Eq. 3.39. Contact between steel and steel.

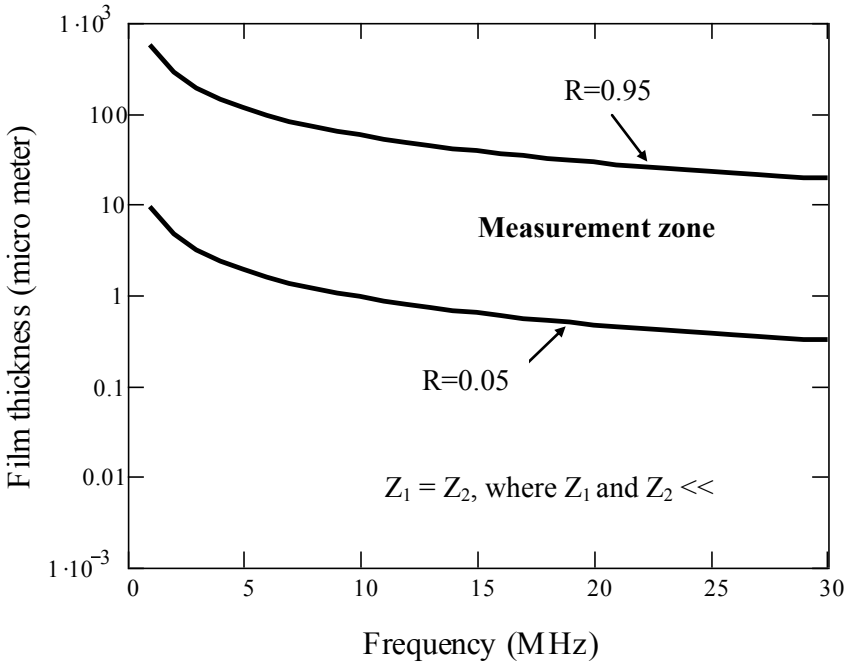

Figure 5.2 Measurement zone for both the first and second medium are acoustically the same and both acoustic impedances are low ($Z_1 = Z_2$, where Z_1 and Z_2 <<) based on Eq. 3.39. Contact between Perspex and Perspex.

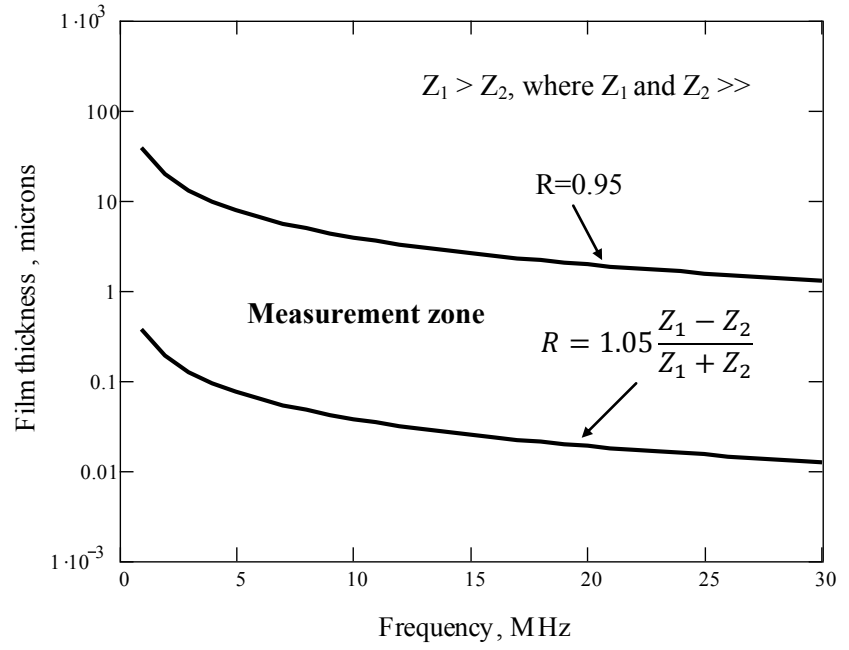

Figure 5.3 Measurement zone for the second medium is acoustically less dense that the first and both acoustic impedances are high ($Z_1 > Z_2$, where Z_1 and Z_2 >>) based on Eq. 3.39. Contact between Inconel and steel.

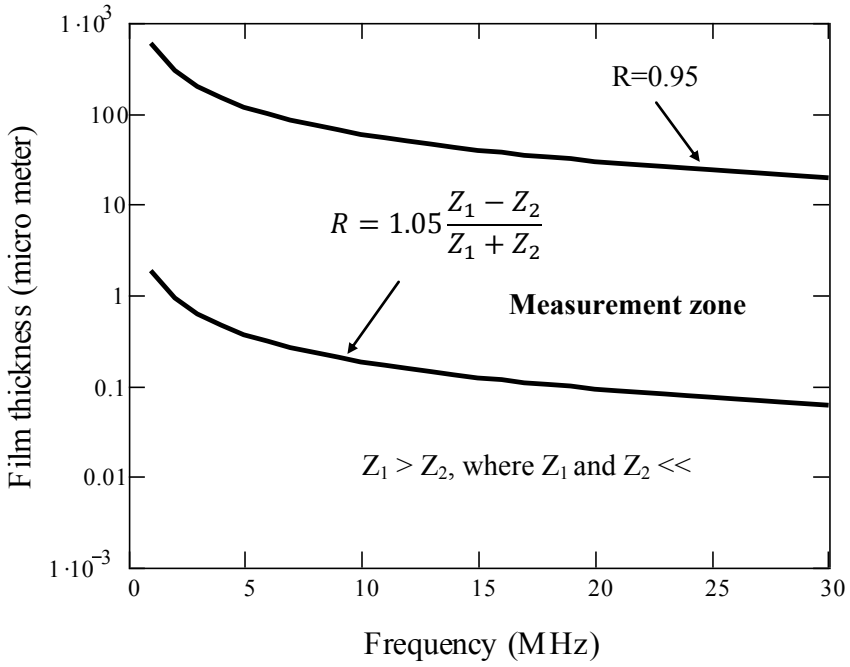

Figure 5.4 Measurement zone for the second medium is acoustically less dense that the first and both acoustic impedances are low ($Z_1 > Z_2$, where Z_1 and $Z_2 <<$) based on Eq. 3.39. Contact between Perspex and rubber)

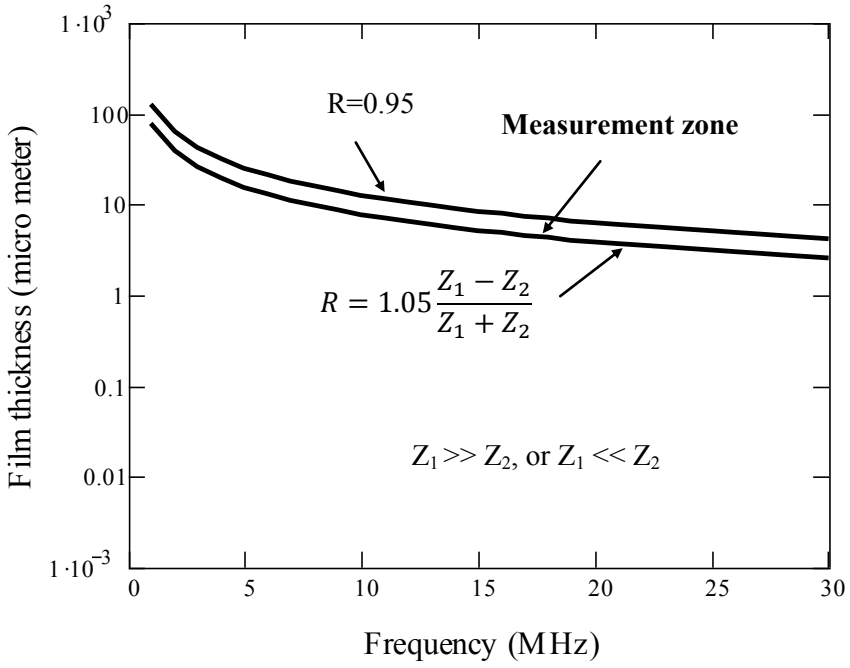

Figure 5.5 Measurement zone for the second medium is acoustically less dense that the first or vice versa ($Z_1 >> Z_2$ or $Z_1 << Z_2$) based on Eq. 3.39. Contact between steel and rubber.

5.3 Theoretical basis of the phase shift method

The reflection coefficient and phase difference vary for different film thicknesses. This can be seen from general equation of reflection coefficient in Eq. 3.37 that contains complex quantity phase and amplitude as restated in Eq. 5.1;

$$R = \frac{(z_1^2 - z_2^2) + z_1^2 z_2^2 (\omega / K)^2}{(z_1 + z_2)^2 + z_1^2 z_2^2 (\omega / K)^2} + i\left[\frac{2 z_1 z_2^2 (\omega / K)}{(z_1 + z_2)^2 + z_1^2 z_2^2 (\omega / K)^2}\right] \tag{5.1}$$

Eq. 5.1 can be separated into reflection coefficient and phase difference using an Argand diagram as stated in Eqs. 3.38 and 3.40 and restated in Eqs.5.2 and 5.3;

$$|R| = \sqrt{\frac{(\omega z_1 z_2)^2 + K^2 (z_1 - z_2)^2}{(\omega z_1 z_2)^2 + K^2 (z_1 + z_2)^2}} \tag{5.2}$$

$$\phi = \arctan\left(\frac{2 z_1 z_2^2 \left(\frac{\omega}{K}\right)}{\left(z_1^2 - z_2^2\right) + z_1^2 z_2^2 \left(\frac{\omega}{K}\right)^2}\right) \tag{5.3}$$

The reflection coefficient and phase difference in Eq. 5.1 can best be expressed by an Argand diagram where the real and imaginary part of the complex number R and phase difference angle ϕ are plotted in Figure 5.6. The reflection coefficient and phase difference angle of the wave were reflected from an interface where the film thickness was somewhere represented by point ***c*** would be given by R and ϕ. For a thick film, $\omega/K \rightarrow \infty$, total reflection and phase difference are obtained: $R = 1$ and $\phi = 0$, which is represented by a vector from the origin to point ***a***. For thin film, $\omega/K \rightarrow 0$, the reflection coefficient is dependent on the acoustic impedance between the two materials: $R = \frac{z_1 - z_2}{z_1 + z_2}$ and phase difference is zero ($\phi = 0$) which is represented by a vector from the origin to point ***b***. The value of ω/K varies from 0 to ∞ stated in the semicircle above real axis and from 0 to $-\infty$ stated in the semicircle below real axis.

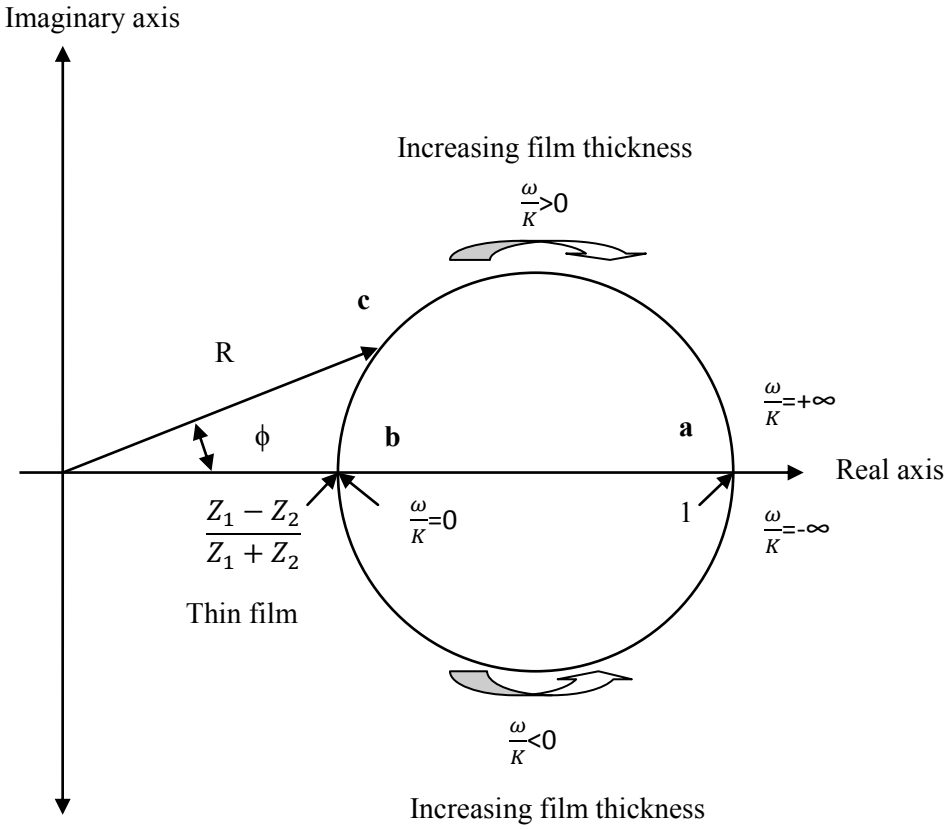

Figure 5.6 The reflection coefficient, *R*, and phase difference, ϕ, are a function of ω/K as shown in an Argand diagram for case of $Z_1 > Z_2$.

In Chapter 3 section 3.3, the theoretical method to calculate film thickness using both amplitude and phase shift methods was discussed. Eqs. 5.2 and 5.3 have been used to plot the relation between reflection coefficient or phase difference and frequency of transducer for different film thicknesses. In the bracket of Eq. 3.41 restated in Eq. 5.4, there are two signs, positive and negative. Each sign will give a measurement region for film thickness.

Positive and negative signs

$$h = \frac{\rho c^2 \left(z_1 z_2^2 \pm \sqrt{\left(z_1 z_2^2\right)^2 - \tan^2 \phi z_1^2 z_2^2 \left(z_1^2 - z_2^2\right)} \right)}{\omega \tan \phi z_1^2 z_2^2} \tag{5.4}$$

For the contact between two similar materials, there is no difference in the measurement zone between amplitude and phase shift methods. However, the contact occurred between two different materials (($Z_1 > Z_2$) or vice versa ($Z_1 <$

Z_2)), there is difference in the region of measurement between amplitude and phase shift methods. The region of measurement for phase method is wider than amplitude method as shown in Figures 3.13 and 3.15 (see Chapter 3 sections 3.3.2 and 3.3.3) for contact case between rubber and Perspex.

For contact between two acoustically dissimilar materials, there is difference in the measurement zone between two materials in contact where the first medium has an acoustic impedance less dense or more dense than the second ($Z_1 << Z_2$ or $Z_1 >> Z_2$). For the case of $Z_1 >> Z_2$, the phase shift method is fail as shown in Figures 5.7a, and 5.8a. Figure 5.7 shows a plot of Eq. 5.4 for various thickness oil films between two acoustically dissimilar materials where the first medium has acoustic impedance less dense than the second ($Z_1 << Z_2$). Whereas, Figure 5.8a is plotted based on Eq. 5.4 where the upper and lower limits of measurement are ϕ = 0.05. The phase difference and the area of measurement are small and impossible to measure oil film thickness. In contrast, for the case of $Z_1 << Z_2$, the phase shift method can be used to measure film thickness (Figures 5.7b and 5.8b). The phase difference is changed from minus to plus for low and high frequency as shown Figure 5.7b. The area of measurement is large as shown in Figure 5.8b where the upper and lower limits of measurement are ϕ = +0.05 and ϕ = -0.05, respectively.

In the case of $Z_1 > Z_2$ and $Z_1 >> Z_2$, the phase difference has two values for oil film as shown in Figures 5.6 and 5.7a. The film thickness will be thin or thick films depended on frequency of the transducer used (see Eq. 5.4). If the oil film is thin, the negative sign will be used in Eq. 5.4 and vice versa. In the experiment, due to the phase shift of signal in phase, it is difficult to determine thin and thick films. The best way is to check the frequency of the transducer, so the range of measurement oil film for each frequency of transducer can be determined using the Figure 5.7a or Eq. 5.4. The boundary between thin and thick films is also checked by using amplitude method for the case $Z_1 > Z_2$. If the value of R approaches $R = \frac{Z_1 - z_2}{z_1 + z_2}$, the oil film will be thin.

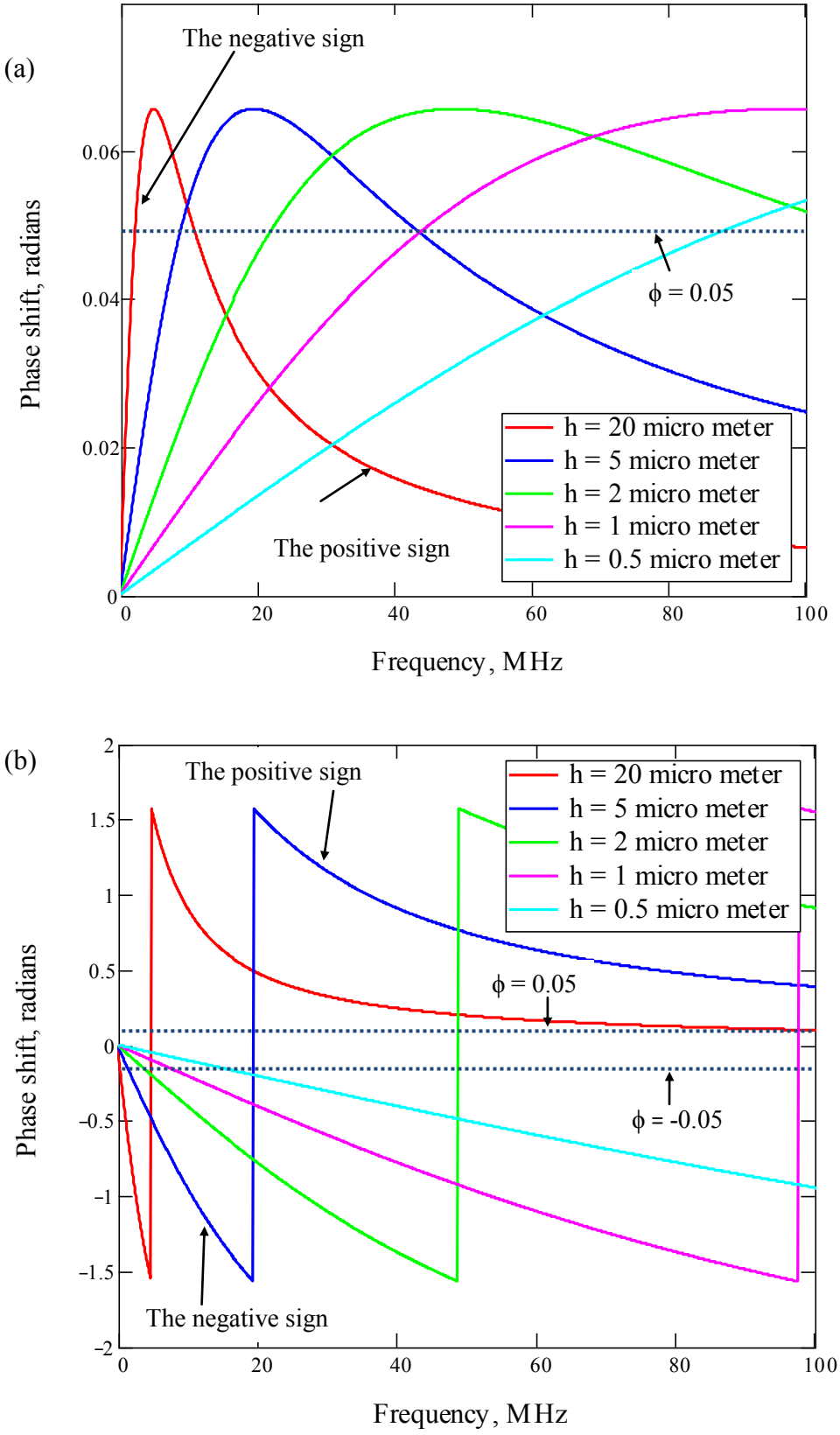

Figure 5.7 Comparison of phase shift for oil film between two different materials based on Eq. 5.4 where (a) the acoustic impedance of the first medium is acoustically more dense that the second ($Z_1 >> Z_2$) and (b) vice versa ($Z_1 << Z_2$). Where Z_1= 46 MRayls and Z_2= 3 MRayls.

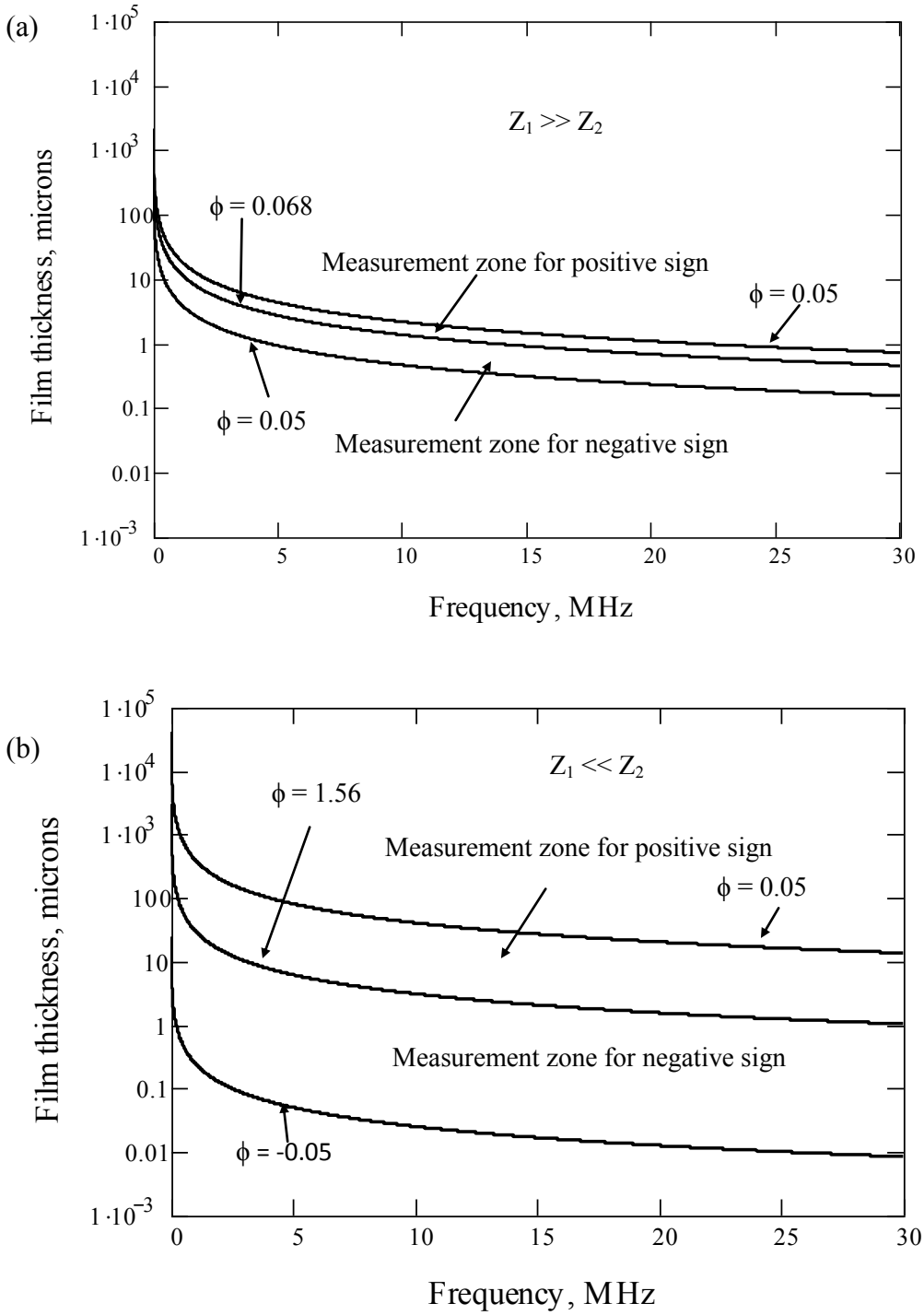

Figure 5.8 Comparison of measurement area of phase method for oil film between two different materials based on Eq. 5.4 where (a) the acoustic impedance of the first medium is acoustically more dense that the second ($Z_1 >> Z_2$) and (b) vice versa ($Z_1 << Z_2$). Where Z_1= 46 MRayls and Z_2= 3 MRayls.

The relationship between reflection coefficient and phase difference (Eq. 3.43) for different contact cases for measuring oil film thickness is plotted as Figure 5.9. This figure shows that the contact cases between steel-steel and Perspex-PTFE

can be employed for both methods. Table 5.2 shows the comparison between amplitude and phase shift methods in capability to measure film thickness. From this table, the contact case between steel and PTFE is difficult to apply the amplitude and phase shift methods due to $R \rightarrow 1$ and $\phi \rightarrow 0$, otherwise for contact case between PTFE and steel, the phase shift method can be used. The range of phase difference is from 0 to $\pi/2$. It also shows that phase shift method is superior than the amplitude method.

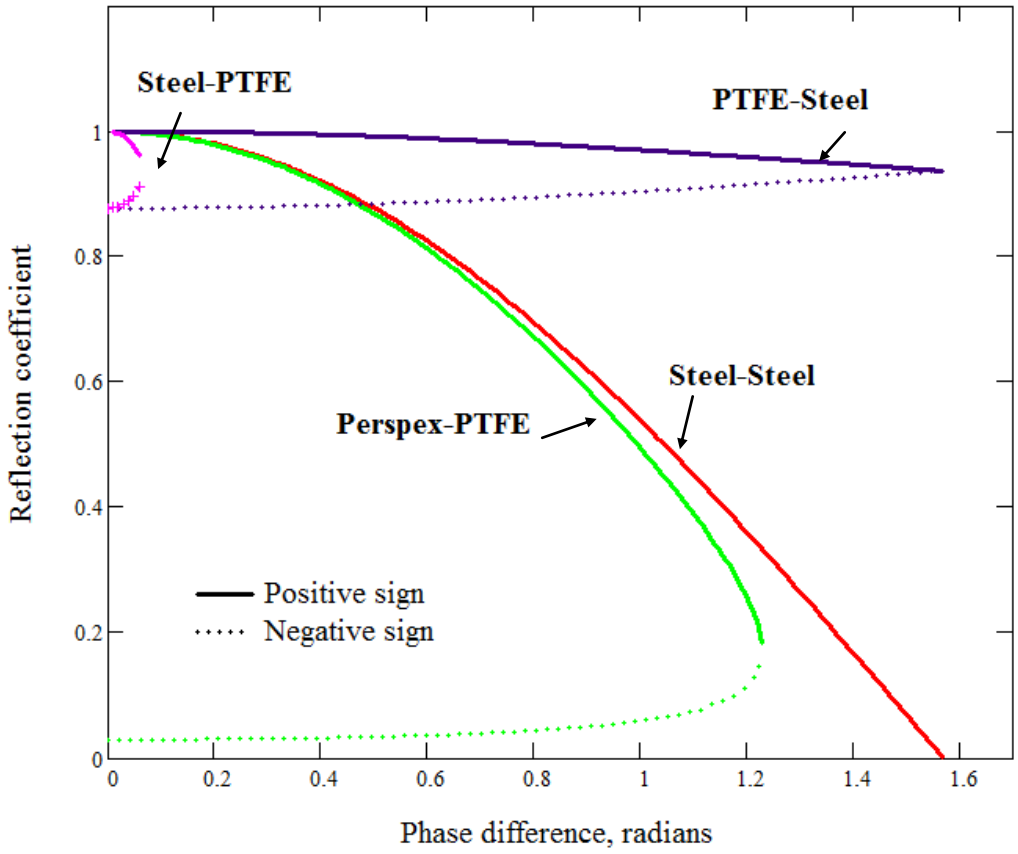

Figure 5.9 Relationship between reflection coefficient and phase difference for several contact materials based on Eqs. 3.42 and 3.43.

Table 5.2 Comparison between amplitude and phase shift methods for several contact materials in capability to measure film thickness.

Contact 1	Contact 2	Amplitude method (R – method)	Phase shift method (Φ – method)
Steel	Steel	√	√
Steel	PTFE	x	x
PTFE	Steel	x	√
Perspex	PTFE	√	√

5.4 The relationship between film thickness, reflection coefficient, and phase difference

Figure 5.10 shows an Argand diagram for several different materials in contact, the frequency of transducer from 0 to 50 MHz and an oil film thickness of 20 μm. From the diagram (Figure 5.10), there are three possibilities that should be considered. They are;

a. For the case of identical material ($Z_1 = Z_2$), red curve, the reflection coefficient amplitude increases from to 1 and the phase difference varies from 0 for a thick film ($K \rightarrow \infty$), to $\pi/2$ for a thin film ($K \rightarrow 0$). The incident wave and reflected wave for the thin film are positive out-of phase.
b. For the case of the first medium is acoustically more dense and greater than the second ($Z_1 > Z_2$ and $Z_1 >> Z_2$), yellow and blue curves. The phase difference varies from 0 to Eq. 3.40 and back to 0 for a thick, moderate and thin film, respectively. The incident wave and reflected wave for thin film are positive out-of phase. The value of phase difference has two values for oil film thickness, thin and thick films. To indicate these values, Eq. 5.4 can be used because in the bracket of Eq. 5.4 has negative and positive signs. The negative sign is for thin films.
c. For the case of the first medium is acoustically less dense and lesser than the second ($Z_1 < Z_2$ and $Z_1 << Z_2$), sky blue and green curves. The phase difference varies from 0 to $\pi/2$ and π for a thick, moderate, and thin film, respectively. The values of phase difference could be negative and positive. If the phase is negative, the incident wave and reflected wave for thin film are negative out-of phase.

Figure 5.11 shows schematically the phase difference and amplitude reduction between an incident and reflected waves between two materials where the first medium is acoustically dissimilar materials less dense and lesser than the second ($Z_1 < Z_2$ and $Z_1 << Z_2$). There is no change of phase difference for thick films but there is a little change of amplitude between an incident and reflected waves. The phase difference is in-phase until it reaches moderate films and then it is changed to be out-of phase when it reaches thin films.

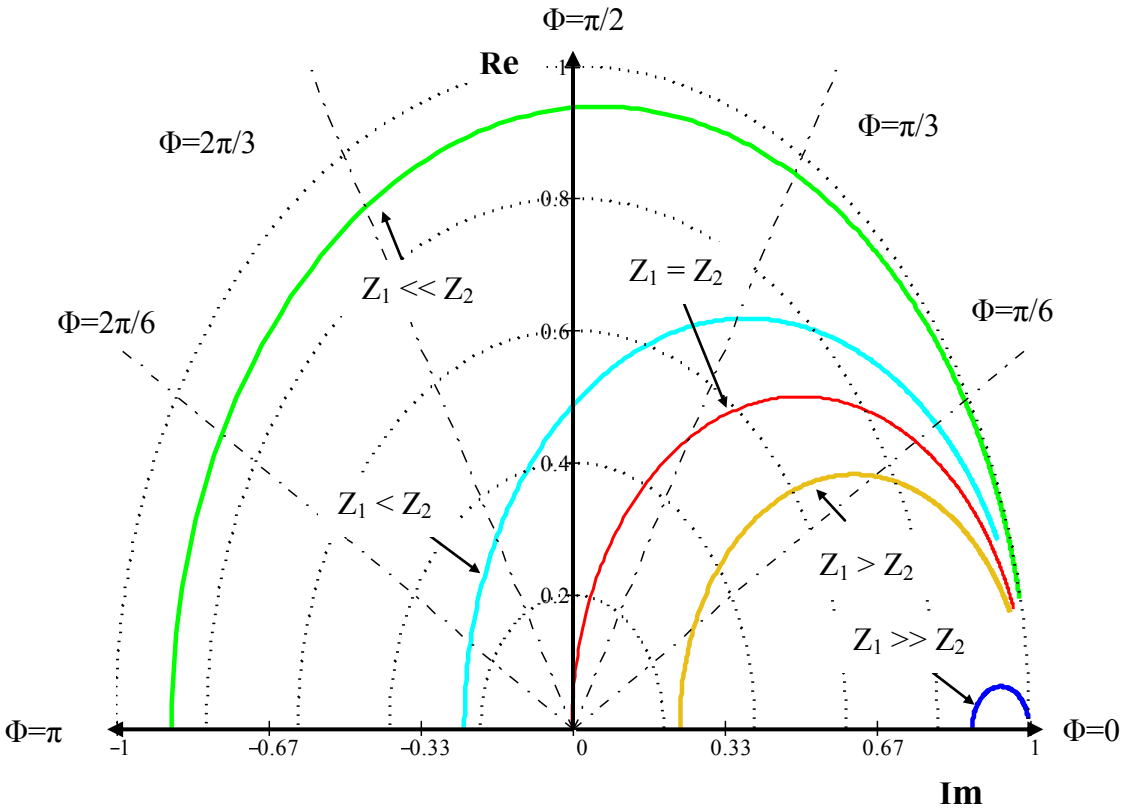

Figure 5.10 Complex reflection coefficient of wave reflected from layers for contacts of different acoustic impedance of materials on an Argand diagram for frequency of transducer from 0 to 50 MHz with film thickness of 20 μm.

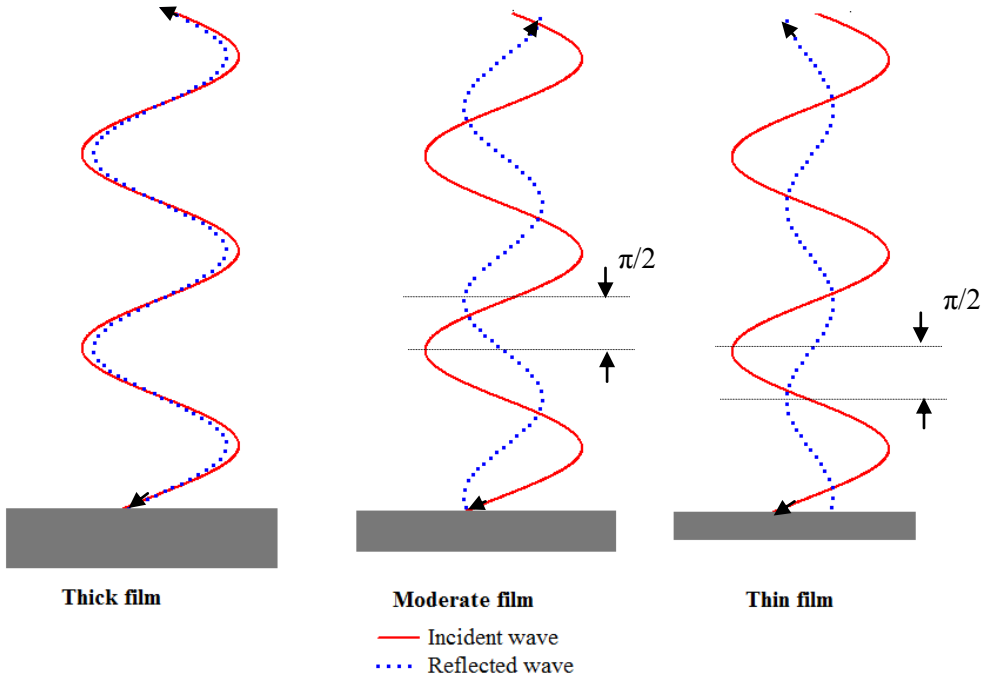

Figure 5.11 Schematic representation of the phase difference and amplitude reduction between an incident (red) and reflected waves (dashed blue) at in-phase for (a) thick film and (b) moderate film and out-phase for (c) thin film for $Z_1 < Z_2$ and $Z_1 << Z_2$.

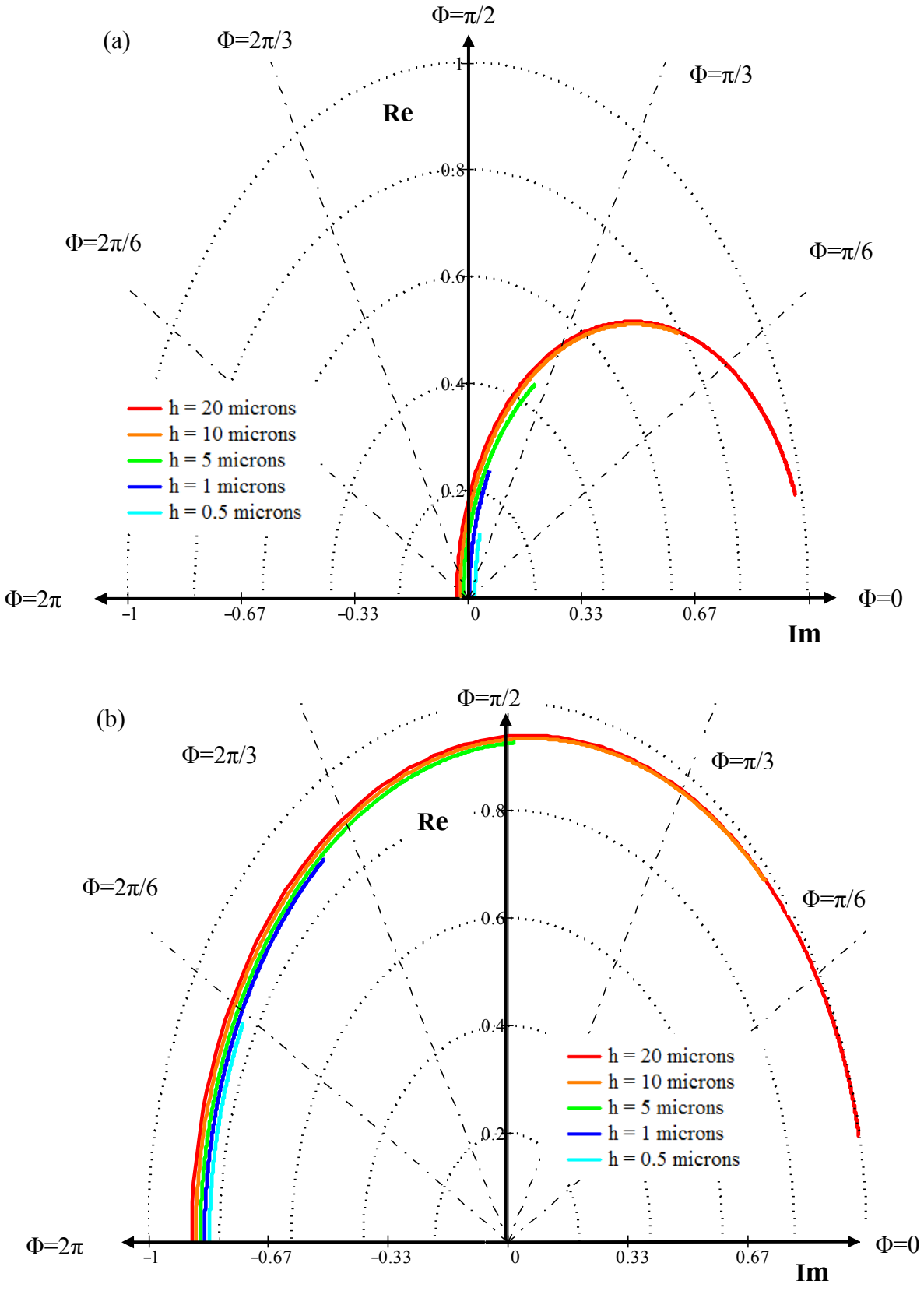

Figure 5.12 Complex reflection coefficient of wave reflected from layers between (a) PTFE and Perspex and (b) PTFE and steel for frequency of transducer from 0 to 50 MHz with different film thicknesses.

The relationship between film thickness, reflection coefficient, and phase difference in an Argand diagram shows in Figure 5.12. Contacts between PTFE-Perspex (Figure 5.12a) and PTFE – steel (Figure 5.12b) are plotted for frequency of transducer from 0 to 50 MHz. In this figure, the measurement of thick film, such as: 20 μm (red curve), is difficult to measure by using amplitude method for high frequency transducer, because the reflection coefficient approaches 1. It is clearly seen in Figure 5.12b contact between PTFE and steel that the red line coincides with the line of reflection coefficient equal to 1.

In the case of thin film, 0.5 μm (light blue curve, Figure 5.12b), the phase difference is greater than 90^0 for contact between PTFE and steel. It means that there is a changed phase from thick film to thin film and the phase shift of reflected signal is out of phase between thick and thin films.

5.5 Materials and experimental procedure

5.5.1 Materials and test specimens

To prove that phase shift method could be employed to measure film thickness between acoustically dissimilar materials, the experiments were carried out on three different contact cases: Perspex-Perspex, Perspex-PTFE, and Perspex-steel. The purpose of Perspex-Perspex contact was to prove that there were no differences of the measurement of film thickness for both methods: amplitude and phase shift methods. The Perspex-PTFE contact was used to show that the measurement of oil film thickness between Perspex and steel could be used phase shift method.

The dimension of each specimen is 95 x 95 mm width and length and 15 mm thick. The dimension of contact area is made in such a way with dimension 20 mm x 20 mm width and length to keep that the surface of contact is flat as shown in Figure 5.13. The Shell Turbo T68 was used as lubricant.

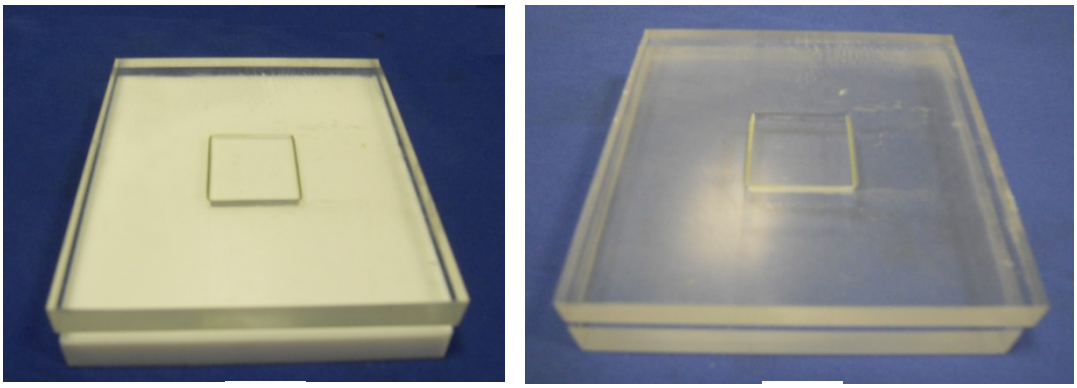

(a) (b)

Figure 5.13 Photograph of specimens used in the experiment; (a) Perspex-PTFE and (b) Perspex-Perspex

5.5.2 Test apparatus

A photograph of test rig is shown in Figure 5.14 where the contact cases (Perspex-Perspex, Perspex-PTFE, and Perspex-Steel) were pressed together with mineral oil applied in contact using hydraulic pressure. The variation of film thickness was controlled by force from hydraulic pressure. A 5 MHz ultrasonic immersion transducer, which was immersed in water bath, was located above the bearing such that it could send and receive pulses perpendicular to the oil film.

An ultrasonic pulser-receiver (UPR) was controlled by PC to drive the transducer. The UPR generated a series of short duration voltage pulses. The piezoelectric element was resonated due to the pulses, thus sending the required ultrasonic pulse through the medium. The element operated in pulse echo mode and, therefore, received reflection back from the oil film. Reflected pulses were digitized in PC. The PC performed the signal processing and displayed with software written in the LabView environment. The schematic diagram of the setup used in this study is shown in Figure 5.15.

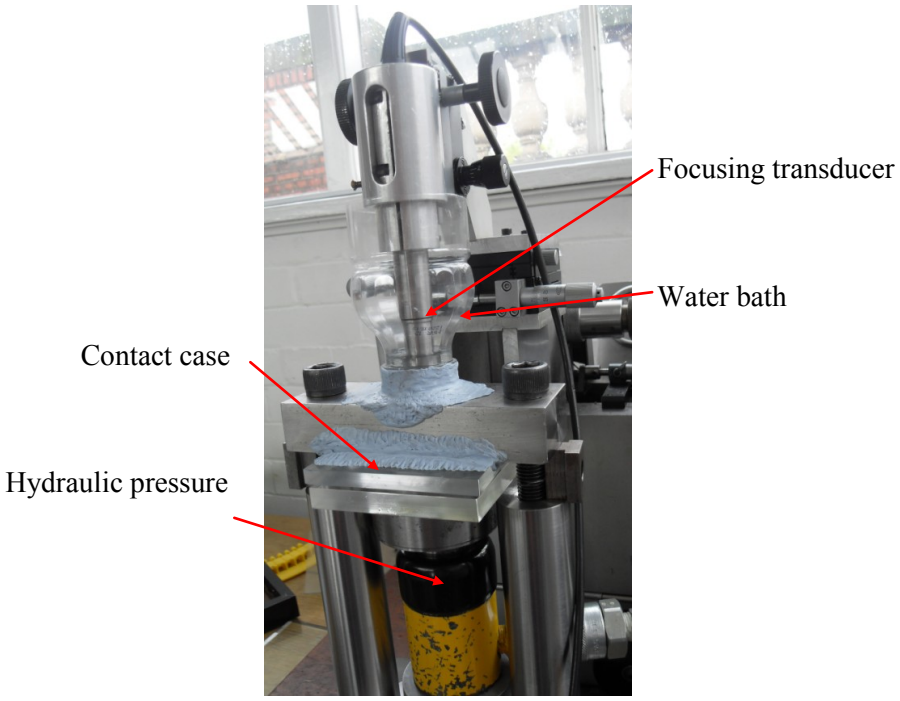

Figure 5.14 Photograph of the test rig to determine film thickness using phase shift method.

The reference signal was recorded first by removing oil layer from the surface contact. A measurement of the reflection was then made from the interface between Perspex plate and the air where the reflected signal will be equal to the incident signal (Figure 4.14a). This reference signal was converted to amplitude and phase spectrums by using an FFT, which were stored as references for later use.

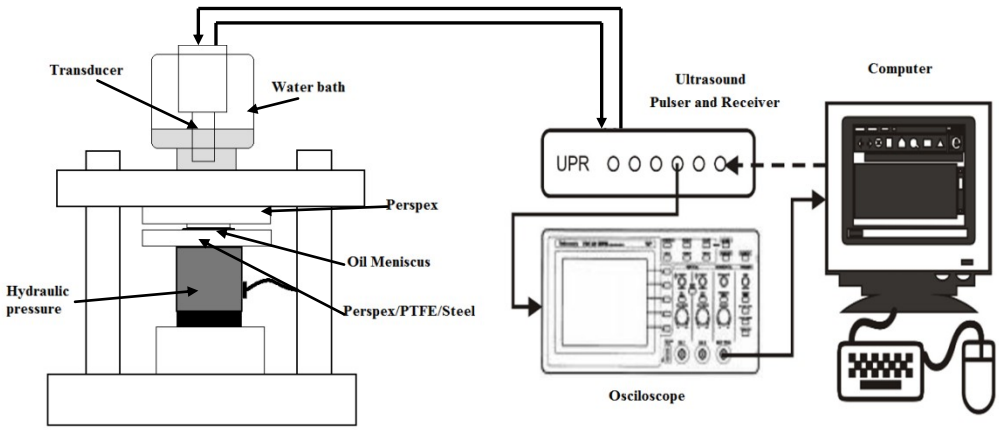

Figure 5.15 Schematic diagram of test rig to determine film thickness using phase shift method.

The contact cases between Perspex-Perspex, Perspex-PTFE, and Perspex-steel were reassembled and reflected pulses were captured and stored for different loads. Each reflected signal from the top and the bottom of Perspex plate was converted from time domain to frequency domain using an FFT.

The fast Fourier transformation of reflected signal in the frequency domain contains both amplitude and phase information. The reflection coefficient spectrum, $R(f)$, is the ratio of the amplitude spectrum from the oil film and the reference amplitude spectrum. The phase difference spectrum, $\phi_R(f)$, is subtraction from the phase spectrum from the oil film and the reference phase spectrum. To determine film thickness, the reflection coefficient and phase difference spectra can then be used in Eqs. 3.39 and 3.41, respectively.

5.5.3 Measuring phase difference

To understand phase shift methods, it is helpful to consider the reflection, transmission and incidence wave at various interface combinations (such as: water-Perspex, Perspex-oil, and oil-steel). The time shift of reflected signal from the top and the bottom of the Perspex plate also must be considered. As it can be seen in Figure 5.16a, the reflected signal from the thick film is shown that the amplitude of reflected signal (b) is reduced but there is no time shift. When there is a combination of reflected signals in the interface (Perspex-oil and oil-Perspex), there is the time shift of reflected signals in the top and the bottom of the Perspex plate as shown in Figure 15.16b due to loading. The load causes a slight deflection of the plate and the result is the Perspex front face moving toward the sensor slightly. If the film thickness is thin, the amplitude of reflected signal is reduced and the time shift of reflected signals in the top and the bottom of Perspex plate is increased.

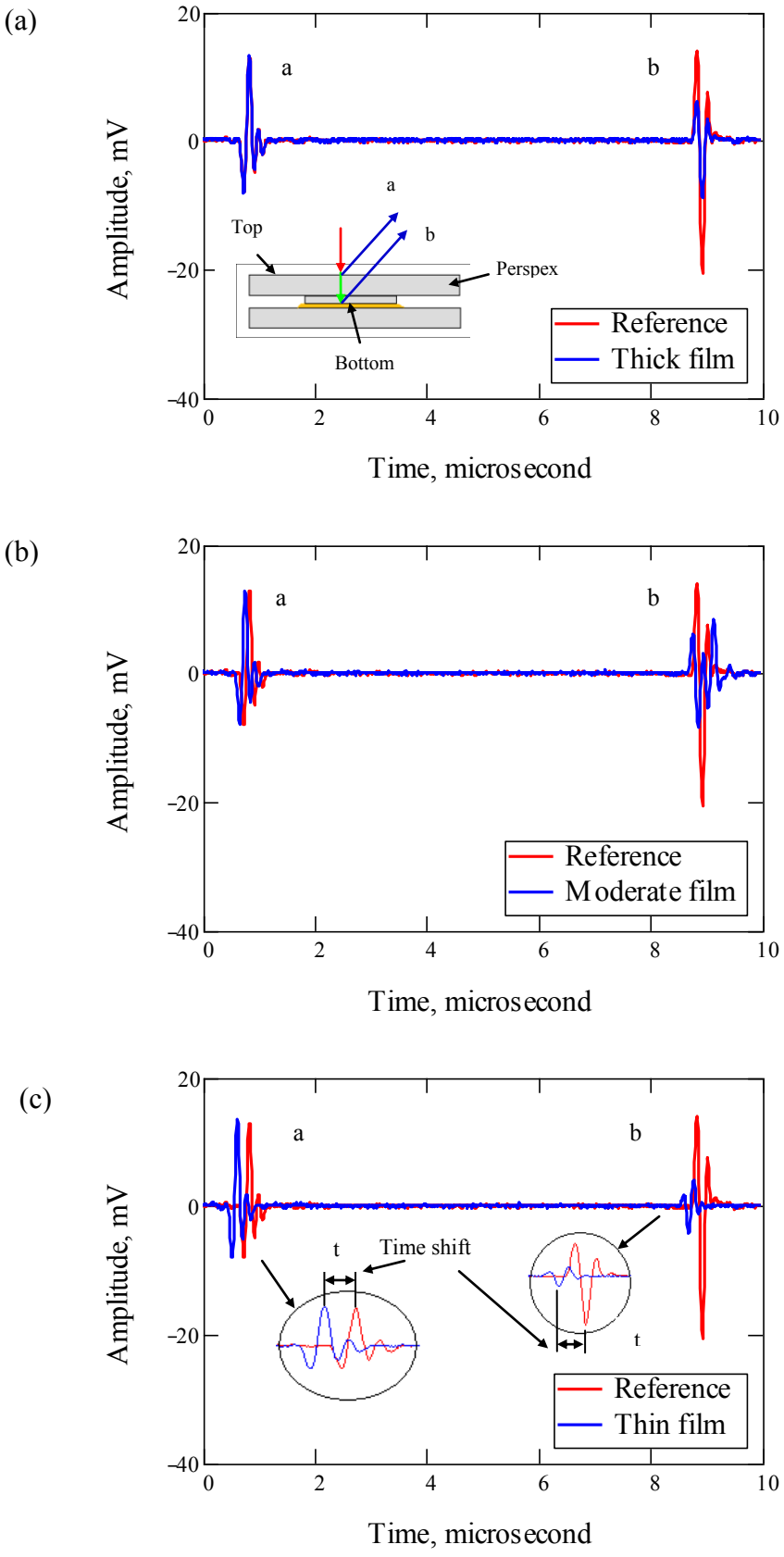

Figure 5.16 Reflected signal from the top and the bottom of Perspex for three conditions: (a) very thick film, (b) moderate film and (c) thin film.

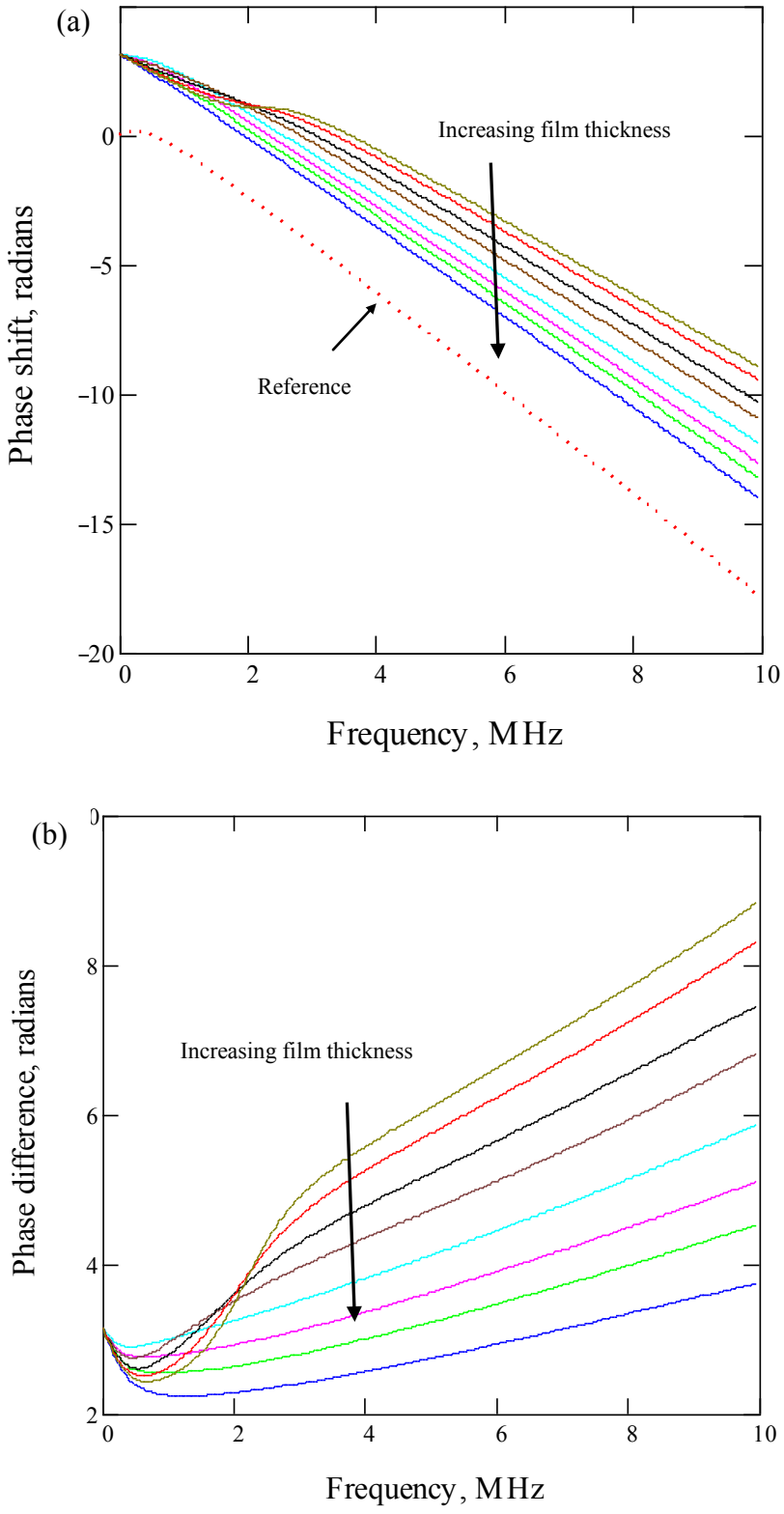

Figure 5.17 (a) The phase shift and (b) phase difference of reflected signal from the bottom surface of Perspex for contact case Perspex-Perspex.

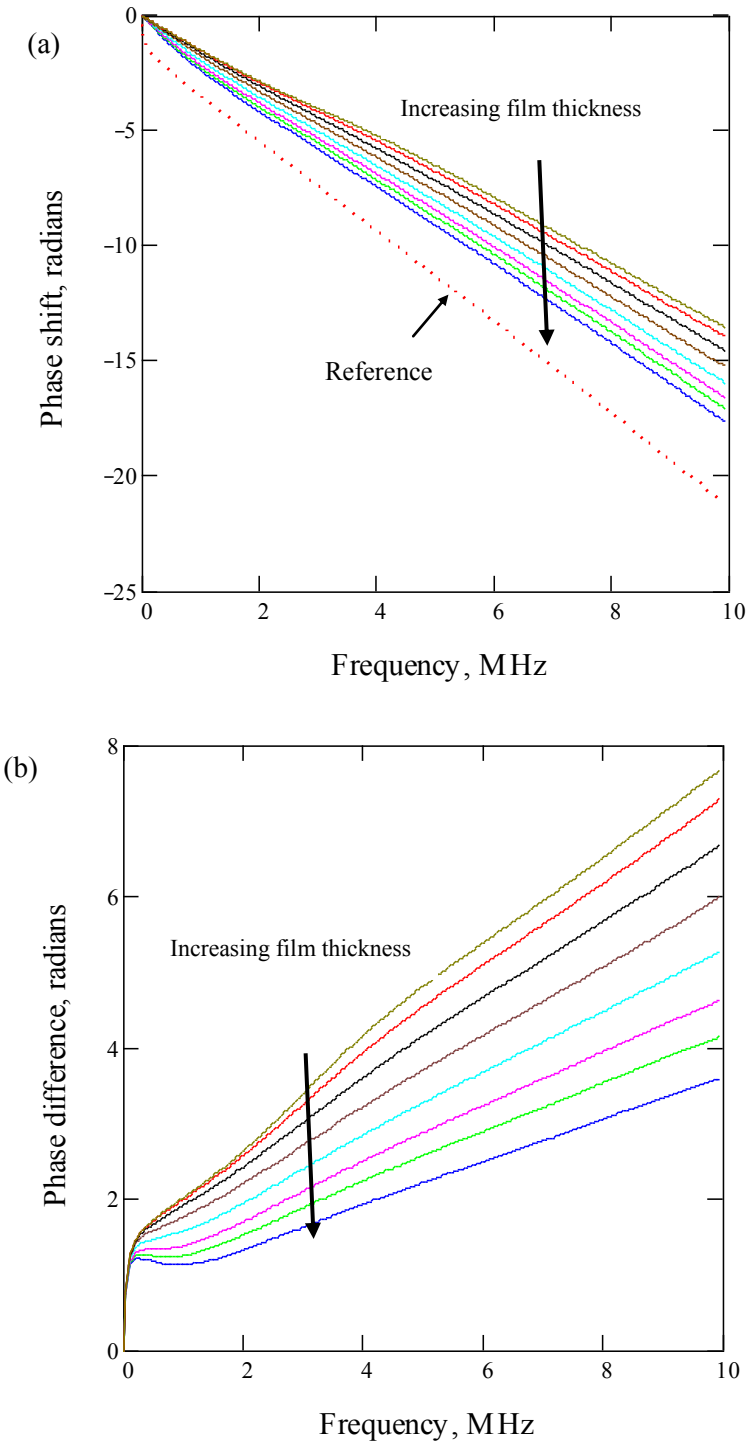

Figure 5.18 (a) The phase shift and (b) phase difference of reflected signal from the top surface of Perspex for contact case Perspex-Perspex.

Because the time shift of reflected signals occurred in the top and the bottom of the Perspex plate due to loading, the measurements of phase difference were carried out in a two-stage measuring procedure. In the first stage, the measurements of reflected signal were taken from the top surface of Perspex plate

and the second stage was measurement of the reflected signal from the bottom of Perspex plate and then the reflected signal from the top and bottom of Perspex plate was converted to phase shift spectrum using an FFT.

For contact case Perspex-Perspex, the phase shifts from top and bottom of Perspex are shown in Figures 5.17a and 5.18a, respectively. The nature of the phase plots is due to the fact that the phase changes continuously with frequency.

Each of phase difference of the top and the bottom surfaces of Perspex plate for contact case Perspex-Perspex was obtained by subtracting each of phase shifts of reflected pulse spectrum of top and bottom surfaces from each of phase shift of reference spectrum of top and bottom surfaces using Eq. 4.5 as shown in Figures 5.17b and 5.18b. To get the final phase difference due to thickness of the oil film, the phase difference of reflected pulse spectrum from the bottom surface was subtracted by the phase difference of reflected signal spectrum from the top surface (the results can be seen in Figures 5.21a, 5.23a, and 5.24 in section 5.6).

5.6 Experimental results

5.6.1 Time shift and changed shape of reflected signal

Figure 5.19 shows the time domain plot of the reflected pulse from a series of oil films for three contact cases: Perspex-Perspex (Fig. 5.19a), Perspex-PTFE (Fig. 5.19b), and Perspex-Steel (Fig. 5.19c). A reference signal reflected from a glass-air interface is compared with subsequent signal reflected from varying oil film thicknesses.

The presence of the oil film between two materials in the contact has two effects on reflected signal. The firstly, the amplitude of the reflected signal was reduced for the contact cases, Perspex-Perspex and Perspex-PTFE, and increased in the contact case, Perspex-Steel. The secondly, the phase of the reflected signal changed the lateral position of the first peak of reference signal.

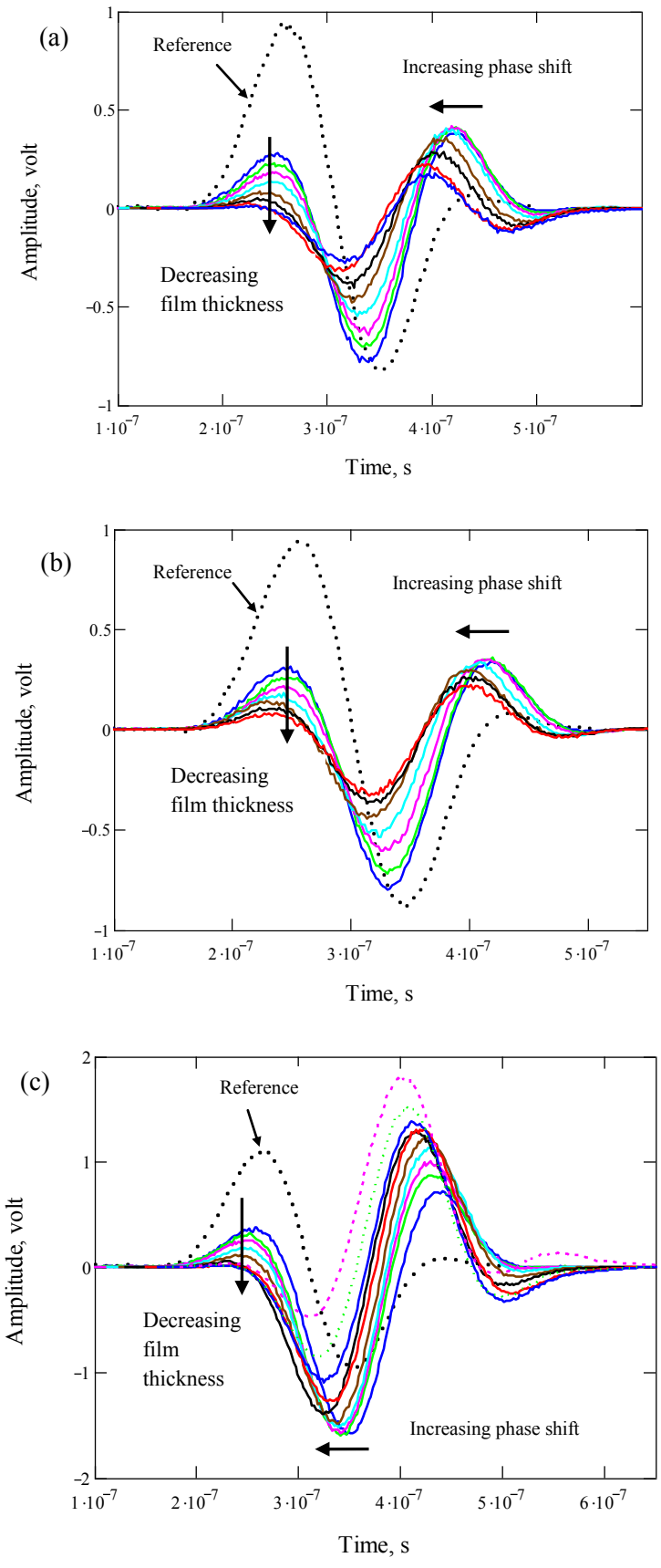

Figure 5.19 Reflected signal from static oil film between (a) Perspex-Perspex plate, (b) Perspex-PTFE, and (c) Perspex-Steel. As the film thickness increases, the amplitude of the pulse reduces and the phase shift increases.

From Figure 5.19c, there are some changes of reflected signal for the contact between Perspex and Steel, where amplitude of reflected signal increases for the thick film and then changes the shape of the signal for the thin film. It means that the phase of reflected signal changes from thick film to thin film. It can be seen in Figure 5.19c where the dash line pink and the dot line green show a change in the phase of the reflected signal.

5.6.2 Contact case 1: Perspex and Perspex

Figure 5.20 shows the reflection coefficient and film thickness for the reflected signal of Figure 5.19a (Perspex-Perspex contact case) from a series of oil film thickness using amplitude method. The reflection coefficient increases with the increased frequency and the calculated film thickness is flat in the range of the bandwidth of the transducer. The flatness of calculated film thickness in the bandwidth area is decreased with the increased oil film thickness. The oil film becomes thicker; it is difficult to get the expected flat calculated film thickness.

In the phase methods, a phase shift FFT of reflected signal from Figure 5.19a can be seen in Figure 5.21. The phase shift is reduced with the increased frequency; this is match with the theoretical study from Eq. 3.40 as shown in Figure 5.7. The film thickness plot as shown in Figure 5.21b is flat in the bandwidth area. The thicker film thicknesses in phase method are larger than amplitude method.

5.6.3 Contact case 2: Perspex and PTFE

The acoustic impedance of Perspex and PTFE is similar (3.2 and 3.13 MRays, respectively). Figure 5.22 shows the reflection coefficient and film thickness spectrums for contact between Perspex and PTFE in a series of film thickness. This figure follows the theoretical equation 3.39 where reflection coefficient increases with increased frequency and film thickness is flat in the range of bandwidth of the transducer. The comparison of film thickness between two methods (Figures 5.22b and 5.23b) shows that the phase shift method gives a result corresponded to the amplitude method.

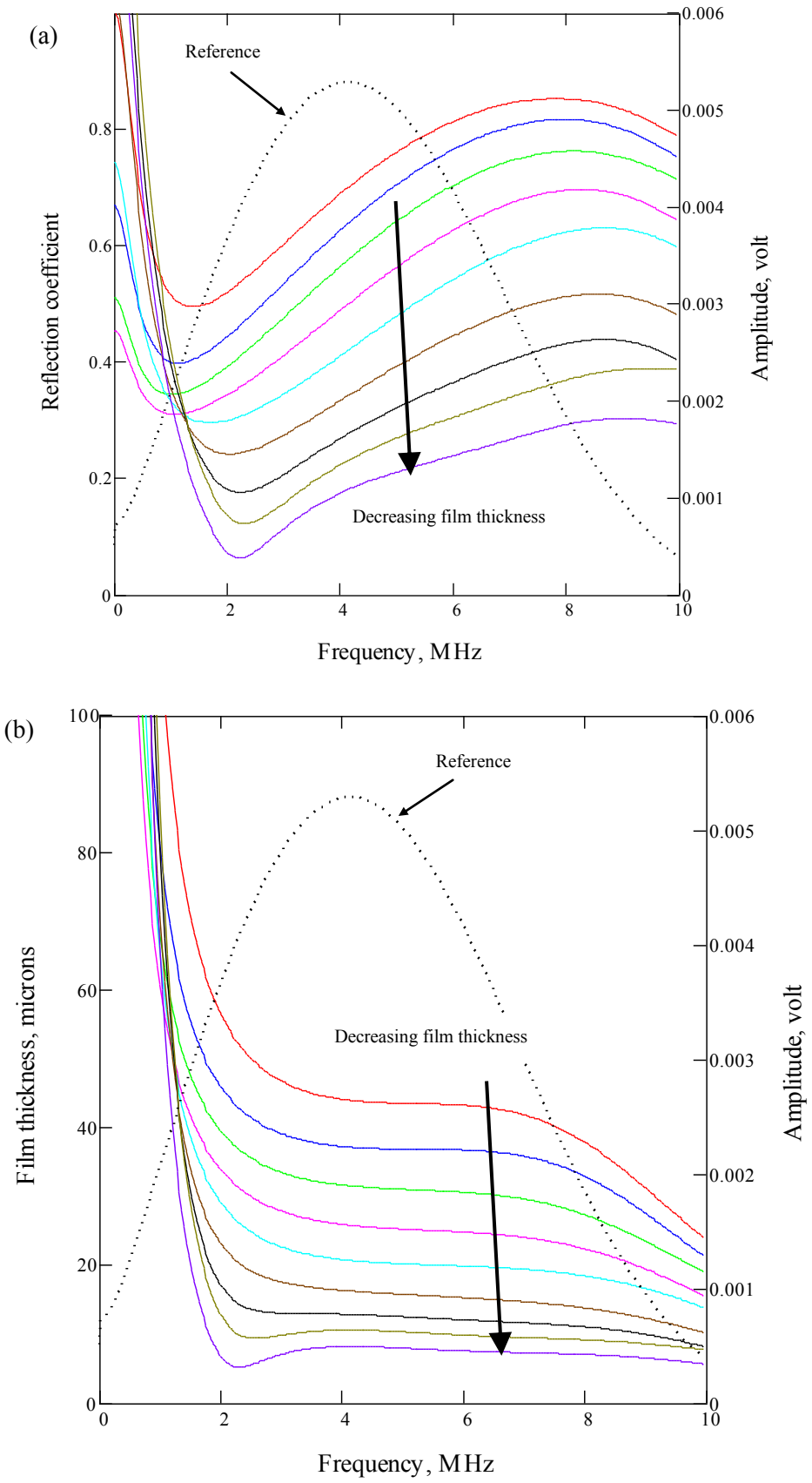

Figure 5.20 Variation of reflection coefficient (a) and film thickness (b) contact between Perspex and Perspex.

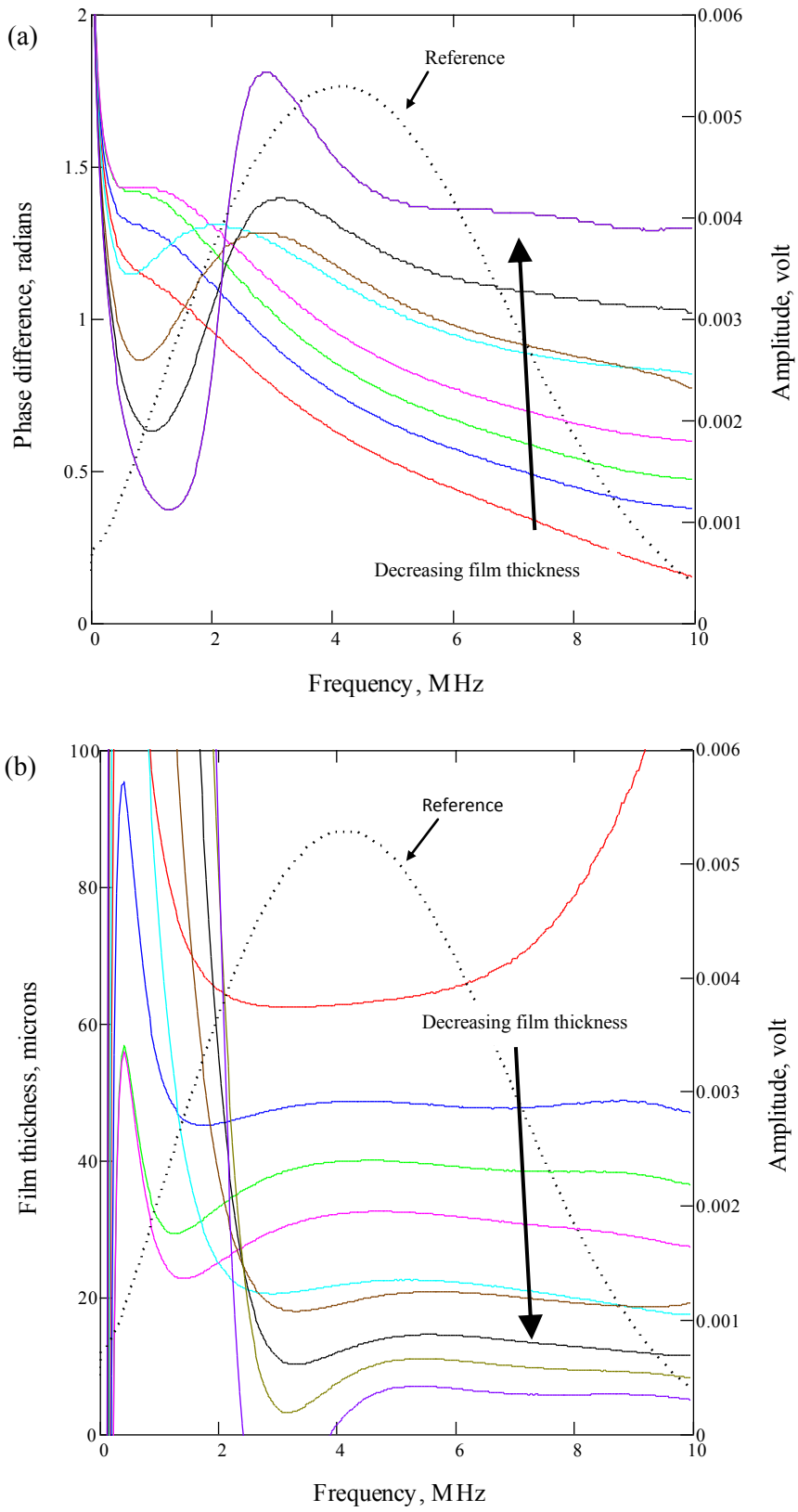

Figure 5.21 Variation of phase difference (a) and film thickness (b) contact between Perspex and Perspex.

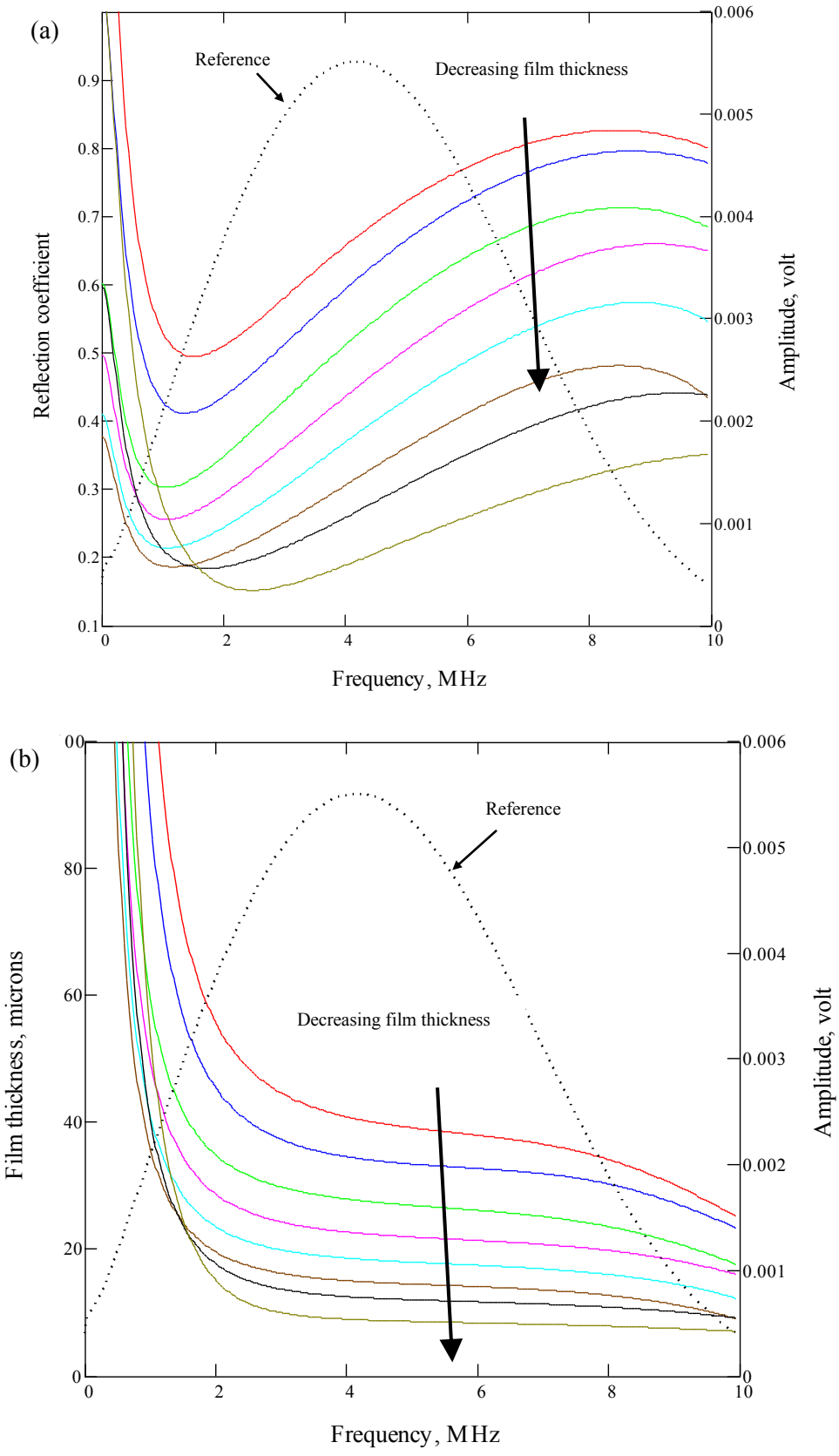

Figure 5.22 Variation of reflection coefficient (a) and film thickness (b) contact between Perspex and PTFE.

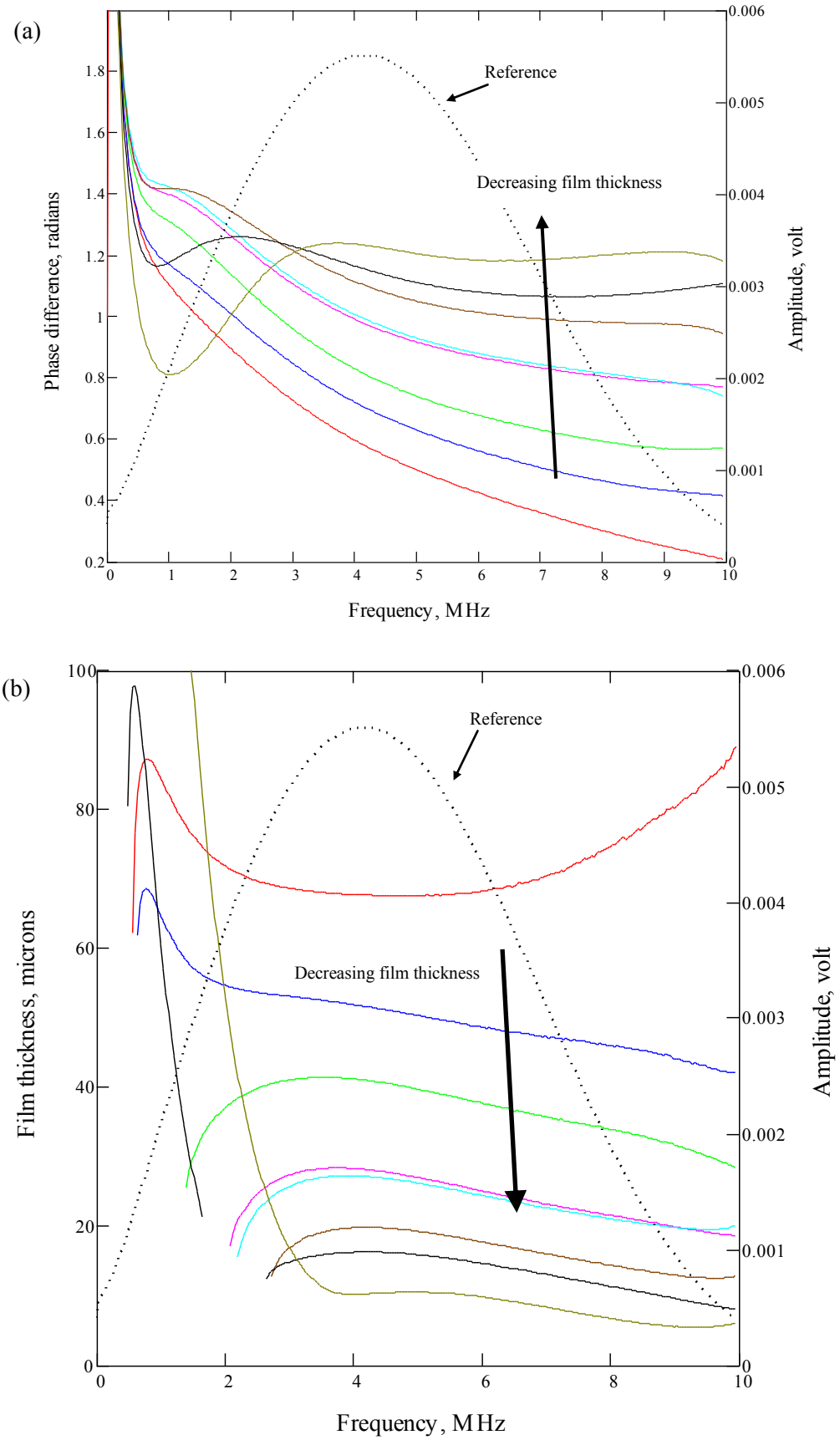

Figure 5.23 Variation of phase difference (a) and film thickness (b) contact between Perspex and PTFE.

5.6.4 Contact case 3: Perspex and Steel

The acoustic impedance of Perspex and steel is very different where the acoustic impedance of Perspex is around one fourteenth that of steel. The amplitude method will perform well to measure film thickness, as the reflection of coefficient approaches one. However, in the phase method, the variation of oil film thickness could be seen in the variation of phase difference as shown in Figure 5.24. In the case of thick film (> 40 μm), the phase difference is in phase but in the thin film (< 40 μm), it is out of phase (air force blue, cadmium green and cadmium orange lines in Figure 5.24).

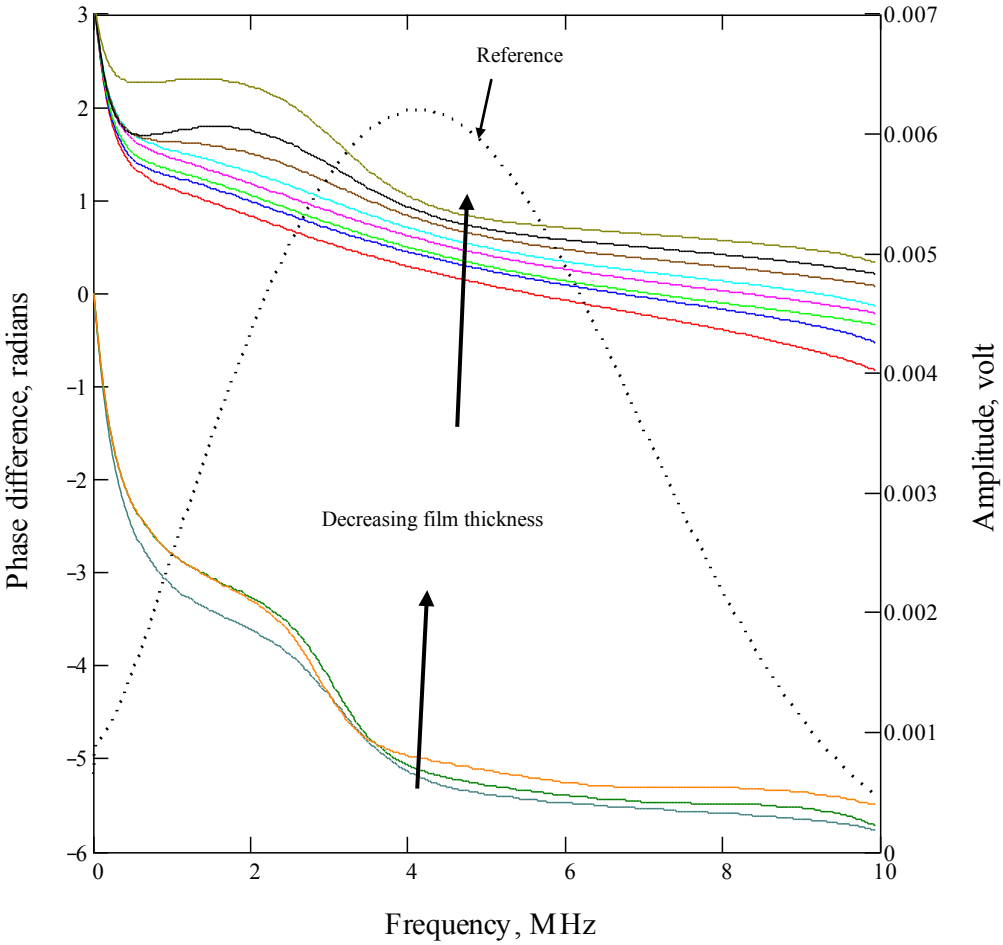

Figure 5.24 Variation of phase difference contact between Perspex and Steel.

The variation of film thickness from Eq. 5.4 for the contact between Perspex and steel is shown in Figure 5.25. In the case of thin film, the value of film thickness is constant in the bandwidth of the transducer. Otherwise, for the very thick film,

the thickness of film is not constant. This suggests that the method will only work with the thin films.

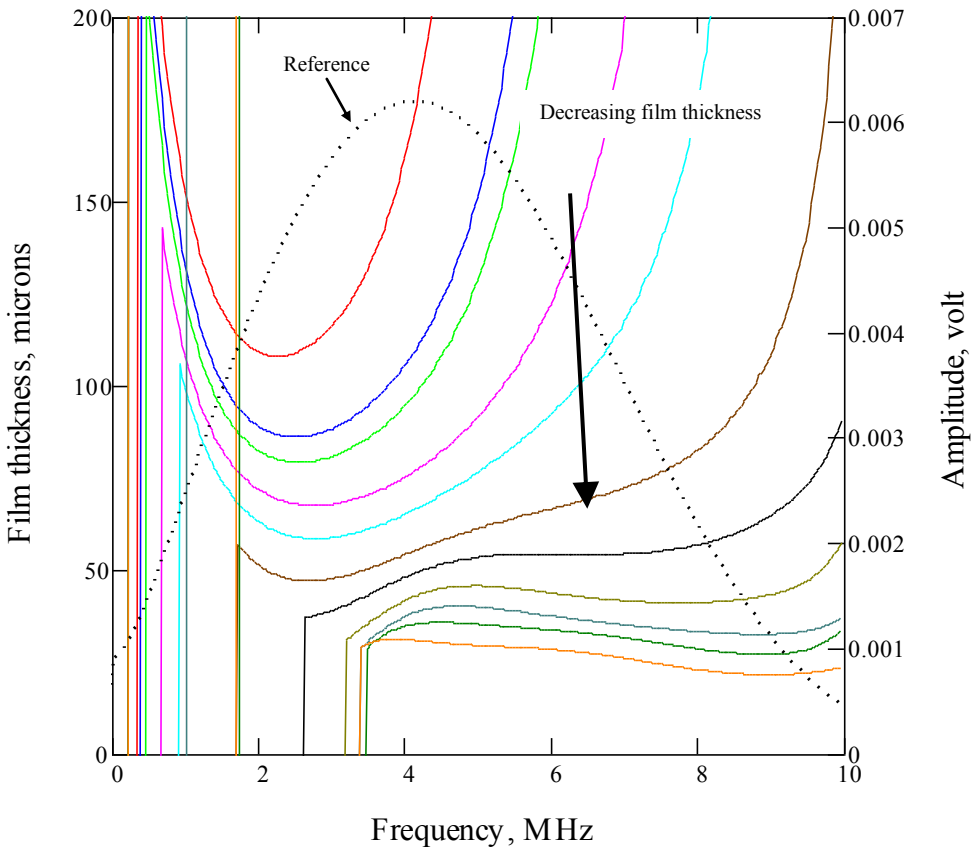

Figure 5.25 Variation of film thickness contact between Perspex and Steel.

5.7 Discussion

5.7.1 Investigation of reflected signal

Figure 5.27 shows the reflected signal from a solid-oil-solid interface, where there are three cases of interface: Perspex-oil-Perspex, Perspex-oil-PTFE, and Perspex-oil-steel. The legend of this graph is shown in Figure 5.26. The oil film is around 95 µm separated by two surfaces which is indicated by ***a*** and ***b:*** top and bottom of plates. From the Figure 5.27, the blue line is reflected signals *of a* and *b* surfaces from the top and bottom plates, respectively and the red line is reference signal. The reflected signal from oil to Perspex is different from oil to PTFE and Steel. The reflected signal of the bottom plate (*b*) from oil-steel (Figure 5.27c) is bigger than oil-Perspex (Figure 5.27a) and oil-PTFE (Figure 5.27b). Therefore, there are

two effects of this reflected signal. Firstly, it will influence the method of measurement and secondly is the ability to measure film thickness.

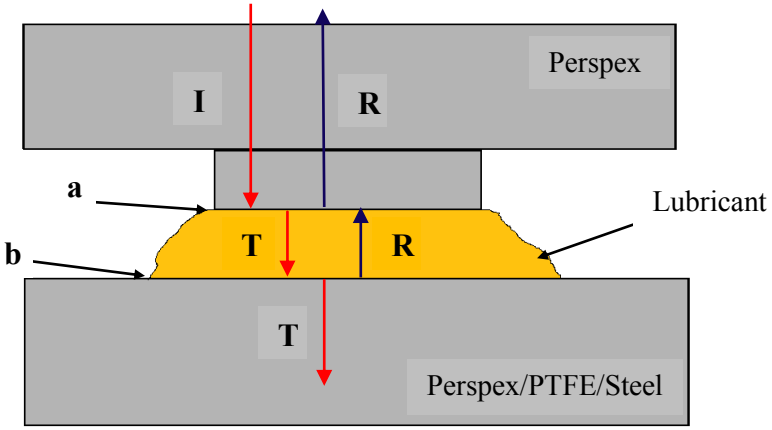

Figure 5.26 The schematic drawing of incident, reflected, and transmitted signals in three media

From Figure 5.27, it shows that as the film becomes thinner, the reflected signal from the surfaces of *a* and *b* will be approach each other. At a certain point, they overlap as shown by the green line in the figure. These overlapping reflected signals, Perspex-oil-Perspex and Perspex-oil-PTFE interfaces (Figures 5.27a and 5.27b), are smaller than reference signal. In contrast, the overlapping reflected signal, Perspex-oil-steel interface, is bigger than reference signal due to uniqueness of its overlapping reflected signal. Therefore, in this case, the amplitude method can be applied for contact Perspex-oil-Perspex and Perspex-oil-PTFE and otherwise amplitude method cannot be used to measure oil film thickness between Perspex and steel due to R > 1. This is unusual case because based on conservation of energy, the reflection coefficient is never larger than 1 (R>1). Therefore, this phenomenon is needed investigation further. By using phase shift method, Figure 5.19c shows that when the oil film becomes thinner, the overlapping reflected signal will be smaller. Therefore, phase of the overlapping of reflected signal would be negative out of phase. When the phase is positive out of phase or thick films, the reflection coefficient is larger than 1. Therefore, from Figure 5.25, it shows that the film thickness is not flat in the bandwidth of transducer. When the reflection coefficient approaches 1, the film thickness is flat in the bandwidth of transducer. It means that the spring-interface model is valid only for thin films but is not for thick films.

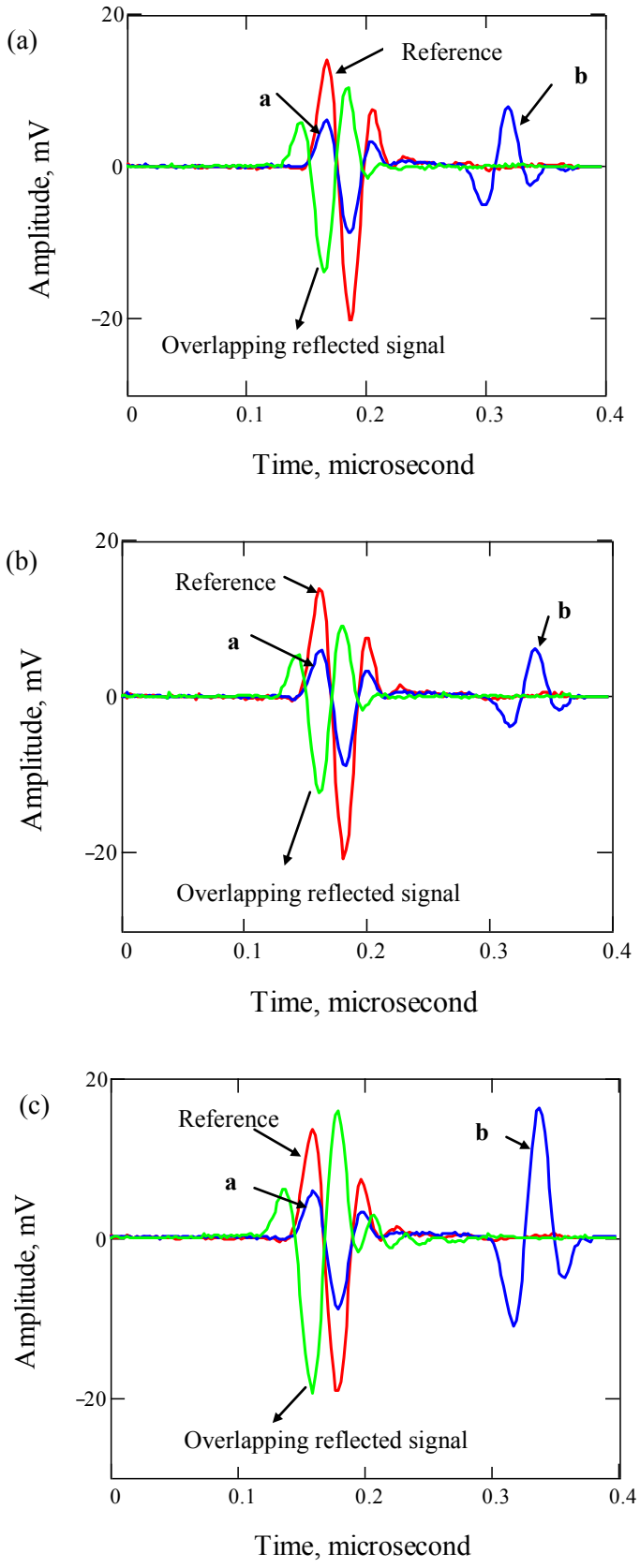

Figure 5.27 The comparison of variation of reflected signal and overlap of reflected signal from **a** and **b** for (a) Perspex-Perspex, (b) Perspex-PTFE, and (c) Perspex-steel.

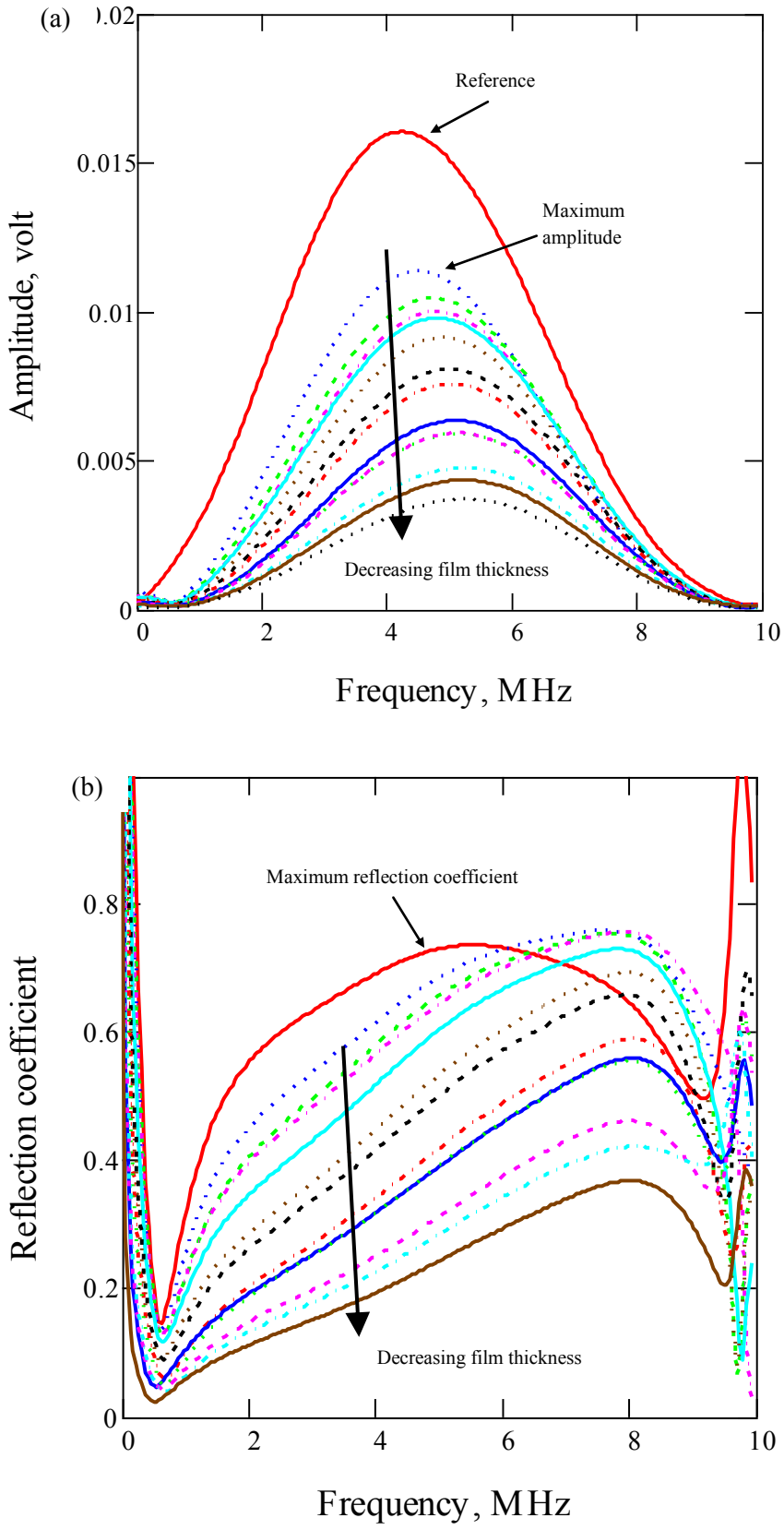

Figure 5.28 (a) The maximum amplitude and (b) reflection coefficient spectra for contact between Perspex and Perspex.

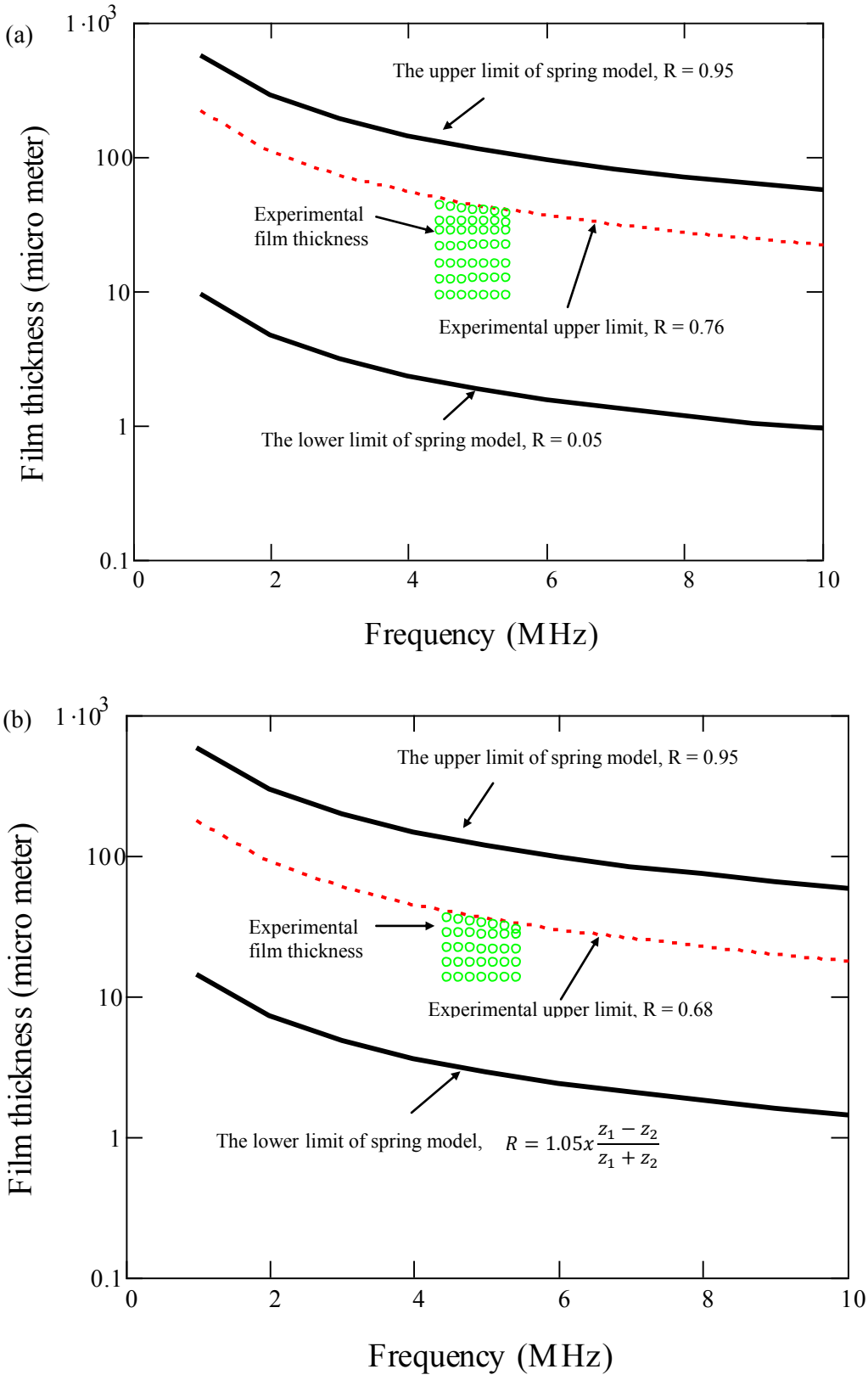

Figure 5.29 Shift of maximum upper limit of measurement using amplitude method: (a) Perspex-Perspex and (b) Perspex-PTFE, using 5 MHz focusing transducer.

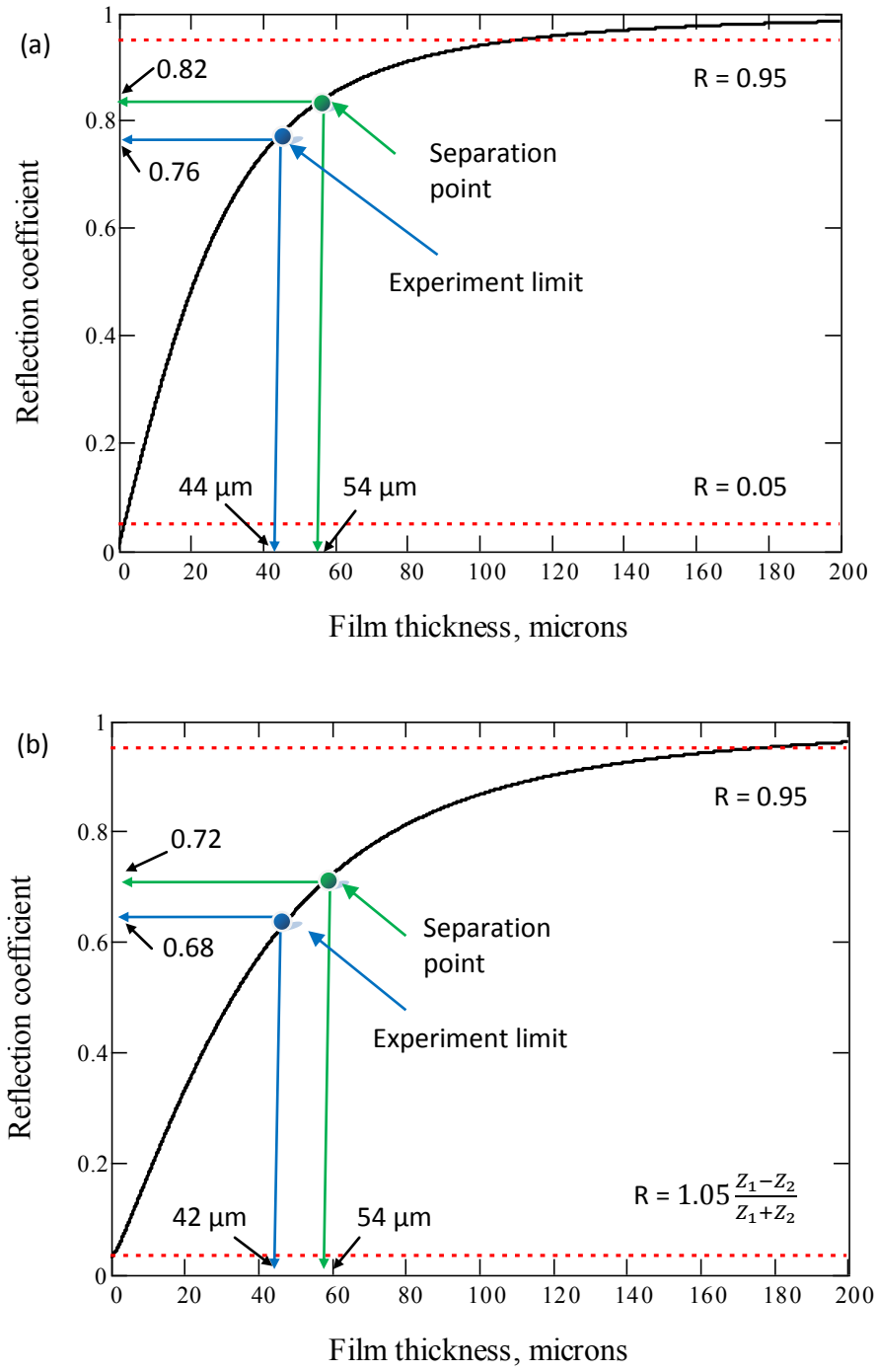

Figure 5.30 Reflection coefficient spectra for 5 MHz frequency transducer for contact (a) between Perspex and Perspex and (b) between Perspex and PTFE.

The maximum upper limit of measurement using amplitude method can also be drawn in Figure 5.30. The separation of reflected signals from the interface when the limitation of ToF model is obtained is shown in green line where the upper limit of R is 0.82 and 0.72 for contact between Perspex-Perspex and Perspex-

PTFE, respectively. The spring interface model is valid when the reflected signals from the interface form single reflection. Therefore, the maximum upper limit of R from the experiment for contact between Perspex and Perspex (5.30a) and between Perspex and steel (5.30b) is 0.76 and 0.68, respectively. These results show a good agreement.

The maximum limitation of measurement of film thickness using amplitude method using Eq. 3.39 had been shown in Figures 5.1 through 5.5, where if the maximum upper limit of reflection coefficient was supposed 0.95. In this experimental study, the maximum upper limit of thicker film was influenced by overlapping the reflected signals in the interface. Figure 5.28 shows the amplitude and reflection coefficient spectrums of contact between Perspex and Perspex. From Figure 5.28a, amplitude maximum is around one third of amplitude of reference signal. It shows that the maximum reflection coefficient never approaches 0.95, but reflection coefficient is around 0.75 at 5 MHz, as shown in Figure 5.28b.

Figure 5.29 shows the comparison between the spring model and the experimental result of the upper limit to measure oil film thickness for contacts: Perspex-Perspex and Perspex-PTFE. From the experimental result, the maximum reflection coefficient depends on the combination of two reflected signals in the interface. The maximum upper limit of reflection coefficient based on Eq. 3.25 and the experimental study was different. Based on the experiment, the maximum upper limit of reflection coefficient was around 0.76 and 0.68 for contact between Perspex and Perspex and Perspex and PTFE, respectively.

5.7.2 Comparison between phase shift and amplitude methods

The spectrum of reflection coefficient and phase difference was recorded from contacts between Perspex-Perspex and Perspex-PTFE and the spring model (Eqs. 3.25 and 3.27) was used to determine the film thickness spectra. The average of film thickness over the frequency between 4.6 and 5.4 MHz was plotted for both methods as shown in Figures 5.31 and 5.32. The comparison of film thickness

between phase and amplitude methods for contact case Perspex-Perspex is shown in Figure 5.31. The agreement between amplitude and phase methods is good for thin films, but in the thicker films, the amplitude method gives a small result.

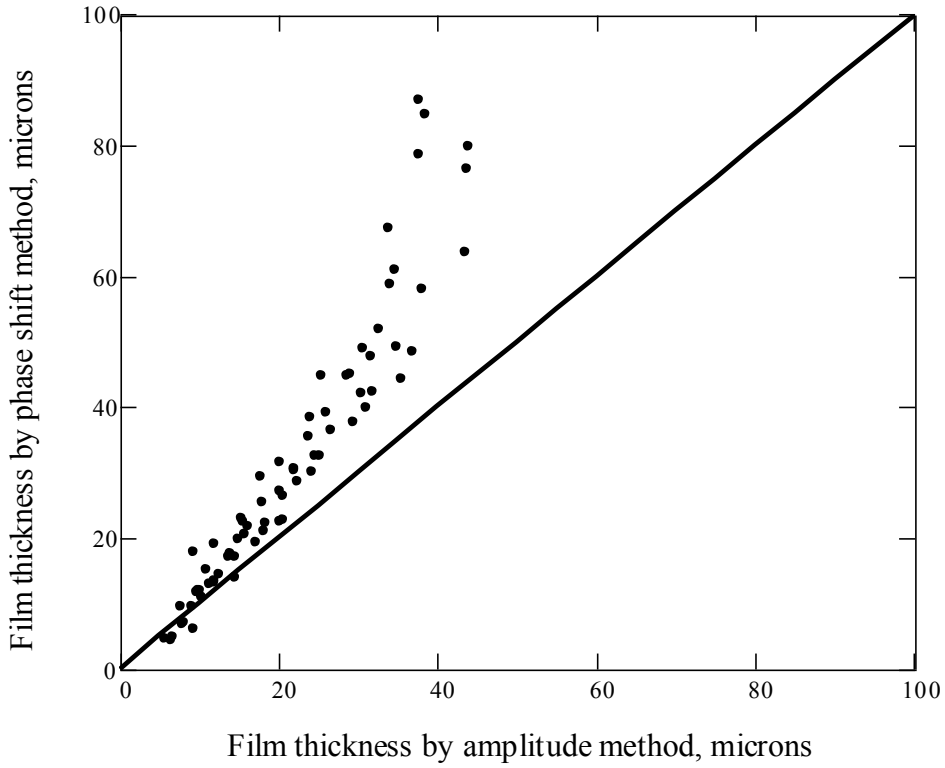

Figure 5.31 Comparison between amplitude and phase methods of oil film thickness where contact between Perspex and Perspex.

Figure 5.32 shows the comparison of film thickness between two methods with contact between Perspex and PTFE. The oil film thickness of the phase method is bigger than amplitude method. Examination of equation 5.3 shows that there is a tangent term; errors in the phase difference are amplified, as the phase difference tends to 0 (i.e. the film thickness tends to infinity) for the thicker films. This leads to an over prediction for thicker films.

Scatter in results is caused by various sources. Firstly, capturing the reflected signal, from the Figures 5.21 and 5.23 the variation of phase difference is not the same pattern of reflection coefficient, there is an error in capturing of film thickness at the top and bottom surface of Perspex. It was difficult to capture the reflected signal simultaneously, so that capturing of reflected signal at the top and the bottom surfaces was not the same. The secondly, the effect of spring, oil was

introduced in the contact too much. Therefore, when the loads were applied, the pressure in the contact was high and the pressure pushed back the force of the hydraulic pressure, the thickness of the film was changed.

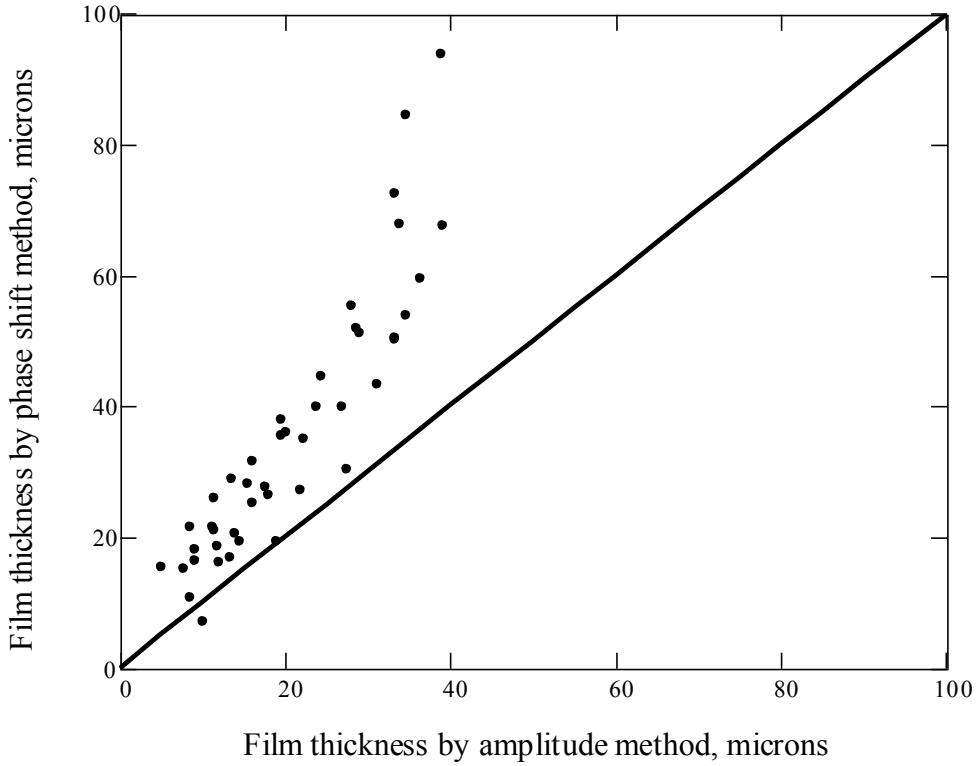

Figure 5.32 Comparison between amplitude and phase methods of oil film thickness where contact between Perspex and PTFE.

5.7.3 Reflection coefficient and phase difference on an Argand diagram

The comparison between theory and experiment of reflection coefficient and phase difference for three contact cases above: Perspex-Perspex, Perspex-PTFE, and Perspex-Steel, was plotted on an Argand diagram as shown in Figure 5.33. In general, from this figure shows that the phase difference between theory and experiment is in a good agreement, but for contact between Perspex and steel the reflection coefficient does not agree well.

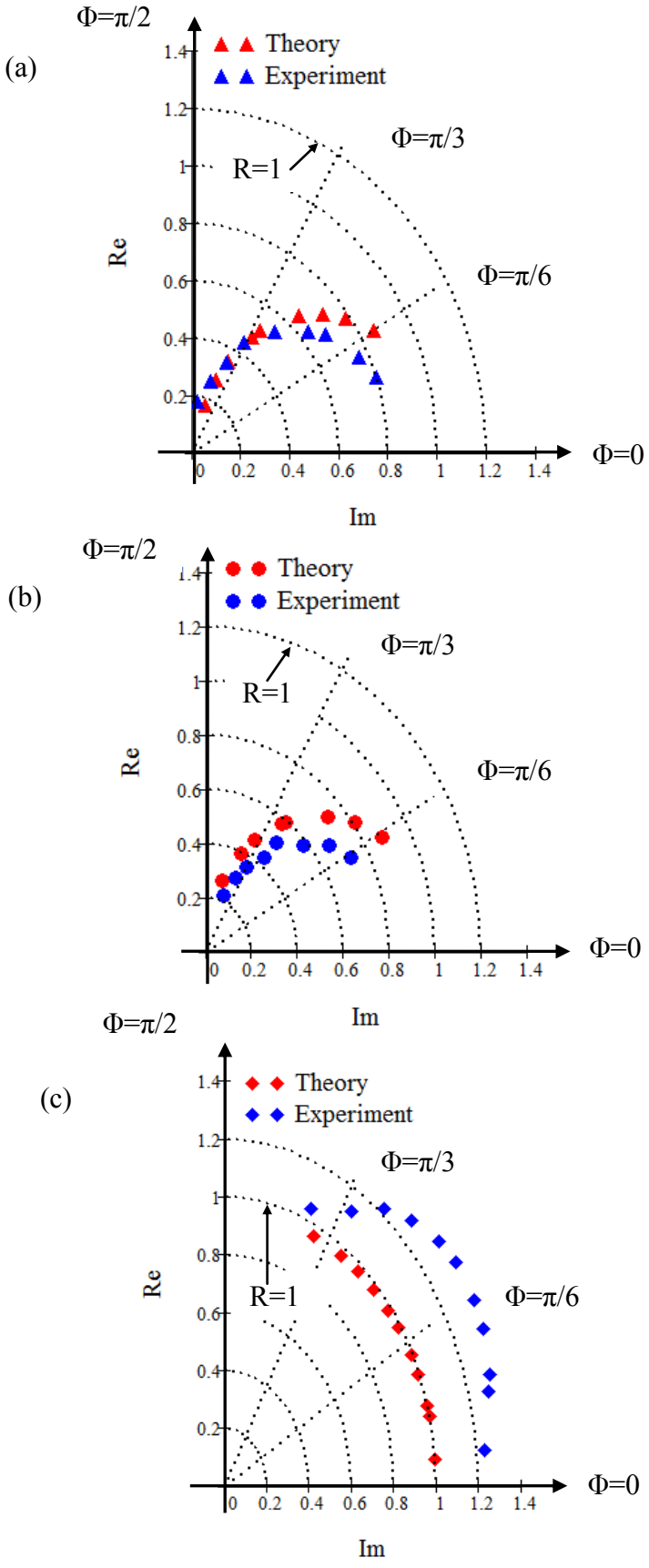

Figure 5.33 Comparison between theory and experiment of reflection coefficient and phase difference plotted on an Argand diagram; (a) Perspex-Perspex, (b) Perspex-PTFE, and (c) Perspex-Steel.

In the case of thin films, both contact cases: Perspex-Perspex (Figure 5.33 a) and Perspex-PTFE (Figure 5.33 b), show good agreement with the theory, but for the thicker films do not. For contact between Perspex and steel (Figure 5.33c), it shows that the reflection coefficient is greater than 1 for the thicker films and for the thin films approaching 1. So the spring-interface model using amplitude method can not apply for this case but the spring-interface model using phase shift method could be apply only for thin films. In this condition, this graph shows that when the reflection coefficient of theory is smaller than 1, the reflection coefficient of experiment will approach 1. In contrast, when the reflection coefficient of theory is equal 1, the reflection coefficient of experiment will be larger than 1 (R>1). At this stage, conclusion can be drawn that if the amplitude of overlapping reflected signal at Perspex-oil-steel interface is bigger than the reference signal (R>1), the spring-interface model using phase shift method is not valid but if the reflection coefficient approaches 1, this method is valid .

5.8 Conclusions

The amplitude and phase shift methods have demonstrated ability to measure oil film thickness between two materials in contact. Two contact cases (Perspex-Perspex and Perspex-PTFE) had been explored using both methods in order to determine oil film thickness. The measurements have revealed that both methods are in good agreement at thin films ($h < 25$ μm). The values of film thickness at thick films ($h > 25$ μm) using the phase shift method are higher than the amplitude method. This is because there is a tangent term; errors in the phase difference are amplified, as the phase difference tends to 0 and the film thickness tends to infinity.

In the case of contact between two acoustically dissimilar materials, the amplitude method is difficult to apply for measuring oil film thickness. This contact has a narrow measurable range because the reflection coefficient approaches 1. Otherwise, the phase shift method can be applied to measure oil film thickness. Even though for thick films ($h > 40$ μm) the result of film thickness is not as good as thin films ($h < 40$ μm), but this method has shown a promising result.

In the amplitude method, the upper limit of film thickness depends on the combination of amplitude of reflected signal in three-layer system. The amplitude of reflected signal is depended upon materials in contact. From the experiment, it shows that the upper limit of measuring oil film thickness shift from R = 0.95 to R=0.76 and R=0.68 for contact cases Perspex-Perspex and Perspex-PTFE, respectively.

Chapter 6

Measurement of film thickness in the iso-viscous elastohydrodynamic regime

This chapter describes the use of the techniques developed in Chapters 4 and 5 to measure oil film thickness in the I-EHL regime. Ultrasonic reflection technique is applied to contacting materials which have low modulus elasticity and acoustic impedance. The experimental results of film thickness in I-EHL regime have been compared with an optical interference method.

6.1 Introduction

The phenomenon of elastohydrodynamic lubrication has reached prominence as a result of the need to understand the lubrication of gears, rolling bearing, and other non-conformal contact machine parts. For this reason, there has been much study on the mechanics of lubrication for high elastic modulus materials where the piezo-viscous properties of the oil play an important role. There are also many machine elements where one or both of the contacting parts are manufactured from low modulus materials such as lip seals, o-rings, and metal on polymer prosthetic joints. In these cases, the contact pressure is insufficient to cause a

substantial increase in viscosity and the elastic deformation is significant relative to the thickness of the fluid film separating them. This is known as the compliant or iso-viscous elastohydrodynamic (I-EHL) regime.

Herrebrough [1968] was the first to provide a numerical solution of an integral equation for constant viscosity for a large range of loading conditions. There have been several other similar solutions (Hook and O'Donoghue [1972], Biswas and Snidel [1976], Hamrock and Dowson [1978], de Vicente *et al.* [2005]). Recently, Venner and Napel [1992] and Venner [1991] used Multi-Level-Multi-Integration (MLMI) methods and proposed a formula for central film thickness, which covers all regimes of lubrication.

Previous experimental studies of I-EHL have been carried out using optical methods. Roberts and Tabor [1968] used an optical interference approach to measure the oil film thickness between a glass plate and a rubber hemisphere. Myant [2010] has used a similar approach to achieve measurements in the 0.02 - 1.25 μm region. He also used a laser induced fluorescence method that enabled measurements in the region 1 - 20 μm.

This chapter describes an ultrasonic reflection method to measure oil film thickness in the I-EHL regime. The test apparatus and materials are shown in section 6.3. The reflection coefficient from the interface between the sphere and disk is shown for range of lubricated and dry, static and dynamic contact conditions. The phenomenon of cavitation in the exit region is shown. The film thickness across a range of applied loads and entrainment speeds are presented. A summary is given at the end of this chapter.

6.2 Iso-viscous elastohydrodynamic lubrication (I-EHL)

Roberts and Tabor [1968] used interferometric results to deduce the film formation between a rubber ball and a flat surface. During squeezing motion (as shown in Figure 6.1a) a trapped "bell" of liquid is observed. The pressure distribution has a maximum value along the center line of the sphere, and this

causes maximum elastic displacement which produces the concavity. During the squeeze action, the central film thickness decreases with time as the liquid is squeezed out. In the last stages of the approach, the edges of the deformed elastic sphere attempt to seal and trap the lubricant in the cavity. Subsequently and over a long period, the lubricant within the cavity exudes laterally and will completely disappear (Moore [1972]).

When a sphere is sliding on a flat surface (Figure 6.1b), a wedge shaped contour forms at the fluid entrance and a constriction appears in the film toward the rear of the contact. In the front part of the contact zone, the pressure build up is due to a narrowing film thickness, whereas the relatively sudden drop in the pressure curve towards the rear part requires a sharp constriction to maintain continuity of the flow without cavitation. The low modulus of rubber implies that the contact pressures are low and that the material can be easily deformed to provide a convenient shape for effective hydrodynamic lubrication.

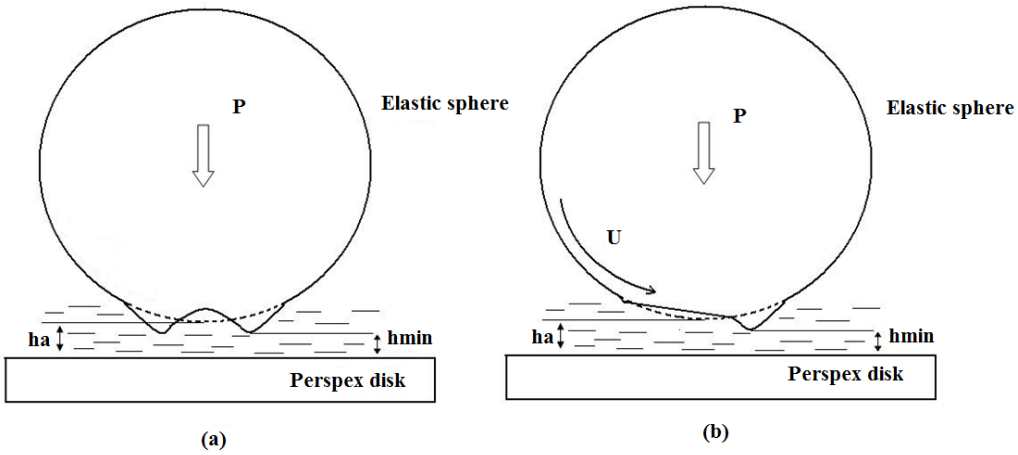

Figure 6.1 Elastohydrodynamic film shape for an elastic sphere (a) approaching a rigid plane surface and (b) sliding on a plane surface.

6.3 Experimental approach

6.3.1 Test apparatus

Figure 6.2 shows a photograph of apparatus used to generate an I-EHL contact under controlled load and speed. The apparatus is a modification of a conventional optical EHL rig where the microscope has been replaced by a

focusing ultrasonic transducer and the glass disk by a Perspex one. A nitrile sphere (19 mm in diameter) was supported on rollers and loaded onto the underside of the Perspex disk. The load was applied vertically upward with a small hydraulic loading cylinder (with test loads of 3.8, 5.5, and 7.3 N).

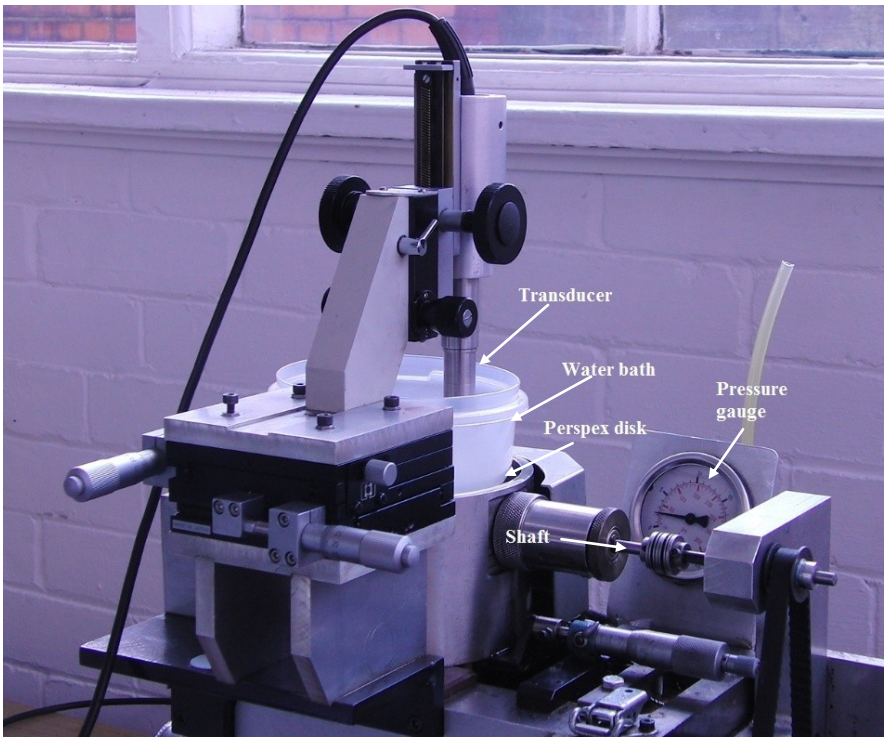

Figure 6.2 Photograph of the I-EHD contact apparatus, showing the ultrasonic transducer and captive water bath above the contact.

The nitrile rubber sphere was rotated at constant speed by an electric motor through a gear box and quill shaft at speeds in the range 5 – 1500 rpm. The flat Perspex disk was held stationary such that the contact was completely sliding. The contact was fully flooded with a mineral oil.

Figure 6.3 shows the schematic layout of the instrumentation. A 10 MHz immersion focused transducer was mounted above the contact in a water bath. The transducer could be positioned using x, y, and z micrometers. Prior to experimentation, it was located directly above the contact region and at a distance such that the wave was focused directly on the contact. This positioning was achieved by searching for the maximum possible reflected signal (which occurs at the centre of the contact at the vertical location of best focus).

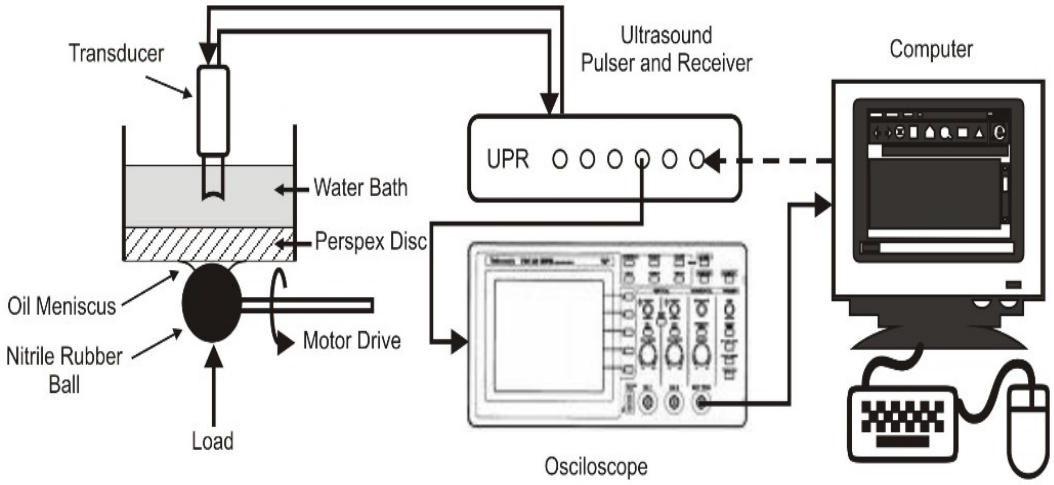

Figure 6.3 Schematic diagrams of ultrasonic apparatus to measure soft EHL film thickness.

The ultrasonic transducer was connected to a pulse-receiver (UPR) that generates a sequence of high-voltage pulses. These caused the piezoelectric transducer to be excited in mechanical resonance. The transducer then emitted a broadband pulse of ultrasonic energy. The pulse reflected from the lubricant layer was received by the same transducer, amplified, and stored on a digital oscilloscope. The UPR and storage oscilloscope were controlled by purpose built LabView interfaces.

6.3.2 Material and test specimens

Figure 6.4 shows a photo of the nitrile spheres, which were used in the experiments. These materials have been obtained in ball form for experimental purposes. The surface roughness was measured using a stylus profilometer as Ra=0.59 μm. The lubricant used was Shell Turbo T68. The disk was cut from standard Perspex sheet. The acoustic properties for the materials used in this work are shown in Table 6.1.

The nitrile sphere had Young's modulus elasticity E of 8.54 MPa. This modulus was determined experimentally by observing the size of the contact area when the sphere was pressed against the Perspex disk and using the Hertz elastic equation (Eq. (4.2)) to back calculate the modulus. The speed of sound in all the materials

was determined by simple time of flight experiments at room temperature and ambient pressure (i.e. by measuring the transmission time of an ultrasonic pulse over a fixed distance). It should be noted that for oil the acoustic impedance varies with pressure (Dwyer-Joyce *et al.* [2003]), however at the low pressure experienced in the I-EHL contacts the effect is not great.

Table 6.1 Acoustic properties of Shell Turbo T68 lubricating oil, Perspex, and nitrile sphere.

	Density ρ (kg/m^3)	**Longitudinal wave velocity *c* (m/s)**	**Acoustic Impedance *z* (MRayls)**
Shell Turbo T68	876	1460	1.28
Perspex	1179	2730	3.22
Nitrile sphere	1262	1618	2.04

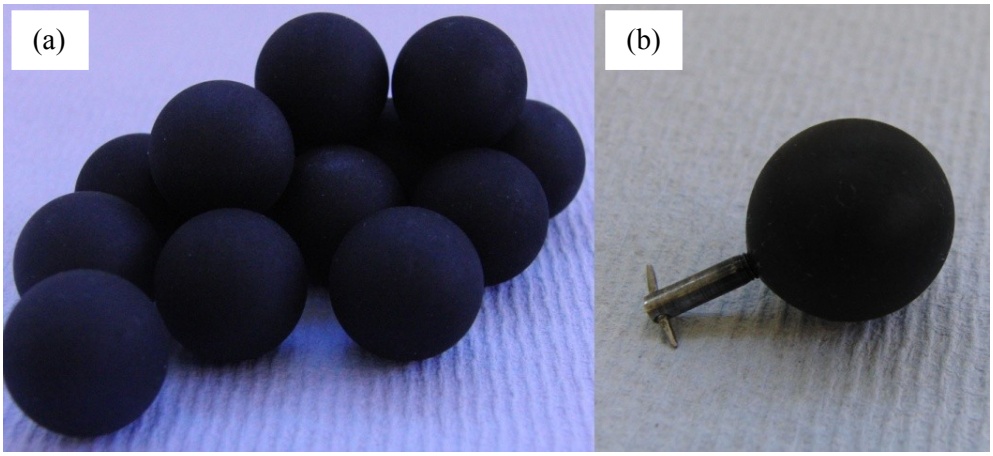

Figure 6.4 Photograph of nitrile rubber sphere (a) and nitrile sphere mounted on a shaft (b).

6.3.3 Transducer selection and focusing

In section 4.3.2, it has explained how to choose ultrasonic transducer in connection with the diameter of contact and spot diameter. Here we define a focusing ratio as the ratio of the spot diameter to the diameter of the contact;

$$\emptyset_r = \frac{d_f}{2a} \tag{6.1}$$

The limit of validity for the ultrasonic pulse to fall within the contact patch is therefore when $\emptyset_r < 1$. Figure 6.5 is the region of measurement used in this work with 10 MHz transducers.

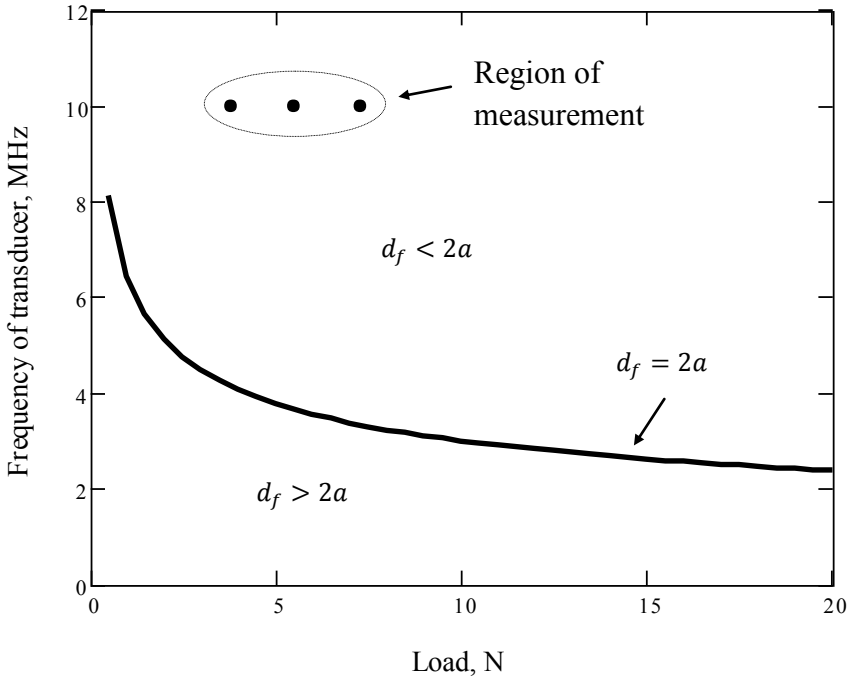

Figure 6.5 Limit condition for measurement such that the ultrasonic beam falls within the area of contact, for a rubber ball loaded against Perspex flat.

6.4 Results

6.4.1 Reflection coefficient profile for a static contact

Figure 6.6a shows the measured reflection coefficient recorded as the transducer is moved across the diameter of an un-lubricated static contact, for a range of applied loads. The reduction in reflection as the centre of the contact is clearly visible. At higher local contact pressure, the surfaces will be in close conformal contact and more of the ultrasonic wave is transmitted. Where no contact is made the reflection coefficient is equal to unity. The reflection coefficient will reach a minimum value, if the contact pressure is sufficient to cause perfect acoustic contact. The minimum value recorded in these experiments is approximately R=0.2. Eq. (3.16) predicts that if the rubber and Perspex had been perfectly bonded the reflection coefficient would be approximately equal to this value.

From this, it is deduced that there is complete, or very close to complete, contact between the ball and Perspex at these contact pressures.

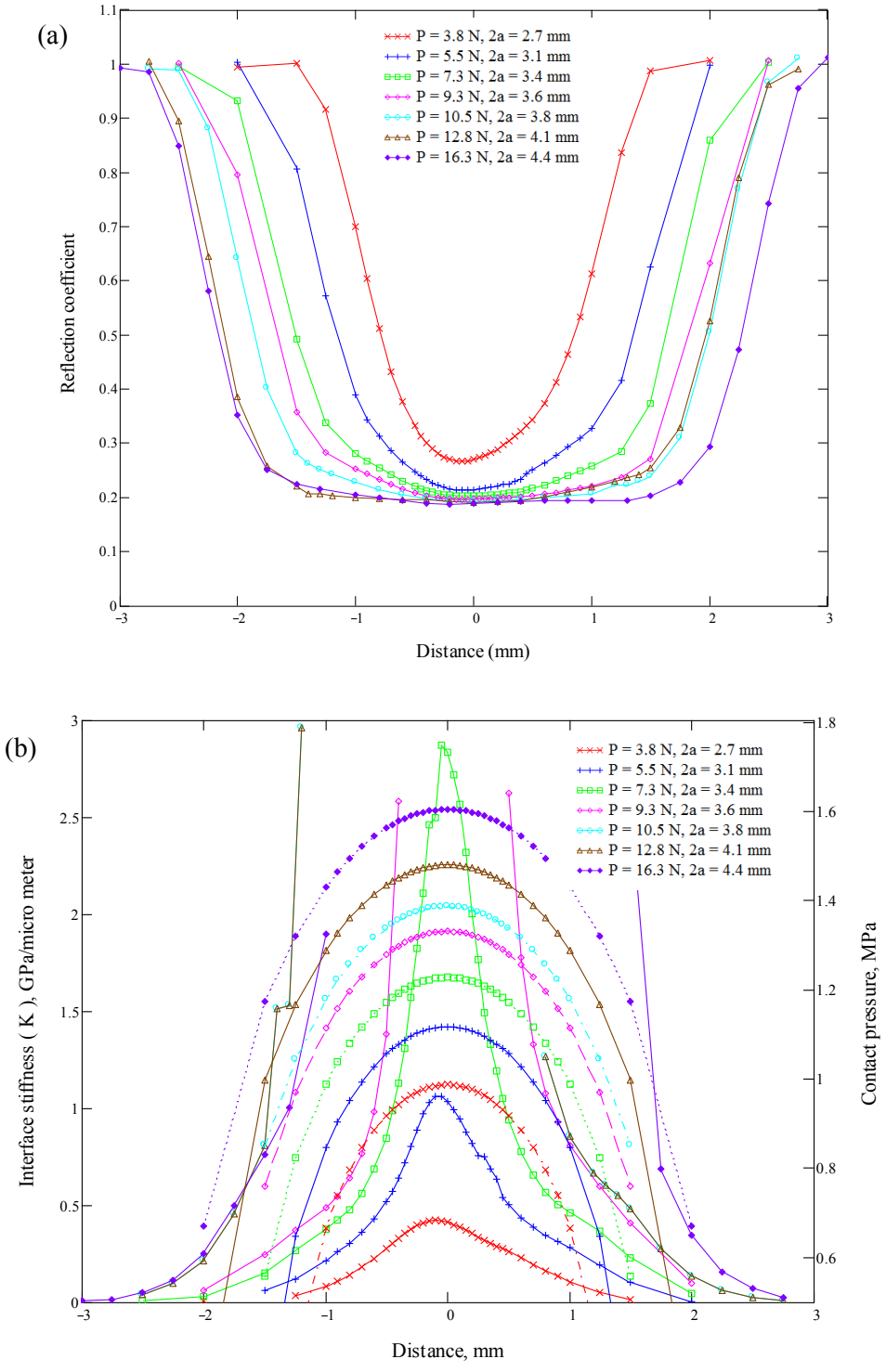

Figure 6.6 (a) Reflection coefficient profiles and (b) interface stiffness profiles and contact pressure, across a dry nitrile sphere-Perspex contact for a range of applied loads. 2*a*=Hertz contact diameter.

Figure 6.6b shows the reflection data of Figure 6.6a converted into interface stiffness (using Eq. (3.17)), where there is complete conformity the stiffness of the interface is infinite. Also shown on this plot is the predicted contact pressure (calculated from the Hertz elastic solution).

Figure 6.7 shows the contact stiffness data for each of the profiles in Figure 6.6b plotted against the local contact pressure. The data from each of the contact cases falls approximately on a continuous curve. As expected for a given local contact pressure, the same interface stiffness is achieved regardless of what the total load on the contact was. The data would also indicate that a pressure of 1.2 MPa is sufficient to cause complete conformity; or that the reflection is so close to that for complete conformity that there is no sensitivity to measure any areas of non-contact.

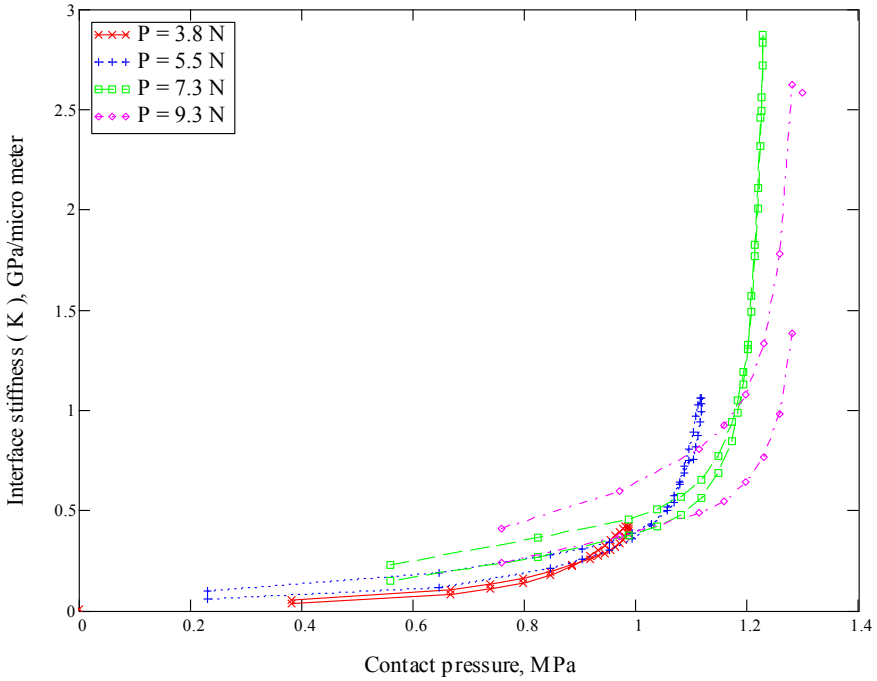

Figure 6.7 Variation of interface stiffness with contact pressure for each of the profiles of Figure 6.6b.

Figure 6.8 shows the case when the oil was introduced to the static contact such that the whole region was flooded. It is expected that oil now fills the air gaps between the asperity contact regions. The reflection coefficient now approaches the minimum value for the all loads across the whole contact region. In this contact, the gaps between contacts bodies are filled now with oil, which adds a

new path for ultrasonic transmission, so that the reflection coefficient is further reduced.

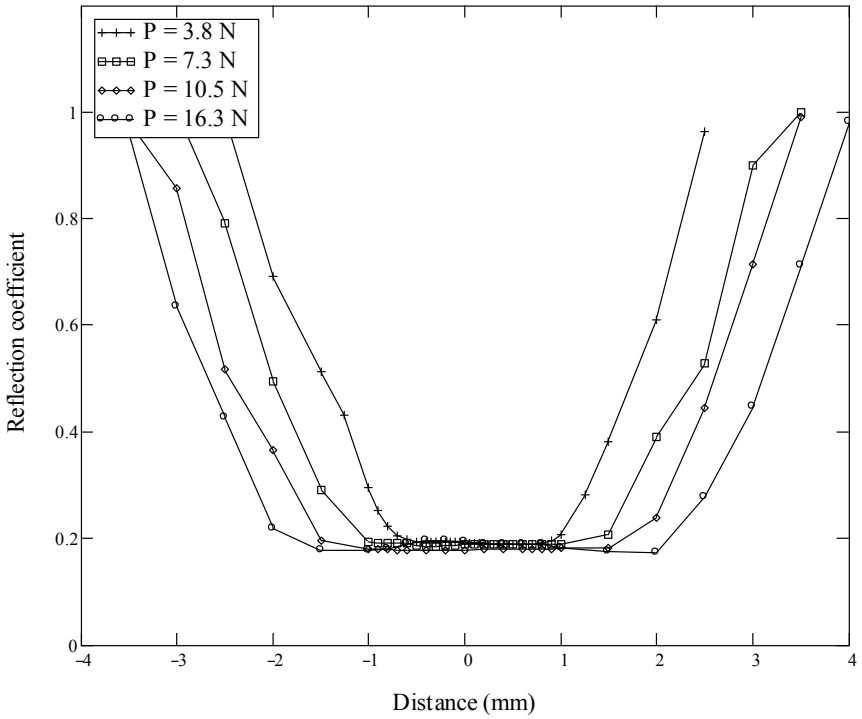

Figure 6.8 Reflection coefficient profiles under different loads for static rubber ball-Perspex contacts submersed in oil.

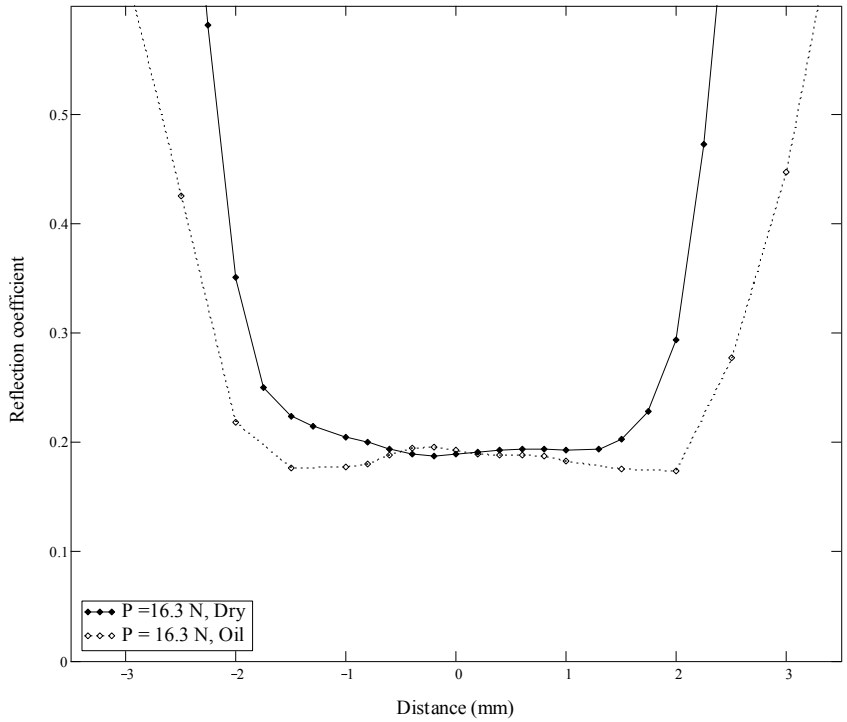

Figure 6.9 Comparison between reflection coefficient profiles measured under dry and wetted conditions, showing the cavity that forms by squeeze action.

Figure 6.9 shows the wet and dry cases compared for the highest load. For the wetted case a slight concavity is observed; this is thought to be some residual squeeze film formation as the oil was drawn into the contact, as predicted by Roberts and Tabor [1968]. At this stage, no attempt has been made to investigate this squeeze film stability with time.

6.4.2 Film thickness profile for a dynamic lubricated contact

Reflection coefficient profiles (similar to those of Figure 6.6a) were recorded for the dynamic lubricated case. Then Eq. (3.39) was used to convert these into oil film thickness profiles. These are shown as Figure 6.10.

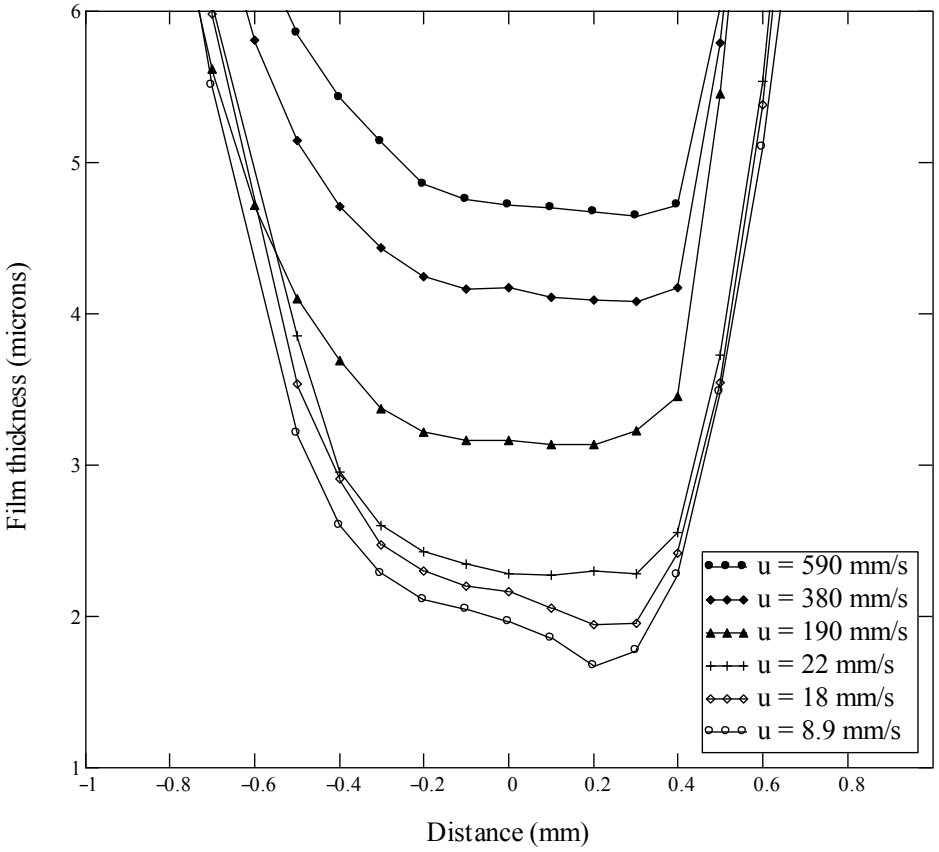

Figure 6.10 Film thickness profiles for six sliding speeds under a contact load of P = 3.8 N (corresponding to a mean contact pressure of 1.04 MPa). Entrainment direction from left to right.

The wedge shaped inlet and the constriction at the contact exit can just be seen for the thinner film cases, as observed by (Robert and Tabor [1968], Myant [2010]). Again, it should be noted that the low spatial resolution (typical focussed spot size

1.12 mm) has a significant blurring effect on the results and so sharp features cannot be observed.

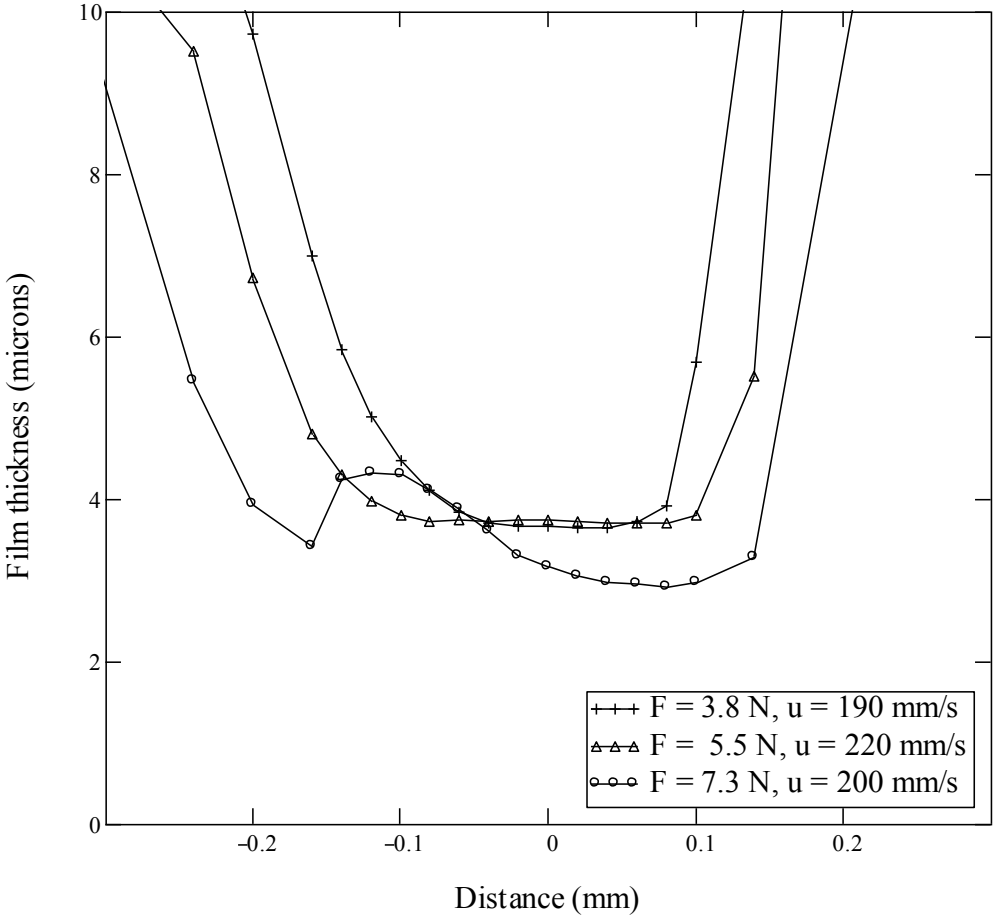

Figure 6.11 Film thickness profile for three applied loads (corresponding to a mean contact pressure of 1.04, 1.18, and 1.29 MPa) and an approximately constant sliding speed. Entrainment direction from left to right.

In Figure 6.11, the sliding speed has been kept approximately constant (to the best of repeatability of the motor control system), and the applied load varied. At the highest load, the wedge shaped inlet has been interrupted. The elastic deformations are large compared with the thickness of the hydrodynamic film, and it might be expected that pressure would be close to the Hertzian distribution for dry contact. It also follows that over the main load-bearing region the film thickness should be of approximately parallel form. However, at the higher load, this is not the case and there is an unusual ripple in the contact entry. It is not clear what has caused this instability to occur only at the high load. Possibly, at the high material strains, the stiffness has proportionately reduced and allowed a greater proportion of the oil to enter the contact. The phenomenon is also reminiscent of

so-called Schallamach waves (Dowson and Taylor [1979]) where frictional sliding occurs by the successive attachment and detachment of material. Of course, in this lubricated case the shear stress will be low, but perhaps large enough, especially at the higher load, to cause some out of plane deformation.

The data is shown as central film thickness plotted against speed for a range of loads in Figure 6.12. The film thickness increases, as entrainment speed increases.

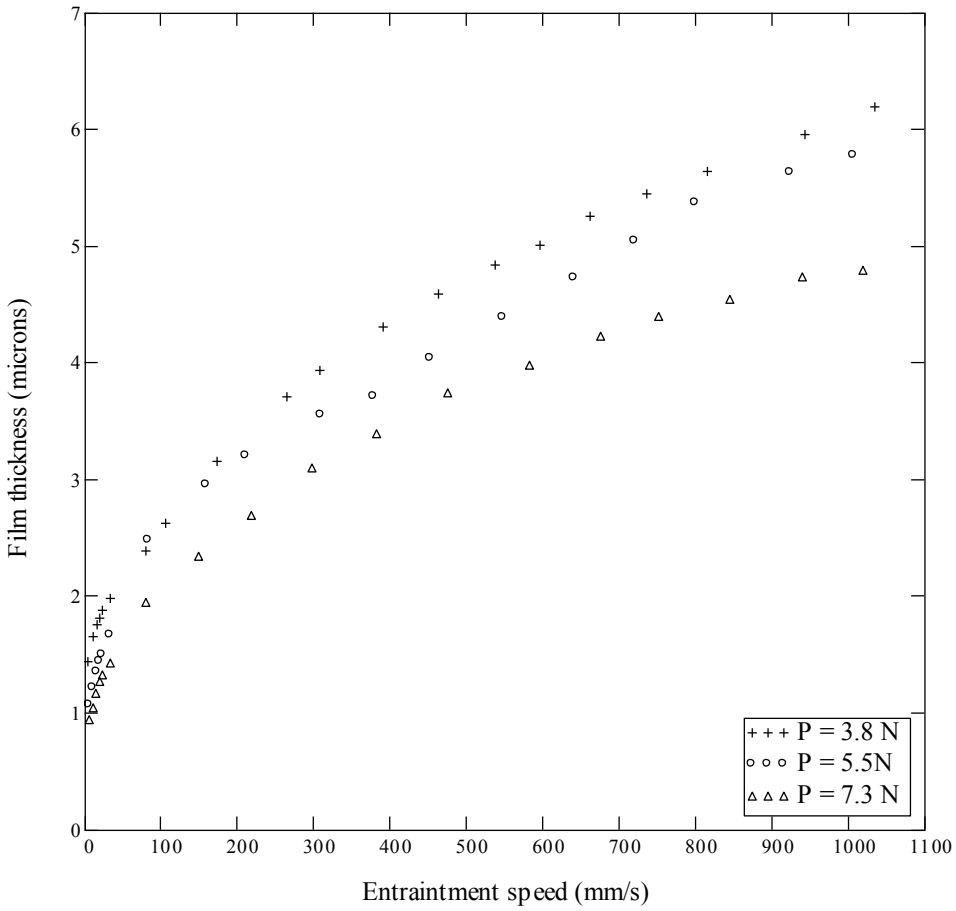

Figure 6.12 Influence speed and load on the central film thickness.

6.4.3 Measurements in the exit region

Cavitation can be generated by the passage of the lubricant through a constriction and sudden expansion. The velocity of the liquid increases at the expense of the pressure around the constriction, then falls below the threshold pressure for cavitation. Tiny bubbles filled with vapor appear and grow rapidly (Silk [1984]). A cavitation boundary is usually observed at the exit to the contact area (as shown

in the photographs of Figure 6.13). The higher the speed, the greater the volume of cavitation that occurs.

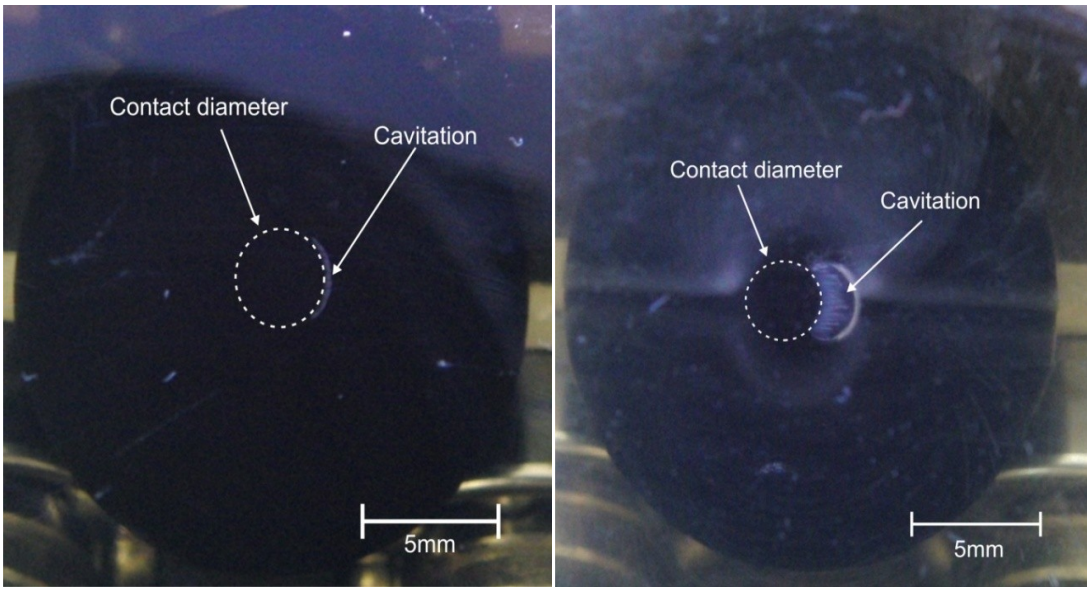

(a) (b)

Figure 6.13 Photograph of cavitation occurring in the exit region at (a) low speed, 33 mm/s (b) high speed, 740 mm/s. Entrainment direction from left to right and P = 3.8 N.

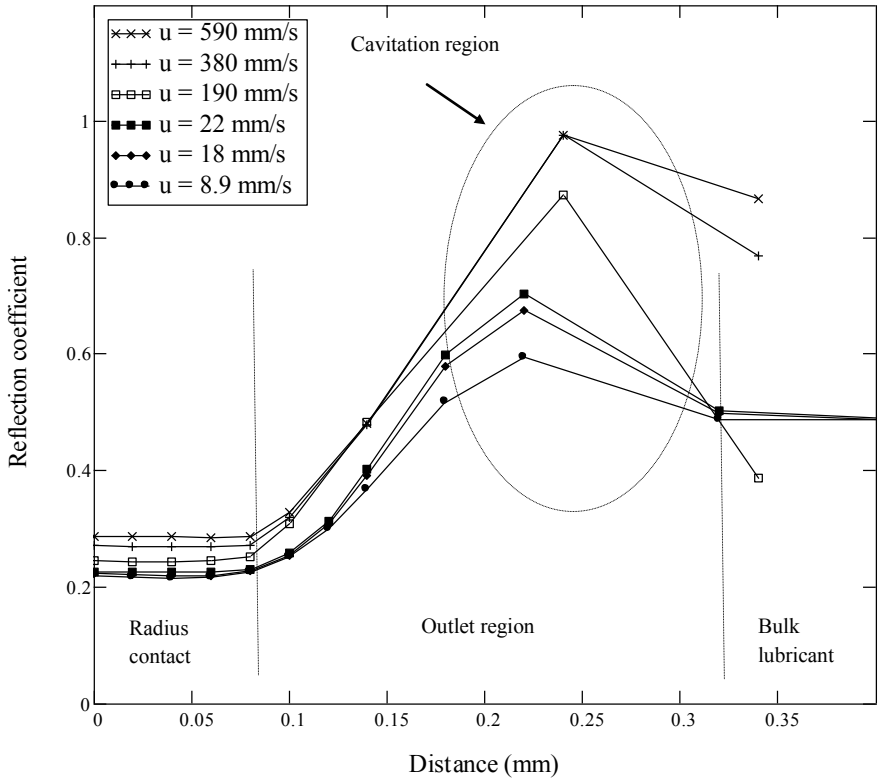

Figure 6.14 Reflection coefficients around the exit region showing cavitation at the higher speeds. Applied load P = 3.8 N.

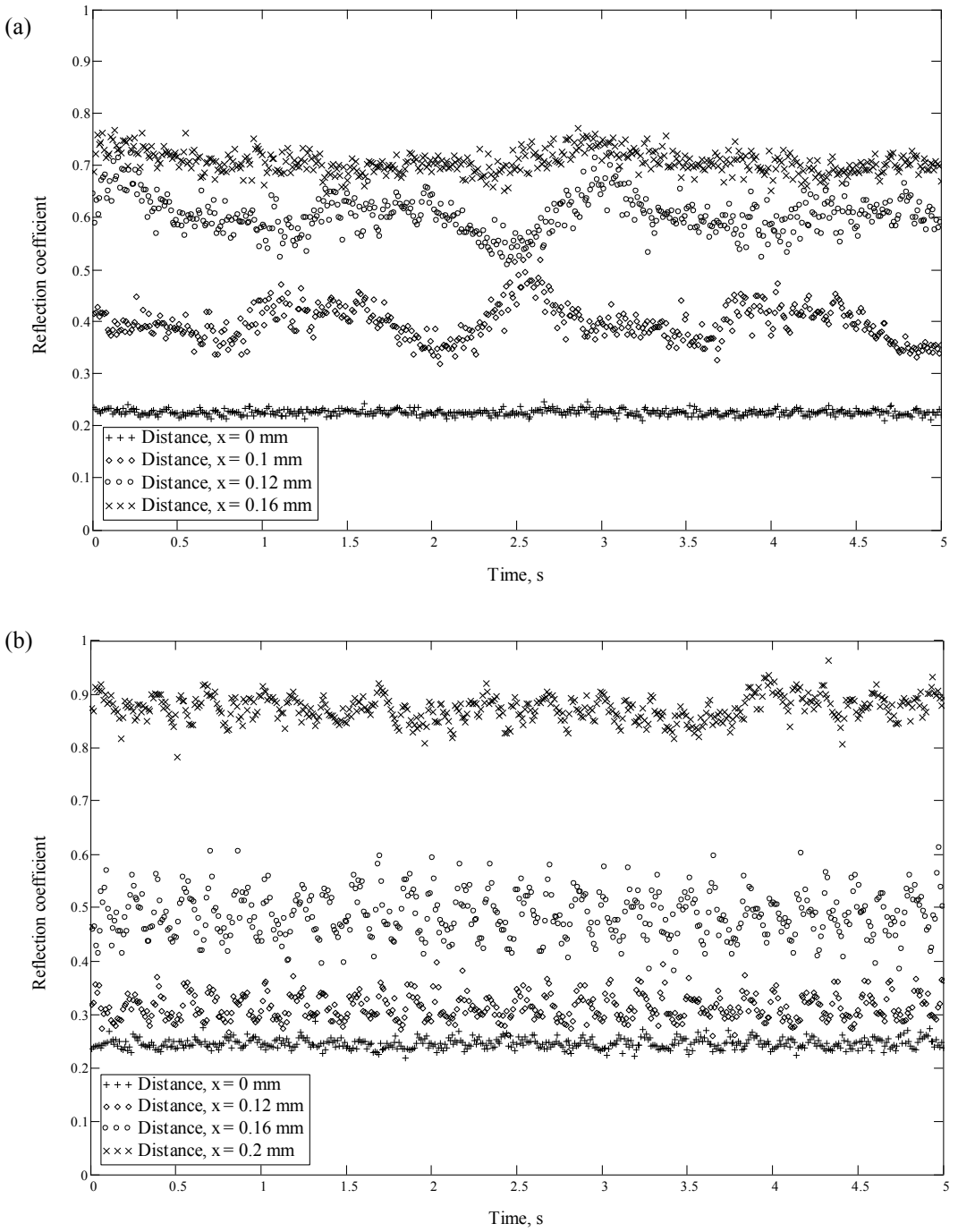

Figure 6.15 Variation of reflection coefficient with time at various points along the contact (*x=0* corresponds to the contact centre line). (a) Low speed, 33 mm/s (b) high speed, 200 mm/s. The phenomenon of cavitation causes a cyclic fluctuation in the reflection.

Cavitation can also be observed from the reflection coefficient results. Figure 6.14 shows the reflection coefficient in the exit region. There are three regions: radius contact, outlet region, and bulk lubricant. The bulk lubricant should have ideally $R = \frac{z_1 - z_2}{z_1 + z_2}$. At the low speeds (8.9, 18, and 22 mm/s) the reflection coefficients are

around 0.6. Whereas at the higher speeds (380 and 590 mm/s), the reflection coefficients increases to 1. This indicates that there is vapour in that region and total reflection occurs at the Perspex-vapor interface.

It is also interesting to observe how the reflection coefficient varies with time in this region. Physically the liquid follows a cycle of rarefaction and pressurization. As a consequence the liquid cavitates, creating small bubbles which in turn are compressed and expanded. Figure 6.15 shows how this dynamic process is recorded by the fluctuation in reflection coefficient.

6.5 Discussion

6.5.1 Comparison with theoretical solutions

The theoretical prediction for the film thickness (Eq. 2.2) suggests that film is proportional to the product of non-dimensionless load and speed ($U^{0.64} \times W^{-0.22}$). The measured film thickness data is plotted on these axes in Figure 6.16, equation 2.2 is also shown as a solid line. The experimental results fall somewhat below the model. Also shown is the data of Myant [2010] obtained using both optical interference and laser induced fluorescence (LIF) techniques for glycerol (GLY) and sunflower oil (SFO). In his experimental studies, fluids of various viscosities were used so that a wide range of model liquid films could be created. This data is also significantly below the theoretical solution.

At the lower film thickness ranges, the data is in closer agreement with the model. At this stage, the source of this discrepancy is not immediately obvious. However, it is worth pointing out that the range the model was established under is somewhat different to the test cases. Figure 6.17 shows a map of the lubrication regimes for a circular point contact. This map, adapted from (Hamrock *et al.* [2004]), shows the four regimes of hydrodynamic lubrication. The map is constructed using the non-dimensionless of viscosity parameter, g_v and the non-dimensionless elasticity parameter, g_e;

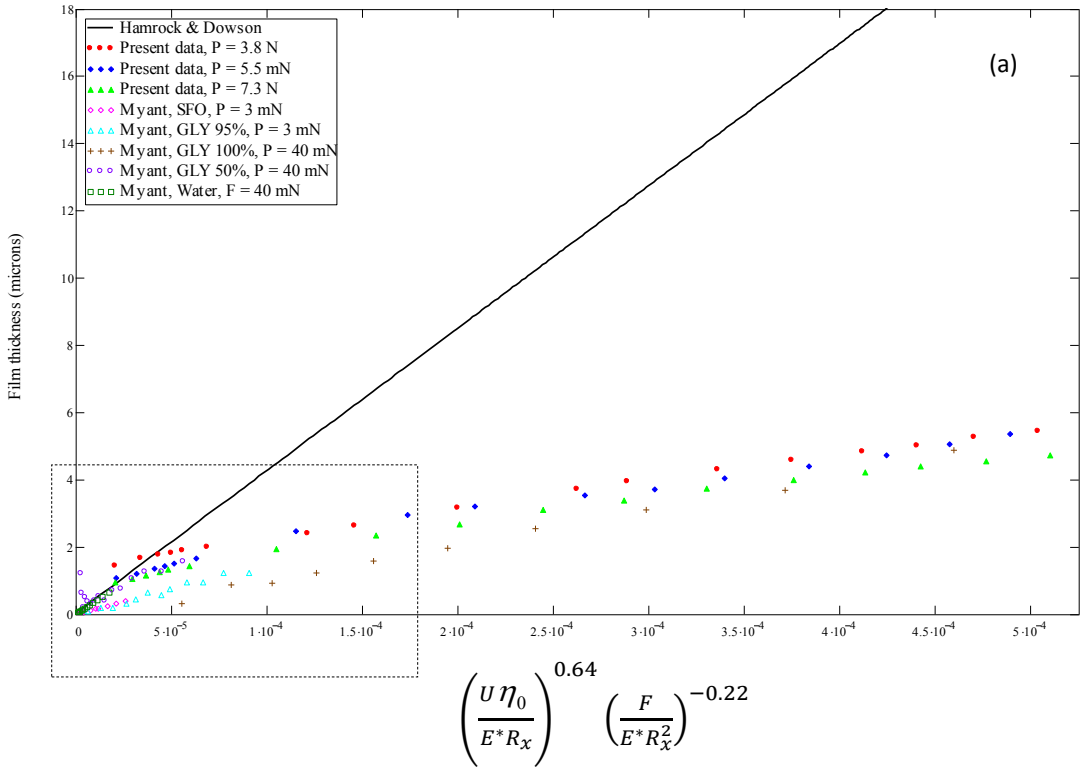

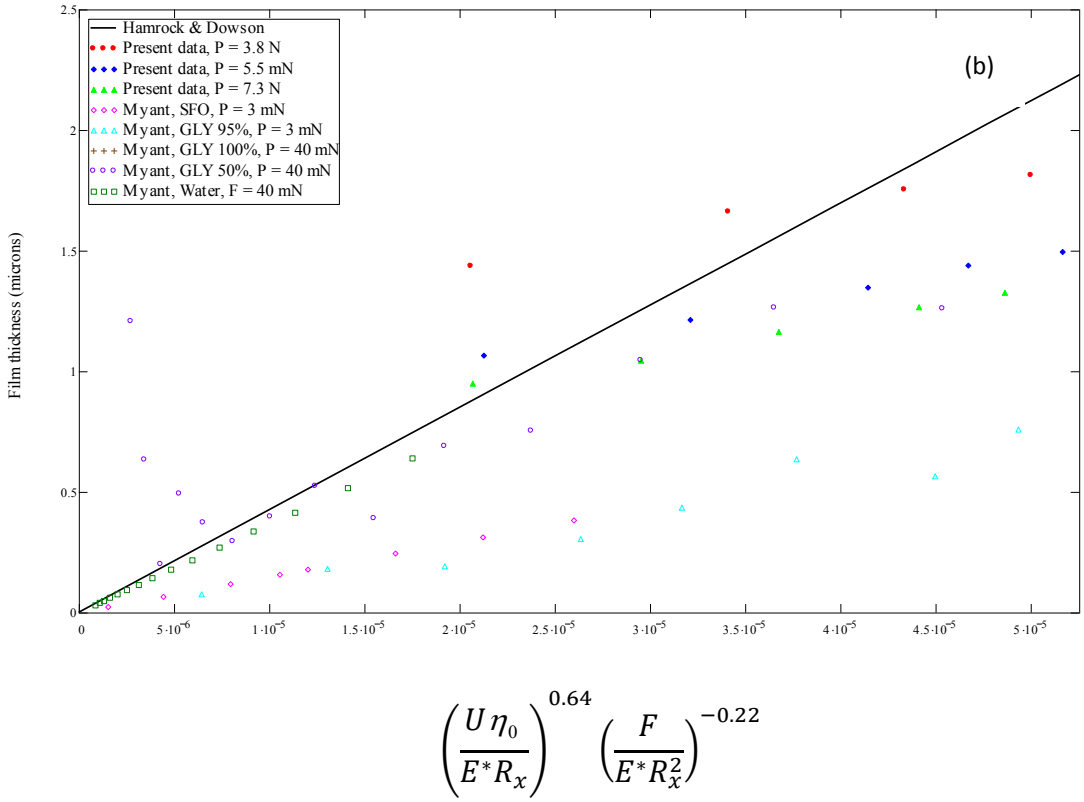

Figure 6.16 Comparison of ultrasonically measured film thickness results with the theoretical solution of Hamrock and Dowson [1978] and the experimental results of Myant [2010]. Lower graph (b) shows an enlarged region of the upper graph (a).

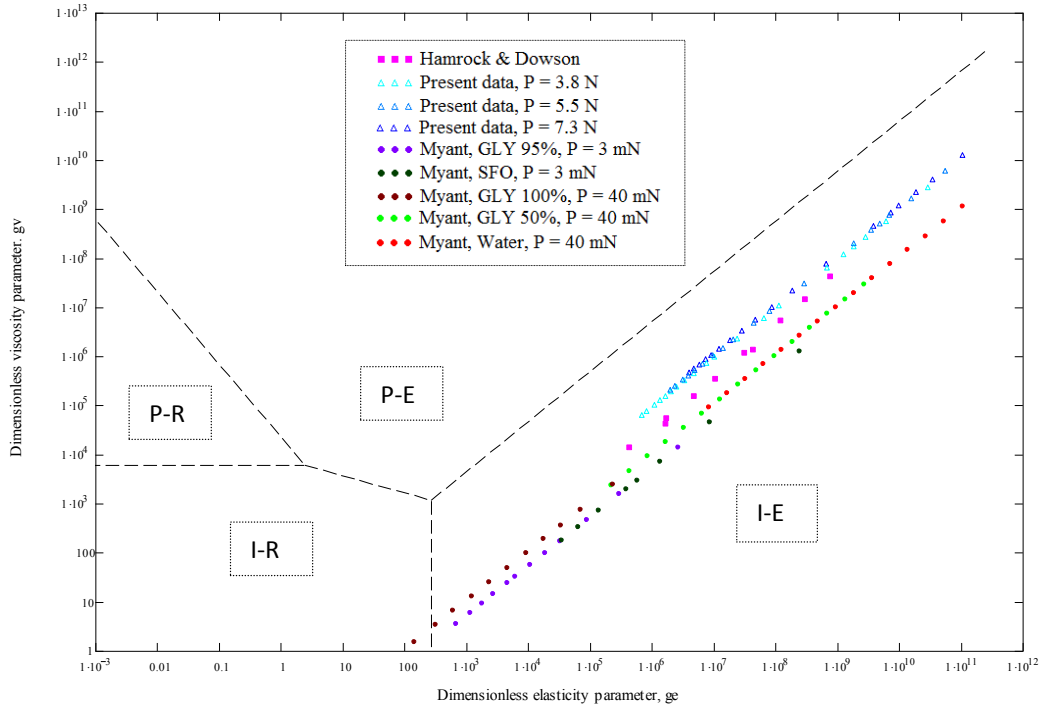

Figure 6.17 Lubrication regime map showing Piezoviscous rigid, *P-R*, Piezoviscous elastic, *P-E*, Isoviscous elastic, *I-E*, Isoviscous rigid, *I-R*. The present experimental data and that if Myant [2010] and the data points used to construct the Hamrock and Dowson model [1978] are shown on the map.

$$g_v = \frac{GW^3}{U^2}$$

$$g_e = \frac{W^{8/3}}{U^2}$$

where $G = \alpha E^*$ and α is the lubricant pressure viscosity coefficient.

The experimental data for the present work, the data of Myant [2010], and the data points used to construct the Hamrock and Dowson [1978] model have been plotted on the regime map of Figure 6.17. It can be seen that the higher film thickness data from this work extends somewhat beyond the range of theoretical solution data points.

6.5.2 Measurement limits

This measurement approach is limited by low spatial resolution measurements of the film in the contact. The 10 MHz immersion transducer used had a focal spot diameter 1.12 mm (from Eq. (4.3)) when ultrasonic wave strikes 10 mm thick of

the Perspex disk. This is fine for the I-EHL case here where the dimensions of the contact patch are larger than this. However, for metal on metal contacts where the contact patch is considerably smaller higher frequency transducers must be used (Dwyer-Joyce *et al.* [2003]). In any event, measurement of the detailed film shape will be difficult at these resolutions. Typically, the maximum practical frequency for this kind of work is ~50 MHz where a commercial transducer might have a focussed spot size of ~100 μm. Polymers and rubbers also tend to attenuate ultrasound at high frequencies particularly. This results in a considerably reduced amplitude and poor signal to noise. Whilst, no problems were experienced in this work with 10 MHz transducers, high frequency work could be more difficult.

The thickness measurement range also depends on the transducer frequency used. The 10 MHz transducer was capable of measurements in the 1 to 100 μm range. In other work (Dwyer Joyce *et al.* [2004]) on metal to metal contacts much lower (down to 50 nm) films have been measureable. This is because the acoustic mismatch between the two solids is lower and so a lower reflection coefficient for perfect contact is obtained. Essentially, the measurement region extends from $0<R<1$ rather than $0.2<R<1$ as in this case. Table 6.2 shows the measureable oil film thickness range for different combinations of bearing material. For the common case of rubber against steel, it is clear that no one transducer would measure a wide range of oil film thickness, and measurements would be difficult.

Table 6.2 Measurable film range for different contact cases for four different frequency transducers.

Contact cases	R_{min}	Measurable film range (μm)			
		5 MHz	10 MHz	25 MHz	50 MHz
Rubber - Perspex	0.20	3.5 – 137.5	1.0 – 68.7	0.6 – 27.5	0.3 – 13.7
Rubber - Steel	0.91	24.9 – 29.3	12.4 – 14.6	4.9 – 5.4	2.5 – 2.9
Steel - Steel	0.00	0.051 – 12.7	0.026 – 6.3	0.001 – 2.5	0.005 – 1.3
PTFE - Steel	0.88	15.0 – 24.4	7.5 – 12.2	3.0 – 4.9	1.5 – 2.4

6.5.3 Constriction and pressure spike

The profiles of lubricant film thickness (Figure 6.8) show constrictions at the contact exit occurred only at low speed. In the inlet region, the pressure is greater

for the higher speed than the lower speed. The pressure approaches closer to a Hertzian profile. Even though for low speed, there is still a significant rise in pressure in the inlet region and the pressure profile remains skewed towards the exit region. This was predicted by de Vicente *et al.* [2005]. Hamrock [1994] investigated the pressure spike and showed they do not occur for the isoviscous solution, so that the film shape for a large load range shows only a slight gap closing at the outlet. The lack of a pressure spike is probably due to the absence of piezo-viscous effects of the fluid in the contact for compliant materials.

6.6 Conclusions

The ultrasonic reflection technique has demonstrated the capability of measuring oil lubricant film thickness in I-EHL regime. The reflection of ultrasonic pulses from the interface between the sphere and disk was recorded for a range of lubricated and dry, static and dynamic contact conditions. Where there is a thin oil film, or very close contact, the ultrasonic pulse is largely transmitted. Conversely where the film is thick, or the interface consists of mostly air gaps and little solid contact, the reflection is high. The transducer was also scanned back and forth across the contact to pick up profiles of reflection.

At high contact pressures (P > 9.3 N) the reflection approaches a minimum value, when perfect contact has been formed. This data point allows the acoustic properties of the nitrile material to be determined. For the case where there is a thin separating liquid film between the surfaces, the reflection coefficient can be used to determine the liquid layer thickness using a simple mathematical analysis.

In this way, profiles of oil film thickness were created for various loads and sliding speeds. The phenomenon of a wedge-shaped constriction in lubricant film was observed, especially at low speeds (8.9, 11 and 22 mm/s). It was also possible to observe cavitation effects on the signal in the exit region at high speeds (380 and 590 mm/s). The measured central film thickness results are compared with published models of the lubrication mechanism and experimental data obtained from optical methods. The oil film thickness was measured in the region of 1 to 6

μm. The data was shown to be consistent with previous published experimental work using optical methods (Myant [2010]) but somewhat lower than theoretical solutions where there is limitation of theory Hamrock and Dowson [1978] for soft EHL contacts.

Chapter 7

Measurements of soft contacts using Rayleigh waves in-situ

In this chapter, the reflection of a Rayleigh wave at the contact between soft and hard materials was investigated. Variable and fixed wedge transducers were employed to generate surface waves. The characteristic of reflected signal of the Rayleigh wave at point and line contacts was carried out. The aim is to explore the possibility of developing a sensor for O-ring and lip seals that is positioned remotely from the contact region.

7.1 Introduction

In Chapter 5, the phase shift method has been explored to measure oil film thickness between two acoustically dissimilar materials in contact using bulk longitudinal ultrasonic waves. This method has shown that it could be employed as an alternative to measure film thickness between hard and soft material. However, there are two drawbacks in measuring a contact by using bulk longitudinal wave between soft and hard materials (such as: rubber and steel), which have mismatched acoustic impedance, are the attenuation and accessibility, as discussed in Chapter 1 section 1.1. If the rubber material is too thick, the bulk

ultrasonic wave will be attenuated. Then the transducer must be mounted on the rubber itself and so the bulk wave must pass normally through the thickness of the rubber and interface. Thus, the accessibility of the transducer is a big issue. Surface waves are proposed as a new method to measure contact between soft and hard materials. The ultrasonic transducer is positioned remotely from the contact region, so it can be applied as a sensor for o-ring and lip seals.

Surface waves, one of the categories of guided waves, can be generated through a variety of different techniques. They are normal beam transducer excitation, a wedge technique, comb transducer, and utilizing a mediator (Rose [1999]). The wedge technique is used in this study. The advantages of the wedge technique are that the surface waves are preferentially excited in just one direction, and in pulse mode the Rayleigh wave pulse generated has the same pulse envelope shape as the acoustic-source pulse (Rokhlin *et al*. [1981]).

Rayleigh waves and other acoustic surface waves are frequently used for non destructive evaluation (NDE) and damage detection. The application of ultrasonic surface wave has been developed experimentally by some authors not only in surface inspection problems but also in many others applications. Rokhlin *et al.* [1981] measured the phase velocity and transmission losses for predicting the strength of adhesive bonds. Schneider *et al.* [1992] developed a method to determine simultaneously the thickness and the elastic modulus of surface layers from surface wave dispersion.

The bulk wave and surface waves are fundamentally different. Mathematically, they are governed by the same set of partial differential wave equations. The fundamental difference is that, for bulk wave, there are no boundary conditions that need to be satisfied by the proposed solution. Otherwise, the solution to a guided wave problem must satisfy some physical boundary conditions that make it difficult to solve analytically (Rose [1999]).

The reflected signal of surface waves at contact between soft and hard materials has been studied experimentally using ultrasonic reflection method. Variable and

fixed wedge transducers were used and reflected signal of surface wave propagation within lubricated and un-lubricated contact was examined.

7.2 Wedge transducer to generate surface waves

7.2.1 Surface waves

The wave equation (Eq. 7.1), as a result of Helmholtz decomposition of the displacement vector, can be divided into two components,

$$\vec{u} = \overrightarrow{\nabla\emptyset} + \vec{\nabla} \times \vec{\psi} \tag{7.1}$$

As for bulk wave, ϕ and $\vec{\psi}$ are potentials for the longitudinal and transverse wave components, respectively, and the corresponding wave equations are given by

$$\frac{\partial^2 \emptyset}{\partial x^2} + \frac{\partial^2 \emptyset}{\partial z^2} + k_L^2 \emptyset = 0 \tag{7.2}$$

$$\frac{\partial^2 \psi}{\partial x^2} + \frac{\partial^2 \psi}{\partial z^2} + k_S^2 \psi = 0 \tag{7.3}$$

Where k_L and k_S are the usual bulk wave numbers

$$k_L = \sqrt{\frac{\rho}{\lambda+2\mu}} \quad \text{and} \quad k_S = \sqrt{\frac{\mu}{\rho}}$$

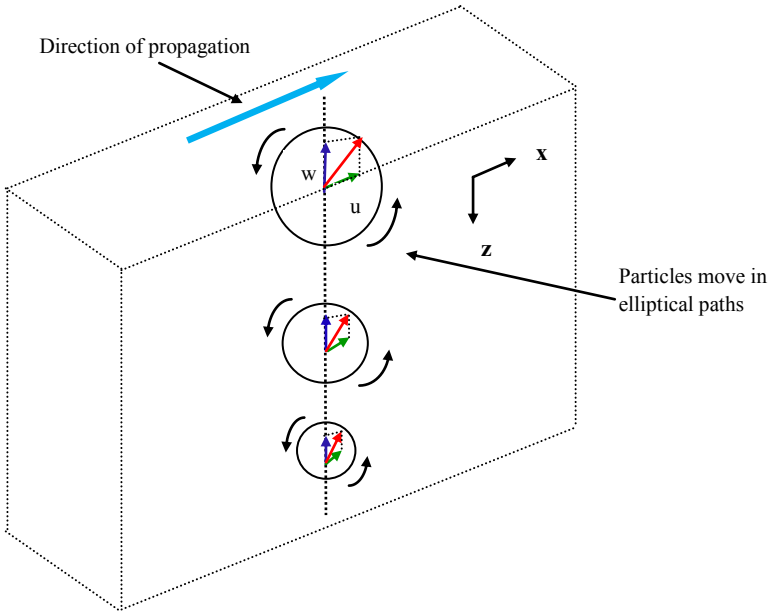

Figure 7.1 Displacement vector elliptical particle motion changed with depth. The solution for the normalized displacements with respect to the unknown

constant A can be obtained as follow;

$$\tilde{u} = \frac{u}{A} = (re^{-qz} - 2sqe^{-sz}) \cos k\,(x - ct) \tag{7.4}$$

$$\tilde{w} = \frac{w}{A} = q(re^{-qz} - 2sqe^{-sz}) \sin k(x - ct) \tag{7.5}$$

where

$$q = \sqrt{1 - \left(\frac{c}{c_L}\right)^2},\ s = \sqrt{1 - \left(\frac{c}{c_T}\right)^2},\ k = \frac{\omega}{c}$$

x in the propagation direction and z is in the depth.

The original expressions (Eqs. 7.2 and 7.3) show two waves, one longitudinal and one transverse, propagating along a boundary. The superposition of two wave leads to surface waves where the vector sum of equation in u and w on the surface gives the ellipse, as shown in Figure 7.1. The elliptical particle motion changes as a function of depth.

7.2.1 Generation of surface waves

The most common method for generating surface waves is using a plastic wedge device, which is based on the conversion of longitudinal wave, which impinges at an angle θ to the boundary of the solid and wedge. A longitudinal mode transducer launches a compressional wave into the plastic wedge having a critical angle, θ_R, at which the energy converts into a Rayleigh surface wave, which propagates with an elliptical particle motion. The elliptical motion occurs as function of depth, with the motion actually reversing after a particular depth. A plot of displacement profile from Eqs. 7.4 and 7.5 with depth is shown in Figure 7.2 for displacement in the x and z axes. The graph shows that the displacement normal to the surface increases at first, and then falls off monotonically with depth.

The wedge transducers use the principles of refraction and mode conversion (as discussed in Chapter 3 section 3.2.2) to produce refracted shear or longitudinal waves. When a longitudinal wave with a velocity c_i arrives at the boundary of an adjacent medium with a Rayleigh wave velocity c_R, the critical angle θ_c of incident for generation of surface wave at the boundary is given by

$$\theta_c = sin^{-1}(\frac{C_i}{C_R}) \tag{7.6}$$

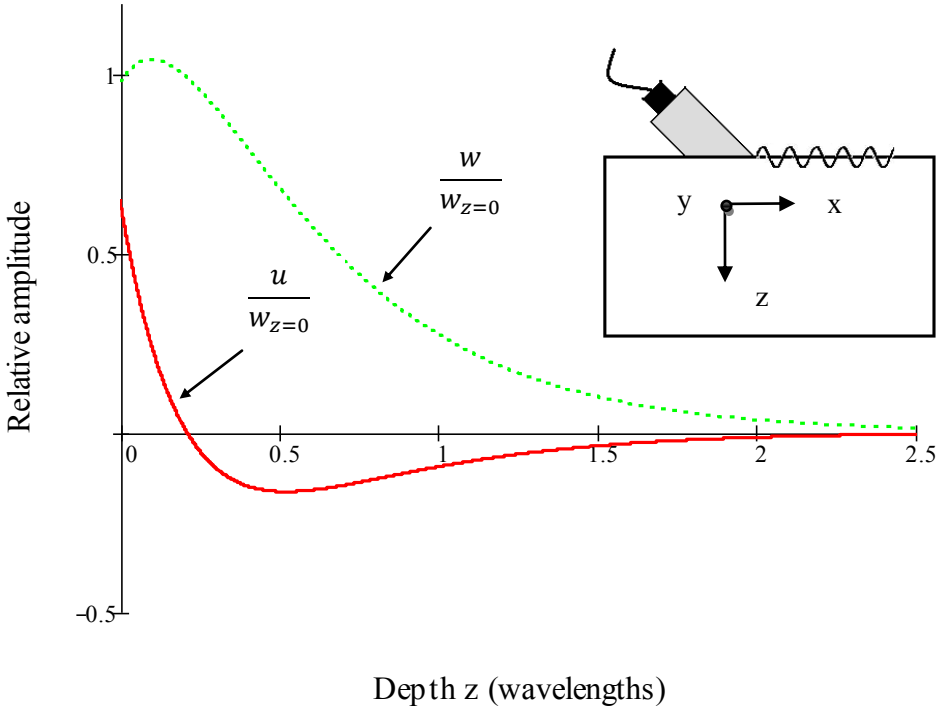

Figure 7.2 Relative Rayleigh wave displacements with depth for a steel half-space: curved are normalized with respect to w_z at z = 0.

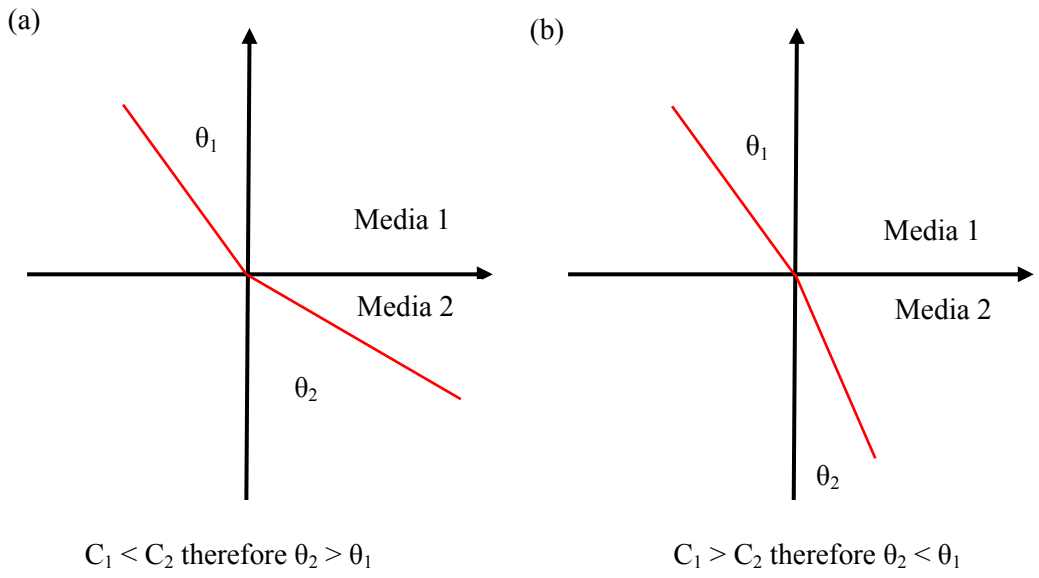

Figure 7.3 Critical angle concepts: (a) $C_1 < C_2$ and (b) $C_1 > C_2$.

In order to generate a surface wave, wedges in a conventional type angle transducer have been designed to use this principle, with c_{1w} the wave velocity in

the wedge material and c_R the surface wave velocity in medium 2. From the Snell's law, application of refracted angle 90^0 yields $c_{1w} \sin 90^0 = c_R \sin \theta_w$, so

$$\sin \theta_w = \frac{c_{1w}}{c_R} \tag{7.7}$$

This technique will work, if c_{1w} is less than c_R, as shown in Figure 7.3.

To get c_R theoretically, it is obtained from the Rayleigh equation (Rose [1999]) which is writen in polynomial form as

$$\eta^6 - 8\eta^4 + 8(3 - 2\xi^2)\eta^2 - 16(1 - \xi^2) = 0 \tag{7.8}$$

The variables of ξ and η are

$$\eta = \frac{c}{c_T} \text{ and } \xi = \frac{c_T}{c_L} \tag{7.9}$$

where c is surface wave, c_T is shear velocity, and c_L is longitudinal velocity.

The equation has one real root, η_R, corresponding to the existence of a Rayleigh surface wave with the properties given by the two potential functions (ξ and η). This root (η_R) depends on Poissons ratio, ν, which is given an approximation solution by Vikotorov (Rose [1999]);

$$\eta_R \approx \frac{0.87+1.12\nu}{1+\nu} \tag{7.10}$$

Combining Eqs. 7.9 and 7.10

$$\frac{c_R}{c_s} = \frac{0.87+1.12\nu}{1+\nu} \tag{7.11}$$

Over the allowed range of ν ($0 < \nu < 0.5$), the Rayleigh velocity, c_R, thus varies from 0.87 c_S to 0.96 c_S. The variation is shown in Figure 7.4. From this figure the surface wave velocity on the medium can be predicted, if the Poisson ratio of medium is known.

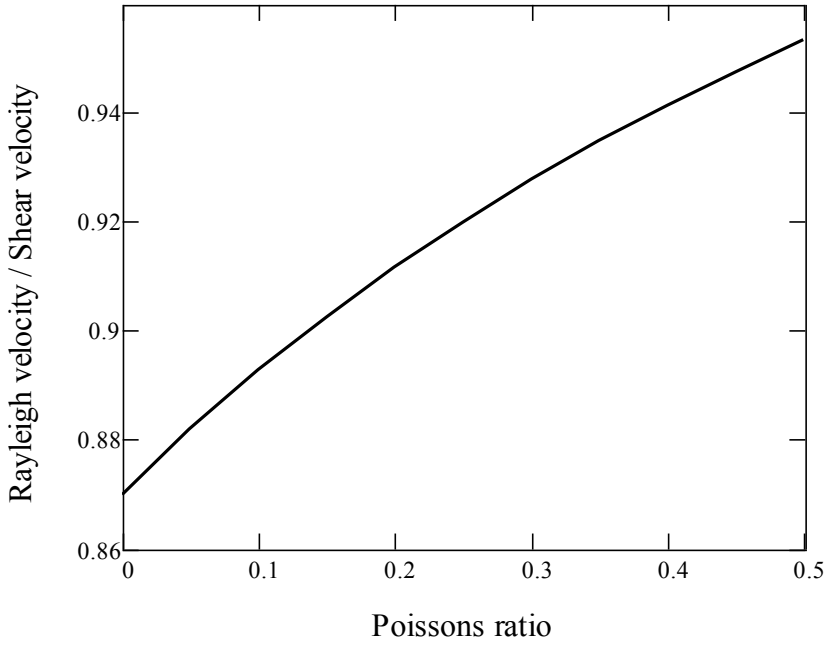

Figure 7.4 Ratio of Rayleigh and shear velocity as a function of Poissons ratio, *v*, using approximation Eq. 7.11.

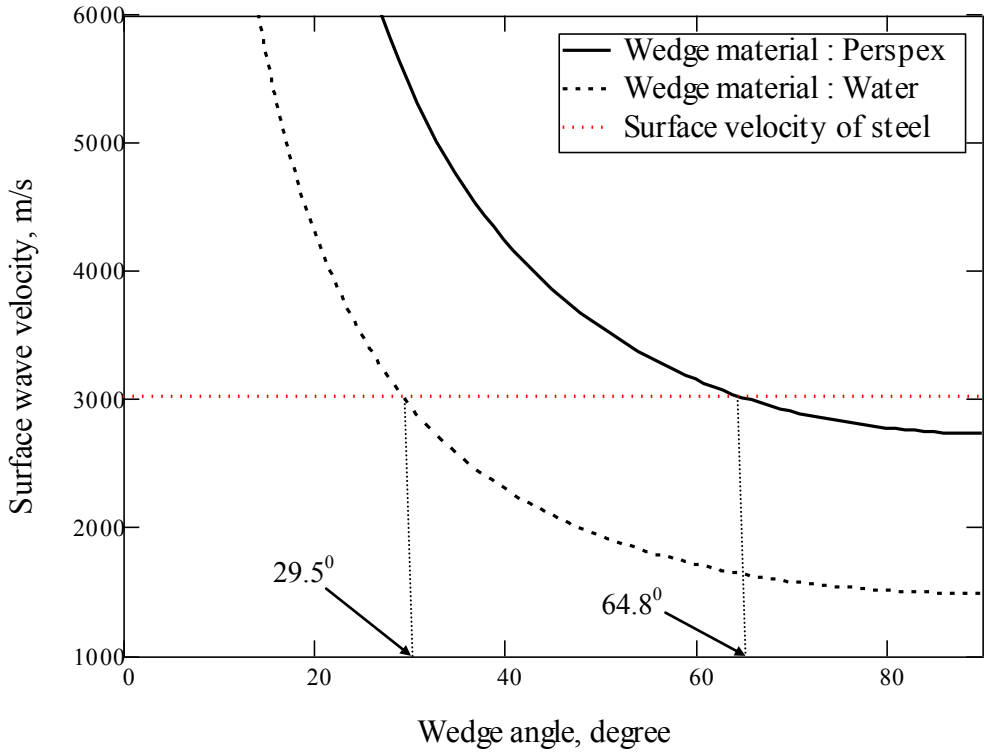

Figure 7.5 The relationship between wedge angle and Rayleigh wave velocity for different wedge materials against steel.

The wedge material may be either liquid or solid. The efficiency of both materials of wedges is 68 % and 35 % respectively based on the rate of attenuation due to leakage from the surface wave into the wedge material (Schneider *et al.* [1992]). Figure 7.5 shows the relationship between the wedge angle and surface wave velocity for wedge materials against steel based on Eq. 7.7. It shows that to generate the surface wave on steel plate using a Perspex wedge required an incident angle of 64.8^0 (based on Eq. 7.11 where surface wave velocity on steel is 3016 m/s and longitudinal wave velocity of Perspex is 2730 m/s). For water coupling wedge, the angle should be 29.5^0.

7.3 Materials and experimental apparatus

7.3.1 Materials

The reflected signal of surface wave propagation was investigated by studying at point and line contact conditions. Two kinds of rubber were used to generate point and line contacts. A nitrile ball of 19 mm diameter and a nitrile cord of 10 mm diameter and 45 mm length were used as shown in Figure 7.6. The two types of nitrile were slightly different. The density was obtained from the manufacture POLIMAX and the speed of sound was obtained from measuring reflection from solid-solid interface (RSS) as stated in section 4.4, as shown in Table 7.1

(a) (b)

Figure 7.6 (a) Nitrile ball and (b) Nitrile cord.

Table 7.1 Properties of materials used in the experiment.

Name of materials	Density (kg/m^3)	Speed of sound (m/s)	Acoustic impedance (MRayls)
Nitrile ball	1262	1618	2.04
Nitrile cord	1300	1890	2.45

7.3.2. Apparatus

To generate Rayleigh surface waves and detect reflected signals, a solid wedge transducer was used. Variable and fixed wedge transducers were employed to generate surface waves, which were excited and detected experimentally with apparatus shown in Figure 7.7. A 2.25 MHz contact longitudinal transducer was used. The transducers, which have elements size of 6.35 and 2.54 mm, respectively, were coupled on the fixed wedge and the variable wedge with the angle at 64.8^0 (see section 7.2).

The reflected surface wave signal the surface of steel has a small amplitude. In order to get a good signal, all interfaces (transducer/acrylic, acrylic/base and base/sample) are covered with a coupling gel to ensure transmission of the ultrasonic wave.

The wedge transducers were placed on a steel plate, with the dimension of 158 mm length, 70 mm width and 7 mm thick. The nitrile rubber ball or cord were mounted on the surface of steel and different loads applied by clamping and applying weights up to 10 kg. The tests were conducted with or without oil introduced in the contact.

The ultrasonic transducers were connected to a pulse-receiver that generates a sequence of high-voltage pulses as stated in Chapter 4 section 4.5.3. These caused the piezoelectric transducers to be excited in mechanical resonance. The transducers then emitted a broadband pulse of ultrasonic energy. The pulse

reflected from the contact was amplified and stored on a digital oscilloscope. The UPR was controlled by LabView program to receive reflection signals from the oscilloscope. The reflection signals were converted into frequency domain using an FFT to obtain the amplitude spectra. The reflection coefficient amplitude was determined by comparing the reflected signal of surface wave on steel plate with and without nitrile rubber.

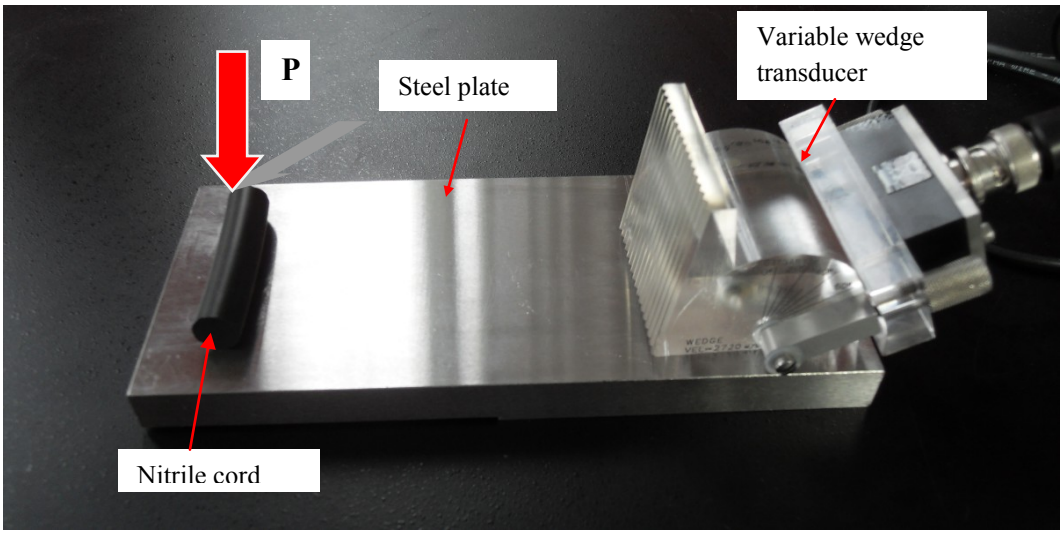

(a)

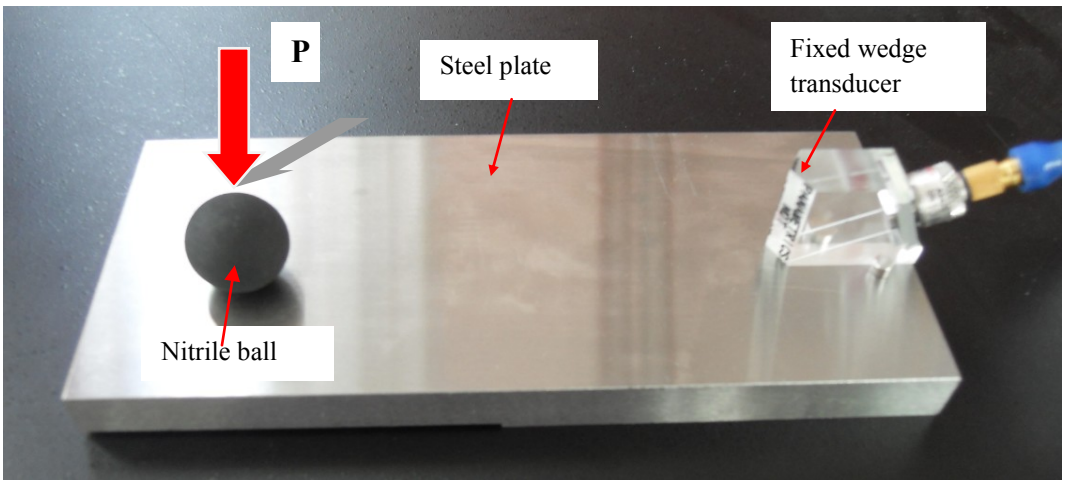

(b)

Figure 7.7 Photograph of experimental apparatus used for measuring contact between nitrile cord (nitrile ball) and steel plate using (a) variable and (b) fixed wedge transducers.

7.4 Results

7.4.1 Typical measurement

A schematic is shown to explain position of reflected signal of surface wave propagation on the surface of steel plate for variable and fixed wedge transducers in Figure 7.8. The position of reflected signal of surface wave propagation on the surface of steel plate using fixed wedge transducer is shown in Figure 7.8a. *BW* is the bottom face reflection from the wedge and *TS* is the reflection coming from the top edge of steel plate, which has high amplitude. The third pulse, *BS*, seen in this figure is the reflected signal of surface wave propagation on the bottom edge of steel plate. Whereas, for variable wedge transducer, the position of reflected signal of surface wave propagation is shown on Figure 7.8b. *TW* and *BW* are reflection from the top and bottom face of the wedge, respectively. *TS* and *BS* are reflection of surface wave propagation coming from the top and bottom edge of steel plate. The *TS* reflection will be monitored in order to detect the presence of contact between steel plate and rubber ball.

The reflected signal of surface wave propagation from the nitrile ball using fixed wedge transducer (see Figure 7.8a for label) can be seen in Figure 7.9 but the amplitude of reflected signal was very small compared to the others as found also by Drinkwater *et al.* [2003]. When the load was applied on the nitrile ball, the nitrile ball and *TS* reflections were reduced proportionally to the applied load. Because the amplitude of reflected signal from nitrile ball was very small, so the *TS* reflection was adopted as criterion of change of the contact between nitrile ball and steel plate.

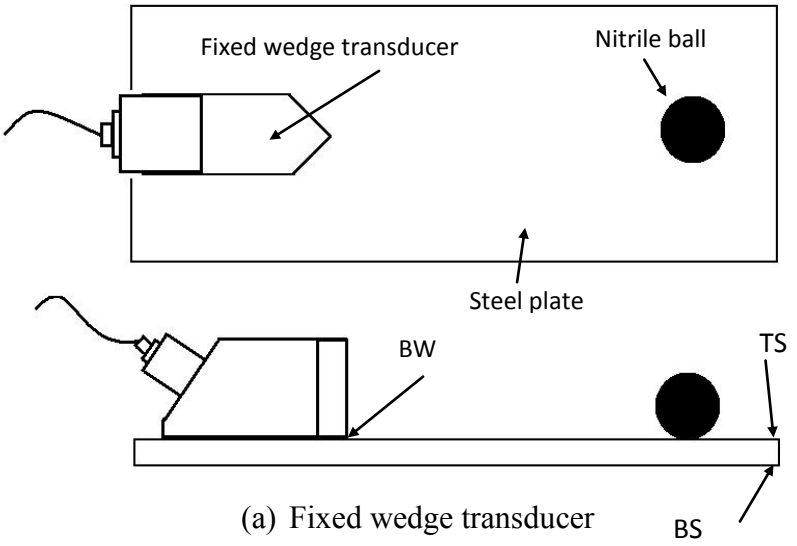

(a) Fixed wedge transducer

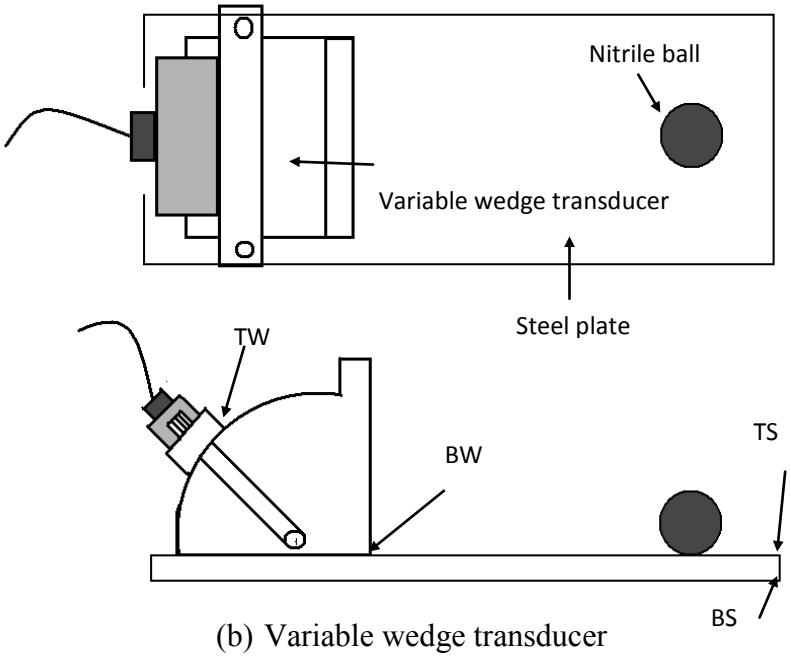

(b) Variable wedge transducer

Figure 7.8 Schematic for describing position of reflected signal from: (a) fixed and (b) variable wedge transducers on the surface of steel plate.

The proportion of amplitude of reflected signal (*TS*) of surface wave propagation is dependent on the degree of contact between two surfaces. When no nitrile ball is present on the surface of steel plate, the energy of reflected signal of surface wave propagation will increase (Figure 7.9a). In Figure 7.9b, when the nitrile ball is present on the surface of steel plate with load 29 N, the amplitude of reflected signal of surface wave propagation (*TS*) is reduced. The reflected signal (*TS*) of

surface wave propagation at the interface will be decreased proportionally, as the percentage of contact increases.

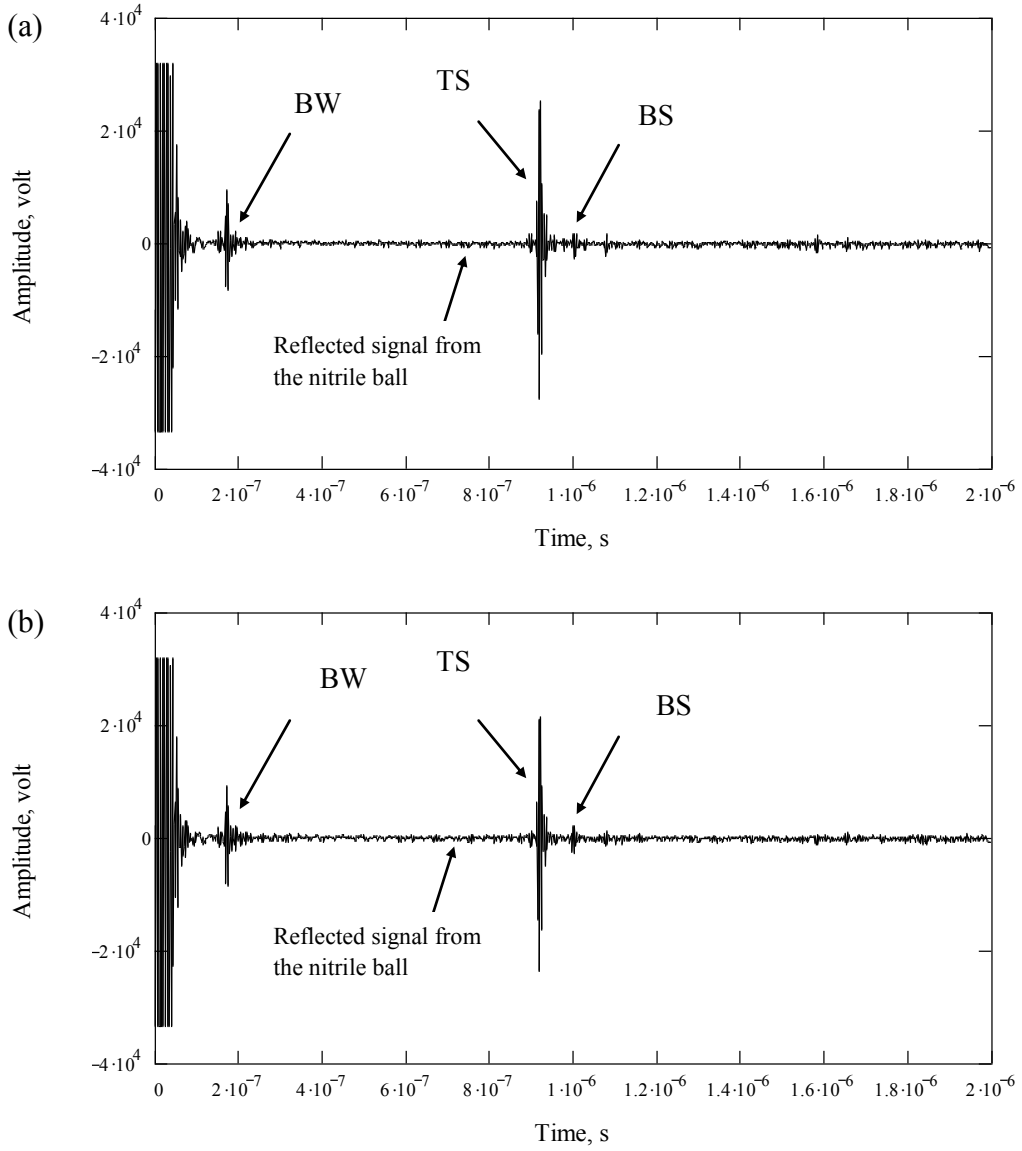

Figure 7.9 The comparison of reflected signal of surface wave propagation on the surface plate of steel between (a) without nitrile ball and (b) with nitrile ball load 29 N using fixed wedge transducer.

7.4.2 Effect of oil

To investigate effect of oil on reflected signal of surface wave propagation on the surface of steel plate, the experiments were conducted by applying oil to the surface of the steel plate using variable wedge transducer (see Figure 7.8b for the label) as shown in Figure 7.10. It was difficult to quantify the amount of oil

applied to the surface of steel plate. In these experiments, two conditions were considered: applying 25 mm width of adhered oil on the steel plate and covering the whole surface of steel plate. In both cases, the thickness of oil was not determined quantitatively.

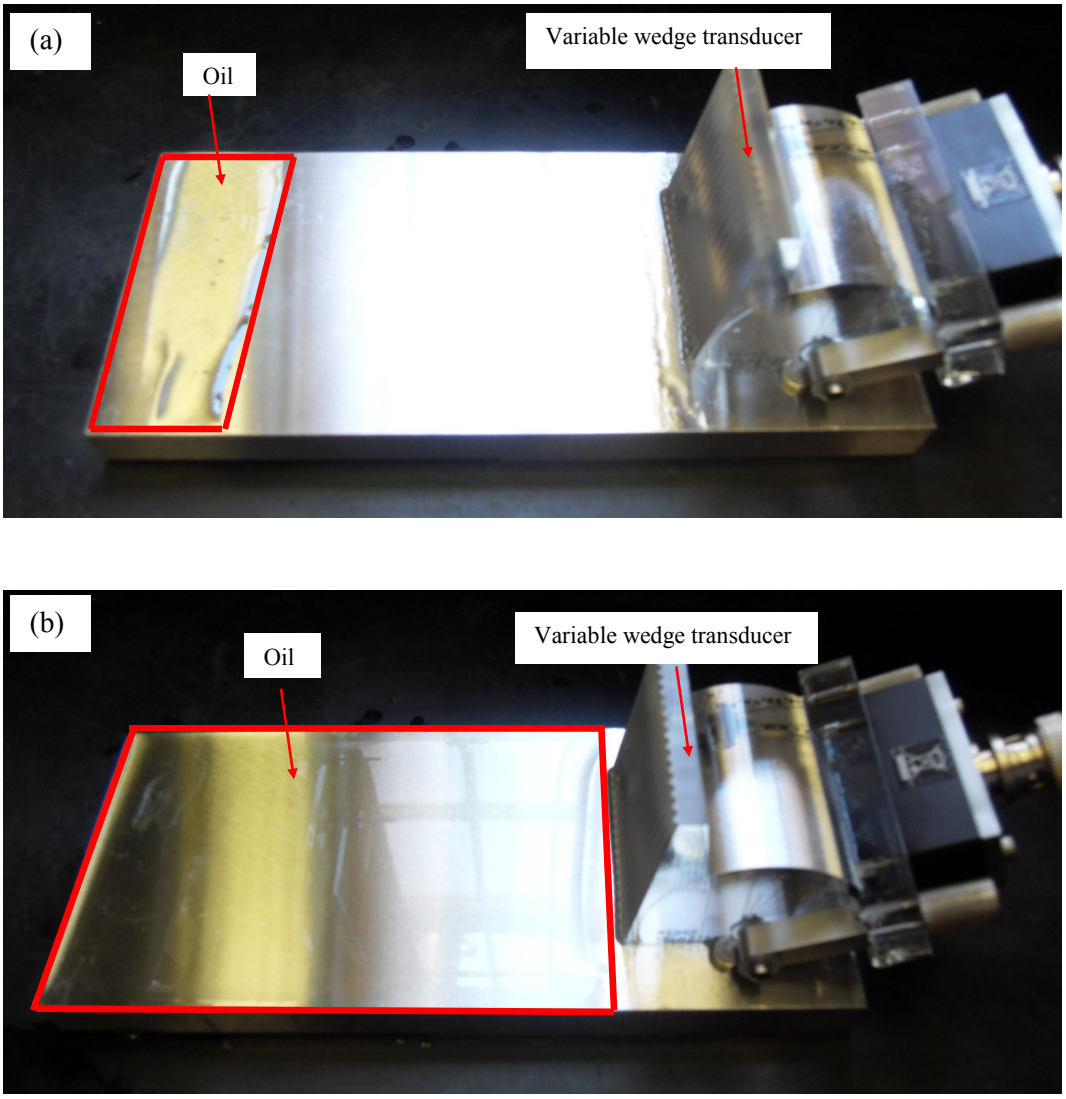

Figure 7.10 The photographs of experimental study: the effect of oil against reflection coefficient of surface wave propagation by (a) applying 25 mm width of adhered oil and (b) covering whole of oil on the surface of steel plate by using variable wedge transducer.

The results of this experiment compared to dry case are shown in Figure 7.11 using the variable wedge transducer. The reflected signal of surface wave propagation was significantly reduced in the liquid. It can be seen from Figure 7.9b that the reflected signal, *TS*, is reduced dramatically then vanished when the

liquid covers the whole surface of steel plate (Figure 7.11c). This is because the energy of surface wave has been absorbed in liquid.

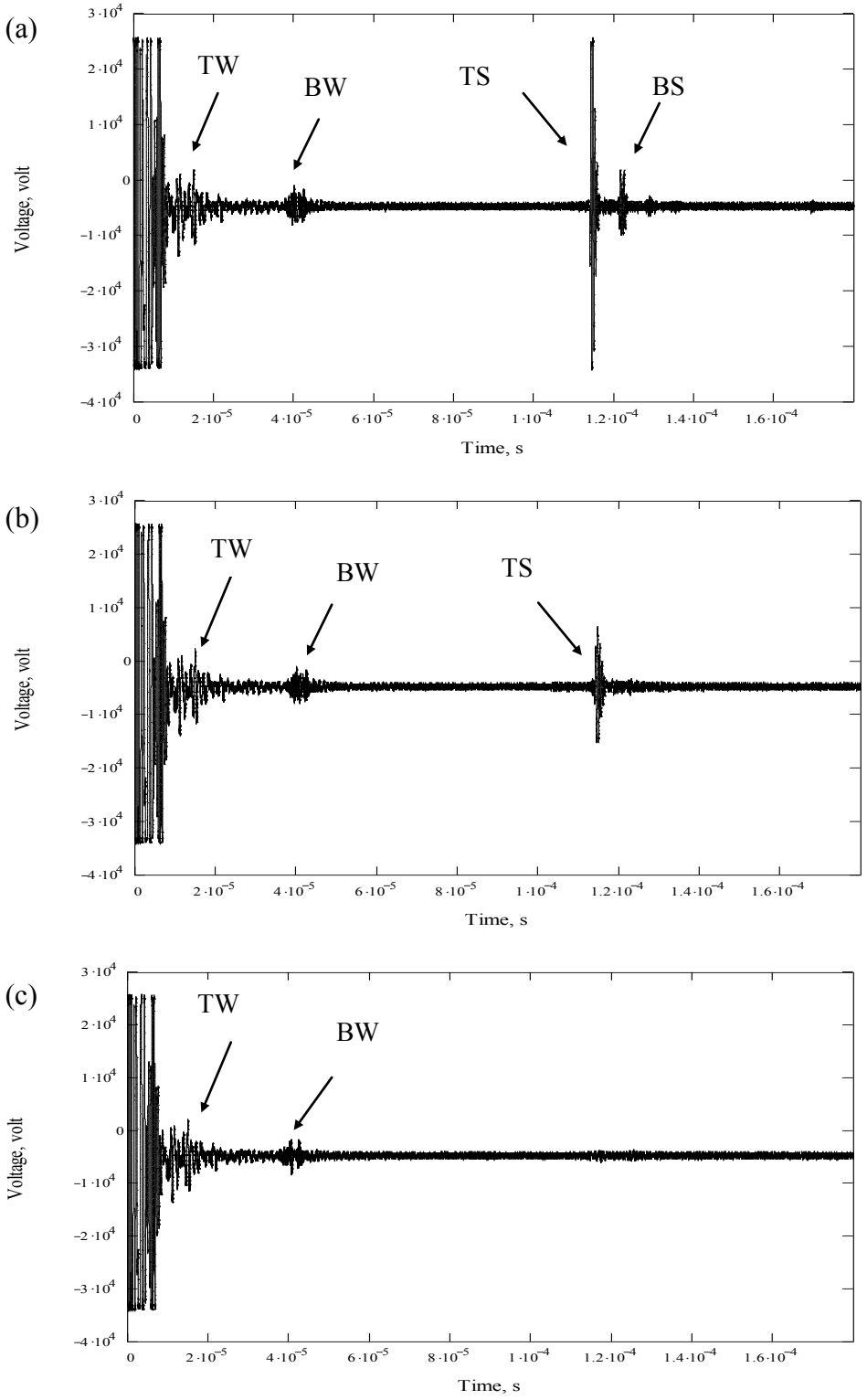

Figure 7.11 The comparison between (a) without oil, (b) with 25 mm width of adhered oil, and (c) cover whole of oil on the surface of steel plates of reflected signal of surface wave propagation by using variable wedge transducer.

7.4.3 Point and line contacts

The influence of load against reflected signal of surface wave propagation at the contact for both wedge transducers was conducted by using point and line contact experiments. The point contact was formed by contact between nitrile rubber ball and steel plate, whereas the line contact was formed by contact between nitrile cord and steel plate. The measurements of reflected signal of surface wave propagation were conducted when the contact between two solids was in dry and lubricated conditions with different loads. The effect of this loading on the reflected signal of the surface wave in the steel plate was measured.

The characteristic of the reflected signal of surface wave propagation at both contacts is expressed by a reflection coefficient. Figure 7.12 shows the steps of digital signal processing from capturing reflected signal to obtain reflection coefficient. The selected signal from the time domain wave (*TS*) is shown in Figure 7.12a by capturing reference signal first by removing nitrile ball and nitrile cord from the surface of steel plate and then by capturing reflected signal when the nitrile ball and nitrile cord are loaded. Each of the reflection pulses is passed through a fast Fourier transform (FFT) to give amplitude against frequency plot (Figure 7.12b). Dividing each signal from different loads by the FFT of the reference signal gives the reflection coefficient spectra (Figure 7.12c).

Figures 7.13 and 7.14 show the reflection coefficient of surface wave propagation at the point and line contacts, respectively, with dry and oil contacts for both wedge transducers. In general, from these figures, it shows that as the maximum contact pressure increases, the reflection coefficient decreases and the reflection coefficient of dry contact is higher than the oil contact. The results of reflection coefficient at point contact are shown in Figure 7.13 by comparing reflection coefficient against maximum contact pressure in dry and oil contacts. The variable wedge transducer has reflection coefficient higher than the fixed wedge transducer for both dry and lubricated conditions. It is notable that the element diameter of transducer would influence the reflected signal of surface wave propagation at

point contact, where element diameter of the variable wedge transducer is larger than the fixed wedge transducer (see section 7.3.2).

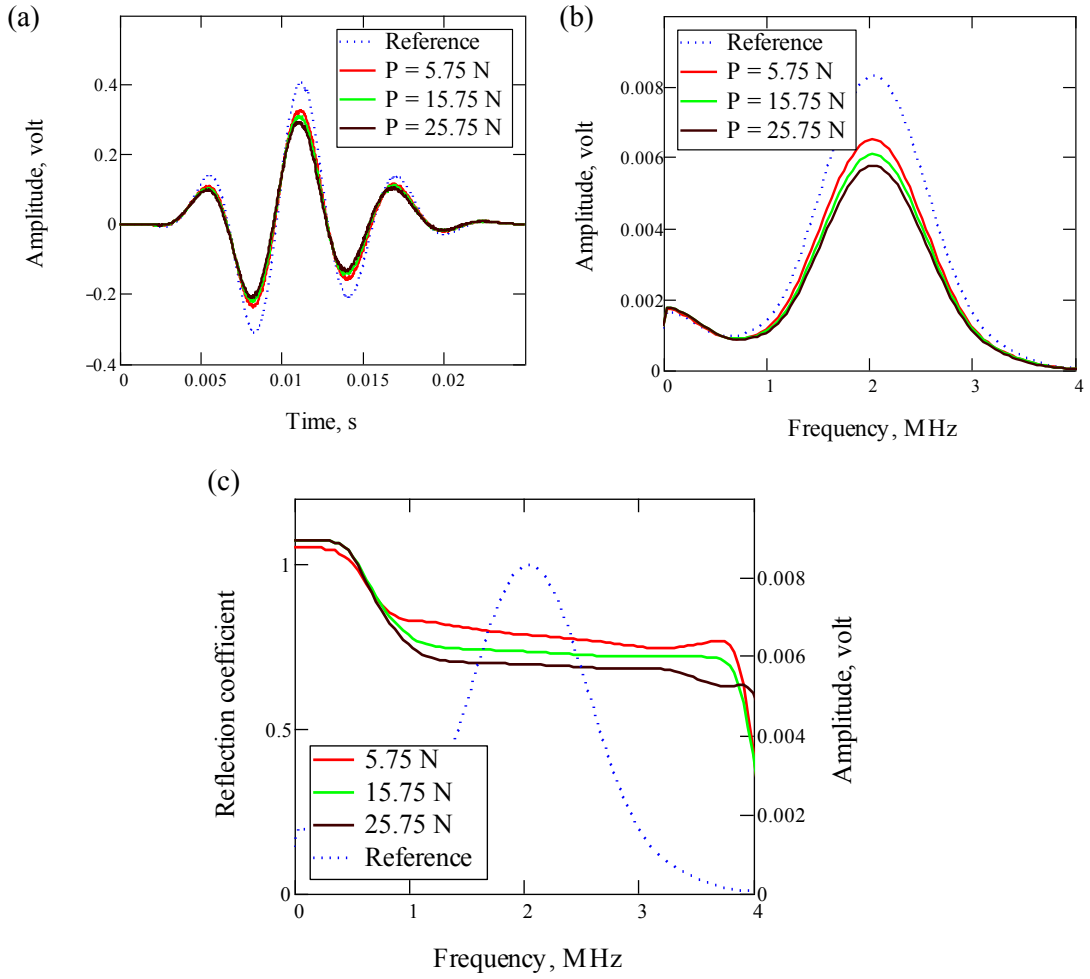

Figure 7.12 The steps of digital signal processing: (a) selected signals (b) FFT, and (c) reflection coefficient.

Figure 7.14 shows the comparison between reflection coefficient and maximum contact pressure at the line contact between dry and lubricated contacts. It can be seen that reflection coefficient for the fixed wedge transducer is a little bit higher than the variable wedge transducer, but the differences of reflection coefficient both wedge transducers are not significant especially at high loads. There is no effect of element diameter against reflected signal of surface wave propagation at line contact for both transducers. Even though the element diameter of both transducers is different, the reflected signal of surface wave propagation both transducers at line contact is almost the same.

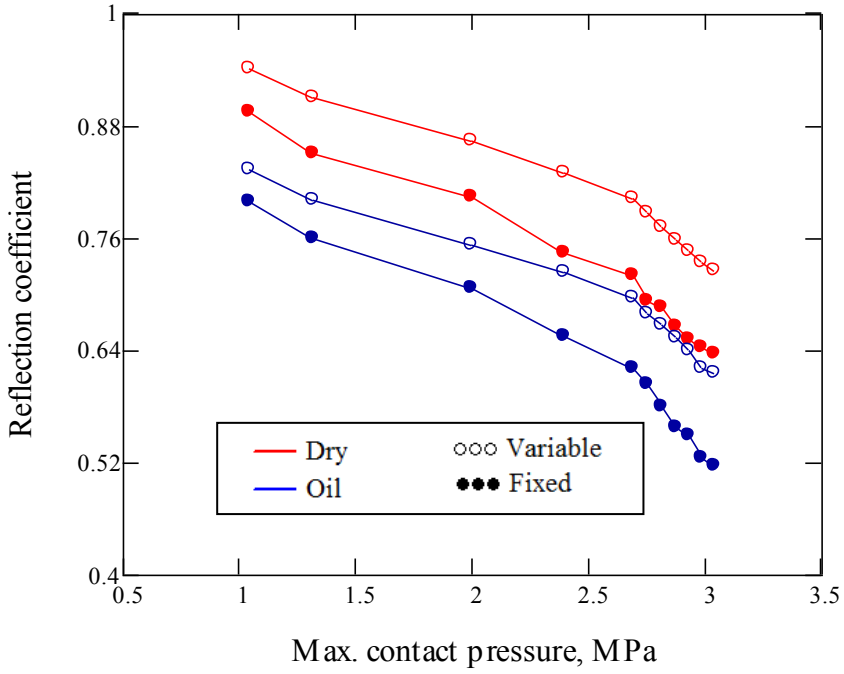

Figure 7.13 The comparison between reflection coefficient and maximum contact pressure for both fixed and variable wedge transducers in dry (red line) and oil (blue line) contacts at point contact (Nitrile ball).

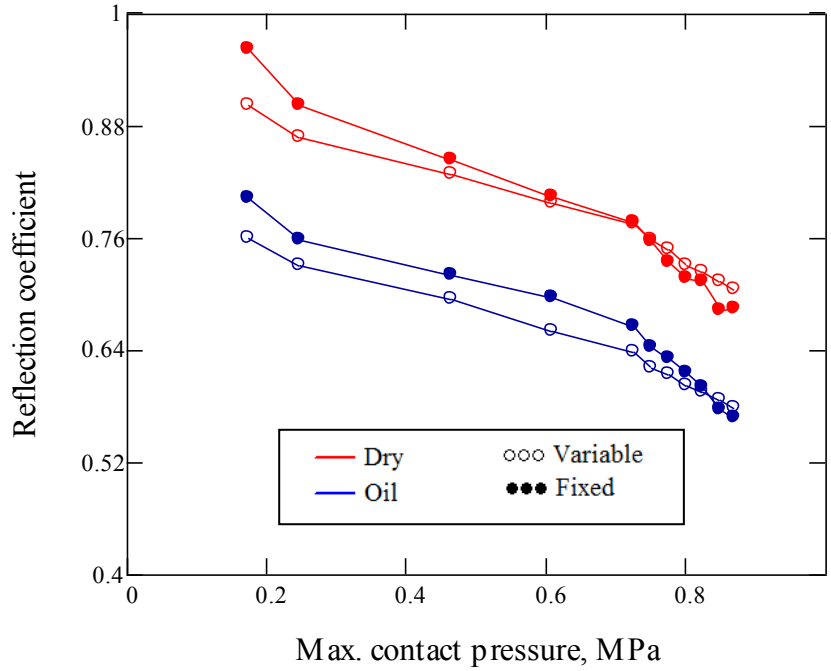

Figure 7.14 The comparison between reflection coefficient and maximum contact pressure both variable and fixed wedge transducers in dry (red line) and oil (blue line) contacts at line contact (Nitrile cord).

The difference of reflection coefficient between point and line contacts was that at point contact, the pulse spreading because of wave transmission from the variable

transducer was outside of the contact area so that the reflection coefficient was higher than for the fixed transducer. At the line contact, on the other hand, most of pulse spreading was in the contact region so that the reflection coefficient was influenced of both the contact geometry and contact pressure. At low pressures ($p < 0.7$ MPa), the geometry of contact is dominant where the reflection coefficient for the fixed wedge transducer is higher than the variable wedge transducer, but at high pressures ($p < 0.7$ MPa), the contact pressure is dominant where the reflection coefficient for the fixed wedge transducer is lower than the variable wedge transducer, as seen in Figure 7.14.

7.4.4 Loading and unloading

Figures 7.15 and 7.16 show reflection coefficient varied through a cycle of loading and unloading for both dry and lubricated conditions using fixed and variable wedge transducers at point and line contacts. Typically, the reflection coefficient at a given pressure on the loading and unloading lines for dry contact is narrower than the lubricated contact for both transducers. It means that there was an effect between oil lubrication and plastic deformation at unloading condition. It should also be noted that in the experiment, it was difficult to control how much oil was applied to the contact for both wedge transducers, so when unloading the oil adhered to the surface of steel plate. At point contact, however, the reflection coefficient between loading and unloading for variable wedge transducer is almost the same for dry and lubricated condition. It is clear that element diameter of variable wedge transducer is bigger than diameter contact so that only a small part of surface wave propagated in the contact interface.

These figures also show that the reflection coefficient at dry contact for fixed transducer, at point and line contacts between loading and unloading lines, is wider than the variable wedge transducer. As similar pattern is seen for lubricated contact. This indicates that the fixed transducer is more sensitive to detect plastic deformation in the contact due to the effect of element diameter. Even though there was difference of reflection coefficient between loading and unloading lines between two transducers, in the case of line contact it is clear as shown in Figure

7.15 that the reflection coefficient between fixed and variable wedge transducer is almost coincide.

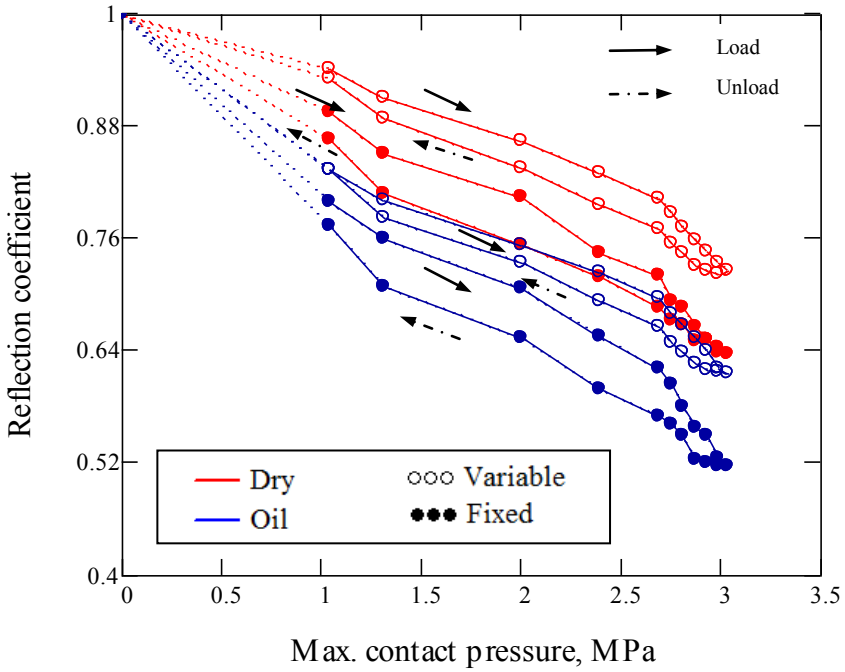

Figure 7.15 The experimental measurement of reflection coefficient of surface wave propagation as a function of maximum contact pressure in dry (red line) and lubricated (blue line) contacts for variable and fixed wedge transducers at point contact.

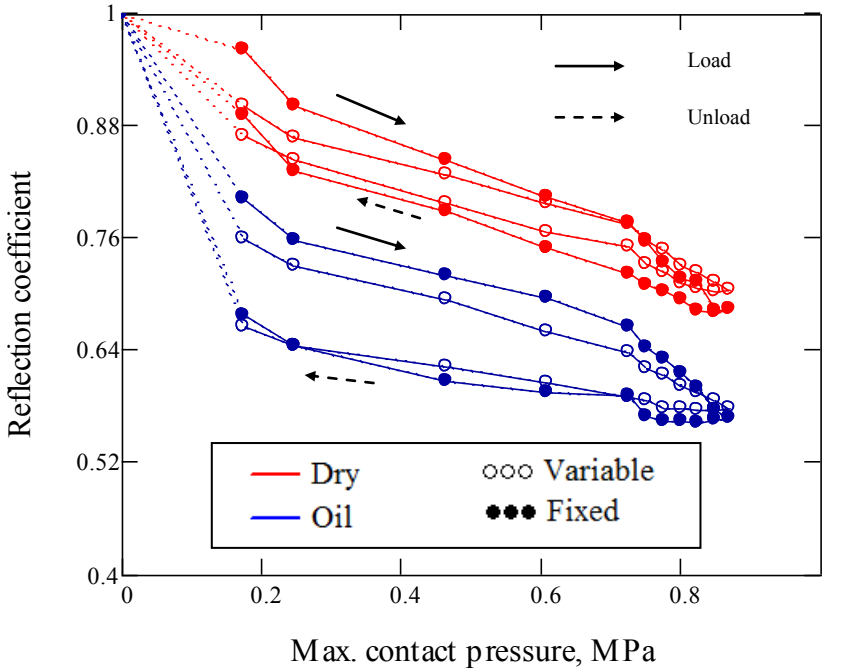

Figure 7.16 The experimental measurement of reflection coefficient of surface wave propagation as a function of maximum contact pressure in dry (red line) and lubricated (blue line) contacts for variable and fixed wedge transducers at line contact.

7.5 Discussion

7.5.1 Propagation of surface wave in solid-liquid interface

The amplitude of surface wave will be decreased when it propagates in fluid, because the surface wave is combination of longitudinal and transversal wave, where the transversal wave cannot propagate in liquid. The propagation of surface wave along a solid-liquid interface is known as Scholte wave where Rose [1999] investigated that the wave amplitude decreases slightly in liquid but rapidly in the elastic half-space as thickness of liquid increases. This wave carries almost all of the energy in the liquid rather than in the solid. This prove can be seen in Figures from 7.13 to 7.16 that the reflection coefficient of lubricated contact is lower than dry contact.

This is one of the drawbacks of this surface wave approved where from Figure 7.11c, the surface wave is difficult to propagate in solid-liquid interface. This is critical for the practical application if this waveform is employed as a method for seal condition monitoring. If the rotating shaft becomes coated in the oil then this could hide the signal from seal-shaft interface. This is therefore a serious limitation of this approach.

7.5.2 Ratio between contact diameter and element contact diameter

At the solid-solid interface, contact between two surfaces occurs at the peaks of the surface roughness. The surface wave cannot propagate along the air gaps left between the contacting regions. As the contact increases, the amplitude reflected signal of surface wave propagation, which is transmitted, will be smaller. The propagation of a surface wave within a point contact will be influenced by not only the contact area, but also the element diameter of transducer. It can be seen in Figure 7.17 that ratio between the contact diameter and element diameter will influence the reflected signal of surface wave propagation in dry and lubricated contact interfaces. This figure was re-plotted from Figure 7.13 by dividing contact diameter and element diameter of beam transducers.

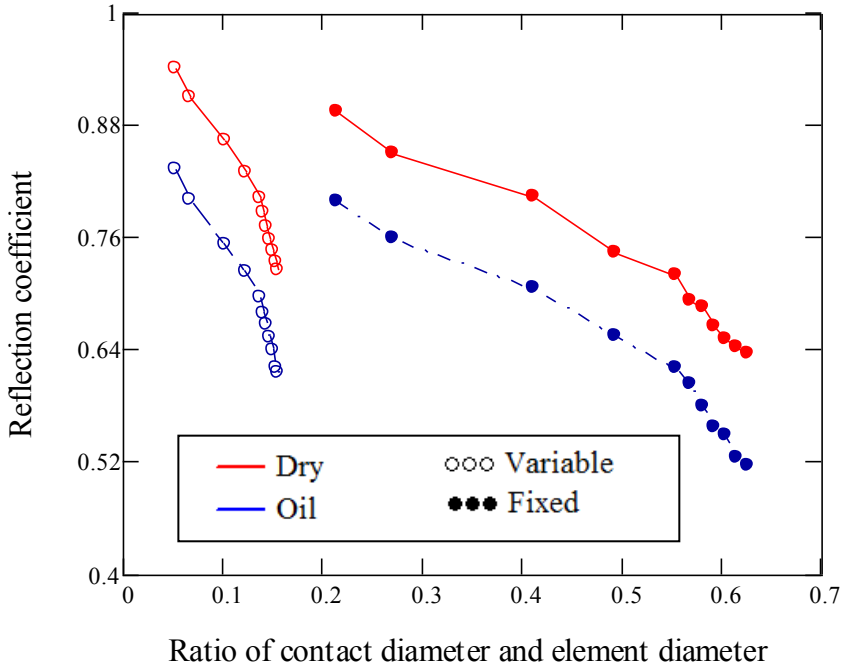

Figure 7.17 The relation of reflection coefficient against ratio contact diameter and diameter contact between fixed (ball) and variable angle beam transducers (circle) in dry (red line) and oil (blue line) contacts at point contact.

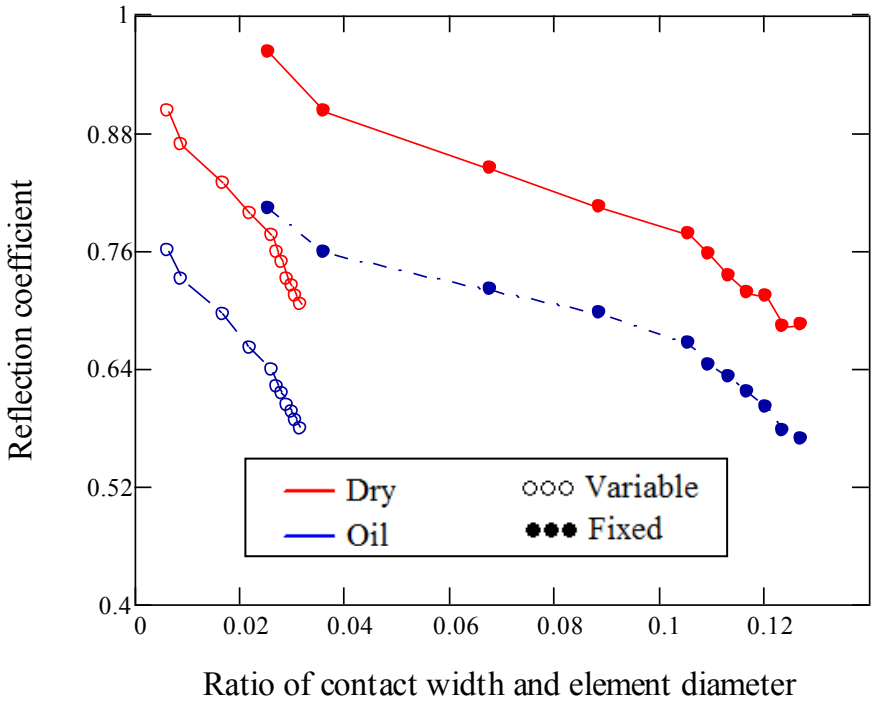

Figure 7.18 The relation of reflection coefficient against ratio contact area and diameter contact between fixed (ball) and variable (circle) angle beam transducers in dry (red line) and oil (blue line) contacts at line contact.

However, in line contact there is no effect of element diameter against reflection coefficient of propagation of surface wave as shown in Figure 7.18. This figure was re-plotted from Figure 7.14 by dividing contact width and element diameter of beam transducers. It can be explained in Figure 7.19. The propagation of surface wave was influenced of the object that obstructs it such as area of contact. In the case of line contact, all of propagation of wave passed through the contact, but in contrast, at a point contact, not all of wave passed through the contact.

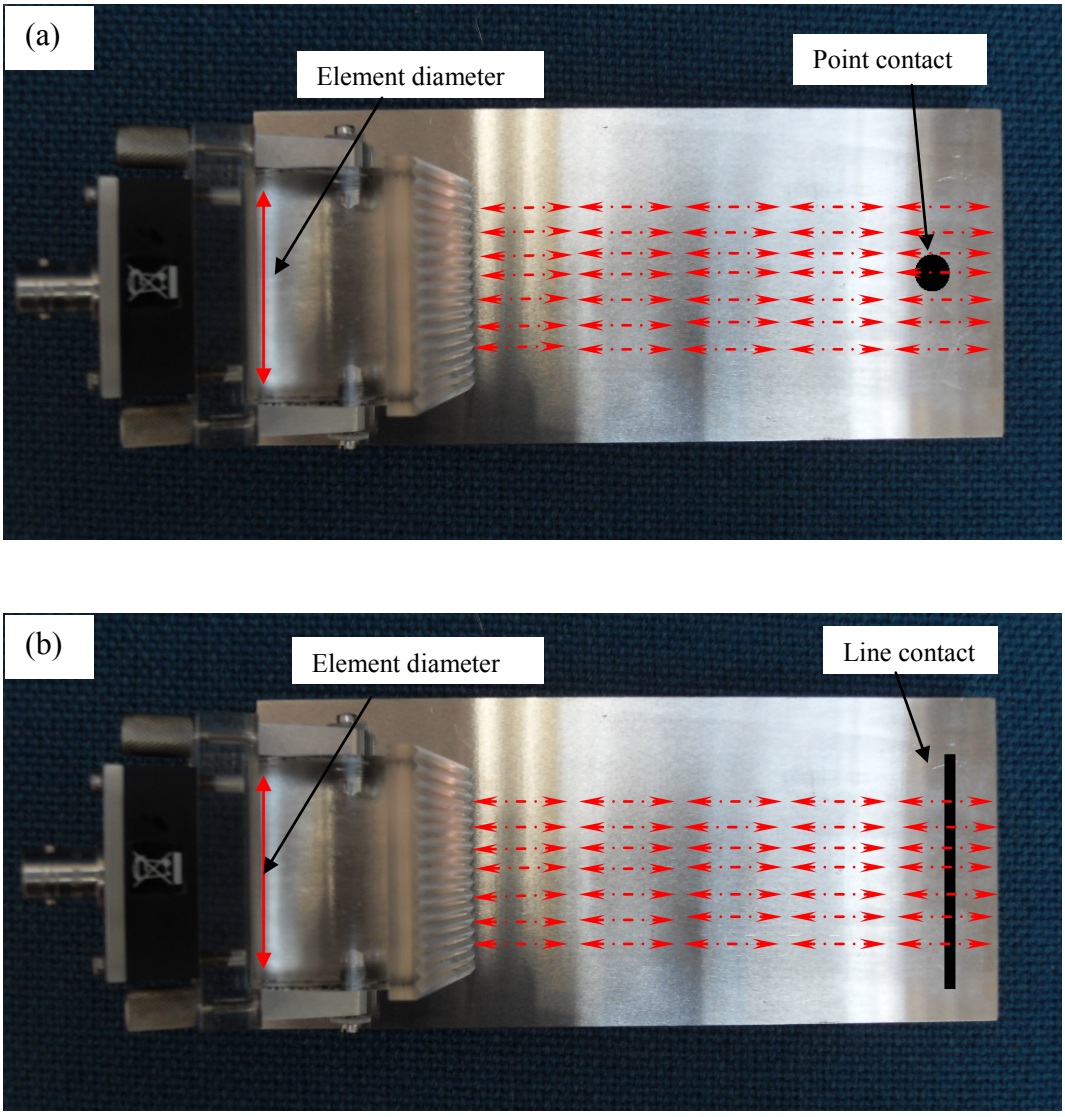

Figure 7.19 Sketch of propagation of Rayleigh surface wave by ignoring beam divergence (a) point and (b) line contacts using variable wedge transducer.

7.5 Conclusions

Measurements of reflection coefficient of surface wave propagation on the surface of steel plate loaded through a solid-solid contact with nitrile rubber have been performed. These measurements were made by using variable and fixed wedge 2.25 MHz transducers, which had 2.54 and 6.35 mm element diameters, respectively. The reflection coefficient of surface wave propagation at point and line contacts was considered. These results show that the principal effect was shown to be decreased amplitude of the surface wave propagation. This effect was caused by leakage of energy of surface wave into the nitrile rubber, where it was dissipated due to high viscoelastic damping. It was shown that the decrease of reflection coefficient was strongly dependent on the compressive load applied across the solid-solid interface. So, the change of reflection coefficient of surface wave propagation due to loading can be used as a sensor to measure contact between soft and hard materials

The surface wave is difficult to propagate along liquid-solid interface. If the thickness of liquid is too thick, the energy of surface waves will be absorbed by liquid. Therefore, this waveform is difficult to employ for seal condition monitoring.

There was no effect of element transducer against the reflection coefficient for line contact where the reflection coefficient between loading and unloading line was almost coinciding. For point contacts, however, there was influence of the element diameter of transducer.

Chapter 8

Conclusions and recommendations

The experimental techniques to investigate oil film thickness and contact between two dissimilar materials using ultrasonic reflection techniques have been performed in Chapters 5, 6, and 7. Whilst in the previous application chapters, individual discussions were presented. The findings of this study are now summarised and suggestions for future work are given.

8.1 Conclusions

Ultrasonic reflection techniques have been applied to measure experimentally the oil film thickness in hydrodynamic (HD) and elastohydrodynamic (EHD) lubrications. These methods have been applied to engineering and biological Tribology, such as ball bearings, journal bearings, piston rings, and metal on metal prosthetic hip joints.

In the contact mechanics, ultrasonic reflection techniques have been used to measure contact pressures distribution and area of contact. These methods have been also applied to the contact between a railway wheel and rail, the interface between two clamped plates in a bolted joint, the interface between a shaft and sleeve in a simple interference fit, the contact between the wheel and axle in a

railway wheel-set assembly (Marshall [2005]), and interface between pin and bush aircraft landing gear (Zhu *et al* [2010]).

The goals of measurement in the machine components above are for design purpose, manufacturing process, or condition monitoring. As a tool for measurement process, ultrasonic reflection has some advantages, such as non-invasive, safe, and portable those are very useful in plant and field conditions. To develop a robust method that can be used in real industrial situations, the methods have been developed and explored for wide application of several types of material in contact. This investigation has focussed on developing phase shift method to measure oil film thickness between two acoustically dissimilar materials, measuring oil film thickness in isoviscous elastohydrodynamic lubrication (I-EHL) regime, and exploring the feasibility of developing a sensor to measure contact between soft and hard material using surface waves.

8.1.1 Phase shift method investigations

The main purpose of this study was to explore phase shift method to measure oil film thickness between two acoustically dissimilar materials in contact. The measurement of oil film thickness was carried out for different contact cases: Perspex and Perspex, Perspex and PTFE, and Perspex and steel. The results obtained from this study are concluded as follows;

1. The amplitude and phase shift methods have demonstrated the capability to measure experimentally oil film thickness between two materials in contact. The results of both methods have been compared to measure oil film thickness for contact between Perspex-Perspex and Perspex-PTFE; the results are in a good agreement for thin films ($h < 25$ μm).
2. The phase shift method has also demonstrated the feasibility to measure the oil film thickness between two acoustically dissimilar materials (Perspex-steel). From the oil film thickness spectrum (Figure 5.25), it shows that this method is valid only for thin films ($h < 40$ μm)

characterized by the value of film thickness is constant in the bandwidth of the transducer (4 – 6 MHz).

3. For the amplitude method, it is not important to which material of the contact pair of the sensor is mounted. In the phase shift method, however, the order of the material pair is critically important. Measuring from a soft to a hard material is possible whilst the opposite is not. This is because in the amplitude method (from Eq. 3.25) there is no effect on the film thickness if the order of the contact pair is changed.
4. The amplitude method is best suited to acoustically similar materials. As they become more dissimilar, the method becomes increasingly more inaccurate. This is because the minimum of reflection coefficient (From Eq. 3.2) approaches 1 when two acoustically dissimilar materials is in the contact. The amplitude method has successfully been used for materials where the difference of the acoustic impedance between two materials is small. This means that measurements of metal on metal ($Z_1 = Z_2$) are practical, but measurement of polymers or rubber on metal ($Z_1 << Z_2$) is not.
5. The maximum upper limit to measure oil film thickness using amplitude method depends upon contact between two materials where the reflected signal in the contact will influence of the combination of two amplitudes of reflected signal on three-layer-system. The results of experiment show that the maximum limitation to measure oil film thickness was shifted from R = 0.95 to R = 0.76 and R = 0.68 for contact cases Perspex-Perspex and Perspex-PTFE, respectively due to corrections regarding limits.
6. The reflection between solid and liquid interface (Perspex and oil) could be used to measure speed of sound of liquid material. By using Eq. 3.2, the acoustic impedance of liquid can be calculated if the acoustic impedance of Perspex is known. Therefore, this method is easier to use than time of flight (ToF) method and the error of speed of sound between ToF and RLS method for Shell Turbo T68 was 0.34%.

8.1.2 Film thickness investigations in I-EHL regime

The aim of the work was to measure of reflection coefficient profile in the contact area, film thickness profile, cavitation in outlet region and central film thickness from a solid-rubber interface (I-EHL) by using ultrasonic reflection. The main results obtained are summarized as follows;

1. The distribution of reflection coefficient from dry and oil wetted static contact has been measured for varying applied loads. Complete contact (i.e. no air gaps) was observed at the central region under high load (P > 9.3 N). In this region, the reflection coefficient approached its minimum value and the stiffness increased to infinity. This data can then be used to measure speed of sound of the nitrile ball. This method has been developed to measure acoustic impedance of low acoustic impedance of materials such as nitrile cord. The error of speed of sound between ToF and RSS method for Nitrile ball was 1.85%.
2. The relationship between the interface stiffness and local contact pressure for dry contact was observed to be uniform regardless of the global load on the contact. The results show that a pressure of 1.2 MPa is sufficient to cause complete conformity; or that the reflection is so close to that for complete conformity that there is no sensitivity to measure any areas of non-contact.
3. Profiles of the oil film thickness were created for various loads and sliding speeds in dynamic lubricated cases. The phenomenon of a wedge-shaped constriction in lubricant film was observed, especially at low speeds (8.9, 11, and 22 mm/s).
4. The phenomenon of cavitation was seen clearly at high speed (380 and 590 mm/s). Cavitation can also be observed from the reflection coefficient results, where in the bulk lubricant, the reflection coefficients are around 0.6 at the low speeds (8.9, 18, and 22 mm/s). Whereas at the higher speeds (380 and 590 mm/s), the reflection coefficients increases towards 1.
5. Oil film thickness was measured in the region of 1 - 6 μm. The data was shown to be consistent with previous published experimental work

(Myant [2010]) but somewhat lower than theoretical solutions (Hamrock and Dowson [1978]).

8.1.3 Rayleigh wave investigations

The objective of investigation of surface wave propagation was to explore the possibility of developing a sensor to measure contact between soft and hard materials. The reflection coefficient of surface wave propagation at point and line contacts was investigate by using two wedge transducers. The results of investigation are summarized as follows;

1. The results show that the reflection coefficient of surface wave propagation in the contact interface between steel and nitrile ball and cord is proportional to the applied load. This reflection coefficient can be used as an alternative method to measure contact between soft and hard materials where the ultrasonic transducer can be placed remotely from the contact location.
2. There is a relationship between element diameter and contact area where at point contact, the reflection coefficient of surface wave propagation between fixed and variable wedge transducers was different. At line contact, however, there was no effect of element diameter against the reflection coefficient for both transducers. This is because the most of energy of surface wave transmission for both transducers passed through the line contact but at the point contact, it was not.
3. The fixed transducer is more sensitive than the variable wedge transducer where the reflection coefficient at the loading and unloading lines is wider than the variable wedge transducer for both contact conditions due to effect of element diameter. However, in general for line contact, both transducers could be used to detect contact, because there is no difference of reflection coefficient at the loading and unloading lines between two transducers, as shown in Figure 7.15. In contrast, at point contact, there was.
4. The drawback of surface wave is that it is difficult to propagate along a liquid-solid interface, because the liquid will absorb the energy of surface wave. This is the reason why this is critical from the practical application if

the surface wave propagation is used as a method for seal condition monitoring. The rotating shaft becomes coated in the oil then this could hide the signal from seal-shaft interface.

8.2 Recommendations for future work

8.2.1 Film thickness measurements: Phase shift method

There was a phase shift of reflected signal on the top and the bottom of measured material (Perspex plate) due to applied load when (see section 5.5.3). Capturing these signals was not done simultaneously and possibility the measured phase shift was changed, so when the using of Eq. 4.5 to calculate phase difference the result was not accurate and then there was an error in calculating of oil film thickness as well. To solve the problem, it is suggested that when the capturing of reflected signal should be carried out synchronously by developing a hardware and software, which can capture the reflected signals instantaneously by using two channels.

The phase shift method has shown the ability to measure film thickness between two acoustically dissimilar materials. This method should be developed further for some real components such as o-rings, lip seals, and metal on polymer prosthetic hip joints by developing an ultrasonic sensor that can attach and propagate on soft material.

8.2.2 Film thickness measurements: I-EHL regime

The experiments that had been carried out were limited to measure film thickness between Perspex and nitrile rubber. To develop further, it is suggested to use different materials, used in seal technology such as Polyurethane and Fluroelastomer, to see effect of some relationships for isoviscous elastohydrodynamic lubrication (I-EHL).

The spatial resolution of an ultrasonic pulse was relatively low because 10 MHz focusing transducer having spot diameter of 1.12 mm was employed and the transducer was moved manually using micrometer, so it was not possible to pick out the detail of constriction at the contact exit especially at low speeds. It is suggested that the transducer should be moved by a step motor that can be moved in x-y direction so that the horseshoe constriction at the contact exit especially at low speeds can be observed.

It was difficult to observe starvation phenomenon in I-EHL regime, where the surface of nitrile ball was not smooth and there was a dimple in the surface. The sort of dimple could act as oil reservoir. In addition, the speed of motor was limited for high speeds. To investigate the starvation phenomenon, it suggests that the surface of the nitrile ball should be smooth and range of rotation speed should be wide by changing the motor driver.

There was a problem in applying the load, where the variation of load was varied from 3.5 N to 7.5 N so it was difficult to apply for low loads. The pressure gauge should be changed with new one that could measure load until 0.1 N. At high loads, there was occurred slip between shaft and nitrile ball. It would be beneficial to find a technology, which can couple between shaft and nitrile ball without the occurrence of slip.

8.2.3 Soft contact measurements: Rayleigh waves

There is a lack of a prediction model for the reflection coefficient and interfacial stiffness in measuring of contact between soft and hard materials by surface wave. Regarding experimental work involving reflection coefficient, it is observed that the general trend of the experimental results is predicted well by the reflection coefficient model. However, no sufficient information about the contacting stiffness was available to compare the theory and the experiment in a quantitative way. It is suggested that a mathematical model needs to be developed for the

relationship between surface wave reflection coefficient and interface stiffness of a soft contact.

The sensor used to generate surface wave would be difficult to apply in field conditions, because it was big and difficult to attach on the surface of shaft. It is recommended to develop small and easily assembled sensors for generating surface waves. There was no effect of the frequency of transducer on measurement so low frequency transducer could be possibly used.

Publications arising from this work

Journal Papers

Wan Ibrahim M K, Gasni, D, and Dwyer-Joyce, R S, Profiling a Ball Bearing Oil Film with Ultrasonic Reflection, Tribology Transactions, 55:4, 409-421, 2012.

Gasni, D, Wan Ibrahim, M K, and Dwyer-Joyce, R S, Measurement of Lubricant Film Thickness in the Iso-Viscous Elastohydrodynamic Regime, Tribology International, 44 (7-8), 933-944, 2011.

Extended Abstracts

Gasni, D, Wan Ibrahim, M K, and Dwyer-Joyce, R S, Ultrasonic Reflection Technique for Measuring Film Thickness in the I-EHL Regime, STLE Annual Meeting 2011 Atlanta, 15 – 19 May 2011, Atlanta , USA.

Wan Ibrahim, M K, Gasni, D, and Dwyer-Joyce, R S, Profiling the Oil Film of a Ball Bearing with Ultrasonic Reflection, STLE Annual Meeting 2011 Atlanta, 15 – 19 May 2011, Atlanta , USA.

References

Anderson W, Salant RF, and Jarzynski J. Ultrasonic detection of lubricating film collapse in mechanical seals. Tribology Transactions 1999; 42: 801-806.

Anderson W, Jarzynski J, and Salant RF. Condition monitoring of mechanical seals: Detection of film collapse using reflected ultrasonic wave. Proc Instn Mech Engrs Part C: J Engineering Tribology 2000;214:1187-1194.

Anderson W, Jarzynski J, and Salant RF. A condition monitor for liquid lubricated mechanical seals. Tribology Transactions 2001;44:479-483.

Ahn H and Kim D. In situ evaluation of wear surface by ultrasound. Wear 2001;251:1193-1201.

Aymerich F And Pau M. Assessment of nominal contact area parameters by means of ultrasonic wave. Journal of Tribology 2004;126:639-645.

Adams MJ, Briscoe BJ, and Johnson SA. Friction and lubrication of human skin. Tribology Letters 2007;26:239-253.

Allen DR and Cooper WHB. A Fourier transform technique that measures phase delays between ultrasonic impulses with sufficient accuracy to determine residual stress in metals. NDT International 1983; 16(4): 205-217.

Avan, EY, Mills RS, and Dwyer-Joyce RS. Ultrasonic imaging of the piston ring oil film during operation in a motored engine - towards oil film measurement**.** *SAE 2010 Power trains Fuels and Lubricants Meeting* San Diego 2010. 2010-01-2179.

Biswas S and Snidle RW. Elastohydrodynamic lubrication of spherical surfaces of low elastic modulus. Trans ASME J Lubric Technol 1976;98: 524-529.

Baik JM and Thompson RB. Ultrasonic scattering from imperfect interfaces: a quasi-static model. Journal of Non-Destructive Evaluation 1984;4:177-196.

Birring AS and Kwun H. Ultrasonic measurement of wear. Tribology International 1989;22(01):33-37.

Baltazar A, Rokhlin S, and Pecorari C. On the relationship between ultrasonic and micromechanical properties of contacting rough surfaces. J Mech Phys Solids 2002;50:1397–1416.

Bongaerts JHH, Rossetti D, and Stokes JR. The lubricating properties of human whole saliva. Tribology Letters 2007;27(3):277-287.

Cheeke JD. Fundamentals and applications of ultrasonic wave. CRC Press LLC; 2002.

Dowson D and Taylor CM. Cavitation in bearings, Ann Rev Fluid Mech 1979; 11: 35-66.

Dowson D and Neville A. Bio-tribology and bio-mimetics in operating environtment. Journal Engineering Tribology Part J: ImechE 2006;220:109-123.

Drotowski RC. Contact elasticity of seals elastomers. Trans ASME J Lubric Technol 1968;94:478-483.

Drinkwater B, Dwyer-Joyce RS, and Cawley P. A study of the transmission of ultrasound across real rough solid-solid interfaces. Ultrasonics symposium; 1994.

Drinkwater BW, Dwyer-Joyce RS, and Cawley P. A study of interaction between ultrasound and a partially contacting solid-solid interface. Proc R Soc Lond A 1996;452:2613-2638.

Drinkwater B and Cawley P. Measurement of the frequency dependence of the ultrasonic reflection coefficient from thin interface layers and partially contacting interfaces. Ultrasonics 1997;35:479-488.

Drinkwater BW, Castaings M, and Hosten B. The measurement of A0 and S0 lamb wave attenuation to determine the normal and shear stiffness of a compressively loaded interface. J Acoust Soc Am 2003;113:3161–3170.

Dwyer-Joyce RS, Drinkwater BW, and Quinn AM. The use of ultrasound in the investigation of rough surface interfaces. ASME J Tribol 2001;123:8–16.

Dwyer-Joyce RS, Quinn AM, and Drinkwater BW. Experimental procedure for mapping Hertzian contact. Science in China Seri A 2001;44:423-430.

Dwyer-Joyce RS, Drinkwater B, and Donohoe CJ. The measurement of lubricant-film thickness using ultrasound. Proc R Soc Lond A 2003;459: 957-976.

Dwyer-Joyce RS, Harper P, and Drinkwater BW. A method for measurement of hydrodynamic oil films using ultrasonic reflection. Tribology letters 2004;17:337 – 347.

Dwyer-Joyce RS. The application of ultrasonic NDT techniques in Tribology. Proc ImechE Part J: J Engineering Tribology 2005;219:347-366.

de Vicente J, Stokes JR, and Spikes HA. The frictional properties of Newtonian fluids in rolling-sliding soft-EHL contact. Tribology Letters 2005;20:3-4.

de Vicente J, Stokes JR, and Spikes HA. Rolling and sliding friction in compliant, lubricated contact. Proc ImechE Part J J Engineering Tribology 2005;220:55-63.

Fraser J, Khuri-Yakub BT, and Kino GS. The design of efficient broadband wedge transducers. Appl Phys Letts 1978;32(11).

Fuji Y, Method for measuring transient friction coefficient for rubber wiper blades on glass surfaces. Tribology International 2007;41:17-23.

Gabelli A and Poll G, Formation of lubrication film in rotary sealing contacts: Part I-Lubricant film modelling. Journal of Tribology Transaction of the ASME 1992;114:280-289.

Gonzales-Valades M, Baltazar A, and Dwyer-Joyce RS. Study of interfacial stiffness ratio of a rough surface in contact using a spring model. Wear 2010;268:373-379.

Hallermeier RJ and Diachock OI. Simple technique for exciting and probing elastic surface wave. J Appl Phys 1970; 41(12).

Hamrock BJ and Dowson D. Elastohydrodynamic lubrication of elliptical contacts for materials of low elastic modulus 1: fully floaded conjuction. Trans ASME J Lubric Technol 1978;100:236-245.

Hamrock BJ. Fundamentals of fluid film lubrication, New York: McGraw-Hill Book Co.; 1994.

Hamrock BJ, Schmid SR, and Jacobson BO. Fundamentals of fluid film lubrication, second edition, Marcell Dekker, 2004.

Harper P. Measurement of film thickness in lubricated components using ultrasonic reflection. PhD Thesis, University of Sheffield, 2008.

Heinrich G and Kluppel M. Rubber friction thread deformation and tire traction. Wear 2008;265:1052-1060.

Herrebrugh K. Solving the incompressible and isothermal problem in elastohydrodynamic lubrication through an integral equation. Trans ASME J Lubric Technol 1968;94:262-270.

Hooke CJ and O'Donoghue JP. Elastohydrodynamic lubrication of soft highly deformed contacts. J Mech Engng Sci 1972;14:34-48.

Hosten B. Bulk heterogeneous plane waves propagation through viscoelastic plates and stratified media with large values of frequency domain. Ultrasonics 1991;29:445-450.

Hooke CJ. Elastohydrodynamic lubrication of soft solids. Elsevier Science; 1997.

Jin ZM and Dowson D. Elastohydrodynamic lubrication in biological system. Proc IMechE J J Engineering Tribology 2005;219:367-380.

Kaneta M, Todoroki H, and Nishikawa H. Tribology of flexible seals for reciprocating motion. Journal of Tribology ASME 2000;122:787-795

Kasolong S and Dwyer-Joyce RS. Observations of film thickness profile and cavitation around a journal bearing circumference. Tribology Transactions 2008;51:231-245.

Kasolong S and Dwyer-Joyce RS. Viscosity measurement in thin lubricant film using shear ultrasonic reflection. Proc ImechE Part J J Engineering Tribology 2008;222:423-429.

Kendall K and Tabor D. An ultrasonic study of the area of contact between stationary and sliding surfaces. Proc Roy Soc Lond A 1971;323:321-340.

Królikowski J, Szczepek J, and Witczak Z. Ultrasonic investigation of contact between solids under high hydrostatic pressure. Ultrasonics 1989;27: 45-49.

Królikowski J and Szczepek J. Prediction of contact parameters using ultrasonic method. Wear 1991;148:181-195.

Królikowski J and Szczepek J. Phase shift of the reflection coefficient of ultrasonic waves in the study of the contact interface. Wear 1992;157:51-64.

Masuko M, and Ito Y. Measurement of contact pressure by means of ultrasonic wave. Ann CIRP 1969;17:289-296.

Marshall MB, Lewis R, Drinkwater BW, and Dwyer-Joyce RS. An approach for contact stress mapping in joints and concentrated contacts. J. Strain Anal 2004:39:339-350.

Marshall MB. An ultrasonic investigation of real engineering contacts. PhD Thesis, 2005, University of Sheffield.

Marshall MB, Lewis R, and Dwyer-Joyce RS. Experimental characterization of wheel-rail contact patch evolution. Journal of Tribology 2006;128:493-504.

Moore DF. The friction and lubrication of elastomers, Pergamon Press; 1972.

Murty GS, and Kumar V. Elastic wave propagation with kinematic discontinuity along a non ideal interface between two isotropic elastic half-spaces. Journal of Nondestructive Evaluation 1991;10(2):39-52.

Myant CW. Experimental techniques for investigating lubricated, compliant, contacts. PhD Thesis, 2010. Imperial College London.

Myant CW, Fowell M, Spikes HA, and Stokes JR. An investigation of lubricant film thickness in sliding compliant contacts. Tribology Transactions 2010;55:684-694.

Nagy PB. Ultrasonic classification of imperfect interfaces. J Nondestruct Eval 1992;11:127-139.

Pau M. Estimation of real contact area in wheel-rail system by means of ultrasonic wave. Tribology International 2003;36:687-690.

Reddyhoff T, Kasolong S, and Dwyer-Joyce RS. The phase shift of an ultrasonic pulse at an oil layer and determination of film thickness. Proc ImechE Part J J Engineering Tribology 2005;219:387-400.

Reddyhoff T, Dwyer-Joyce RS, Harper P. Ultrasonic measurement of film thickness in mechanical seals. Sealing Technology July 2006:7-11.

Reddyhoff T. Ultrasonic measurement technique for lubricant film. PhD Thesis, 2006, Sheffield University.

Reddyhoff T, Dwyer-Joyce RS, Harper P. A new approach for the measurement of film thickness in liquid face seals. Tribology Transactions 2008;51:140-149.

Poll G, Gabelli A, Binnington P, and Qu J. Dynamic mapping of rotary lip seal lubricant films by fluorescent image processing. Proceedings of the 3th Annual Conference on Fluid Sealing, BHRA, 55-57,1992.

Poll G and Gabelli A, Formation of lubricant film in rotary sealing contacts: Part II-A new measuring principle for lubricant film thickness. Journal of Tribology Transaction of the ASME 1992;114:290-296.

Polijaniuk A and Kaczmarek J. Novel stage for ultrasonic measurement of real contact area between rough and flat parts under quasi-static load. ASTM J Test Eval 1993;21:174-177.

Robert AD, Tabor D. Short communication: Fluid film lubrication of rubber – an interferometric study. Wear 1968; II: 163-166.

Rokhlin SI and Wang YJ. Analysis of boundary condition for elastic wave interaction with an interface between two solids. J Acoust Soc Am 1991;89:503-515.

Rose JL. Ultrasonic wave in solid media. Cambridge University Press 1999.

Silk MG. Ultrasonic transducers for nondestructive testing. Hilger, Bristol, 1984.

Sugimura J, Hashimoto M, and Yamamoto Y. Study of elastohydrodynamic contacts with fluorescence microscope. Thinning Films and Tribology Interfaces 2000:609-617.

Stachwiak GW and Batchelor AW. Engineering Tribology second edition, Butterworth-Heinemann, 2001.

Stokes JR and Telford JH. Measuring the yield behaviour of structured fluids. Journal Non-Newtonian Fluid Mech 2004;124:137-146.

Tattersall HG. The ultrasonic pulse-echo techniques as applied to adhesion testing. J Phys D Appl Phys 1973;6:819-832.

Tohmyoh H and Saka M. Dry-contact techniques for high-resolution ultrasonic imaging. IEEE, Transactions on Ultrasonics, Ferroelectrics, and Frequency Control 2003;50(6):661-667.

Venner CR. Multilevel solution of the EHL line and point contact problem. PhD Thesis, 1991, University of Twente, Enchede, The Netherland, ISBN 90-9003974 0.

Venner CH and Napel WE. Multilevel solution of the elastohydrodynamically lubricated circular contact problem. Part 2: Smooth surface results. Wear 1992;152:369-381.

Wedeven L D. Optical measurements in elastohydrodynamic rolling-contact bearing. Imperial College London, University of London Press, 1970.

Zhang J, Drinkwater BW, and Dwyer-Joyce RS. Calibration of ultrasonic lubricant-film thickness measurement technique. Meas Sci Technol 2005;16:1784-1791.

Zhang J, Drinkwater BW, and Dwyer-Joyce RS. Monitoring of lubricant film failure in a ball bearing using ultrasound. Trans ASME J Lubric Technol 2006;128:612-618.

Zhang J and Drinkwater BW. Thin oil film thickness distribution measurement using ultrasonic arrays. NDT&E International 2008;41:596-601.

Zhu J, Pugh S, and Dwyer-Joyce RS *et al*. Experiments and the pressure distribution and frictional torque in articulating pin joints. Proc IMechE Part J J Engineering Tribology 2010;224:1153-1162.